DYNAMIC SOIL-STRUCTURE INTERACTION OF REINFORCED CONCRETE BURIED STRUCTURES UNDER THE EFFECT OF DYNAMIC LOADS USING SOIL REINFORCEMENT NEW TECHNOLOGIES

Soil-structure interaction of buried rigid and flexible pipes under geogrid-reinforced soil subjected to cyclic loads

Ahmed M. M. ELSHESHENY

Submitted for the Degree of
Doctor of Philosophy

Faculty of Engineering and Informatics
University of Bradford

2019

ABSTRACT

Ahmed M. M. Elshesheny

Soil-structure interaction of buried rigid and flexible pipes under geogrid-reinforced soil subjected to cyclic loads

Keywords: Buried rigid pipes, Buried flexible pipes, Geogrid-reinforced soil, Incrementally cyclic loading, Large-scale laboratory tests, Material testing, Numerical investigation, Strain gauges, Pressure cells.

Recent developments in constructions have heightened the need for protecting existing buried infrastructure. New roads and buildings may be constructed over already existing buried infrastructures e.g. buried utility pipes, leading to excessive loads threatening their stability and longevity. Additionally applied loads over water mains led to catastrophic damage, which result in severe damage to the infrastructure surrounding these mains. Therefore, providing protection to these existing buried infrastructure against increased loads due to new constructions is important and necessary.

In this research, a solution was proposed and assessed, where the protection concept would be achieved through the inclusion process of geogrid-reinforcing layers in the soil cover above the buried infrastructure. The controlling parameters for the inclusion of geogrid-reinforcing layers was assessed experimentally and numerically. Twenty-three laboratory tests were conducted on buried flexible and rigid pipes under unreinforced and geogrid-reinforced sand beds. All the investigated systems were subjected to incrementally increasing cyclic loading, where the contribution of varying the burial depth of the pipe and the number of the geogrid-reinforcing layers on the overall behaviour of the systems was investigated. To further investigate the contribution of the controlling parameters in the pipe-soil systems performance, thirty-five numerical models were performed using Abaqus software. The contribution of increasing the amplitude of the applied cyclic loading, the

number of the geogrid-reinforcing layers, the burial depth of the pipe and the unit-weight of the backfill soil was investigated numerically.

The inclusion of the geogrid-reinforcing layers in the investigated pipe-soil systems had a significant influence on decreasing the transferred pressure to the crown of the pipe, generated strains along its crown, invert and spring-line, and its deformation, where reinforcing-layers sustained tensile strains. Concerning rigid pipes, the inclusion of the reinforcing-layers controlled the rebound that occurred in their invert deformation. With respect to the numerical investigation, increasing the number of the reinforcing-layers, the burial depth of the pipe and the unit-weight of the backfill soil had positive effect in decreasing the generated deformations, stresses and strains in the system, until reaching an optimum value for each parameter. Increasing the amplitude of the applied loading profile resulted in remarkable increase in the deformations, stresses and strains generated in the system. Moreover, the location of the maximum tensile strain generated in the soil was varied, as well as the reinforcing-layer, which suffered the maximum tensile strain.

ACKNOWLEDGMENTS

First of all, all praise is due to **ALLAH** alone, Lord of all the creations, for giving me the ability to complete this thesis.

Secondly, I would like to express my deepest appreciation to ***Dr. Mostafa Mohamed***, who helped in every step in the research, for his intellectually stimulating guidance, his insightful comments and encouragement, always believed in me and never hesitated to provide relentless support and motivation at all times. I also would like to express my deepest thanks to ***Dr. Therese Sheehan***, for her assistance, encouragement and above all her accurate support during the writing.

I am also grateful to the Government of Egypt for the financial support for this research throughout my PhD research period.

It would be outrageous if I missed mentioning my father, ***Mohamed Elshesheny***, who was and still my main motivator. I would like to thank ***my mother***, ***brother and sisters***.

I would further like to express my deepest appreciation to my wife, ***Nancy Elrefaey***, for her unconditional patience, support and her continuous encouragement. Also, to my beloved sons, ***Omar and Yousuf***.

Furthermore, I would like to express my gratitude to all the staff in the Department of Civil Engineering for their sincere and continuous support throughout years. I wish to express my deepest thanks and sincere gratitude to my colleagues, ***Khaled Aqoub and Othman Shalookh***, for their assistance and valuable consultation.

CONTENTS

LIST OF FIGURES

LIST OF TABLES

NOMENCLATURE

$\in$	Meridional eccentricity
B	Width of the reinforcing layer
B_f	Footing width
B_n	Nominal width of the tested geogrid-specimen
c	Cohesion
C	Factor depends on the geometry of the reinforcing layer
$c\|o$	The initial cohesion yield stress corresponding to zero plastic strain
C_c	Coefficient of curvature
C_s	Settlement of the crown
C_{st}	Strain of the crown
C_u	Coefficient of uniformity
D	Diameter of the pipe
d	Soil's cohesion in the meridional plane (p-q)
D_{10}	Effective grain size
D_{50}	Medium grain size
D_c	Sand density at certain cycle of the applied loading profile
$d\mathcal{E}_{ij}$	Total increase in the strain
$d\mathcal{E}_{ij}^{e}$	Elastic strain increment
$d\mathcal{E}_{ij}^{p}$	Plastic strain increment
D_i	Sand density before applying loading profile (initial density)
Dr	Relative density
E	Elastic modulus
e	Deviatoric eccentricity
e_{max}	Maximum void ratio
e_{min}	Minimum void ratio
E_{slip}	Elastic slip between two interacted surfaces in a contact pair
$\mathcal{E}$	Strain
$\mathcal{E}_{nom}$	Engineering strain
$\mathcal{E}_{true}$	True strain
F	Applied Force

F_c	Cap surface
f_{cu}	Compressive strength
F_{max}	Maximum tensile force
F_s	Settlement of the footing
F_t	Transition surface
g	Plastic potential function
G_s	Specific Gravity
H	Burial depth of the pipe
h	Spacing between the first reinforcing layer and the footing
I_S	Settlement of the invert
I_{st}	Strain of the invert
J	Secant stiffness
k	Hardening parameter
K	Material stress parameter
L	Length of the specimen
$L1$	First reinforcing layer
$L2$	Second reinforcing layer
$L3$	Third reinforcing layer
$L4$	Fourth reinforcing layer
LL	Lower layer
N	Number of the reinforcing layers
N_m	Average number of tensile elements within one-meter width of the tested product
n_s	Number of tensile elements within the tested specimen
p	Hydrostatic pressure/Equivalent stress
Ph	Loading phase
q	Mises equivalent stress
R_{mc}	Measure of the shape of the yield surface in the deviatoric stress
R_{mw}	Polar radius
S_r	Ring stiffness
S	Stress deviator
Sg	Segment
SL_{st}	Strain of the spring-line

t	Average thickness
T_{max}	Maximum tensile strength
u	Spacing between the reinforcing layers
UL	Upper layer
υ	Poisson's ratio
y	Deflection
β	Soil's friction angle in the meridional plane (p-q)
γ_d	Dry unit weight
$\gamma_{d(max)}$	Maximum dry unit weight
$\gamma_{d(min)}$	Minimum dry unit weight
δ	Friction angle between the soil and the geogrid reinforcement
ΔD	Vertical diameter of the pipe after loading
Θ	The deviatoric polar angle
μ	Coefficient of friction between the soil and the geogrid reinforcement
σ_{II}	Intermediate principal stress
σ_{ij}	Current stress state
σ_n	Normal stress
σ_{nom}	Engineering stress
σ_{true}	True stress
τ	Shear stress
$\tau_{critical}$	Critical shear stress in a contact pair, where slip occurs for the 1st time
Φ	Internal friction angle
Ψ	Dilatancy angle

ABBREVIATIONS

C3D8R	Eight node continuum brick element with reduced integration
EMC	Extended Mohr-Coulomb
EPS	Expanded polystyrene blocks
FEA	Finite element analysis
FEM	Finite element method
HDPE	High-density Polyethylene
ITM	Induced trench method
LVDT	Linear variable differential transducer
M3D3	Three node triangular elements
PVC	Poly-vinyl chloride
SDR	Standard dimensional ratio
SIDD	Standard Installation Direct Design
SP	Superplasticizer
SRHDPE	Steel-Reinforced High-Density Polyethylene
SS20	Tensar square biaxial geogrid reinforcing layers
TDA	Tire-derived aggregate
uPVC	Polymeric un-plasticized
W/C	Water/Cement ratio

CHAPTER 1

INTRODUCTION

1.1 Background

The worldwide construction industry is increasing enormously to meet the needs and expectations of the population, particularly to overcome increasing population and traffic congestion problems. Consequently, potential construction of new houses, infrastructure, transportation links, new roads and maybe buildings over already existing buried infrastructure, e.g. pipes, might be required. This could lead to potential risks on existing buried structures due to additional loads and stresses.

To maintain the safety of these structures, one of the following solutions should be followed; i. relocating buried infrastructures, which is often costly and time consuming, ii. enhancing load transfer within the soil cover above these structures, to minimize adverse impacts of new development. Several techniques such as soil compaction, replacement of weak soil and soil stabilizing using chemicals and geosynthetics inclusion are available nowadays to enhance soil cover performance above buried structures (Fang and Daniels, 2006).

Pipelines are considered one of the most important infrastructures, as they facilitate modern life. Buried pipes are extensively used for strategic purposes, such as mineral transfer. The behaviour of buried pipes and soil cover needs to be well understood to provide economical and practical solutions for future challenges.

The behaviour of buried pipes depends upon both their response to external loading and their interaction with surrounding soils. Flexible pipes deform towards an oval/heart shape in response to loading and are able to develop significant lateral earth pressure from their surrounding embedment. Rigid pipe materials have a small deflection upon loading, which is too small to develop any lateral earth pressures. The pipe takes load, and bending moments are developed in the pipe walls. Rigid pipes also attract an increased backfill load upon burial and obtain a reaction from their bedding in response (BS, 2010a).

Consequently, the main concern in flexible pipes is their deformation. However; cracks formation, i.e. tensile failure, is the main danger affecting rigid pipes (BS, 2010a).

In the case of a rigid pipe, it has high circumferential and flexural stiffness, which is significantly higher than the surrounding soil stiffness; in addition, it suffers insignificant deformation. Consequently, differential settlement occurs between the soil prism located above the pipe and the adjacent soil portions surrounding it generating a passive arching mechanism due to the generated shearing stresses between them. Therefore, the generated forces in the soil prism above the pipe and part of the generated forces in the adjacent soil portions will be directed towards the pipe, which will apply more loads to the pipe, in addition to the geostatic pressure of the soil prism (Vaslestad et al., 1993; Peter et al., 2018).

Unlike the rigid pipes, flexible pipes have relatively lower stiffness and can deform, consequently, the soil prism located above it will settle more than the adjacent soil portions, generating active arching mechanism. Due to the active arching, part of the generated loads in the soil prism above the pipe will be directed to the adjacent soil portions, where the applied loads over the pipe will be the geostatic pressure of the soil prism in addition to the remaining part of the generated loads inside it. However, these relatively reduced loads would generate significant deformation in the pipe, which may lead to its failure according to its diametric strain.

It is therefore crucial that solutions are proposed and tested to provide protection by reducing the transferred stresses to the buried rigid and flexible pipes.

Leaves, straw, and woodchips were mixed with soil and used as lightweight backfills over pipes (Spangler, 1958; Larsen and Hendrickson, 1962; McAffee and Valsangkar, 2004). The main purpose of adding these materials to the soil cover was to enhance the ability of the soil to sustain tensile stresses and strains by creating new composite material of higher properties compared with soil. However, the problem of these materials was their decomposition with the passage of time. Based on this idea, adding geogrid-reinforcing layers to the soil would achieve similar behaviour to the soil cover, where a composite

material with enhanced properties will be formed, particularly its shearing strength. Consequently, the formed soil cover will have better ability to mitigate the transferred stresses through it, where lower value of loads and stresses will be transferred to the buried pipes, which would provide enhanced degree of protection to these pipes.

1.2 Aim and objectives of the research

The main aim of this research is to acquire deeper understanding of the generated load transfer mechanisms in the investigated unreinforced and geogrid-reinforced pipe-soil systems due to the application of incrementally increased cyclic loading. The contribution of varying the burial depth of the pipe and the number of the geogrid-reinforcing layers on the overall behaviour of the systems was investigated. This was achieved through both the experimental and numerical investigations to assess, i. the generated load transfer mechanisms between the soil and the ribs of the geogrid-layers, ii. the formed interaction between the pipe and the soil. The variation of the burial depth of the pipe and the number of the reinforcing layers would influence the following:

1- Settlement of the footing.
2- Deformation of the pipe.
3- Transferred pressure to the crown of the pipe.
4- Generated strains along the crown, invert and the spring-line of the pipe.
5- Generated strain in the geogrid-reinforcing layers.

1.3 Investigation methodology

The aim of this research would be achieved through performing a series of stages, as presented in the following sections.

1.3.1 Stage one, experimental material testing

In stage one, an experimental material-testing process will be performed on all the components of a full model, i.e. soil, flexible pipe, rigid pipe and geogrid-reinforcements, to identify the mechanical properties of these components.

1.3.2 Stage two, experimental investigation of buried flexible pipes

In stage two, laboratory large-scale physical models will be performed to investigate the behaviour of buried flexible pipes under geogrid-reinforced and unreinforced soil beds while applying incrementally increasing cyclic loading profile. The contribution of two main parameters will be investigated in this phase, the burial depth of the pipe (*H/D*=1.5, 2, 2.5 and 3) and the number of the geogrid-reinforcing layers (*N*=0, 1 and 2).

1.3.3 Stage three, experimental investigation of buried rigid pipes

In stage three, the performance of buried rigid pipes under geogrid-reinforced and unreinforced soil beds while applying incrementally increased cyclic loadings will be experimentally investigated using a fully instrumented laboratory rig, varying both the burial depth of the pipe (*H/D*=1.5, 2 and 2.5), and the number of the geogrid-reinforcing layers (*N*=0, 1 and 2).

1.3.4 Stage four, numerical investigation of buried flexible pipes).

In stage four, the performance of buried pipes in geogrid-reinforced and unreinforced sand beds while applying cyclic loading will be investigated numerically. Three-dimensional, 3D, finite element models will be generated to simulate stage two, and perform a parametric study to investigate the contribution of variable parameters on the performance of the system, using finite element package Abaqus v.6.14. The investigated parameters will be as follows:

1- Burial depth of the pipe (*H/D*=1.5, 2, 2.5 and 3).
2- Number of the geogrid-reinforcing layers (*N*=0 to 4).
3- Unit weight of the soil (loose – medium – dense).
4- Amplitude of the applied cyclic load.

1.4 Thesis outlines

This thesis consists of eight chapters. A brief description of the chapters is presented as follows:

Chapter 1 introduces the context of the research proposed and briefly describes the thesis structure and content.

Chapter 2 shows a comprehensive critical review of the performed investigations in the area of buried structures performance, and the points that may require further research.

Chapter 3 illustrates the experimental material testing of the used components in this research, the calibration of the used instruments and the laboratory-testing rig.

Chapter 4 presents the experimental investigation of buried flexible pipes.

Chapter 5 demonstrates the experimental investigation of buried rigid pipes.

Chapter 6 illustrates description of the numerical method and the constitutive models for the materials used in the numerical investigation of the problem.

Chapter 7 discusses the numerical investigation of buried flexible pipes.

Chapter 8 identifies the conclusions of the current research and the proposed recommendations for future researches in this area.

1.5 Dissemination of the work presented in the thesis

Some of the findings of this research have already been disseminated in the following peer-reviewed papers:

1- Elshesheny, A., Mohamed, M. and Sheehan, T. Behaviour of buried flexible pipes under the application of incrementally increasing cyclic loading. 2nd Annual Innovative Engineering Research Conference, AIERC2018, Bradford, United Kingdom, October 2018. (Published).

2- Elshesheny, A., Mohamed, M. and Sheehan, T. (2019). Buried flexible pipes behaviour in unreinforced and reinforced soils under cyclic loading. Geosynthetics International, 26, No. 2, 184–205. [https://doi.org/10.1680/jgein.18.00046]. (Published).

3- Elshesheny, A., Mohamed, M. and Sheehan, T. (2019). Performance of buried rigid pipes under the application of incrementally increasing cyclic loading. Soil Dynamics and Earthquake Engineering Journal, 125, 1-13. [https://doi.org/10.1016/j.soildyn.2019.105729]. (Published).

4- Elshesheny, A., Mohamed, M. and Sheehan, T. (2019). Protection of buried rigid pipes using geogrid-reinforced soil systems under cyclic loading. (Submitted and under review).

5- Elshesheny, A., Mohamed, M., Nagy, N. and Sheehan, T. (2019). Numerical performance of buried pipes under geogrid-reinforced soil subjected to cyclic loading. (Submitted and under review).

CHAPTER 2

LITERATURE REVIEW

2.1 Introduction

Buried structures are widely used for several purposes that serve and improve quality of life. These structures might be new or already existing infrastructure, which will share space with other infrastructure, e.g. roads and buildings, where additional loads will be subjected to them. These applied additional loads would cause detrimental effects, e.g. increased stresses, strains and deformations, to the buried structures, which would threaten their stability and longevity. Consequently, protecting these buried structures became a necessity to maintain their durability safely. Since these buried structures are located underneath the ground surface, enhancing the performance of the soil cover above them would provide protection to these structures (Lay and Brachman, 2014).

In the past, people used trees roots, leaves, straws and some plants like bamboo, wood and mixed them with soil. Furthermore, they used mixtures of mud or clay with wood and trees roots to construct houses. It was found that these mixtures provided more stability and durability to the constructed houses than a single mud/clay did. Consequently, the idea of using reinforcing elements to interact with the natural soil in order to enhance its performance was generated, leading to the initiation of the reinforced soil system that can be considered a composite material whose properties are better than the natural soil alone (as reinforced concrete idea). Unfortunately, the long-term behaviour of these admixtures was unstable as they were organic materials, which would decompose with time passing leading to further problems (Spangler, 1958; Larsen and Hendrickson, 1962; McAffee and Valsangkar, 2004).

During the last decades, these organic materials were replaced by the geosynthetic reinforcing elements. The integrated composite system which could be generated from the interaction between the natural soil and the geosynthetic reinforcing elements, e.g. reinforced soil, had enhanced performance compared with only soil, where its short-term and long-term

behaviour is stable. The use of such reinforced soils as a backfill cover above the buried structures would provide protection to them, even under the application of relatively increased loads.

2.2 Reinforced soil system components

Any reinforced soil system consists of at least two main components (may be increased according to the function of the system) to create composite material that can sustain different types of load. As long as the main concern in this research is to provide safety for buried structures, then one more element will be added to the reinforced soil system (Mitchell and Villet, 1987; Babu, 2006). Consequently, the system consists of:

1- Backfill soil.
2- Reinforcing elements.
3- Buried structure.

2.3 Backfill soil

Backfill soil is the fill material by which the buried structure is covered. According to its mechanical properties, it might be the excavated natural soil or a new imported soil. A fairly wide range of backfill materials have been used for reinforced soil applications. Suitable quality backfill material can frequently be found near the construction site. Typically, predominantly granular materials, such as clean sand, gravel and silty sand have been used for backfill soil. Clayey and silty soils have been used successfully in some applications. As experience of the performance is gained, these soil types may be selected for use as a good backfill material. Systems such as reinforced earth and retained earth specify certain minimum backfill soil properties, usually in terms of maximum allowable amount of fine solids, plasticity and a minimum effective friction angle (Berg et al., 2009). According to the British Standard Specifications, the backfill soil should be granular, well-graded, well-compacted and clean of organic materials (BS, 2010a). The following points show the effect of the soil:

1- The lower the soil friction angle, the higher the internal horizontal earth pressure to be resisted by reinforcements.

2- The lower the soil friction angle, the lower the apparent friction coefficient for frictional reinforcing systems and the bearing value for passive reinforcement systems.
3- The higher the plasticity of the backfill, the greater the possibility of creep deformations, especially when the backfill is wet.
4- The greater the percentage of fines in the backfill, the poorer the drainage and the more severe the potential problems from high water pressures.
5- The more fine grained and plastic the backfill, the more potential there is for corrosion of metallic reinforcement.

Thus, when high quality backfill is easily available, it should be used. Otherwise, soil properties should be enhanced by using reinforcing elements, forming reinforced soil system.

2.4 Reinforcing elements

Reinforcing elements are mainly defined as tensile elements that can sustain tensile forces and strains. The main function of these elements is to enhance the soil's performance through resisting the generated shear and tensile stress and strains in it, which by turn will generate a new composite material with enhanced mechanical properties compared with the original soil. When the soil is subjected to any type of loads, for example vertical load, then the soil's particles will be deformed according to the soil's characteristics as well as the type and amplitude of the load. Due to the occurring deformation, shear stresses are generated in the soil. To reach its equilibrium state, the soil's particles tend to realign in order to be able to resist the occurred shear stresses. Shear stresses generate both compressive and tensile strains. The soil has high ability to sustain the compressive strain and the load generated due to it. Unfortunately, the soil cannot resist the generated tensile strains. Consequently, the inclusion of the reinforcing elements becomes necessary, because they are considered tensile elements that can sustain tensile strains (Jewell, 1996). The following points can describe the function of the reinforcement:

1- Reduction of the shear force that has to be carried by soil (resist tensile strain component).

2- Enhancement of the normal stress acting on the shear surface by increasing the available shearing resistance in soil.

2.4.1 Different types of reinforcing materials

Reinforcement varies according to its material. There are metallic and non-metallic reinforcement. Metallic reinforcements are mainly made of steel that can be shaped to form any type of metallic reinforcement. Non-metallic reinforcements are mainly made of fibres and vary according to the formation process, stiffness and aperture shape (Elias et al., 1997; Babu, 2006; Koerner, 2009).

2.4.1.1 Metallic reinforcement

Steel reinforcements have been used for many years in its various forms. It can be shaped as sheets, grids, meshes, strips, bars and rods, as shown in Figure 2.1. The inclusion of all the previous forms of steel reinforcements provides the reinforced soil with tensile sustainability, which would lead to a reduction in its deformation (increase in its bearing capacity). Steel has been used inside soil in many forms, for example, pipelines and reinforcing layers. But using steel as a reinforcing material will require the proper knowledge of important parameters such as tensile strength, friction coefficient between the soil and the steel reinforcing elements, Young's modulus and stress-strain behaviour (strain compatibility) (Babu, 2006).

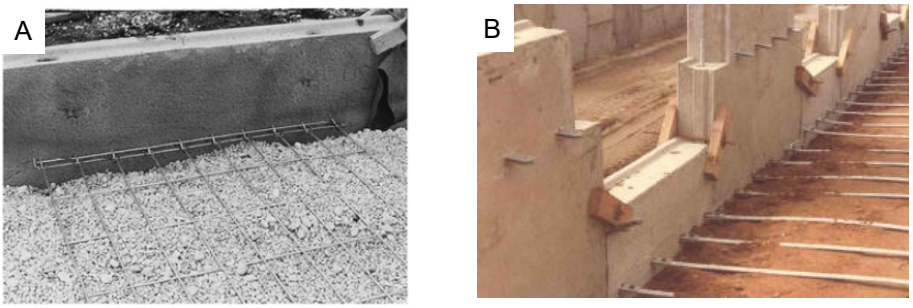

Figure 2.1 Different shapes of metallic reinforcement, (Babu, 2006)
A: Grid reinforcement. B: Strip reinforcement.

The main disadvantage of steel reinforcement is corrosion, which is mainly an electrochemical process. It happens when there is a potential difference between two points that are electrically connected in the existence of an

electrolyte. In the case of steel reinforced soil system, pore water containing oxygen and dissolved salts creates the conditions for the existence of corrosion. To overcome this problem, galvanized steel or black steel may be used as a reinforcing material. Using such types of steel as reinforcement will ensure safety for certain periods of time depending on the design surface life and the surrounding environment (Babu, 2006).

2.4.1.2 Non-metallic reinforcement (Geosynthetics)

Geosynthetics are mainly fabrics, which can be used in geotechnical engineering. Geosynthetics material can be either woven or non-woven fabrics. They are made from polymers (Jewell, 1996). Once geosynthetics were invented, people used them in construction processes, especially in reinforced soil systems because of its benefits, which can be defined as follows:

1- Quick construction.
2- High resistance to weather conditions.
3- Earthworks reduced volume.
4- Ability to use poor quality soil.
5- Ease of placement (installation).
6- Ability to mitigate soil defects.
7- Cost saving construction.

There are many types of non-metallic reinforcement and they vary according to the manufacturing process, stiffness, aperture shape and how they transfer stress from and to the soil, e.g. load transfer mechanisms, (Jewell, 1996). Figure 2.2 illustrates theses different types.

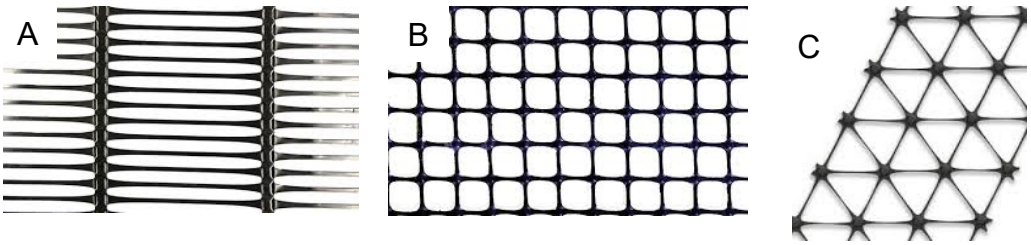

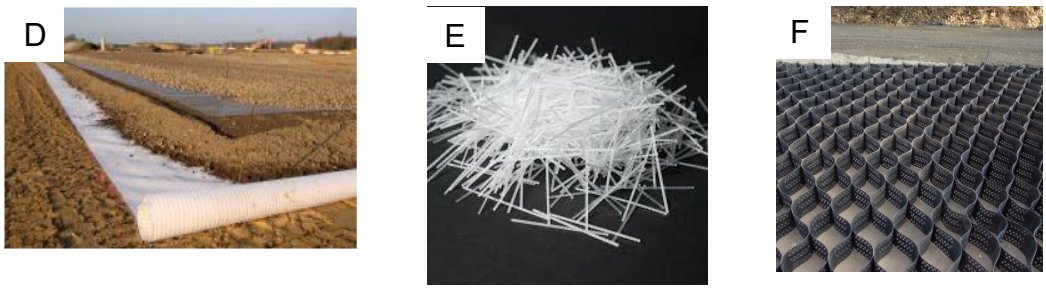

Figure 2.2 Different types of Geosynthetic reinforcements, (Jewell, 1996)
A: Uniaxial. B: Biaxial. C: Triaxial. D: Geotextiles. E: Fibres. F: Geocell.

2.4.2 Geogrid reinforcing layers

Geosynthetics can be defined as being a family of products for earthwork applications made generally from thermoplastic polymers. A geogrid is an oversized screen (usually with apertures of one inch or larger) which captures aggregate or soil particles and interlocks them as well as creates friction zones with soil particles to create a mechanically stabilized earthwork system. The geogrid serves to redistribute the load and thus protect the structure from failure due to the relatively large applied concentrated load.

Use of geosynthetic reinforcing layers has spread widely to many engineering purposes. There are many types of the reinforcing layers according to the tensile strength and geometry. Geogrid reinforcing layers may have uniaxial, biaxial and triaxial apertures, as illustrated in Figure 2.2. Uniaxial reinforcing layers can provide resistance, stiffness and strength in only one direction, where biaxial reinforcing layers can provide resistance in two perpendicular directions, i.e. principle directions, (Qian et al., 2012). On the other hand, due to the innovation in engineering applications, the need for uniform resistance in all directions has led to the invention of triaxial reinforcing layers (Qian et al., 2010; Dong et al., 2011; Qian et al., 2011; Qian et al., 2012).

Tensar International (2010), Dong et al. (2011) and Chen et al. (2012) showed that the stiffness of the biaxial geogrid is very high, if it was loaded in its principle directions, and is weak in other directions, in particular at 45^{o}, where its strength might reach zero, as illustrated in Figure 2.3. On the other hand, the triaxial geogrid almost has equal stiffness in all directions.

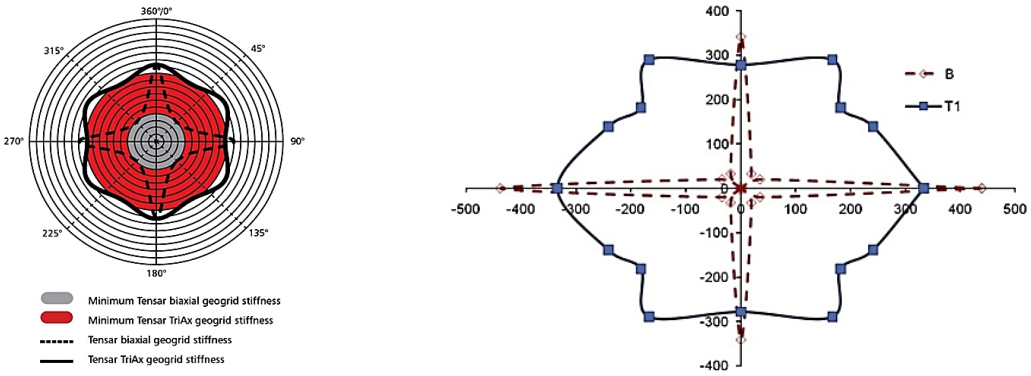

Figure 2.3 Radial stiffness of biaxial and triaxial geogrid reinforcement (kN/m), (Tensar International, 2010; Dong et al., 2011)

2.4.3 Soil-reinforcement interaction

Transfer of stresses between soil and reinforcements of high strength and tensile stiffness involves different mechanisms depending on the following parameters:

1- The characteristics of the soil as well as the reinforcing layers.
2- The state of deformation of the reinforced soil system itself.

Consequently, the soil-reinforcement interaction can be achieved, once the load transfer mechanism between both of them is well identified and understood.

2.4.4 Load transfer mechanisms

Soil is considered a good material to sustain compression loads. In case of the application of loading profile to the soil, then lateral and vertical deformations are generated in the soil, where its values would decrease due to the inclusion of the reinforcing layers because of the interaction between the reinforcing layers and the soil according to the state of the interaction mechanism. The inclusion of the reinforcing elements in the soil generates inward lateral stress (confining stresses). This lateral stress resists the shearing stress that was generated as a result of the application of the applied loading profile (Babu, 2006). The following mechanisms identify how the load could be transferred between the soil and the reinforcement (Villard et al., 2016):

1- Frictional load transfer (skin friction).
2- Passive earth resistance (bearing resistance).

3- Deflection or elongation of the reinforcement (membrane resistance).
4- Combination between mechanisms according to the properties and geometry of the reinforcing layers and the soil.

In addition to these mechanisms, arching and soil expansion mechanisms are generated inside the soil transferring stresses inside it, and the inclusion of the reinforcing layers inside the soil mass positively contribute to the performance of these two mechanisms.

The inclusion of the reinforcing elements in the soil generates a bond between them. The main two mechanisms that have the greatest influence on stress transfer and bond creation between both the soil and the reinforcement are the frictional and the passive earth resistance mechanisms (Jewell, 1996; Elias et al., 1997; Sieira et al., 2009; Wang et al., 2016). When the reinforced soil system is subjected to a loading profile, then the trapped soil particles in between the apertures of the reinforcing layers, in case of using grid reinforcement, tend to move laterally because of the generated shearing stresses inside the soil. Due to the existence of the reinforcing layers, this lateral movement of the trapped soil particles is significantly reduced and becomes dependent on the deformation of the transverse ribs of the reinforcing layers, due to the occurred interaction between the soil and the transverse ribs of the reinforcing layers, which could be defined as the passive earth resistance. Along the longitudinal ribs and the upper and lower surfaces of the reinforcing layer, the load can be transferred between the soil and the reinforcing layers due to the friction that occurs between them. Both of those mechanisms are generated due to the existing elongation that occurs in the reinforcing layers, in the case of using grid reinforcement or any reinforcing layer that contains both longitudinal and transverse elements as illustrated in Figure 2.4 (Sieira et al., 2009).

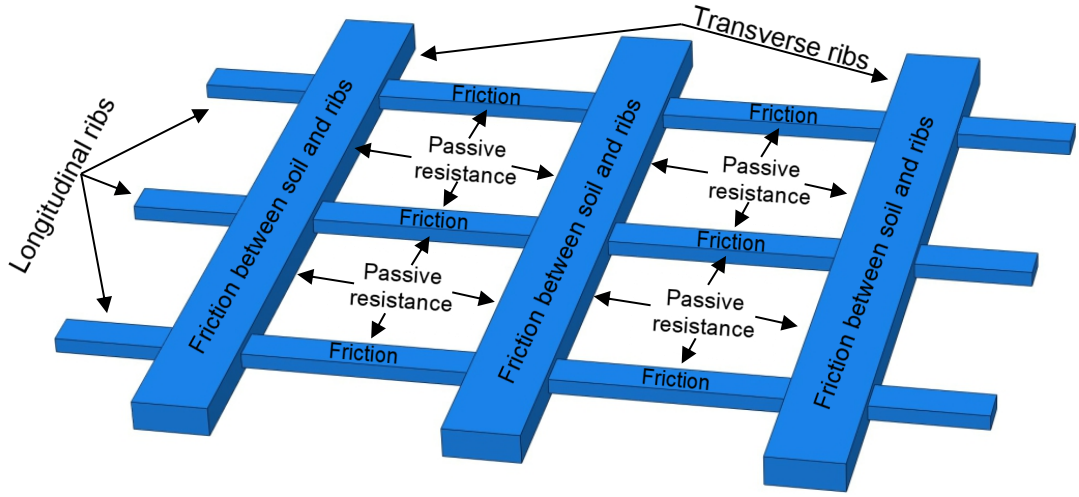

Figure 2.4 Longitudinal and transverse ribs of the reinforcing

In many systems, both mechanisms are active and the relative contribution of each is indeterminate according to the geometry of the reinforcing elements. Together they determine the bond strength that controls the maximum rate of change of axial force in the reinforcement along its length. They depend on the transferred stresses, reinforcing layer's material elongation, nature and properties of the reinforcement and the soil, geometry of the reinforcing layers and load-extension properties of both longitudinal and transverse elements (Palmeira, 2009).

On the other hand, the membrane mechanism contribution of the reinforcing layer depends mainly on the deformation that occurs in the layer. It requires significant layer deformation to contribute to the system stability (Jewell, 1996; Gourc and Villard, 2000; Briancon and Villard, 2008; Le Hello and Villard, 2009). This deformation helps in increasing the angle formed between the original and the deformed positions of the reinforcing layer, as illustrated in Figure 2.5. Consequently, the vertical component of the tensile force generated in the reinforcing layer is increased. This component opposes the applied force direction and reduces its value, leading to enhanced system stability.

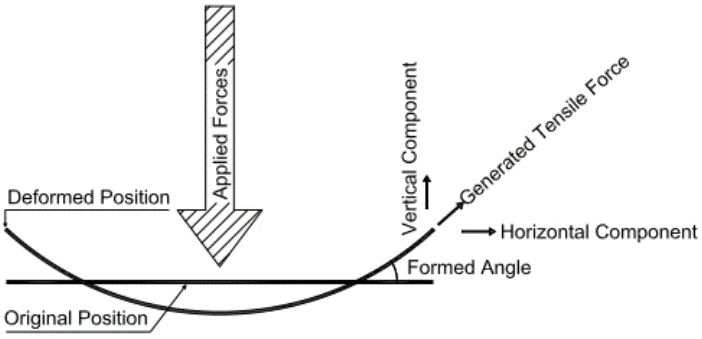

Figure 2.5 Reinforcing layer membrane mechanism

The contribution of the reinforcing layers in enhancing the reinforced soil system behaviour is governed by its tensile strength and its stiffness. The tensile strength of the reinforcing layer is an indication of the allowable sustained tensile forces, which will positively influence the passive earth resistance mechanism when it is increased. On the other hand, increasing the layer stiffness, i.e. elastic modulus, will lower its ability to deform, which will negatively influence the membrane mechanism contribution.

2.5 Buried structures

Any structure located underneath the ground surface can be defined as a buried structure, and according to its importance, a certain level of protection should be provided to it. There are different types of buried structures such as:

1- Shelters (airplane shelter – anti-explosion shelters).
2- Tunnels (usually located beneath roads).
3- Utility pipes (water, petroleum products and sewage transfer).
4- Control units.
5- Storages.

Among the illustrated buried structures, pipes are considered to be one of the most important and widely used structures, which would require a particular attention for long-term protection against increased loading from future development. In this research, the investigated buried structures were pipes.

2.5.1 Pipes classification

Pipe materials are divided for structural design purposes into three categories:

1- Rigid pipe.
2- Semi-rigid pipe.

3- Flexible pipe.

Generally, any pipe that can sustain at least a 2% vertical diametric deflection without generating structural instability is defined as a flexible pipe, otherwise it is a rigid one (Moser and Folkman, 2001). The behaviour of these materials depends upon both their response to external loading and their interaction with surrounding soils. Rigid pipe materials have a small deflection on loading, which is too small to develop any lateral earth pressures. The pipe takes load, and bending moments are developed in the pipe walls. Rigid pipes also attract an increased backfill load upon burial and obtain a reaction from their bedding in response. Semi-rigid pipe materials tend to exhibit a range of behaviour from rigid to flexible; however, the main concern in this research is about flexible and rigid pipes. Flexible pipes deform towards an oval/heart shape in response to loading and are able to develop significant lateral earth pressure from their surrounding embedment (BS, 2010b).

Pipes of different materials are classified according to the strength criterion required to be proven in testing or otherwise established in design. If the strength of pipes is established in a crushing test, they are classified as rigid. Table 2.1 illustrates the pipe's classification.

Table 2.1 Pipe classification, (BS, 2010b)

Pipe type	Classification	Pipe type	Classification
Clay	Rigid	Thick walled steel	Semi-rigid
Concrete	Rigid	Thermoplastics	Flexible
Reinforced concrete	Rigid	Glass reinforced plastics	Flexible
Ductile iron	Semi-rigid	Thin walled steel	Flexible

2.5.2 Differences in pipes response

Considerable researches on the behaviour of buried pipes under variable configurations of soil beds and various loading conditions have been carried out using experimental and numerical models. These studies investigated the improvement in the behaviour of the pipe, for both flexible and rigid. Table 2.2 illustrates the main differences between flexible and rigid pipes behaviour and properties.

Table 2.2 Differences between rigid and flexible pipes

Rigid pipe	Flexible pipe	Reference
Clay or concrete pipes	Thin steel or polymer pipes	BS 9295 (BS, 2010b)
Insignificant deflection and remarkable bending moment are sustained	Remarkable deflection is sustained	BS 9295 (BS, 2010b)
High circumferential and flexural rigidity (*EA* & *EI*)	Low circumferential and flexural rigidity (*EA* & *EI*)	(Lay and Brachman, 2014)
Main concern is about the generated tensile strains and the formed cracks	Main concern is about the increase in its deformation	BS 9295 (BS, 2010b)
Long-lasting mineral conduit	Short to long-lasting mineral conduit	(Lay and Brachman, 2014)
Under loads the pipe settle keeping its circular cross-section until receiving significant reaction forces and stresses from the bedding layer	Under loads the pipe significantly deform, where its crown deformation controls the deformed cross-section of it	(Abolmaali and Kararam, 2009)
Increased loads due to the passive arching mechanism is sustained as a result of its non-deformable nature	Reduced loads due to the active arching mechanism is sustained because of its deformable nature	(Young and Trott, 1984; Vaslestad et al., 1993; Peter et al., 2018)

2.5.3 Loads affecting buried pipes

Variable techniques are available for installing a pipe under the ground surface; however, the most common one is the trench installation technique. In this technique, the installation process of a pipe under the ground surface requires the removal of a natural soil layer, installing the pipe, and then backing the soil over the pipe once more. This process will cause disturbance to the natural soil, leading to a differential settlement between the backed soil and the adjacent soil portions. According to the type of the pipe and the differential settlement that occurred between the backed soil and the adjacent soils, the load transfer path will be determined, either directed towards the pipe or away from it (BS, 2010b).

In the case of rigid pipe installation, the stiffness of the rigid pipe is higher than the surrounding soil's stiffness. Consequently, the soil prism located above the pipe will settle less than the adjacent soil portions surrounding it, generating a

passive arching mechanism due to the generated shearing stresses between the different soil portions. Consequently, the generated forces in the soil prism above the pipe and part of the generated forces in the adjacent soil portions will be directed towards the pipe, which will apply more loads to the pipe, in addition to the geostatic pressure of the soil prism.

Unlike the rigid pipe, the flexible pipe can deform, consequently, the soil prism located above it will settle more than the adjacent soil portions generating active arching mechanism. Due to the active arching, part of the generated loads in the soil prism above the pipe will be directed to the adjacent soil portions, where the applied loads over the pipe will be the geostatic pressure of the soil prism in addition to the remaining part of the generated loads inside it. Figure 2.6 illustrates the transferred loads to the pipe and the generated stresses shortly after (BS, 2010b).

According to the stress distribution along the rigid pipe, as illustrated in Figure 2.6-C, it is obvious that significant value of stresses are generated between the invert of the pipe and the bedding layer as well as those generated along the crown of the pipe. Due to the stiffness variation between the pipe and the soil, stress concentration zone was generated between the invert of the pipe and the bedding layer. The rigid pipe can be considered a support to the whole system, where loads and stresses are transferred to the bedding layer underneath it through the invert. Consequently, the generated stresses along the invert are higher than those generated along the crown. On the other hand, in the flexible pipe, it is clear that reduced value of stresses are generated along the invert and the crown according to the deformable nature of the pipe.

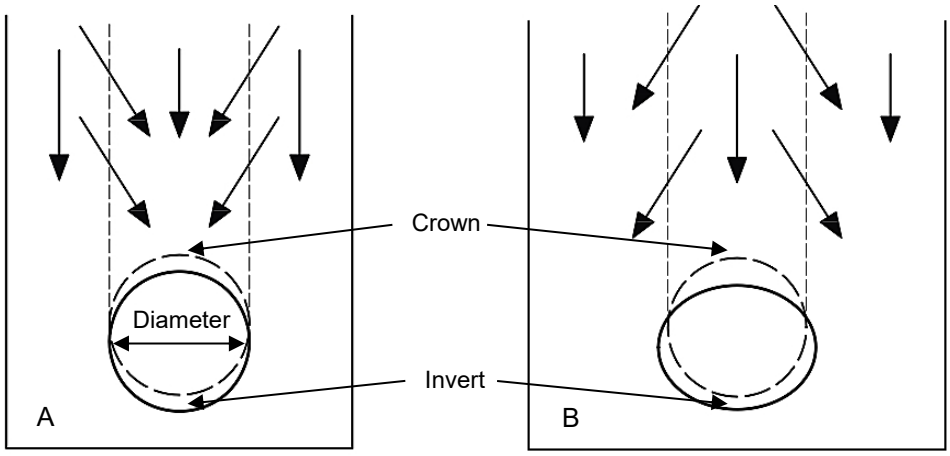

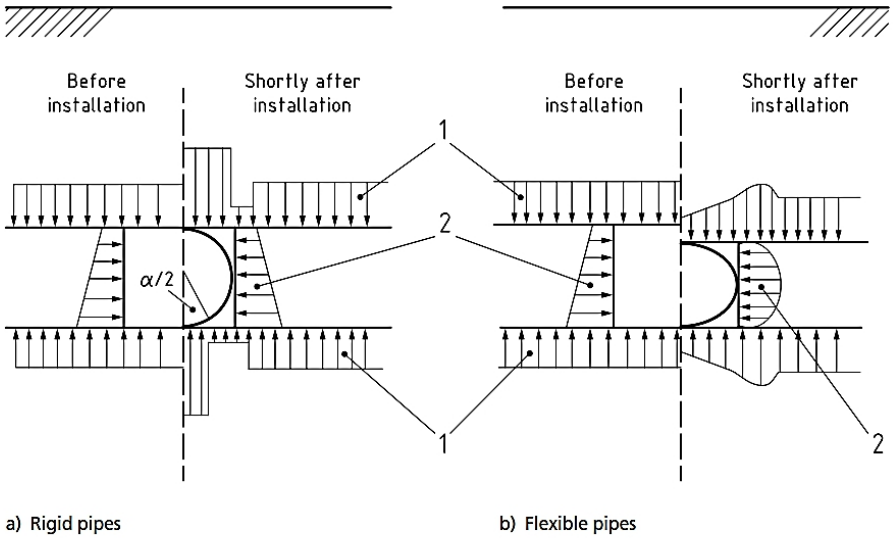

Figure 2.6 Load transferred and stresses generated in rigid and flexible pipes A: Rigid pipe. B: Flexible pipe. C: Generated stresses. (BS, 2010b)

2.5.4 Pipe installation techniques

Due to the generated active arching mechanism while using a flexible pipe, the value of the transferred loads and stresses to the pipe will be reduced. Consequently, the installation technique of a flexible pipe, where a trench is excavated and the pipe is installed inside it and then a backfill cover is backed above the pipe, provides a certain degree of safety for the pipe. On the other hand, because of the low deformable nature of the rigid pipes, the following installation techniques could be followed:

1- Trench installation method,
2- Embankment installation method,
3- Jacking installation method,
4- Induced trench method (*ITM*).

The selection of which technique is to be used depends on the location where the pipeline will be installed as well as the expertise level (Ahmed, 2016). Figure 2.7 illustrates the different installation techniques.

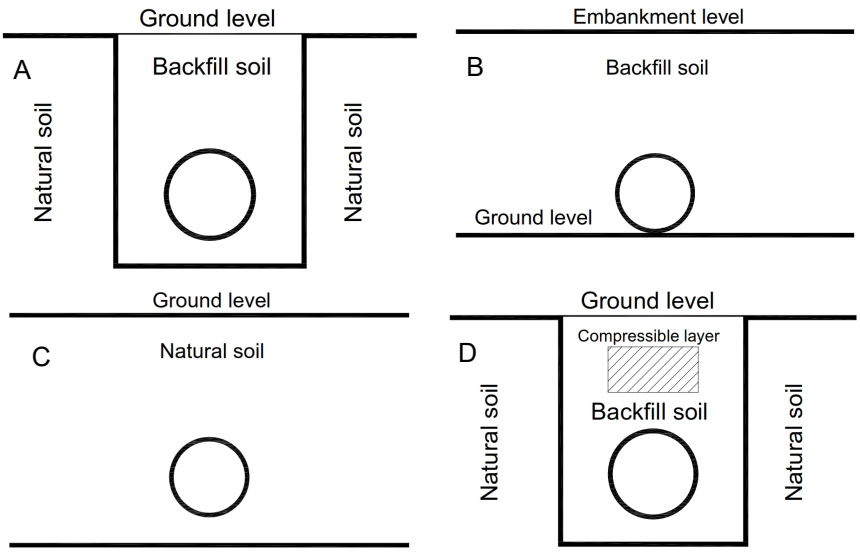

Figure 2.7 Different installation techniques
A: Trench. B: Embankment. C: Jacking. D: *ITM*.

2.5.4.1 Trench installation method

In the trench installation method, the pipeline installation method follows specific steps as follows:

1- Excavating the natural soil to form trench according to the required depth.
2- Installing the pipeline at its predesigned level.
3- Backing the backfill cover above the pipe, while applying compaction to it.

In the trench installation method, the main load affecting the pipe is the live load, where the self-weight of the soil can be relatively small and its influence on the pipe can be negligible.

2.5.4.2 Embankment installation method

In the embankment installation method, the pipe is initially located on the ground surface and an embankment of high depth is installed over it, where no trenches are excavated. The main concern in this installation method is the own-weight of the soil. The influence of the live load in this case is relatively small compared with the self-weight of the soil.

2.5.4.3 Jacking installation method

The jacking installation method relieves the pipe from the generated increased loads and stresses, where no disturbance of the backfill soil occurs as no trenches are excavated. This results in a significant reduction in the generated bending moment in the walls of the pipe as a result of the development of the lateral support, e.g. horizontal soil resistance, (BS, 2010b). The main concern in this method is the difficulty of the replacement process of any damaged portion of the pipe. Moreover, the pipe used in this installation method must be sufficiently strong to withstand the applied jacking forces during the installation process.

2.5.4.4 Induced trench method (ITM)

In all the previous installation methods, the pipe suffers an increase in the applied loads and stresses over it due to the generation of passive arching mechanism. To reduce the generated stresses and loads along the pipe walls, the Induced Trench Method (*ITM*) was used. Initial studies using *ITM* were conducted by Anderson (1913); Marston (1922) and Marston (1930). *ITM* was reintroduced by Spangler (1950) as Marston and Spangler (*M-S*) theory. The theory was about using compacted backfill over the buried pipe and the surrounding soils, then a trench of the same width of the pipe was excavated, where a thin compacted backfill layer remained above the pipe. The trench was then filled with loose lightweight material, which had a high compressibility, leading to the formation of active arching. The generated active arching contributed in transferring the applied stresses and loads to the adjacent soil portions to the pipe.

2.6 Previous studies on flexible pipes

In this section the behaviour of buried flexible pipes from previous research work will be reviewed according to the different parameters influencing the overall behaviour of the investigated systems.

2.6.1 Behaviour investigation methods

In order to understand the influence of a specific parameter on the behaviour of a buried pipe under reinforced and unreinforced soil, an experimental

investigation is highly recommended, as it provides real and accurate data. Various experimental investigations on the buried pipe behaviour was performed (Selvadurai, 1989; Mir Mohammad and Moghaddas 2001; Bueno et al., 2005; Arockiasamy et al., 2006; Rajkumar and Ilamparuthi, 2008; Tafreshi and Khalaj, 2008; Palmeira and Andrade, 2010; Srivastava et al., 2012; Mehrjardi et al., 2013; Bartlett and Lingwall, 2014; Corey et al., 2014; Hegde et al., 2014; Ahmed et al., 2015; Mehrjardi et al., 2016). However, its realistic response, investigating the effect of certain parameter on the buried pipe experimentally will consume too much time and effort. Therefore, the role of the numerical analysis to perform these investigations will rise. Various numerical research projects on the behaviour of buried pipes have been introduced (Perkins and Edens, 2003; Arockiasamy et al., 2006; Rajkumar and Ilamparuthi, 2008; Tafreshi and Khalaj, 2008; Hussein et al., 2009; Zhuang, 2009; Chen et al., 2011; Hussein and Meguid, 2013; Ahmed et al., 2015; Hussein and Meguid, 2016).

Field and finite element tests to investigate the behaviour of different buried pipe materials such as, *HDPE*, *PVC* and metal large diameter pipes under the application of live loads were performed by Arockiasamy et al. (2006). It was reported that the buried flexible pipe is well protected if it is buried under highly compacted graded silty sand. Increasing the burial depth of the pipe significantly reduces the pressure transferred to it.

The finite element method, was used to investigate the short-term and long-term behaviour of buried corrugated *HDPE* pipes by Kang et al. (2009), and the results were compared with those attained by analytical equations. It was reported that the *FEM* results, in particular deflection results, were smaller than the analytically calculated results, because of the suggested approximations that tend to simulate the reality, such cohesion value approximation. Kang et al. (2009) also demonstrated that pipe deflection depends mainly on the applied load variation, e.g. earth pressure and live load, whereas the pipe time-dependent properties have a limited contribution to its deflection.

Two laboratory tests and *FEM* investigation of road surface settlement as well as the Steel-Reinforced High-Density Polyethylene Pipe, *SRHDPE*, settlement was presented by Cao et al. (2016). In the two laboratory tests, the pipe was

buried in a compacted sand trench covered by aggregate in the first test and sand in the second test. The results illustrate that surface deformation is dependent substantially on the deformed soil above and below the pipe, as the pipe deformation was negligible compared with the road surface settlement, under the application of cyclic loading. Increasing the burial depth of the pipe significantly reduced the road surface settlement.

It should be considered that a three-dimensional simulation of the soil-pipe interaction is imperative because of the generated longitudinal strain in the pipe. In case of using two dimensional modelling (plane strain), the longitudinal direction of the pipe will be neglected and the generated strain in this direction will tend to be zero, which doesn't represent the actual case of the buried pipe. Moreover, in the case of modelling reinforced soil, e.g. geogrid-reinforced soil, the three-dimensional modelling will allow the simulation of the load transfer mechanisms, particularly the passive earth resistance, unlike the case in the two-dimensional modelling, which will ignore this mechanism and produce inaccurate outcomes. To avoid the boundary conditions effect (reaction interference), the simulated testing box dimensions must be at least six times the dimensions of the test specimen (Perkins and Edens, 2003; Arockiasamy et al., 2006; Hussein et al., 2015; Hussein and Meguid, 2016).

2.6.2 Effect of backfill density

High quality backfill material of relatively high density is greatly recommended in order to reduce the generated stresses and strains on the buried pipe. Soil's density variation under the application of cyclic and static loads was investigated (Mir Mohammad and Moghaddas 2001; Rajkumar and Ilamparuthi, 2008; Tafreshi and Khalaj, 2008; Srivastava et al., 2012).

It is considered that the soil's density is an important factors affecting the pipe-soil interaction. Increasing the soil's relative density around the pipe will significantly reduce its deformation, where improved degree of lateral support will be provided to the pipe allowing it to resist the occurred deformations in its walls due to the applied loads. In dense sand and under sufficient pipe burial depth, the failure mode occurred due to excessive settlement of the loading

plate, while the pipe remained safe. On the other hand, using loose sand will cause failure mode due to both surface settlement and pipe deformation.

Srivastava et al. (2012) contradicted the previous conclusions by claiming that, in case of burying the flexible pipe in loose and medium density sand, the ultimate bearing capacity of the system will be increased. Conversely, when the pipe is buried in very dense sand, the ultimate bearing capacity of the system will be reduced. The reason is that the stiffness of the pipe is relatively higher than the stiffness of the loose and the medium density sand; consequently, the existence of the pipe inside these soils will enhance its performance. Unlike the case of burying the pipe in dense sand, where the pipe's stiffness is relatively close to the soil's stiffness, consequently, the stiffness of the whole system will be reduced resulting in reduced ultimate bearing capacity of the system. Also, sudden failure will occur in both cases, because of the buckling failure of the buried pipe.

2.6.3 Effect of backfill material type

According to the British Standards, (BS, 2010a), the backfill used within the reinforced zone shall be selected to meet the properties required by the design and the project specifications. The selection of the backfill material depends on some factors, such as fill workability, function and environment of the structure and long-term behaviour, fill layer thickness and maximum particle size, drainage properties, fill-reinforcement interaction and fill-internal friction and cohesion. Unsuitable fills such as organic soils, soluble materials and strongly swelling materials, shall not be used.

The variation of the backfill material type will significantly affect the generated stresses on the buried pipe. Regular soils like, sand, clay and gravel are used as backfill materials to reduce stresses on a buried pipe. Because of its high compressibility and energy absorption, a backfill mixture of sand and rubber was investigated (Mehrjardi et al., 2012; Tafreshi et al., 2012). It can be considered that, using a rubber-sand mixture enhances the soil's surface settlement because it has higher energy absorption more than sandy soil. Therefore, it reduced the plastic deformation under repeated loading condition. Increasing the rubber percentage in the mixture will force the soil to behave like

a rubber-like behaviour because of the mixture's high compressibility, which will lead to more deformation in the soil's surface as well as the pipe's diameter under cyclic load (fatigue phenomenon). Using a rubber-sand mixture will reduce the pipe's diameter deformation, if it was used as a layer over the buried pipe when it is surrounded by well-compacted sandy soil. This could be attributed to the compaction of the sand, which provides lateral support to the pipe, reducing its diameter deformation due to vertical stresses.

2.6.4 Effect of compaction

The compaction process of the backfill soil surrounding the buried pipe has a great effect on enhancing the performance of the system. Soil compaction is investigated by Arockiasamy et al. (2006). It can be considered that when the pipe deforms in the heart shape, where the crown is flattened and the shoulders tend to be curved, then the pipe is buried in a well-compacted soil. For a higher soil compaction under cyclic load application, the measured deflection at the 50^{th} cycle may be considered the initial deflection (Arockiasamy et al., 2006). In case the measured pressures at the haunch and the invert of the pipe are approximately equal, then the pipe receives good support from the soil through the lower portion of the pipe. That means a good degree of compaction of the bedding soil.

Using easily compacted soil which has low sensitivity to moisture content reduces the magnitude of the developed strains in the buried pipe as a result of compaction forces (BS, 2010a).

2.6.5 Effect of the burial depth of the pipe

The burial depth of the pipe has a great role in its stability under increased stresses and strains. The burial depth of the pipe is investigated, (Mir Mohammad and Moghaddas 2001; Arockiasamy et al., 2006; Rajkumar and Ilamparuthi, 2008; Tafreshi and Khalaj, 2008; Hegde et al., 2014). Increasing the burial depth will reduce the pipe deformation, but will increase the soil surface settlement. The reason for this phenomenon is that the thickness of the soil layer above the pipe (compressible layer) will be increased leading to an increase in the air gaps in the soil, which will lead to an increase in the settlement due to load application (increased embedment depth - load

application - reduction in air gaps - compacted soil - more surface settlement). On the other hand, the stresses transferred to the pipe will be reduced with the increase of its burial depth; consequently, reduced deformation will influence the pipe. Arockiasamy et al. (2006) reported that using well-compacted soil cover will significantly reduce the soil surface settlement. This conclusion contradicts the previous assumption and then burying the pipe at large depths will not increase the soil surface settlement in case of performing compaction to the soil cover, before applying loads to the system.

A buried pipe in well-compacted soil will remain undamaged under load application, even if failure occurred to the above soil due to surface settlement. Increasing the burial depth of the pipe and using stiffer pipe material, distributes the applied pressure on its crown to the other regions of the pipe (spring line, haunch and invert) more effectively than burying a lower-stiff pipe material under shallow burial depth. This helps significantly in reducing the vertical pipe deformation. The measured pressure at the pipe's crown, invert and spring lines in the case of burial depth equal to *1D* and *2D* (*D* is the pipe's diameter) are considered very small relative to those measured at a burial depth of *0.5D* (Arockiasamy et al., 2006). Consequently, increasing the burial depth will significantly reduce the transferred stresses to the pipe's portions.

2.6.6 Effect of loading type

The behaviour of the buried pipe varies widely according to many parameters. One of these parameters is the nature of the applied load, either, monotonic or cyclic load. Many researchers investigated the behaviour of buried flexible pipe under different loading conditions (Perkins and Edens, 2003; Arockiasamy et al., 2006; Rajkumar and Ilamparuthi, 2008; Tafreshi and Khalaj, 2008; Hussein et al., 2009; Zhuang, 2009; Chen et al., 2011; Hussein and Meguid, 2013; Ahmed et al., 2015; Hussein and Meguid, 2016). However, a wide range of these research projects were investigated under static loading. Very few researchers have studied the system's behaviour under cyclic loading. Consequently, investigating behaviour of buried pipes under applied cyclic loading is required.

Full-scale field tests were conducted to investigate the behaviour of buried plastic pipes under the application of repeated loading, i.e. heavy vehicle

(Faragher et al., 2000). Two series of tests were performed for pipes buried in compacted sand and gravel. It was noted that an excessive vertical diametric strain occurred during the initial loading cycles, and with further load cycles, a significant reduction in diametric strain was noticeable. It was also noted that variation of the surrounding soil type has a little effect on the deformation rate accumulation of the pipe. According to these findings, an equation that can predict the behaviour of the pipe under loading cycles was proposed, but it was limited to applicable loads during the highway construction phase only. The proposed equation cannot predict the system behaviour due to applied external loads.

The behaviour of small-diameter pipe was investigated under the application of repeated loading, experimentally (Brachman et al., 2000; Mir Mohammad and Moghaddas 2001; Tafreshi and Khalaj, 2011). It was reported that the first loading pulse significantly affects the settlement of the soil surface and pipe deformation compared with those measured during subsequent cycles. In addition, the behaviour of the buried pipe depends mainly on the soil density, its burial depth and the amplitude of the applied load.

It can be considered that the application of cyclic loading is more common than static loading because the cyclic loading can be produced from several real cases, such as machine foundation, truck and train loading, which can be considered a base for the design of new road or railway. The stresses generated from the application of static load are considered to be of a higher value than the stresses resulting from cyclic loading. However, the main danger that faces the buried pipe due to cyclic loading is fatigue, in which the stresses are applied and removed over the pipe many times unlike the stresses generated from static loading.

2.6.7 Effect of geosynthetic reinforcement inclusion

Several researchers investigated the inclusion of geosynthetic reinforcing elements in the backfill soil to enhance its behaviour in order to reduce the generated stresses and strains affecting the buried pipe under static load (Selvadurai, 1989; Rajkumar and Ilamparuthi, 2008; Tafreshi and Khalaj, 2008;

Hussein et al., 2009; Hussein and Meguid, 2013; Corey et al., 2014; Ahmed et al., 2015; Hussein and Meguid, 2016).

Using geogrid reinforcement will enhance the pipe-soil system and will reduce the required burial depth to achieve a safe system, as well as reducing the generated stresses around the pipe, particularly, at the crown and the invert of the pipe. This became achievable because of the interlocked soil inside the geogrid apertures, which generated a passive earth resistance mechanism besides the frictional load transfer mechanism between the soil and the geogrid reinforcement.

The effect of the aperture size is more significant than the stiffness of the used geogrids forming the geocell. Dash (2011) investigated the effect of using two types of geocell, one of them has an aperture size five times larger than the other. It was found that wall of the geocell with the smaller aperture provided more confining pressure to the interlocked soil. In addition, reducing the aperture size will provide a greater reinforcement area, which will generate more bearing resistance between the geocell walls and the interlocked soil. Consequently, the bearing capacity of the reinforced soil will be increased.

Hegde et al. (2014); Hegde and Sitharam (2015) and Hegde et al. (2016) investigated experimentally the behaviour of small diameter *PVC* buried pipes in geocell and geogrid reinforced sandy and soft clay beds under the application of a static plate load test. It was reported that using a combination of geocell and geogrid reinforcing systems significantly reduced the transferred pressure and the generated strain in the pipe, where the measured pressure on the pipe's crown becomes almost negligible while using combination of geocell and geogrid reinforcement at a burial depth more than (*1.5B*), where; (*B*) is the footing width. In addition, the pipe location, its burial depth, significantly influenced the system behaviour.

Using geogrid and geotextile reinforcing layers to improve the soil's resistance to provide safety to buried pipe against sudden damage was investigated by Palmeira and Andrade (2010). It was concluded that, using enveloped reinforcement provided the best safety to the system by increasing the required applied sudden load, which can cause accidental damage to the pipeline regardless the type of the reinforcing layers.

Nevertheless, limited studies investigated the behaviour of buried flexible pipes beneath reinforced soil zones subjected to cyclic loading (Tafreshi and Khalaj, 2008), but using small-scale laboratory tests. It was reported that, the inclusion of the reinforcing layers in the soil has a significant effect on reducing the deformation of the pipe and soil surface because of the higher provided shearing resistance of the new formed composite material, i.e. reinforced-soil. Jones and Cooper (2005) investigated experimentally, the stability of road surface over voids, where multiple reinforcing layers were used under the application of cyclic loading. It was reported that generally, the magnitude of the generated tensile force in the lower reinforcing layer had the highest value ever, and the contribution of each reinforcing layer in resisting the generated tensile force depended on the void diameter and its burial depth. Laboratory model tests on strip footings resting on unreinforced and geogrid-reinforced sand with an inside void subjected to a combination of static and cyclic loading were investigated by Asakereh et al. (2012), where the void was represented by using a flexible can. It was reported that void dimensions controlled the system stability. When the void was located within the footing failure zone, the footing settlement was significantly increased. Increasing the distance between the void and the soil surface as well as increasing the reinforcing layers number had a great effect on enhancing the system stability and reducing the footing settlement. Studies on cyclic loads demonstrated that most of the deformation and settlement occurred during the initial stage of cyclic loading.

In general, the inclusion of geosynthetic reinforcing element will greatly enhance the behaviour of the reinforced soil system by reducing the soil's surface settlement, and the pipe's deformation through reducing the vertical plastic deformation and providing improved degree of the lateral support. This can be achieved while using sufficient length of the reinforcing layers (sufficient anchorage length) above the buried pipe which enables the formation of a strong bond between the soil and the reinforcing layers (interlocked soil and friction in the case of using geogrid and geocell reinforcement, and friction in the case of using geotextile reinforcement). Due to this strong bond and under the application of high load, significant deformation will be generated in the reinforcing layers, generating the membrane mechanism of the reinforcing

layers, which significantly contributes in reducing the generated stresses and strains in the reinforced soil mass as well as the buried pipe.

The generated strain in the pipe was reduced due to the inclusion of reinforcing layers because of the reduced shearing stresses generated due to load application. The reinforcement stiffness has great role in reducing the transferred stresses to the pipe's crown.

According to the illustrated previous researches, most of the investigations were performed under the application of static loading, where very few researches considered the application of cyclic loading. Most of the researches did not investigate the generated strain in the reinforcing layers and the pipe, and the transferred pressure to the crown of the pipe.

2.7 Previous studies on rigid pipes

The most common methods to investigate the behaviour of buried rigid pipe are the experimental and the numerical methods. Several researchers have used these two methods under different conditions.

2.7.1 Experimental investigation of buried rigid pipes

In order to investigate the behaviour of buried rigid pipes, field tests and full-scale tests were performed (Gilley and Gabriel, 1993; McGrath et al., 2000; Wong et al., 2006; Kim et al., 2009; Rakitin and Xu, 2013; Sheldon et al., 2013; Lay and Brachman, 2014; Peter et al., 2018). Buried pipe behaviour was originally investigated by Anderson (1913) and Spangler (1933), where the initial investigation was about the diametric change calculations due to applied static loads.

Field response of cast-in-place plane concrete pipe under the application of vertical loads was investigated by Gilley and Gabriel (1993). It was concluded that providing lateral support to the spring-line of the pipe could maintain its stability under vertical loads, and keep tensile stresses below the cracking threshold.

Full-scale field tests were conducted to investigate the pipe-soil interaction for different types of pipes including a concrete pipe during backfilling by McGrath et al. (2000). Variable trench conditions, backfill materials and compaction methods were investigated. It was reported that the variation in the installation

method significantly influenced the pipe performance, in addition using soft bedding layer significantly reduced the generated peak pressure along the invert of the pipe.

Four full-scale field tests were performed to monitor the short-term and long-term, duration of 20 months, generated stress envelope surrounding buried concrete pipes in different sites with different configurations, e.g. soil cover, trench geometry, pipe diameter and in-situ backfill soil type, under the application of heavy traffic loads by Wong et al. (2006). Measured stresses around the pipe were compared with those predicted from Ontario Provincial Standards and Standard Installation Direct Design (*SIDD*). It was reported that *SIDD* reasonably predicted stresses around the pipe, while the Ontario Provincial Standards method was found to provide an overly conservative prediction of soil stresses at the invert of the pipe.

Field tests of pipe culverts of different materials, including concrete, to investigate the joints behaviour under the application of static and dynamic loading were performed by Sheldon et al. (2013), where dynamic loading was represented by moving truck with different speeds. It was observed that the crown of the pipe experienced the maximum deflection, where the spring-line deflection was 50% less than the crown deflection. Shearing stresses across the joint caused a perpendicular separation, which was usually larger than the longitudinal one, which was caused by the joint relative rotation.

The generated bending moment in a reinforced concrete pipe with 1400 mm diameter, subjected to heavy traffic loading under the variation of the soil cover depth and the position of the load with respect to the pipe was investigated using centrifuge and full-scale tests by Rakitin and Xu (2013). It was reported that good agreement between the centrifuge and the full-scale test was achieved. The pipe experienced the most unfavourable condition when the loading axle was exactly above the crown of the pipe. Increasing the soil cover would lead to an increase in the initial stresses in the pipe as a result of the increased own-weight of the soil, however; it reduced the influence of the traffic load. It should be noted that the applied loading was a static loading, and further researches investigating the influence of cyclic loading are required.

Full-scale physical testing of reinforced concrete pipe buried under variable height compacted granular backfill subjected to single design truck axle load was investigated by Lay and Brachman (2014). The load was applied through four phases, where the first one was monotonic phase divided into sub-phases with 15 minutes between each of them to allow stability in the pipe pressure. The first phase was followed by three cyclic phases with significantly reduced amplitude and duration compared with the first phase. It was reported that maximum measured strain was noticed at the inner crown of the pipe at the shallowest burial depth, which can be attributed to the loose bedding layer. Increasing the pipe burial depth significantly decreased the generated strain along the pipe different portions. The applied cyclic loading had no effect on the generated strain in the pipe, which could be attributed to the small amplitude of the cyclic load as well as its low duration and number of cycles.

Full-scale, controlled laboratory testing of reinforced concrete buried pipe with simulated erosion voids using air bladders under the application of surface load was investigated by Peter et al. (2018). It was reported that the erosion existence negatively affected the pipe performance, where the generated bending moments and strains were increased. The most affected portion of the pipe was its spring-line, where the soil lateral support was decreased. Under increased applied load, soil failure dominated system failure, because of the weak soil-pipe interaction.

Large-scale test on concrete pipeline buried in loose granular soil subjected to seismic loading, which was represented by the application of permanent lateral ground displacement through controlled hydraulic movement of one half of the testing basin was investigated by Kim et al. (2009). Visual inspection of the tested pipeline illustrated considerable damage due to cracks generation, as bending moment and axial force excessively affected the pipeline.

According to the illustrated field and full-scale tests, it was observed that buried rigid pipes performance under surface loads and during installation was investigated, however the behaviour due to applying cyclic/repeated loading was not investigated. Moreover, the generated tensile strain along the crown, invert and spring-line of the pipe need to be clearly investigated to allow the prediction of the tensile failure of the pipe, i.e. cracks formation.

2.7.2 Numerical investigation of buried rigid pipes

Numerical models were performed to investigate the behaviour of buried rigid pipes and structures (Abolmaali and Kararam, 2009; Nagy et al., 2010; Abolmaali and Kararam, 2011; Kraus et al., 2013; Meguid and Kamel, 2014; Alzabeebee et al., 2016; Alzabeebee et al., 2017). The influence of the bedding layer thickness under the variation of the backfill height in an embankment installation method, where applied load is the soil own-weight, was investigated numerically by Abolmaali and Kararam (2009). It was concluded that pipe invert experienced the highest tensile stresses and strains in the pipe as it is considered the pipe's support. The findings of Lay and Brachman (2014) illustrated that maximum tensile strain was generated along the crown of the pipe as a result of the thick loose bedding layer beneath the invert. More tensile stresses were applied to the pipe with the increase in the backfill height and the decrease in the bedding layer thickness. Highly compacted bedding layer contributes in increasing the applied tensile stresses along the pipe invert as it can be considered a stiff layer that can apply reaction forces to the pipe, unlike loose bedding layer, which can mitigate transferred forces and pressure to it.

Dynamic compaction effect on buried concrete pipe was investigated numerically by Abolmaali and Kararam (2011). Applied loads were simulated using two phases, where the first one was monotonic loading representing the compacting plate weight and the second one was repeated loading representing the compaction process. The influence of four different pipe diameters, variable backfill cover, side-fill material density and applied compaction forces positions was investigated. It was found that using higher backfill cover and compacted side-fill material contributed in reducing the pipe deformation, as more lateral support is provided to the pipe. The effect of backfill height was minimized with the increase in the pipe diameter. The most critical position of applying compaction forces to the system is exactly above the pipe joint, which agreed with the findings of Rakitin and Xu (2013) regardless of the loading nature, and the least one is above the side-fill material.

Large-scale laboratory tests and finite element tests on buried concrete pipe to investigate its fatigue behaviour was investigated by Kraus et al. (2013). It was reported that due to the application of fatigue loading test, the measured vertical

displacement can be considered negligible, however visual observation of the pipe after the testing process illustrated that crack damage occurred near the jointed area on the crown of the pipe. This damage was a result of the method by which the pipe was installed inside the testing tank, where the pipe was in contact with the wall openings of the testing tank, which allowed significant interaction between them.

Moreover, three dimensional finite element models were used to investigate the influence of an erosion void on the behaviour of buried concrete pipe by Meguid and Kamel (2014). It was concluded that an increase in the earth pressure around the pipe occurred, compared with the case at which no erosion existed. Earth pressure increased for more than 100% and 30% when the void was located at the spring-line and the invert of the pipe, respectively.

Three dimensional finite element models were used to investigate the behaviour of buried rigid pipes under the existence of poor haunch support and the variation of the backfill height, where own-weight of the soil and surface traffic loading were applied by Alzabeebee et al. (2016). It was reported that increasing the backfill height non-linearly decreased the generated soil pressure along the crown of the pipe. Generated soil pressure along the invert significantly increased, up to 210%, because of the poor haunch support. Soil pressure distribution was changed, where the maximum soil pressure was generated along the invert instead of the crown of the pipe.

In order to estimate the soil pressure on a buried concrete pipe due to the variation of its diameter and the soil cover height above it under the application of traffic live load, three-dimensional finite element models were investigated by Alzabeebee et al. (2017). It was concluded that the maximum vertical displacement of the pipe non-linearly decrease while increasing the diameter of the pipe. In addition, the increase in the backfill cover contributed to redistributing the thrust forces around the pipe without increasing its maximum value.

According to the aforementioned numerical investigation, cyclic loading was applied over buried rigid pipes to represent the compaction efforts of the soil and its influence on the behaviour of the pipe. In addition, a fatigue-loading test was performed to investigate the pipe performance; however, the tested model

did not represent the field/real case because of the generated interaction between the pipe and the walls of the tank. Consequently, more investigation of the buried rigid pipe behaviour under the application of cyclic loading is highly recommended.

2.7.3 Load reduction over buried rigid pipes, *ITM*

To reduce the generated tensile stresses and strains along the pipe walls, the Induced Trench Method (*ITM*) was used, as illustrated in Figure 2.7-D. Initial studies using *ITM* were conducted by Anderson (1913); Marston (1922) and Marston (1930). Due to the lack of information concerning the lightweight material properties at that time, *ITM* long-term behaviour was debated. Long time ago, leaves, baled straw, sawdust and woodchips were mixed with soil and used as lightweight backfill over the pipe (Spangler, 1958; Larsen and Hendrickson, 1962; McAffee and Valsangkar, 2004). The problem of these materials was its decomposition with time passing. Vaslestad et al. (1993); McAffee and Valsangkar (2008); Kim et al. (2010); Turan et al. (2013); Witthoeft and Kim (2016); Meguid et al. (2017); Meguid and Youssef (2018) and Ni et al. (2018) investigated the performance of buried rigid conduits after adding a compressible layer above it, such as superlight expanded polystyrene blocks (*EPS*) and tire-derived aggregate (*TDA*).

Vaslestad et al. (1993) investigated the load reduction on deeply buried rigid pipes and boxes, using experimental full-scale tests, due to the applied overburden pressure. Superlight expanded polystyrene blocks were used as compressible materials to mitigate the transferred load and pressure to the pipe crown. It was reported that measured vertical pressure on the pipe crown was reduced to less than 30% due to the inclusion of the compressible blocks. Long-term monitoring over 3-years illustrated that the pressure value did not increase.

Kim et al. (2010) investigated the inclusion of expanded polystyrene blocks to reduce transferred pressure to buried rigid pipe, experimentally. Multi-blocks were used, where block width was equal to the pipe diameter. An agreement of the results between Kim et al. (2010) and Vaslestad et al. (1993) was observed, where the inclusion of the polystyrene blocks significantly reduced the transferred pressure to the pipe.

Witthoeft and Kim (2016) performed experimental and numerical models to investigate the performance of using *EPS* geofoam layers as compressible material to reduce earth pressure over buried rigid pipes. It was concluded that the system performance depended on the *EPS* layer properties, stiffness, strength and creep effects, where these properties were highly correlated with the density of the *EPS* material. Lower *EPS* density results in lower stiffness, which will enhance the system performance due to the increase in the *EPS* compressibility, i.e. pressure reduction on the rigid pipe.

Meguid and Youssef (2018) investigated the contribution of tire-derived aggregate (*TDA*) layer above buried rigid pipe, instead of the superlight expanded polystyrene blocks. It was reported that average measured pressure above the pipe was reduced by 30% compared with using granular backfill material above the pipe. *TDA* was an accepted replacement of superlight expanded polystyrene blocks in the *ITM*.

Ni et al. (2018) performed plane-strain numerical models to investigate the influence of using pure *TDA* as a compressible material above buried rigid pipe under high embankments. *TDA* layer width, thickness and spacing between it and the pipe were investigated. It was reported that using a *TDA* as a compressible material provided similar beneficial effects on rigid pipes as other commonly used materials did, where the invert and crown pressure were significantly reduced and a slight decrease in the lateral pressure was observed along the spring-line. The earth pressure surrounding the pipe was reduced with the increase in the *TDA* layer width unlike increasing its depth.

According to these researches, the behaviour of the buried pipes while inserting a compressible material, i.e. *ITM*, was performed under the application of soil own-weight, i.e. embankment installation, where the pipe was deeply buried under the surface of the soil. Since the main concern in the *ITM* was to maintain buried conduit stability through reducing transferred strains and stresses to it, the inclusion of geogrid reinforcing layers instead of the compressible material was adopted in this research, considering the researches where leaves, baled straw and woodchips were mixed with soil to generate lightweight backfill. A new composite material i.e. backfill cover, which can sustain higher load profiles

and provide more system stability was created due to the inclusion of the reinforcing layers in soil.

2.8 Summary

Pipes are considered one of the most important infrastructures because of their importance in transferring different minerals. They are mainly classified as; rigid, semi-rigid and flexible. The main concern in the rigid pipes is the generated tensile strain, which would generate cracks in case its value exceeded the tensile strength of the rigid pipe material. On the other hand, in the case of flexible pipe, the main concern is the increased deformation of its cross-section due to the applied loads to it.

Different methods are available to install a pipeline underneath the ground surface. Concerning the flexible pipe, there is no advantage to a mechanism over another, where active arching mechanism is generated reducing transferred pressure to the pipe, regardless the used installation mechanism. On the other hand, while using a rigid pipe, a passive arching mechanism is generated increasing the transferred pressure to the pipe threatening its safety. Consequently, the *ITM* installation technique is preferred while installing a rigid pipe, where the compressible material contributes in converting the generated passive arching mechanism into an active one reducing the transferred pressure to the pipe.

In the past, different admixtures were added to mud and clay to enhance their properties. Based on this idea, geosynthetic-reinforcing layers could be added to the backfill cover over the buried pipes to provide safety to them by reducing the transferred loads and pressures to these pipes. The inclusion of the geosynthetic reinforcing layers in the backfill cover above a buried pipe will generate a new composite material, i.e. reinforced soil, with improved properties compared with only soil, particularly the shearing strength. The reinforced soil system has the ability to mitigate and distribute the applied loads and transfer reduced pressure and load to the buried pipe. This could be achieved through the generated load transfer mechanisms between the soil and the reinforcing layer, frictional, passive earth resistance and the membrane mechanisms.

According to the previous studies, most of the investigations in the case of using buried flexible and rigid pipes were performed considering static loading, which does not represent the real case of loading, and very few researches considered experimental cyclic loading. Generated strain along the invert, crown and spring-line of the pipe need more investigations. Deformation and generated strains in the reinforcing layers need to be investigated.

Consequently, investigating the behaviour of buried flexible and rigid pipes under geogrid-reinforced and unreinforced sand beds due to the application of incrementally increasing cyclic loading will be performed in this research. The research will focus on the following points:

1- Deformation of the strip footing.
2- Deformation of the buried flexible/rigid pipe, particularly its crown and invert.
3- Transferred pressure to the crown of the pipe.
4- Generated load transfer mechanisms inside the pipe-reinforced-soil system.
5- Generated strains along the pipe, particularly its invert, crown and spring-line.
6- Generated deformations and strains in the geogrid-reinforcing layers, while using single and multi-geogrid-reinforcing layers.

It should be noted that the incrementally increasing cyclic loading would be applied until failure occurs in each investigated system, depending on the configuration of the system.

CHAPTER 3

MATERIAL TESTING AND TESTING RIG

3.1 Introduction

The behaviour of geogrid reinforced soil to enhance the soil cover located above flexible or rigid buried pipes, can be investigated by various methods. One of these methods is experimental testing, which provides a clear understanding of the true behaviour of the integrated elements, which forms the problem. In order to clearly investigate this behaviour, two main steps must be followed:

1- Material testing phase.
2- Testing rig identification.

This chapter describes in details the laboratory tests, by which the mechanical properties of the used materials are investigated. In addition, the testing rig to be used is clearly identified.

3.2 Material testing phase

Buried pipes in geosynthetic reinforced soil systems consist of three main elements:

1- Soil (backfill material).
2- Geosynthetic reinforcing layers (Geogrids).
3- Buried pipe (flexible and rigid).

The mechanical properties of each element must be clearly identified to understand its influence on the integrated system behaviour. In addition, the interaction between the soil and the geogrid reinforcing layers must be determined.

3.2.1 Soil

Relatively uniform silica sand is used in this research, as granular backfill material. To clearly identify the mechanical properties of this sand, the British Standard Specifications, are followed BS 1377-1:2016 (BS, 2016a).

3.2.1.1 Sieve analysis test

The particle size distribution of the used sand was obtained from a sieve analysis test, as shown in Figure 3.1. The particle sizes of the silica sand ranged between 0.3 and 1.0 mm, and its properties are illustrated in Table 3.1. According to the outcomes of the sieve analysis test, sand was classified as Even-Graded sand, as illustrated in Table 3.2.

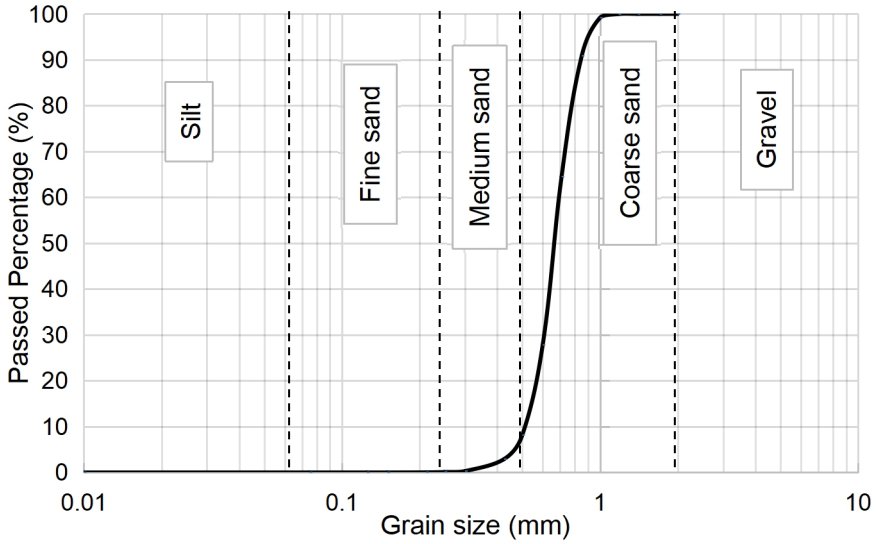

Figure 3.1 Particle size distribution curve

Table 3.1 Sand properties identifying its grade

Description	Value
Coefficient of uniformity, C_u	1.35
Coefficient of curvature, C_c	1.0
Effective grain size, D_{10} (mm)	0.52
D_{30} (mm)	0.61
Medium grain size, D_{50} (mm)	0.67
D_{60} (mm)	0.71

Table 3.2 Granular material classification guide

Shape of grading curve	C_u	C_c
Multi-graded	< 15	$1 < C_c < 3$
Medium-graded	$6 < C_u < 15$	< 1
Even-graded	< 6	< 1
Gap-graded	Usually high	Usually < 0.5

3.2.1.2 Compaction test (Proctor)

In order to identify the dry unit weight of the used silica sand, γ_d, as well as its optimum water content ratio, a compaction test was performed. It was concluded that the dry unit weight of the sand was 16.4 kN/m^3, and the optimum water content was 7.9%, as shown in Figure 3.2.

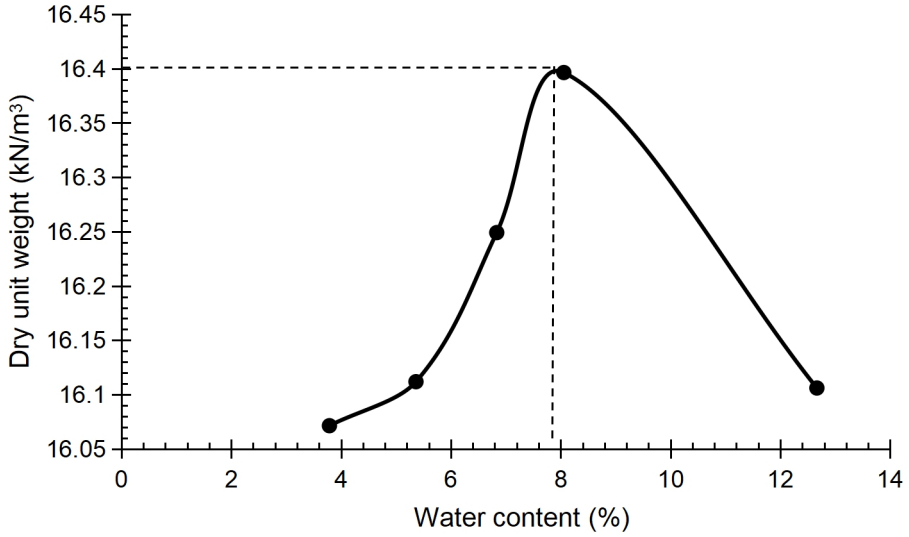

Figure 3.2 Compaction test outcomes

3.2.1.3 Shear strength properties

The most important properties of any granular material are its shear strength, represented by internal friction angle Φ, and the cohesion, c. A direct shear test was performed to investigate the sand cohesion and internal friction angle, as shown in Figure 3.3. Table 3.3 illustrates the shear strength values of the silica sand. It had dimensions of 60mm side length.

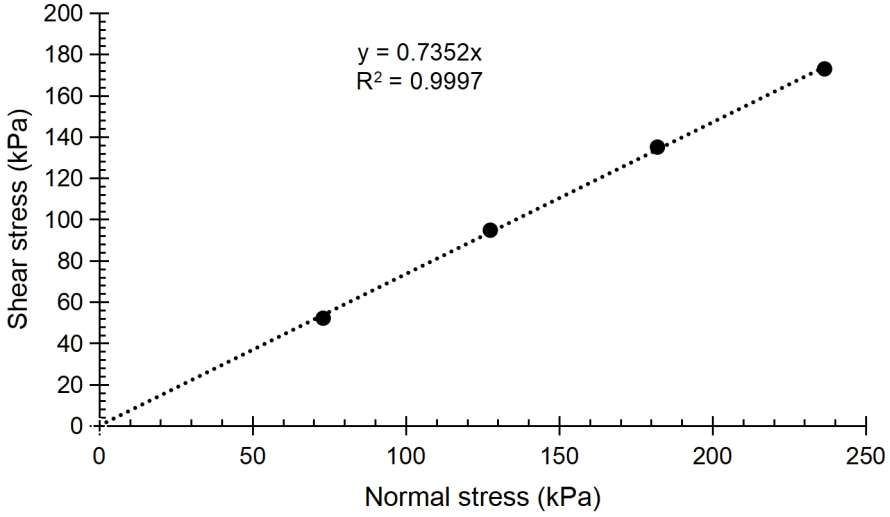

Figure 3.3 Direct shear test outcomes

Table 3.3 Shear strength properties of the silica sand

Description	Value
Friction angle (degree), Φ	36.5
Cohesion (kPa), c	0.0

3.2.1.4 Triaxial test

To identify the elastic modulus of the sand, *E*, a triaxial test on three samples was performed. In order to prepare sand sample, the sand was poured into a cylindrical membrane, 38 mm in diameter and 76 mm in length, where sand density in the three tests was kept constant through fixing the sand mass that will fill the volume of the membrane. In addition, the sand was poured on three layers where each of them was slightly compacted. For the three specimens the applied cell pressure was 50 kPa, 100 kPa and 150 kPa. Figure 3.4 illustrates the stress-strain relation of the silica sand. The initial slope of the curve in each case was determined and the elastic modulus was calculated. The average of the three resulting elastic moduli (54.3 MPa, 54.9 MPa and 56.2 MPa) was considered to be the sand elastic modulus, where its value was 55 MPa.

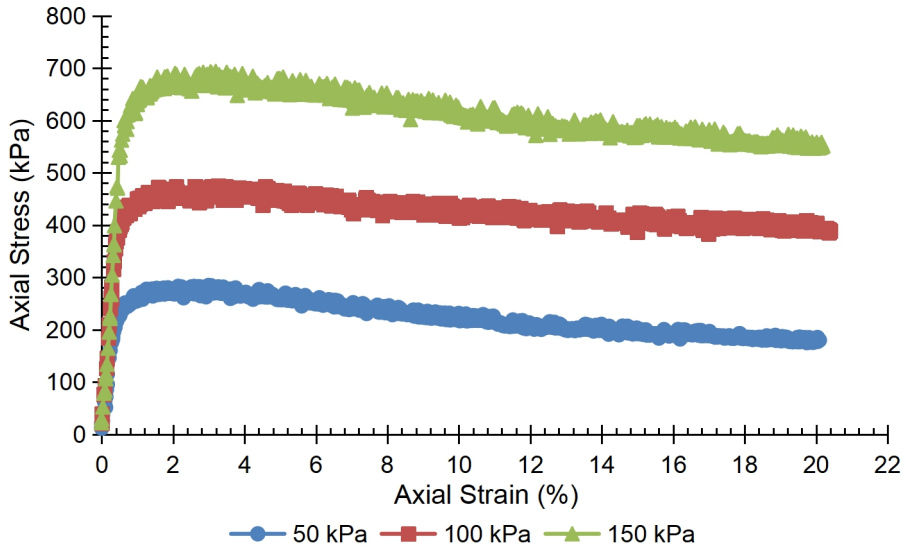

Figure 3.4 Stress-strain relation of the silica sand

3.2.1.5 Relative density

The relative density of the soil required the identification of the maximum and minimum unit weights of the soil (BS, 2016a). This could be achieved through using a funnel to fill a mold with the sand, where the sand was dropped from a height of 12.7 mm (half-inch). The mass and the volume of the sand were calculated and the minimum unit weight of the sand was calculated, $\gamma_{d(min)}$. To calculate the maximum unit weight, a weight was added to the sand surface inside the mold, where a shaker was used to remove the air gabs. The new

volume of the sand was calculated, where its mass remained constant. According to the new volume, the maximum unit weight of the sand was calculated, $\gamma_{d(max)}$. This test was performed three times, where the average values of the maximum and the minimum unit weights of the sand were considered. The relative density of the sand was calculated according to Eq (3.1), (Das, 2019).

$$D_r\ (\%) = (\gamma_{d(max)}\ (\gamma_d - \gamma_{d(min)})) / (\gamma_d\ (\gamma_{d(max)} - \gamma_{d(min)}))\ 100 \quad (3.1)$$

In addition, the maximum and minimum void ratios, e_{max}, e_{min}, of the sand were calculated according to Eqs (3.2) and (3.3), respectively.

$$e_{max} = (G_s\ \gamma_w / \gamma_{d(min)}) - 1 \quad (3.2)$$

$$e_{min} = (G_s\ \gamma_w / \gamma_{d(max)}) - 1 \quad (3.3)$$

Where; G_s represents the specific gravity of the sand and γ_w refers to the unit weight of the water.

The values of the maximum and minimum unit weights of the sand, its maximum and minimum void ratios and its specific gravity are presented in Table 3.4.

Table 3.4 Values of $\gamma_{d(max)}$, $\gamma_{d(min)}$, e_{max}, e_{min} *and* G_s of the sand

Description	Value
Maximum dry unit weight (KN/m^3)	17.1
Minimum dry density (KN/m^3)	15.3
Maximum void ratio, e_{max}	0.7
Minimum void ratio, e_{min}	0.5
Specific Gravity, G_s	2.6

3.2.2 Geosynthetic reinforcing layers

Geosynthetic reinforcing layers are mainly tensile elements that can sustain tensile forces and strains. Due to the applied external cyclic loading, tensile forces and strains are generated in the soil. Consequently, Tensar square biaxial geogrid reinforcing layers, *SS20*, are used in this research because of its availability, and it has the smallest aperture. In order to investigate the stress-strain relationship of the geogrid reinforcing layers, a tensile test must be performed as an initial step. According to the British Standard Specifications on

multi rib geogrid specimens (BS EN ISO 10319:2015 (BS, 2015), at least five specimens of the geogrid layers must be tested in each direction. The samples were tested by using the INSTRON machine as shown in Figure 3.5.

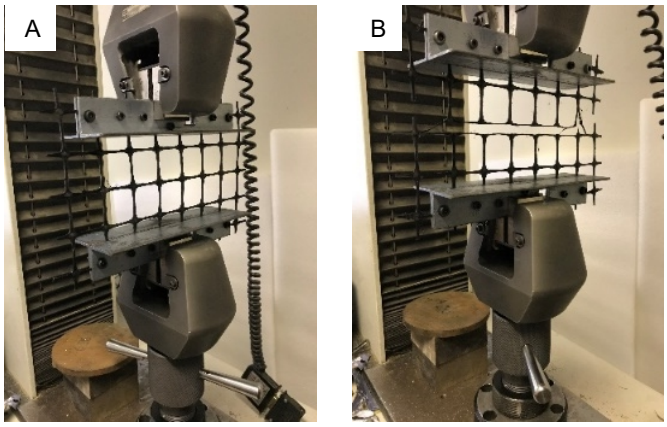

Figure 3.5 Tested reinforcing layers specimens
A: Before testing. B: After testing.

The results show a relationship between the tensile force, F_{max}, and the extension generated in the test specimen. According to the British Standard Specifications, these data should be converted into force per unit width (tensile strength, T_{max}, kN/m) and strain, as shown in Figure 3.6.

The tensile strength can be considered the main feature of the geogrid reinforcement, which is as important as the modulus of elasticity for other materials. The results show that there are two portions defining the relation between the tensile force and the strain, linear and nonlinear. The linear portion represents the elastic behaviour of the geogrid reinforcement and the nonlinear portion represents its plasticity. Consequently, the nonrecoverable deformation of the reinforcing layers due to the applied loads is clarified. In addition, using plasticity inputs to define the behaviour of the geogrid reinforcement in the finite element analysis is required.

3.2.2.1 Elastic modulus calculations

One of the most important mechanical properties of the used geogrid reinforcing layers is its elastic modulus, E, which can be calculated from the tensile test results. The plastic properties and the elastic modulus of the geogrid layers are essential parameters to correctly illustrate its behaviour, especially in the finite

element simulations. In field applications, the tensile strength of the geogrid layers is the most important property. It is clear that the resulting tensile force must be converted into tensile strength, which is the main feature of the geogrid reinforcing elements. According to the British Standard Specifications (BS, 2015), Eq (3.4) can be used to calculate the tensile strength of the reinforcing layer.

$$T_{max} = F_{max}\, C \qquad (3.4)$$

Where; T_{max} : maximum tensile strength.

F_{max} : maximum tensile force.

C : factor depends on the geometry of the reinforcing layer.

For geotextiles, knitted fabrics, geonets and geomats, C, can be calculated according to Eq (3.5):

$$C = 1 / B_n \qquad (3.5)$$

Where; B_n : nominal width of the specimen in meters.

For geogrids with one, two and three axes (uniaxial, biaxial and triaxial geogrids), C, can be calculated according to Eq (3.6).

$$C = N_m / n_s \qquad (3.6)$$

Where; N_m : average number of tensile elements within one meter width of the tested product.

n_s : number of tensile elements within the tested specimen.

In order to calculate the elastic modulus of the geogrid reinforcing layers, its secant stiffness, J, should be divided by its average thickness. Eq (3.7) illustrates the calculations of the secant stiffness (kN/m). Eq (3.8) illustrates the calculations of the elastic modulus (kN/m^2).

$$J = F\, C\, 100 / \varepsilon \qquad (3.7)$$

$$E = J / t \qquad (3.8)$$

Where; ε : is the strain value at the end of the linear phase of the resulting data.

t : the average thickness of the tested specimen.

According to the previous equations, the stress-strain relation of the geogrid reinforcing layers material can be identified, as shown in Figure 3.7. Based on the findings of the stress-strain curve of the geogrid reinforcing layer, the calculated value of the elastic modulus is 300 MPa.

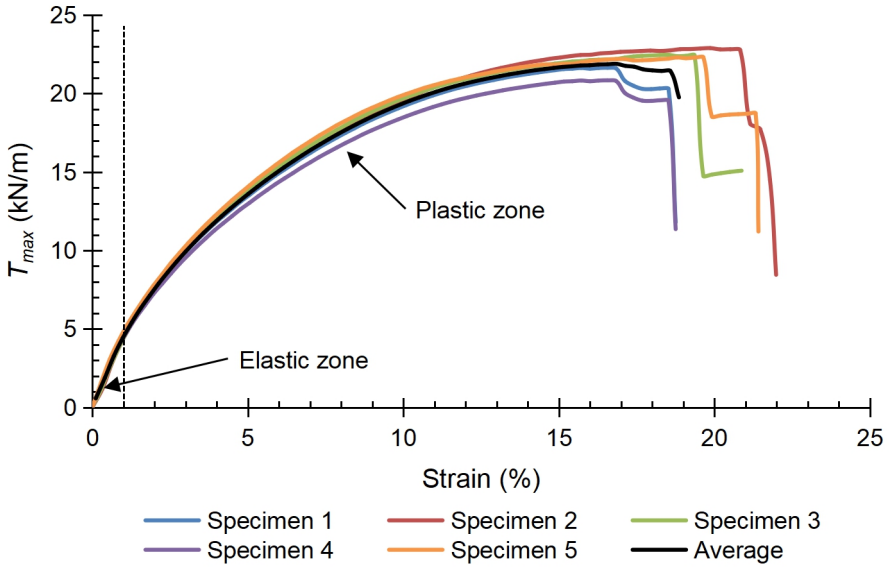

Figure 3.6 Tensile strength - strain relation of the reinforcing layers

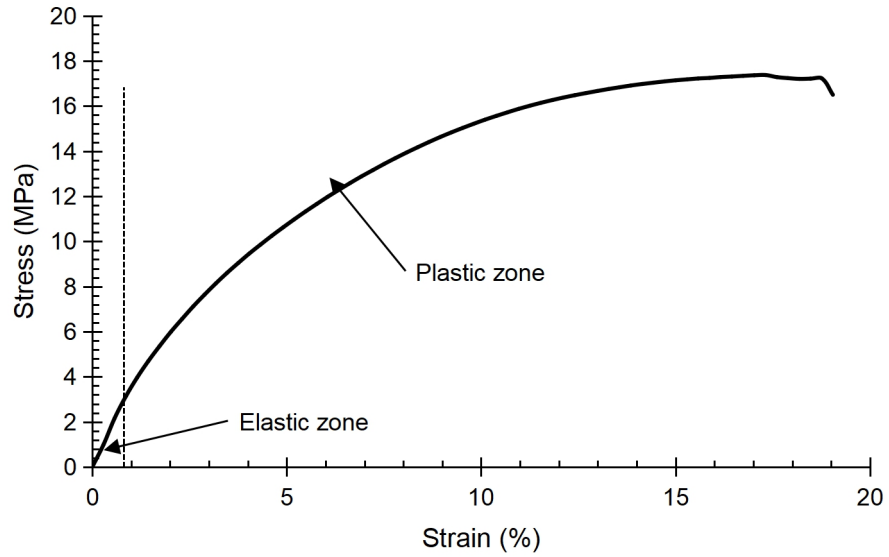

Figure 3.7 Stress-strain relation of the reinforcing layers

3.2.3 Pipe

There are two types of pipes studied in this research, flexible and rigid. The procedures for testing each type depends on its nature. Flexible pipes have the ability to deform under the applied loads; consequently, its elastic and plastic behaviours need to be identified. Concerning the rigid pipes, knowledge of its compressive strength is essential in order to identify its behaviour.

3.2.3.1 Flexible pipe (HDPE)

The British Standard identified the exact methods to test a flexible pipe in order to obtain its exact mechanical properties. Two main tests are illustrated:

1- Tensile test to identify its elastic modulus and its plastic properties, BS EN ISO 527-1:2012 (BS, 2012).
2- Ring stiffness determination test to identify its resistance to the applied loads, BS EN ISO 9969:2016 (BS, 2016b).

Tensile test

The tensile behaviour of the plastic flexible pipe is similar to any other plastic material, which is governed by its stress-strain relation. Consequently, the investigation of the pipe tensile behaviour is essential. The British Standard Specification, illustrated that three standard specimens of the plastic pipe, as illustrated in Figure 3.8, must be formed and tested under tensile test, where, the average results are to be considered.

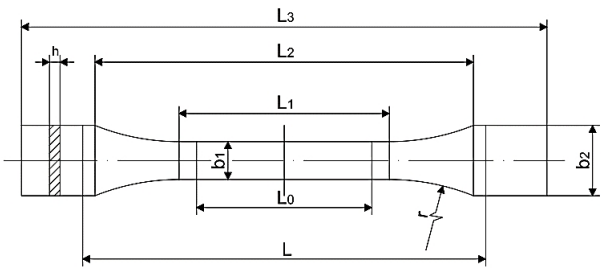

Dimensions details in (BS, 2012) Real specimen

Figure 3.8 Tensile testing specimen details

The INSTRON machine was used to perform the tensile tests, as shown in Figure 3.9.

Figure 3.9 Tensile testing of the plastic pipe specimen

The tensile testing results of the three specimens are presented in the form of the tensile force-extension relation. By dividing the tensile force by the initial cross section area, and the extension by the initial gauge length, the stress-strain relation of the pipe material can be determined, as shown in Figure 3.10. It is clear that the stress-strain relation has two portions, linear and nonlinear; consequently, it is essential to take into consideration the plastic behaviour of the pipe, especially in the finite element modelling. The elastic modulus of the pipe was investigated from the tensile test, where its value was 700 MPa.

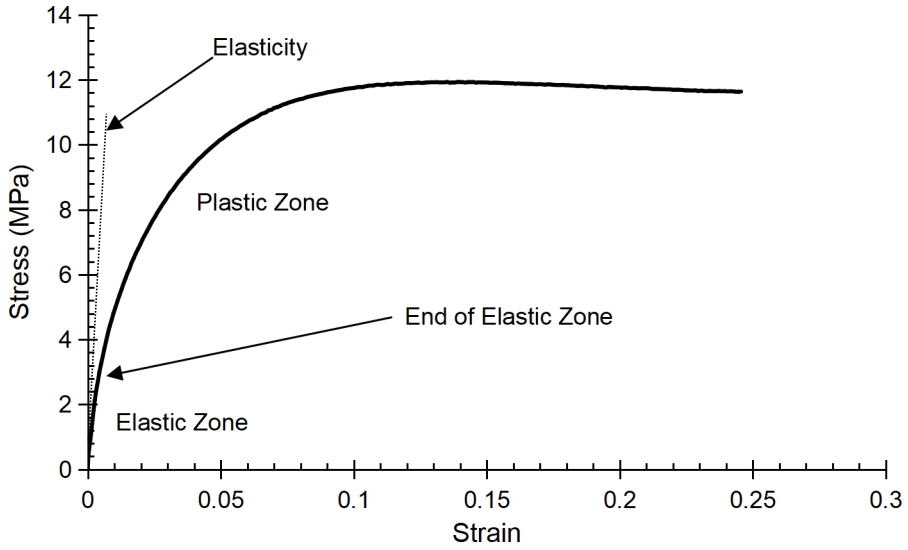

Figure 3.10 Stress-strain relation of the plastic pipe

Ring stiffness test

The ring stiffness can be determined according to the relation between the applied compressive force on the pipe and the generated deflection in the pipe

vertical diameter. The ring stiffness of the pipe is an important property, which depends on the ratio between the pipe diameter and its wall thickness, known as the standard dimensional ratio, *SDR,* and it shows the ability of the pipe to withstand applied loads. A lower *SDR* leads to a higher ring stiffness and vice versa (BS, 2009a). Three pipe specimens were tested according to the British Standard. The length of each sample was 300 mm with a diameter of 200 mm and a wall thickness of 5 mm. The main variation between the tested specimens was the orientation angle. The angle differed by 120 degrees starting from a zero angle with respect to the loading plates. Figure 3.11 illustrates the specimens before and after applying compressive load with constant rate of crosshead movement, using the INSTRON machine.

The required force to generate 3% vertical diametric strain of the pipe is used to calculate the ring stiffness of the pipe as illustrated in Eq (3.9). The ring stiffness was calculated three times, according to each test result, and an average value was calculated. Figure 3.12 illustrates the Load-Deflection curve of the tested specimens. Table 3.5 illustrates the calculated ring stiffness value of the three specimens and the average value.

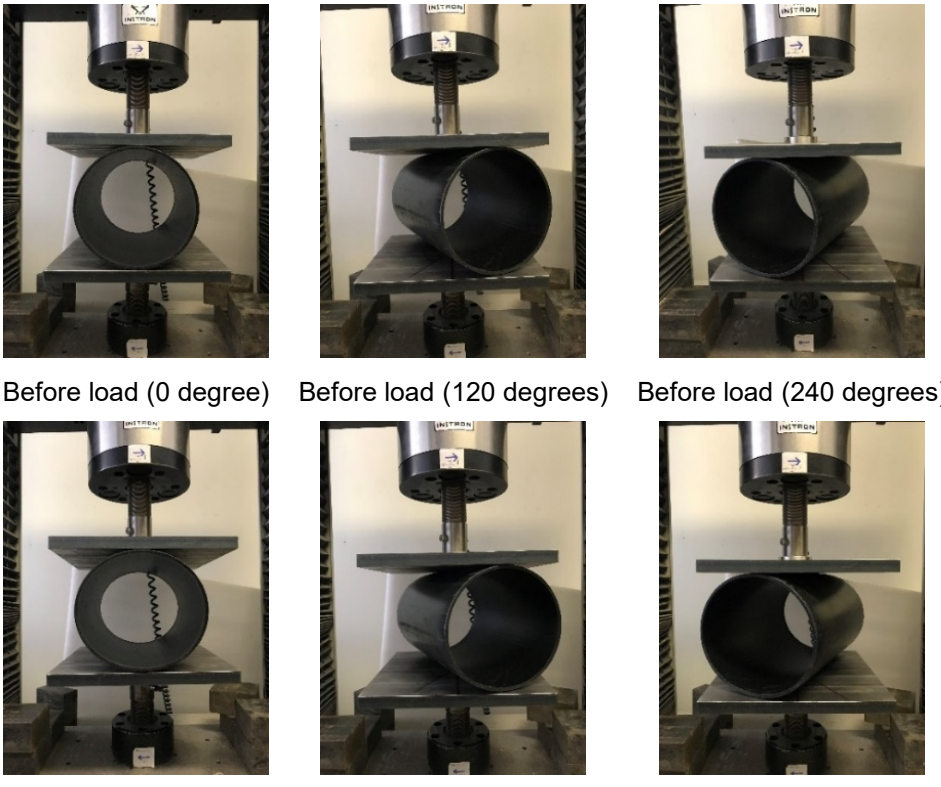

Before load (0 degree) Before load (120 degrees) Before load (240 degrees)

After load (0 degree) After load (120 degrees) After load (240 degrees)

Figure 3.11 Flexible pipes ring stiffness determination

According the British Standard, (BS, 2009a), a pipe with an *SDR* value of 41 and an elastic modulus of 3200 MPa, should have a ring stiffness of approximately 4 kPa. The pipe used in this research has an *SDR* value of 40, but the elastic modulus is 700 MPa, which is lower than the mentioned value in the specifications. That is why the ring stiffness of the used pipe is not in the defined range according to the British Standard.

$$S_r = \left(0.0186 + 0.025\frac{y}{D}\right)\frac{F}{L\,y}10e6 \qquad (3.9)$$

Where; S_r : the ring stiffness, in kPa.

F : the force corresponding to 3% strain in the pipe diameter, in kN.

y : the deflection corresponding to 3% strain in the pipe diameter, in mm.

L : the specimen length, in mm.

D : the pipe diameter, in mm.

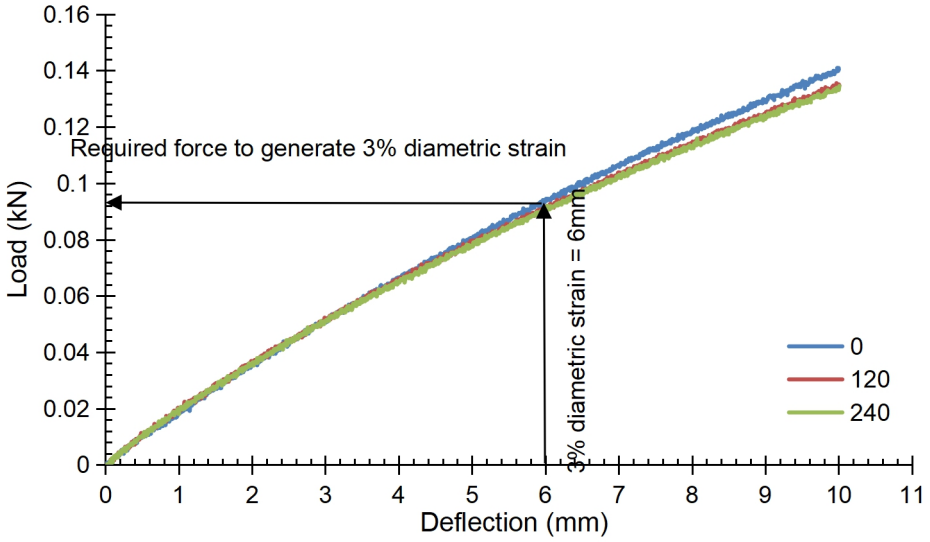

Figure 3.12 Load-Deflection curve of the tested specimens

Table 3.5 Calculated ring stiffness value

Orientation w.r.t loading plate, degrees	0	120	240	Average
Ring stiffness, kPa	1.011	0.976	0.963	0.983

3.2.3.2 Rigid pipe (concrete)

The available rigid pipes in the market have relatively high dimensions compared to the used testing tank, where the minimum available diameter is 350 mm, which is more than one-third the height of the testing tank. Consequently, casting concrete pipes to test them became an essential issue. A

casting frame was manufactured in the laboratory. It consisted of two stiff plastic pipes, outer and inner pipes, and a hardwood base to hold the casting frame. The inner pipe had a cut along its length to simplify the casting frame dismantling process. A wooden supporting system was manufactured to ensure the circularity of the inner pipe. The outer pipe consisted of two halves, where clamps were used to hold them together. After combining all of the system components, a hard-tape was used to cover the cuts in the inner and outer pipes to keep the mortar inside the casting frame, and a thin layer of lubricating oil was painted on the pipes walls to simplify demoulding the concrete pipe from the casting frame. Figure 3.13 illustrates the casting frame components. The wall thickness of the concrete pipe was 14 mm and its diameter was 230 mm; consequently, coarse aggregate with a maximum particle size of 10 mm was used. In addition, Superplasticizer, *SP*, was added to the mixture to increase its workability. A vibrating table was used to remove air voids from the concrete. The concrete mixture used to cast the concrete pipe is illustrated in Table 3.6.

Pipe casting frame

Outer pipe

Inner pipe

Hardwood base

Supporting system

Figure 3.13 Rigid pipe casting frame components

Table 3.6 Concrete mixture ingredients

Ingredients	Water/Cement ratio (*W/C*)	Cement Kg/m^3	Coarse Agg. Kg/m^3	Fine Agg. Kg/m^3	Water Kg/m^3	*SP* %
Value	0.42	500	850	820	210	0.5

Concrete compressive strength

The main property of the concrete is its compressive strength, f_{cu}, and to determine it, specimens were loaded to failure by using a compression testing machine, as specified in the British Standard, (BS, 2009b). The value of the maximum sustained load by the specimen was recorded, and according to the specimen geometry, the compressive strength of the concrete can be calculated. The compressive loading rate must be in the range of 0.6 ± 0.2 MPa/sec, and the load must be applied gradually to the specimen, where no loading shocks or pulses are allowed as initial loading. Cubes of 10 cm side length were used for the compressive strength test specimens. Each concrete mixture was tested by preparing six cubes, where three of them were tested after 28-days to determine the mixture compressive strength, and the other three were tested on the same testing day as the pipe. The average reading of each three cubes was considered. In this research, the defined mixture ingredients were used to cast ten pipes and the testing cubes. Table 3.7 illustrates the compressive strength of the concrete after 28-days and at the pipe-testing day.

Table 3.7 Average compressive strength of the concrete mixtures

Mix.	f_{cu} after 28-days, MPa			f_{cu} at the pipe testing day, MPa			Days till pipe testing
1	68.77	Avg. = 68.4	Standard deviation = 3.13 %	70.71	Avg. = 73.5	Standard deviation = 3.04 %	56
2	72.53			75.96			62
3	73.94			76.39			77
4	65.56			73.22			84
5	65.59			69.23			97
6	66.74			70.75			90
7	65.78			70.14			99
8	68.59			76.44			70
9	70.96			76.97			94
10	65.52			75.32			35

The compressive strength was designed to be constant for all the pipes, however; as the pipes were cast from different batches of concrete mixtures and the age of concrete specimens was different at the day of testing, the strength of concrete slightly varied as shown in Table 3.7, which was similar to

the findings of Zinkaah et al. (2019). There were unavoidable conditions that played a great role in varying the compressive strength of the concrete mixtures, for example:

1- Temperature of the laboratory.
2- Moisture content of the aggregates at the mixing time.
3- Any slight variation in the weights of the concrete mixture ingredients.
4- Elapsed time until pipe testing day.
5- Distribution of coarse aggregates, as concrete is a heterogeneous material.

3.2.4 Geogrid-soil friction angle

The inclusion of the geogrid reinforcing layers in the soil creates a new composite material defined as geogrid reinforced-soil, which has enhanced mechanical properties compared with those of the soil alone. The friction between the geogrid layers and the soil can be obtained experimentally, by using a large direct shear test, as illustrated in Figure 3.14. Hence, the value of the coefficient of friction, μ, can be obtained using the slope of the normal stress-shear stress relation. The friction angle between the soil and the geogrid layers, δ, is usually considered to be equal to approximately two-thirds of the soil internal friction angle, Φ, (Latha and Somwanshi, 2009; Mehdipour et al., 2013). The experimentally calculated friction angle between the soil and the geogrid-reinforcing layers was $\delta = 23°$, as illustrated in Figure 3.15. There is a slight variation between the experimentally determined geogrid-soil friction angle, $\delta = 23°$, and the approximate value, 2/3 the soil-soil friction angle = 24.3°. Following Coulomb failure criterion, the interface between the soil and the geogrid presented an apparent cohesion of 22.8 kPa, matching the findings of Liu et al. (2009) and Vieira et al. (2013).

Figure 3.14 Large shear test

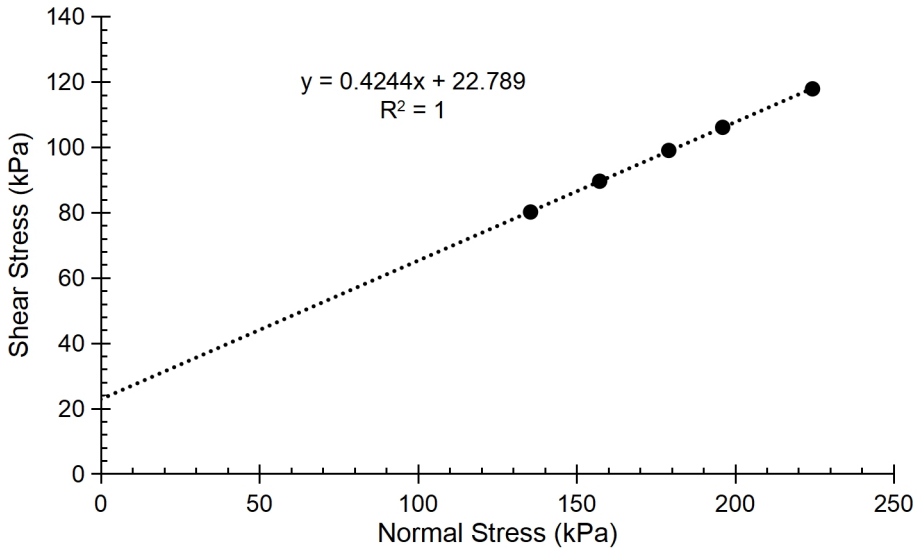

Figure 3.15 Large shear test outcomes

3.3 Testing rig design

Successful experimental testing requires testing components that really describe the true behaviour of the physical problem. In this research, the behaviour of flexible and rigid pipes, buried under unreinforced and geogrid-reinforced silica sand subjected to incrementally increasing cyclic loading through rigid strip footing, is investigated. Consequently, a full description of the following points is essential:

1- Testing tank.
2- Loading system.
3- Strip footing.
4- Measuring instruments.
5- Sand pouring technique.

3.3.1 Testing tank

According to the British Standard Specifications, (BS, 1997), the minimum trench width, i.e. testing tank length, must be at least the greater of either 1.5 times the outside diameter of the pipe plus 300 mm or the outside diameter of the pipe plus 400 mm. Consequently, it can be concluded that the minimum length of the testing tank should be 600 mm and 645 mm for the flexible and rigid pipes, respectively. On the other hand, to avoid the boundary condition effect, i.e. reaction interference, the testing box length must be at least six times the dimensions of the test specimen (Perkins and Edens, 2003; Arockiasamy et al., 2006; Hussein et al., 2015; Hussein and Meguid, 2016). Consequently, the length of the testing tank must be at least 1200 mm and 1380 mm for the flexible and rigid pipes, respectively. According to the previous recommendations, using a testing tank of 1500 mm in length will ensure achieving the real conditions of the physical problem in both the flexible and rigid pipes testing.

In this research, the investigation process of the buried pipes behaviour will take into consideration the burial depth of the pipe relative to the pipe diameter ratio, *H/D*, which varies from 1.5 to 3 for flexible pipes, and from 1.5 to 2.5 for rigid pipes. Consequently, a tank depth of 1000 mm would be enough to investigate the burial depth variation of the pipes.

Therefore, the testing tank was constructed using hardwood of 20 mm thickness. Figure 3.16 illustrates the testing tank details. The tank dimensions are 1500 x 1000 x 1000 mm. Rigid steel sections were used as stiffeners at four places in the tank to ensure its rigidity. The height of the tank was 1000 mm, but it was constructed as two halves, each one of them was 500 mm in height, where two steel stiffeners were used at each half. To ensure that there was no relative displacement between the two halves, 12 mm diameter bolts were used to fix them together, 10 bolts on each long side and 5 bolts on each short side.

To ensure the rigidity of the tank base, it was rested over four I-beams. These I-beams were distributed along the tank length, where two of them were located at the edges and the spacing between every two consecutive I-beams was 500 mm. Rectangular opening in one long side of the tank was made, and the material was replaced by transparent Perspex of 20 mm thickness. Its

dimensions were 430 mm in length, and 70 mm in width. Its function was to enable visual observation of the flexible pipes deformation and to inspect the occurred cracks in the rigid pipes. A small hole in the tank base, a circle of 20 mm diameter, was made to allow the installation of one Linear Variable Differential Transducer (*LVDT*) to measure the deformation of the pipe invert. A mechanism was developed to enable measurement of crown deformation at the mid length of the pipe using a rigid rod with a nail connected to its centre. The nail was put to touch the inner surface of the pipe, whereas the rod was hung over two *LVDTs* from the outside of the tank. The crown deformation was considered as the average value of the two *LVDTs'* measurements. Smooth Polyethylene sheet was used to cover the whole internal surface of the tank to minimize the generated wall friction as much as possible.

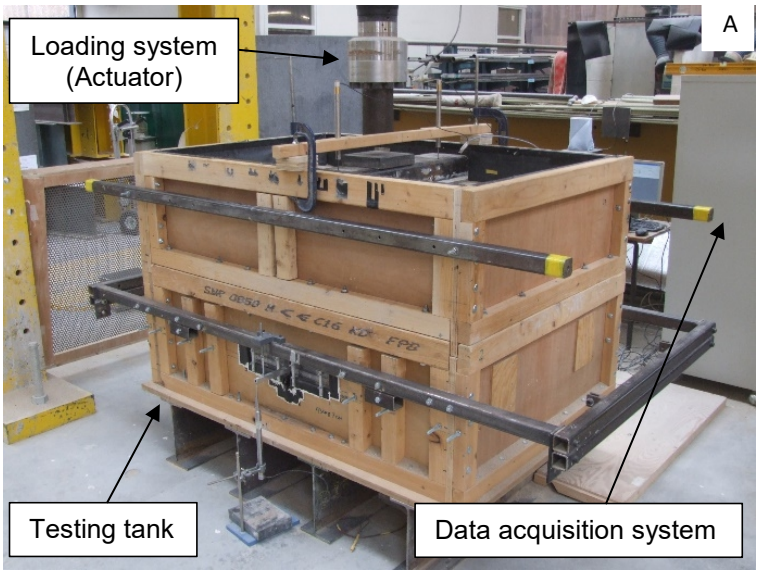

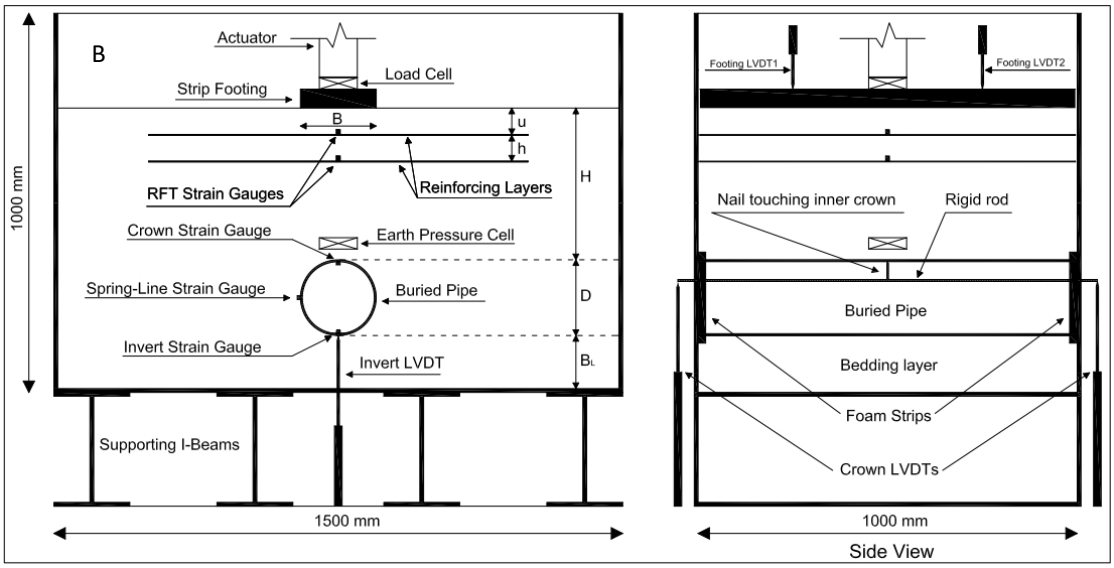

Figure 3.16 Experimental testing rig
A: Physical rig. B: Schematical diagram.

3.3.2 Loading system

The loading system consisted of a loading frame, which could stably hold an actuator, as illustrated in Figure 3.16. An advanced Servo Hydraulic Actuator system installed by ServoCon Ltd, was used to apply and control loads. In addition, to monitor the value of the applied load, an independent precise load cell was installed on top of the loading area. Computer software was used to control the actuator, where different loading regimes, including monotonic and cyclic loads, could be applied. It could apply monotonic and cyclic loads up to 1000 kN with different frequencies and numbers of cycles. In this study, all tests were carried out whilst applied cyclic loads were controlled and set at predetermined values.

3.3.3 Strip footing

Rigid rectangular steel strip footing was utilised in this investigation. The dimensions of the strip footing were 990 mm in length and 200 mm in width. The length of the footing was less than the width of the tank by 10 mm to avoid wall friction. In all experiments, the footing was located exactly in the centre of the tank and the load was applied precisely on its centre to eliminate any detrimental effect of load eccentricity. A heavy-duty sand paper, with approximately the same average particle size as the used silica sand, was glued to the footing base to represent full bond interaction between the footing and the underlying sand, which reflects the applied pressure by traffic loads, as illustrated in Figure 3.17. The footing settlement was measured using two *LVDTs* installed on its surface, where the average value was considered, as shown in Figure 3.16.

Figure 3.17 Strip footing

3.3.4 Measuring instruments

To be able to investigate the behaviour of the physical model, all of the transferred loads, generated deformations, strains and stresses in the different model components must be accurately measured. Two different data acquisition systems were used in this research to enable the measuring process of the applied and the generated loads, pressures, deformations and strains. A load cell, pressure cell and five *LVDTs* were connected to the 1st system. The system could measure up to 20 channels simultaneously, with a minimum time interval of 500 ms. On the other hand, all of the used strain gauges in the physical model were connected to the 2nd system, which could measure up to 16 channels simultaneously, with a minimum time interval of 500 ms.

3.3.4.1 Load and pressure measurement

The applied load to the system is directly transferred to the centre of the strip footing, which converted the load to applied pressure and transferred it to the system beneath it. This pressure would be mitigated inside the soil until it reached the pipe. A load cell was installed between the actuator and the strip footing to measure the applied load to the system, and an earth pressure cell was installed 3 cm above the pipe crown to measure the transferred pressure to it, as illustrated in Figure 3.18.

The load and the earth pressure cells were connected to data acquisition system, which generated results in volts. Consequently, the calibration process for both of them was needed to enable the conversion of the generated volts into engineering outcomes.

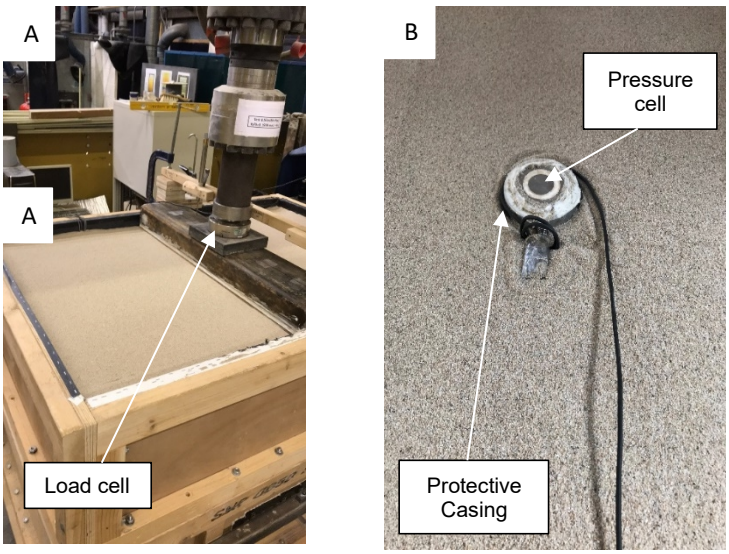

Figure 3.18 Load and pressure measuring instruments
A: Load cell. B: Earth pressure cell.

Load cell calibration

To be able to calibrate the load cell, the INSTRON machine was used to apply different values of known compressive loads, and the load cell was connected to the data logger system, as illustrated in Figure 3.19. The data logger system was adjusted to measure voltage in mV units due to the variation of the applied load on the load cell.

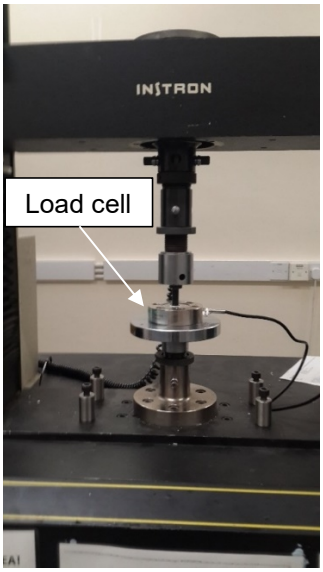

Figure 3.19 Load cell calibration process

Figure 3.20 illustrates the calibration curve of the load cell. It is clear that the curve represents a linear relationship between the applied load and the generated voltage.

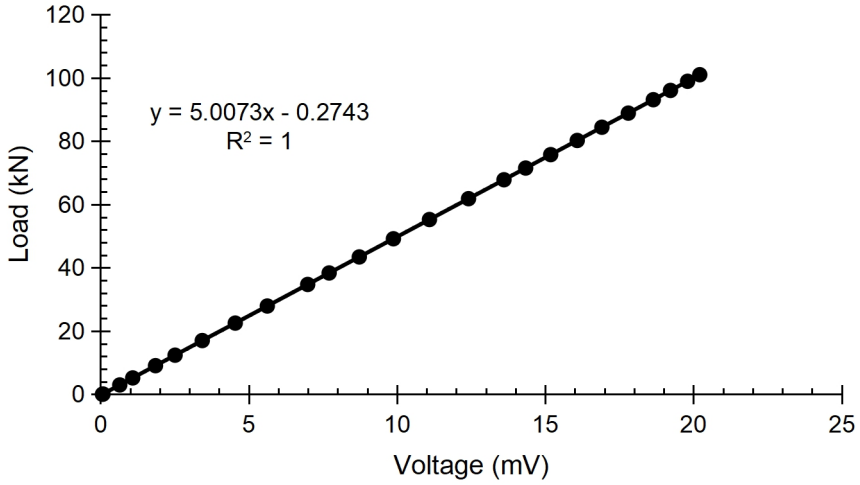

Figure 3.20 Load cell calibration curve

Earth pressure cell calibration

To be able to calibrate the earth pressure cell used in the research, GDS pressure device was used to apply water pressure to the pressure cell, as illustrated in Figure 3.21. A new device to calibrate the earth pressure cell was manufactured in the laboratory to enable the process of applying water pressure to the pressure cell, (Mirzababaei, 2012). The earth pressure cell was connected to the data logger system, where it was adjusted to measure voltage in mV units due to the variation of the applied water pressure on the pressure cell. The applied pressure to the cell needed to be only water pressure, and any additional air pressure had to be removed by using the air removal valve.

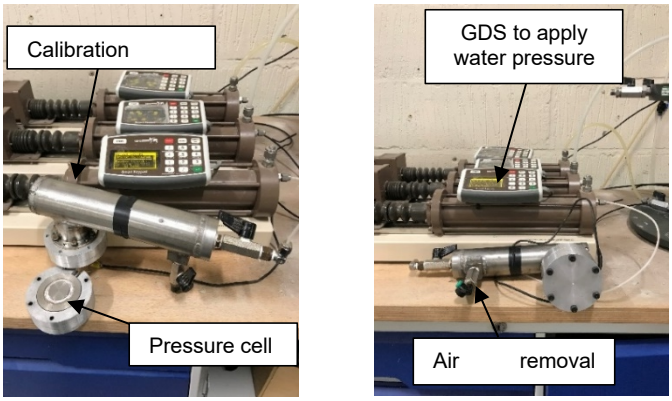

Figure 3.21 Earth pressure cell calibration process

Figure 3.22 illustrates the calibration curve for the earth pressure cell. It is clear that the curve represents a linear relationship between the applied pressure and the generated voltage.

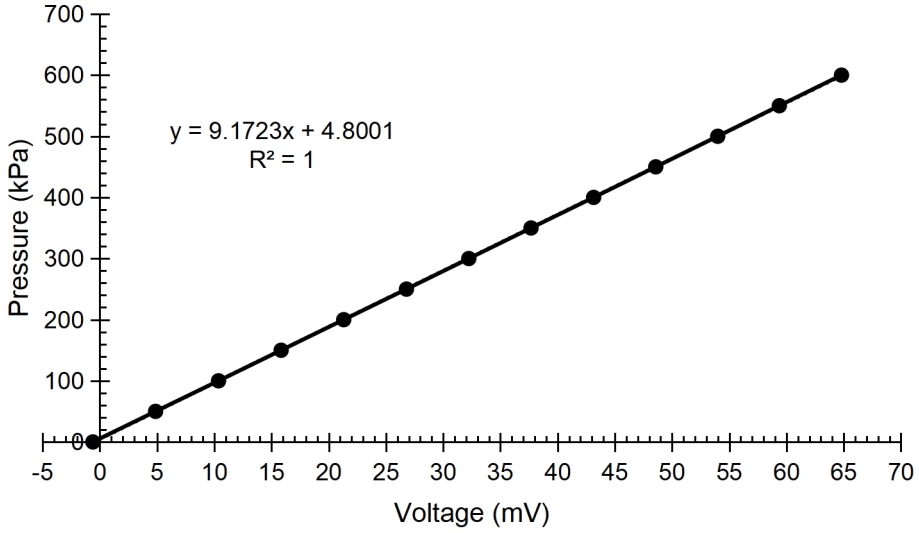

Figure 3.22 Earth pressure cell calibration curve

3.3.4.2 Displacement measurement

Investigating the behaviour of the buried pipe requires the determination of the deformation that occurred in both the pipe and the strip footing. This process requires the usage of Linear Variable Differential Transducers *(LVDTs)*. A total number of five *LVDTs* were used in this research. Two *LVDTs* were installed above the strip footing to measure its settlement, two *LVDTs* were used to measure the deformation of the pipe crown, and the last one was used to measure the pipe invert deformation, as illustrated in Figure 3.23.

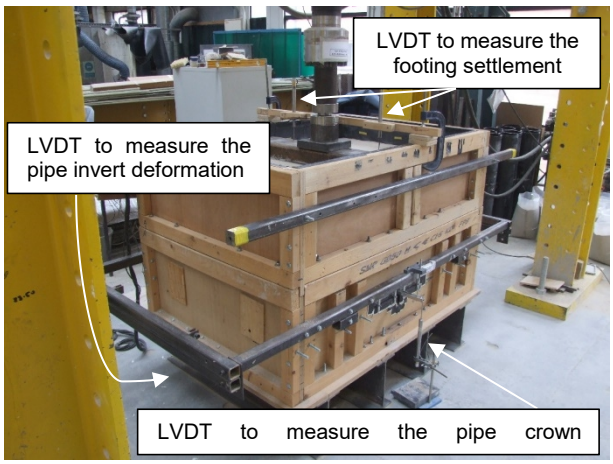

Figure 3.23 Distribution of the installed LVDTs

The calibration process of the *LVDTs* required the usage of a stand, and steel plates with known standard lengths. The stand had to keep the *LVDT* in a vertical position, and the steel plates were used to lift it, as shown in Figure 3.24.

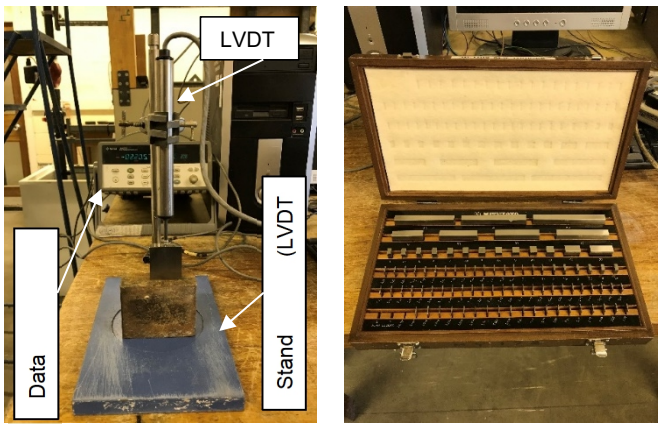

LVDTs holder Standard plates

Figure 3.24 Calibration process of the LVDTs

The LVDTs were connected to the data logger system, where it was adjusted to measure voltage in V units due to the variation of the LVDT movement. Figure 3.25 illustrates the calibration curves of the five LVDTs. It is clear that there is a linear relationship between the change in distance and the generated voltage.

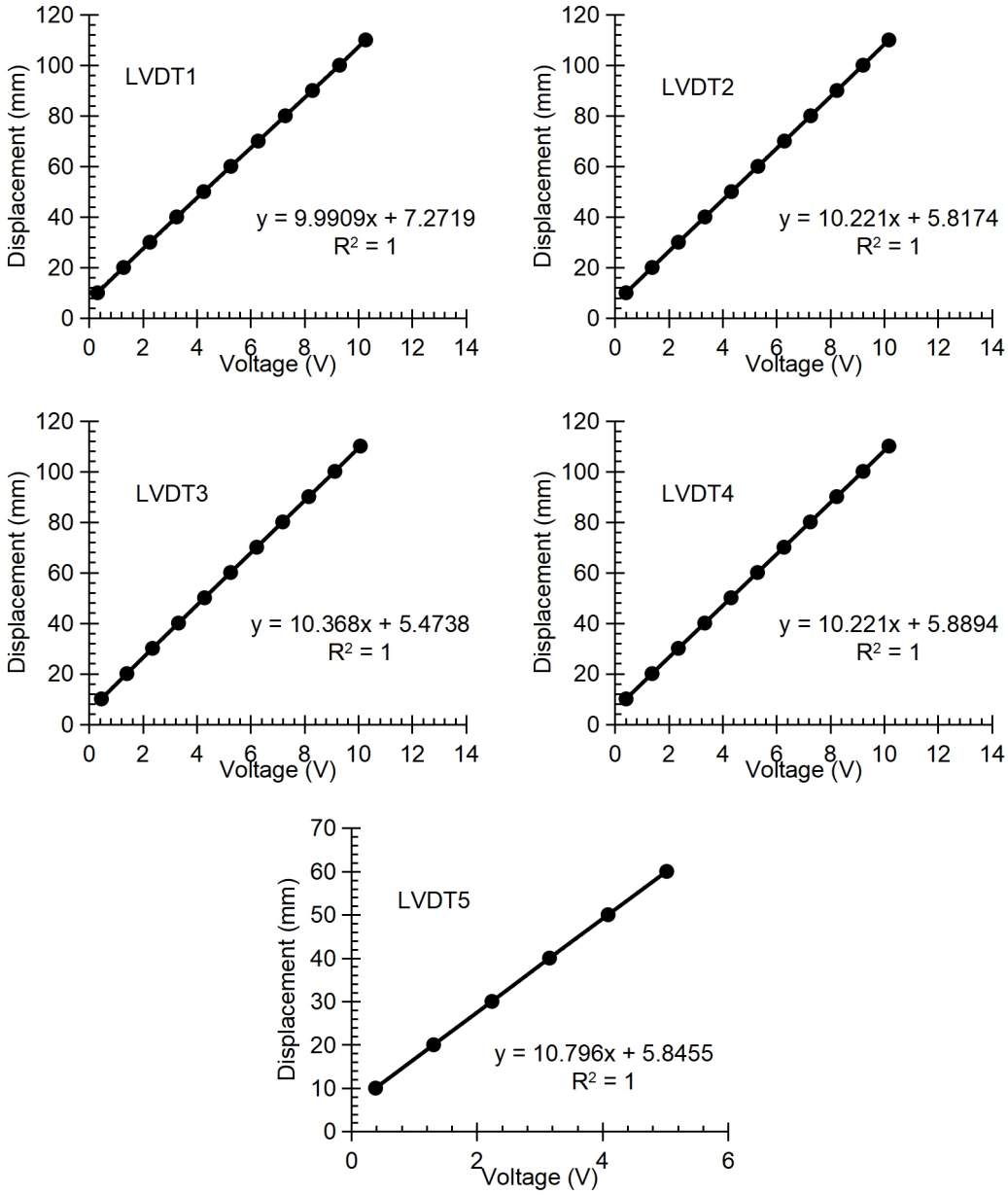

Figure 3.25 Calibration curves of the LVDTs

3.3.4.3 Strain measurement

In this research, the applied loads to the footing were transferred to the system beneath it, creating stresses and strains in each of the elements that formed the integrated system. Measuring the generated strain in each element is important to identify its contribution to the system stability. Three main elements were influenced by the generated strain:

1- Reinforcing layers.
2- Plastic pipe.
3- Concrete pipe.

Each one of these elements had its own stress-strain behaviour, and according to it, the generated strain in it differed. Strain measurement requires the installation of strain gauges to accurately record the generated strain in each element. It should be noted that after installing the strain gauges, a protective adhesive layer covered them to provide protection against the sand particles friction.

Reinforcing layers strain

The reinforcing layers were defined as tensile elements that had the ability to sustain the generated strains in the reinforced soil system. Mainly, the sustained strains by the reinforcing layers were tensile strains, and to record it, one strain gauge was attached to the middle longitudinal rib of each reinforcing layer, which was parallel to the length of the tank. According to the geometry of the reinforcing layer, the width of the rib was 2.4 mm (Tensar, 2012). Consequently, specific type of strain gauges had to be used to fit in this narrow width. FLKB-2-23 strain gauge had a gauge width of 1.5 mm, which made it a suitable strain gauge to be attached to the reinforcing layers, as shown in Figure 3.26. The strain gauges were attached with a half bridge circuit arrangement. It had a 120 Ω resistance and a 5% strain measuring limit.

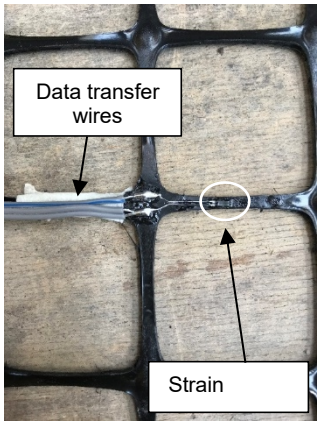

Figure 3.26 Strain gauge attached to the reinforcing layer

Flexible pipe strain

The flexible pipe used in this research was subjected to stresses that generated tensile and compressive strains, along its spring and top lines, respectively. Measuring these strains required the installation of strain gauges. One FLKB-2-23 strain gauges was used to measure the strain generated in the pipe, as

shown in Figure 3.27. One strain gauge was mounted at a location, on the crown and the spring-line, exactly in the middle section of the pipe, where its measurement direction was perpendicular to the longitudinal pipe direction.

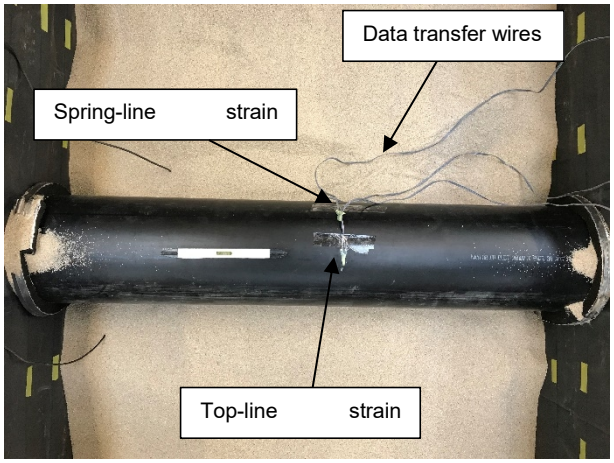

Figure 3.27 Strain gauge attached to the flexible pipe

Rigid pipe strain

Similar to the flexible pipe case, compressive and tensile strains were generated in the rigid pipe. According to its nature, tensile strains were generated at the inner top and invert lines, as well as the outer spring-line of the pipe, where the generated strains were measured using one PL-60-11 strain gauge mounted at each location. The measurement direction was perpendicular to the longitudinal pipe direction, as illustrated in Figure 3.28. This strain gauge has the ability to cover relatively larger area than the FLKB-2-23 strain gauge. The strain gauges used were attached with a half bridge circuit arrangement. They had 120 Ω resistance and 2% strain measuring limit.

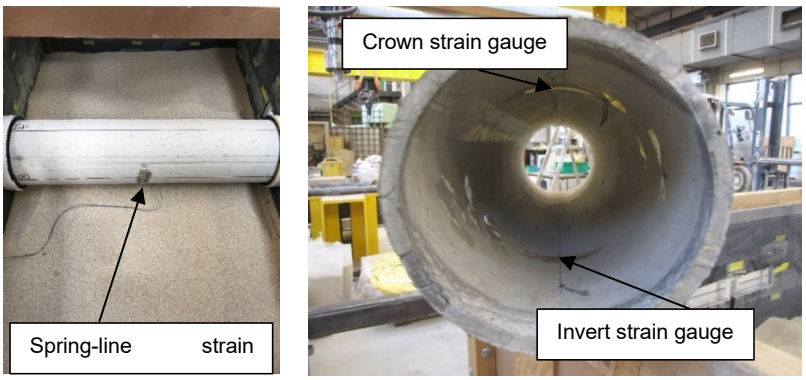

Figure 3.28 Attached strain gauge to the rigid pipe

3.3.4.4 Measuring instruments accuracy

The calibration process of the used measuring instruments enabled the identification of the conversion equation for each one of them. Mainly, the data logger measured volts, and by using the generated calibration equations, it could be converted into the mechanical property that the instrument measured. After this process, the accuracy of this equation had to be tested. It could be done by measuring the variation between the measured and the calculated values. Table 3.8 illustrates the accuracy of the used instruments in this research.

Table 3.8 Accuracy of the used instruments

	Load cell	Pressure cell	*LVDT1*	*LVDT2*	*LVDT3*	*LVDT4*	*LVDT5*
Accuracy (%)	0.11	0.07	0.29	0.16	0.03	0.81	0.32

3.3.5 Sand pouring technique

Unit weight of the sand is one of the most important factors that would affect the behaviour of the tested systems. Consequently, to get reliable outcomes from this research, the tested sand needed to have the same unit weight. To get this relatively constant unit weight, a raining technique was used (Rad and Tumay, 1987). The main factors that controlled the unit weight of the sand through the raining technique were:

1- Sand drop height.
2- Sieve opening.

The sand initial drop height was 500 mm through the raining sieve (zero level), where it was poured until reaching a height of 400 mm. After that, the sieve was lifted by using four wooden pieces of 100 mm in height at the corners of the tank to keep a constant distance between the sieve and the sand surface, as illustrated in Figure 3.29. The apertures of the raining sieve were circular in shape, of 5 mm diameter, which kept the sand particles dropping at a constant speed. To assure the proper usage of the raining technique, Aluminium cups of known volume were used at different places inside the tank to measure the unit weight of the sand. The ratio between the poured sand density and the maximum dry density according to the Proctor test was 99%.

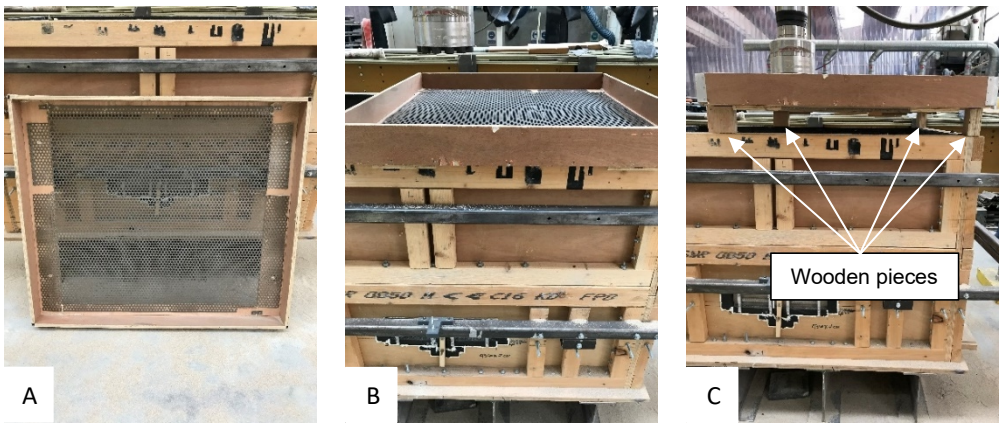

Figure 3.29 Raining sieve and its lifting method
A: Used sieve. B: Sieve at zero level. C: Lifted sieve.

3.4 Experimental testing scheme

Two main parameters are studied in this research, the burial depth of the pipe relative to its diameter, *H/D*, and the number of the geogrid-reinforcing layers included in the system for both the flexible and the rigid pipes. Concerning the spacing between geogrid-layers, h/B_f, and the spacing between the topmost geogrid-layer and the soil surface, u/B_f, an optimum value of 0.35 was chosen (Mir Mohammad and Moghaddas 2001; Mehrjardi and Tafreshi, 2008; Tafreshi and Khalaj, 2008).

Table 3.9 illustrates the details of the testing scheme for the flexible pipes. A total of 13 large-scale tests were predesigned to investigate the variation of the burial depth of the pipe and the number of the reinforcing layers. One test was repeated to assure the accuracy of the testing process and its reliability.

Table 3.9 Testing scheme details for the flexible pipes

Test series	Test type	Tests	Test configuration					Tests No.
			RFT. No.	u/B_f	h/B_f	L/B_f	*H/D*	
A	Unreinforced	*T1:T4*	-	-	-	-	1.5, 2, 2.5, 3	4
B	Reinforced	*T5:T8*	1	0.35	0.35	5		4
C		*T9:T12*	2					4
D	Repetition of T7	*T13*	1				2.5	1

- *RFT* represents reinforcements. *u* refers to the spacing between the reinforcing layers. *h* represents the spacing between the first reinforcing layer and the footing. B_f represents the width of the footing.

Table 3.10 illustrates the details of the testing scheme for the rigid pipes. A total of 10 experimental tests were predesigned to investigate the behaviour of

buried rigid pipes under different burial depths and number of the reinforcing layers. Details of the testing schemes are illustrated in Figure 3.16-B.

Table 3.10 Testing scheme details for the rigid pipes

Test series	Test type	Tests	Test configuration					Tests No.
			RFT. No.	u/B_f	h/B_f	L/B_f	H/D	
A	Unreinforced	*T1:T3*	-	-	-	-	1.5, 2, 2.5	3
B	Reinforced case	*T4:T6*	1	0.35	0.35	5		3
C		*T7:T9*	2					3
D	Repetition of T4	*T10*	1				1.5	1

3.5 Experimental testing preparation

To enable the investigation process of the behaviour of buried flexible/rigid pipes under geogrid-reinforced sand beds, the following steps were followed in each test to prepare reliable tests.

First of all, the tank was filled with a 15 cm of bedding layer by using the raining technique. After that, sand surface was carefully levelled off horizontally. One *LVDT* was installed underneath the tank through the formed hole in the tank base to measure the deformation of the invert of the pipe. This *LVDT* was attached to a light steel rod connected to a cap, which was in contact with the invert of the pipe. After that, the pipe was gently placed exactly in the centre of the testing tank to avoid any load eccentricity. To make sure that the pipe was cantered, a measuring tape was used to measure the distance between the pipe and the walls of the tank from both sides, where these two lengths must be equal. In addition, a spirit level was used on the top of the pipe to make sure that it was positioned in a horizontal level. Two foam strips were used at the edges of the pipe to seal the clearance between the pipe and the tank walls to prevent the sand from entering these areas.

The sand was poured over and around the pipe to fill the tank using the raining technique, where the used sieve was lifted every 100 mm to make sure that the distance between its screen and the sand level was constant (500 mm). Once the sand level was above the crown of the pipe with 10 mm, a pressure cell was placed over the crown of the pipe, exactly at the centre of the pipe. The spirit level was used to make sure that the pressure cell was horizontal. The sand was poured once more until reaching the predesigned level of the reinforcing layer, where the sand was levelled once more. The reinforcing layer was placed in the tank, where it was exactly centred in it. The wires of the strain gauge and

the pressure cell were attached to the tank wall away from the centre of the tank to maintain its safety. The sand was poured again through the sieve until reaching its predesigned level. The sand was levelled one last time, where the footing was placed gently exactly at the centre of the tank to prevent any load eccentricity. The spirit level was used to make sure that the footing was horizontal.

At this stage, the used instruments were installed in position. The rigid rod was inserted inside the pipe through the prepared openings in the tank walls, where the top of the attached nail to it was in contact with the inner crown of the pipe. Two *LVDTs* were installed to be in contact with the two edges of the rigid rod to measure its deformation. Two *LVDTs* were installed on the upper surface of the footing to measure its deformation. It was taken into consideration that a spirit level was used to make sure that all the used *LVDTs* were exactly vertical to prevent any inclination in it, which would cause inaccuracy in the measured deformations.

A load cell was installed between the footing surface and the actuator to measure the applied load to the tested system and make sure that it was identical to the predesigned loading profile.

Before starting the test, i.e. loading, the data acquisition systems were switched on and data were captured to make sure that the complete response was measured.

After ending the test, the loading was slowly released, and all the *LVDTs* were removed from their positions. The footing was removed from the tank. The sand surface was gently excavated until reaching the reinforcing layer surface, where its deformation was manually measured.

After that, the reinforcing layer and the sand were removed from the tank, where the sand was stored in plastic bags, where it was used for the next test.

3.6 Summary

Investigating the behaviour of any system requires a comprehensive understanding of its components behaviour and their mechanical properties. In this research, the behaviour of buried rigid/flexible pipes in unreinforced and geogrid-reinforced soil under the application of incrementally increasing cyclic

loading was investigated by using large-scale laboratory tests. Experimental tests were performed to determine the mechanical properties of the silica sand, geogrid-reinforcing layers and rigid/flexible pipes. A wooden testing tank was used to perform the laboratory testing. Tank dimensions were chosen to enable the simulation of the real case of the buried pipe, as recommended by the British Standard and previous studies. A rigid steel strip footing was used to transfer the cyclic loading to the tested systems. To maintain constant unit weight of the tested sand, a raining technique was used. Due to the application of external cyclic loading, deformations, stresses and strains were generated in the system. These responses were measured using different measuring instruments such as *LVDTs*, pressure cell, load cell and strain gauges. To accurately identify the system response, a calibration process was performed on the measuring instruments.

CHAPTER 4

BEHAVIOUR EVALUATION OF BURIED FLEXIBLE PIPES

4.1 Introduction

Any structure beneath the ground surface level can be considered a buried structure, and a certain level of protection must be provided according to the structure importance.

Establishing new highway embankments and buildings often requires construction over existing underground utilities, such as pipelines. Embankments and buildings constructed over such utilities often induce significant additional earth pressures causing overstressing and/or unacceptable deformations of the buried pipes, resulting in interruption of service for both the utility and the structure itself. Buried pipes are used mainly for water supply and drainage besides many other strategic applications such as transportation of energy and mineral resources like oil, liquefied natural gas, coal slurries and mine tailings. They are manufactured from different materials in various shapes, sizes and are subjected to live and gravity loads. The main concern in designing flexible pipes is its deformation due to the applied loads. According to its importance, flexible pipes behaviour is investigated in this chapter.

The inclusion of the reinforcing layers in soil creates new composite material that can sustain higher load profiles and provide more system stability. Soil reinforcement technique is a quick, easy and relatively cheap technique to construct in comparison with other preventative techniques, and can be used in many of the engineering applications. Adding reinforcing layers enhance the system stability through the generation of load transfer mechanisms such as, frictional, passive earth resistance and membrane effect. In this chapter, the protection concept of flexible pipes using geogrid-reinforcing layers is investigated and evaluated.

4.2 Investigated system components

In this chapter, the behaviour of buried *HDPE* pipe in geogrid-reinforced and unreinforced silica sand under the application of incrementally increasing cyclic loading is investigated. The investigated system consists of:

1- Silica sand (backfill material).
2- Geogrid reinforcing layers (Tensar *SS20*).
3- *HDPE* pipe (flexible pipe).

In this chapter, two main parameters are studied, the burial depth of the pipe relative to its diameter, *H/D*, and the number of the geogrid-reinforcing layers inclusion in the system. A total of 13 large-scale tests are conducted, presented and discussed. Width of the reinforcing layer, *B*, spacing between topmost reinforcing layer and soil surface, *u*, and spacing between reinforcing layers, *h*, are kept constant. Figure 4.1 illustrates a schematical diagram of the tested systems.

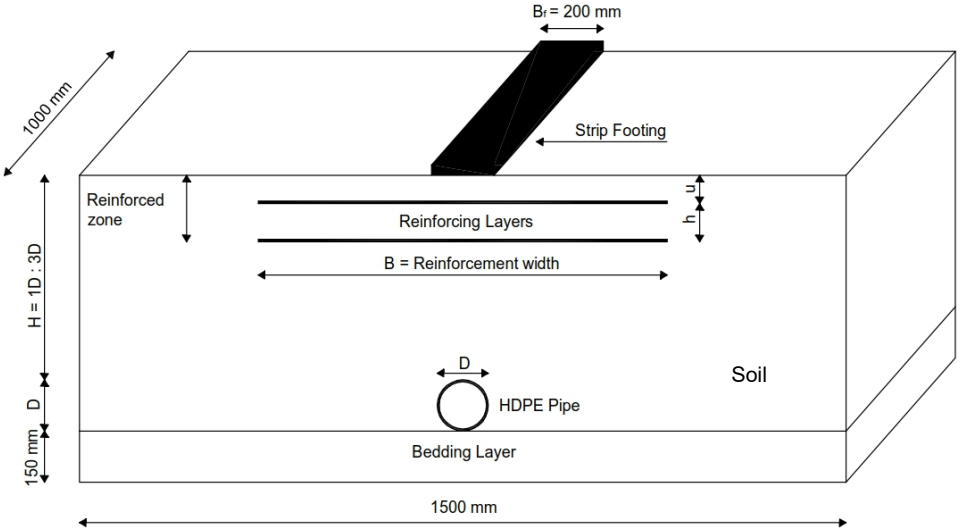

Figure 4.1 Schematical diagram of tested system

4.3 Applied loading profile

According to the British Standard, NA to BS EN 1991-2:2003, the applied load to a buried pipe results from variable sources, in particular vehicles or traffic loads. Based on the axle load and number of wheels per axle, the wheel load can be calculated. Consequently, the applied pressure on a buried pipe can be determined (BS, 2003). Axle load ranges from 50 to 230 kN and can produce a wide range of applied stresses on the pipe-soil systems. The contact area between the wheel and soil can be considered as a square of 0.35 m side

length. Consequently, applied pressure approximately ranges from 200 to 950 kPa. It should be noted that, there is no pavement layer overlying the surface of the soil in this investigation. Consequently, the applied load on the soil surface should be reduced as suggested by Mehrjardi and Tafreshi (2008) and Tafreshi and Khalaj (2008).

The applied load profile to the system consists of monotonic loading followed by cyclic loading. To determine a realistic value for the monotonic loading, a buried HDPE pipe underneath unreinforced soil was tested under static load until failure, as illustrated in Figure 4.2. It was concluded that the failure occurred at load of 21.6 kN. To assure that the initial applied monotonic load will not lead to failure before applying the cyclic loading, the monotonic load amplitude was chosen to be less than the failure load, where its value was 18 kN.

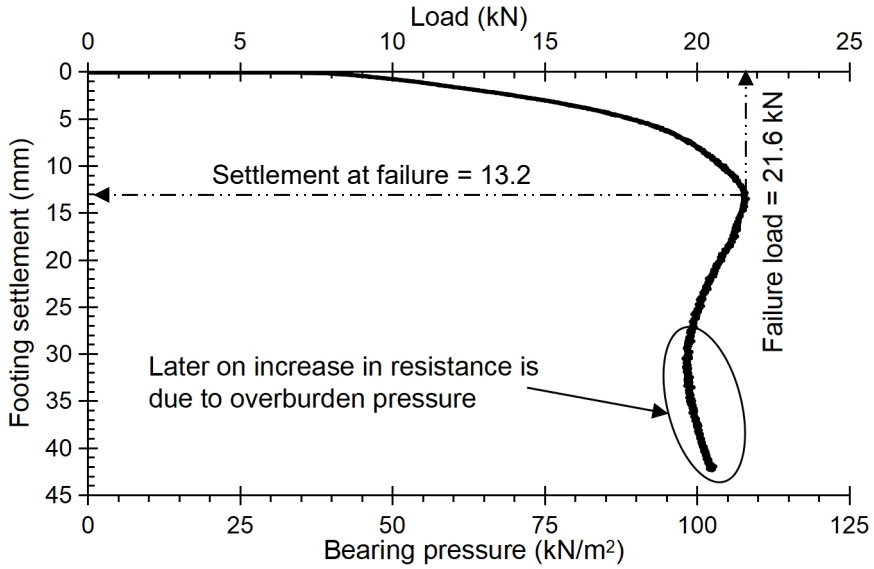

Figure 4.2 Monotonic load amplitude determination

After monotonic loading application, it was followed by cyclic loading of 5 kN amplitude. The following load phases were performed by increasing the mean value of cyclic loading by 5 kN. The first phase was continued for 3000 cycles whereas only 1000 cycles were performed in all subsequent phases. The increase in load phases was continued until the system failed. The used data acquisition systems had the ability to record measurement readings at a minimum time interval of 500 ms. Therefore, a load frequency of 0.5 Hz was selected in this investigation so that, four readings per loading cycle can be recorded to capture the behaviour. The load increment represents different

vehicle capacities over the system, or load increase while time passes due to additional applied loads. Figure 4.3 illustrates the applied loading profile. The value of the applied loading phases is summarised in Table 4.1.

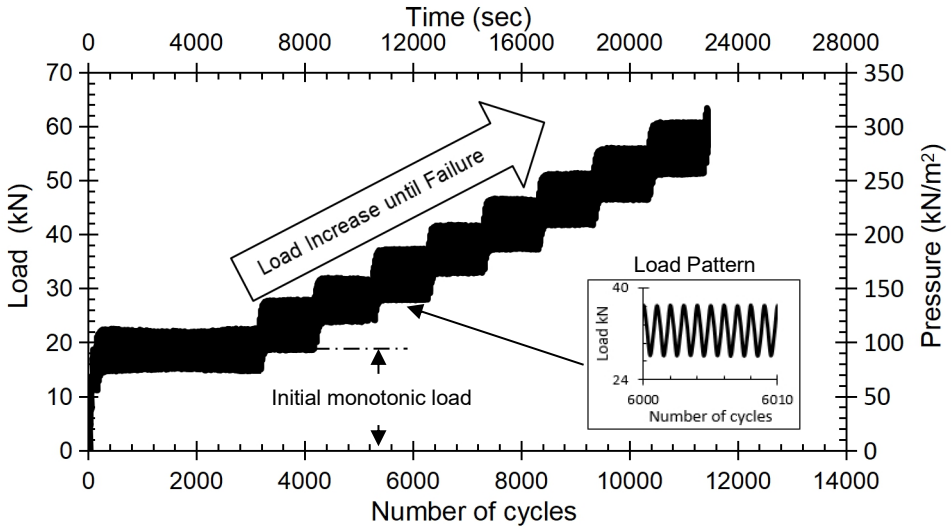

Figure 4.3 Applied loading profile of 0.5 Hz

Table 4.1 Value of the applied cyclic loading phases

Test series			Load phase	Mean load (kN)	Load range (kN)		Amplitude (kN)
					Min.	Max.	
Series C	Series B	Series A	Phase 1	18	13	23	5
			Phase 2	23	18	28	5
			Phase 3	28	23	33	5
			Phase 4	33	28	38	5
			Phase 5	38	33	43	5
			Phase 6	43	38	48	5
			Phase 7	48	43	53	5
			Phase 8	53	48	58	5
			Phase 9	58	53	63	5

4.4 Results and discussions

In this section, the influences of pipe burial depth and number of reinforcing layers on the behaviour of unreinforced and reinforced soil-pipe systems were assessed and discussed. Measurements of footing and pipe deformation, pipe and reinforcement generated strain as well as transferred pressure to the pipe crown are presented and discussed. The followed testing scheme in this chapter is illustrated in Table 3.9. It should be noted that the settlement of the pipe and footing is presented as a ratio of the pipe diameter. i.e. normalised values; and the footing width is equal to the pipe diameter.

4.4.1 Unreinforced case

Series A of the testing scheme examined the contribution of *H/D* variation to the behaviour of buried pipes in unreinforced sand. The tested systems sustained a maximum of three loading phases, as illustrated in Table 4.1, until the occurrence of failure.

4.4.1.1 Footing settlement

Results for the footing settlement ratio, F_s/D, with loading cycles increase are presented in Figure 4.4. The settlement is normalized relative to the pipe diameter. It is clear that increasing the burial depth of the pipe significantly reduced the settlement of the footing until reaching *H/D* = 2.5, i.e. Test 3, in addition, allowing pipe-soil system to sustain more load phases until reaching the failure point. Figure 4.5 shows the settlement of the footing at the end of each loading phase with burial depth increase.

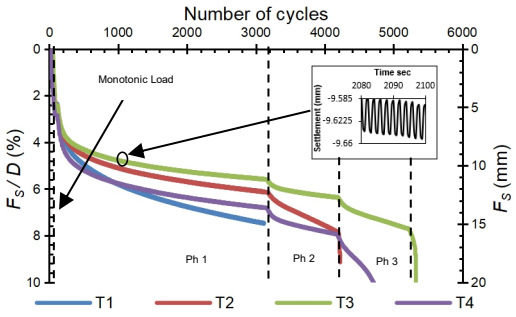

Figure 4.4 Footing settlement ratio against number of cycles, Series A

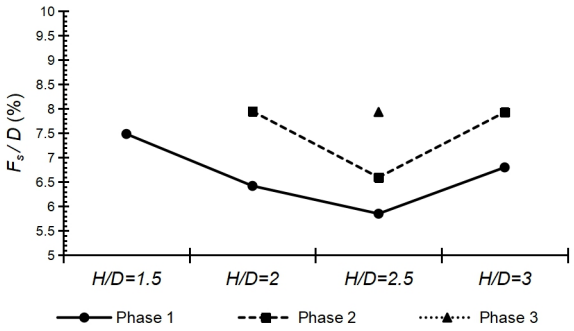

Figure 4.5 Footing settlement ratio at the end of load phases

Under the application of the 1st loading phase, the maximum footing settlement occurred at *H/D*=1.5, where the normalized settlement value reached 7.49% (14.97 mm), and this settlement was followed by system failure. With the increase of the burial depth, the footing settlement rate and values were reduced, and its normalised value reached 6.42% (12.84 mm) and 5.85% (11.7 mm), with enhancement ratio of 14.23% and 21.84%, at *H/D*=2 and 2.5 respectively. Nevertheless, when the burial depth reached H/D=3, the behaviour of the footing settlement deteriorated, and normalized settlement started to increase, where it reached 6.8% (13.6 mm) with an enhancement ratio of only 9.15%, with respect to *H/D*=1.5.

In the 2nd loading phase, the first burial depth, *H/D*=1.5, could not sustain the load and failure occurred. At *H/D*=2, the normalized footing settlement reached 7.95% (15.9 mm) and at *H/D*=2.5, the normalized settlement reached 5.59% (13.19 mm) with an enhancement ratio of 17%. It can be noted that the settlement rate during the 2nd loading phase at *H/D*=2 increased compared with the 1st loading phase, which indicates that system failure approaches. The same behaviour occurred once more, where the normalized settlement started to increase at *H/D*=3, and it reached 7.93% (15.86 mm) with approximately no enhancement at all. During the 3rd phase, the only system that sustained this load was when the burial depth of the pipe was *H/D*=2.5, resulting in a normalized settlement value of 7.94% (15.87 mm), followed by system failure.

At *H/D*=3, the footing settlement was increased due to increased soil volume between the footing and pipe. In addition, the pipe was located too far away from the footing, which led to significant reduction in its contribution to the system stability. As a result, the cyclic loading would cause a significant increase in the density of the soil cover, which is directly reflected on the settlement.

To further inspect the relationships for footing settlement, Figure 4.5 was plotted for the settlement ratio at the end of each loading phase with increasing burial depth. It is clear that a change in the attained settlement occurred with the increase in burial depth. The results suggested that a *H/D* of 2.5 was an optimum value for the system behaviour. This can be attributed to the obvious reduction in footing settlement at *H/D*=2.5.

4.4.1.2 Transferred pressure to the pipe

Figure 4.6 shows measured data for the soil pressure above the pipe crown at the mid-point of the pipe length. At the 1st loading phase, the maximum transferred pressure to the pipe reached 90.5 kPa, at *H/D*=1.5. With the increase of burial depth, the pressure value is reduced and it reached 65.5 kPa, 52.5 kPa and 43.39 kPa at *H/D*=2, 2.5 and 3 respectively, resulting in an improvement of 27.6%, 42% and 52%. The transferred pressure reached 72.75 kPa, 59.34 kPa and 48.41 kPa at *H/D*=2, 2.5 and 3 respectively, at the 2nd loading phase. The improvement ratio was 18.43% and 33.46% at *H/D*=2.5 and

3. At the 3rd loading phase, the only system that sustained this load is when the burial depth of the pipe reached *H/D*=2.5, and the pressure value was 62.77 kPa.

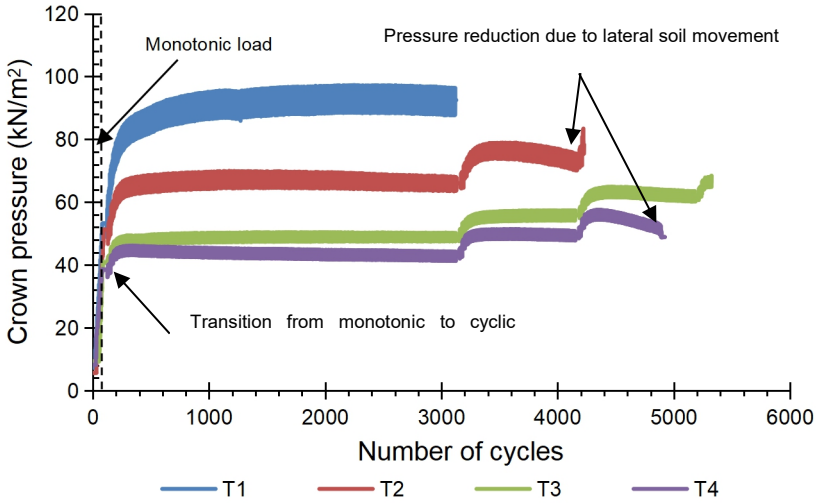

Figure 4.6 Transferred pressure to the pipe in Series A

It was obvious that the transferred pressure started to increase during the first 300 cycles in each loading phase, and then its magnitude began to stabilise. Increasing the burial depth of the pipe allowed for more soil to interact in the distribution of loads around and on the pipe leading to a significant reduction of measured pressure at the pipe crown, which is a good match with the results of Arockiasamy et al. (2006). The applied load on the footing led to the formation of differential settlement between the immediate soil beneath the footing and adjacent soils. This differential settlement caused the generation of shear stresses between these soil zones, which can be defined as an arching effect (Terzaghi and Peck, 1967).

Once the generated tensile strains exceeded the shear resistance of the soil, the arching effect failed leading to a system failure. The generated active arching played a significant role in reducing the transferred cyclic load to the underground inclusion, especially at higher burial depths which allowed the generation of a full arching mechanism (Aqoub et al., 2018).

Consequently, the transferred pressure to the pipe was reduced with the burial depth increase, due to the generation of the arching mechanism. It is obvious that system failure initiation could be predicted from the sharp inclination of the

pressure curve, where an increased tensile strain forced the soil to move laterally leading to stress redistribution and stress reduction over the pipe.

4.4.1.3 Crown settlement

Normalised crown settlement, C_s/D, under variation of H/D is presented in Figure 4.7. The results clearly illustrated that increasing the burial depth of the pipe has a great role in reducing settlement of pipe crown, as well as enabling the system to sustain more load phases. Figure 4.8 illustrates the settlement of the pipe crown at the end of each loading phase with burial depth increases.

Under the application of the 1st loading phase, it is clear that all the burial depth ratios sustain the applied loads with obvious variation in the crown settlement. The crown settlement reached 10 mm (5%), 6 mm (3%), 4.52 mm (2.26%) and 3.36 mm (1.68%) for H/D=1.5, 2, 2.5 and 3, respectively.

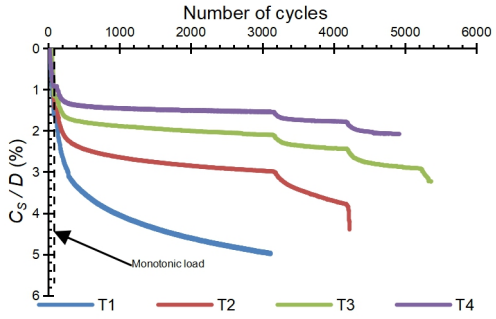

Figure 4.7 Crown settlement ratio in Series A

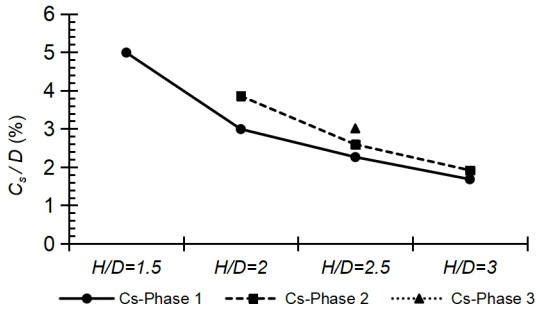

Figure 4.8 Pipe crown settlement with load phases increase

Once the load is increased until reaching the 2nd phase, the system where H/D=1.5 could not sustain the applied load, and the system failed. It can be noted that, at H/D=1.5, the pipe failed once its vertical diametric strain reached 5%, matching the results of Mehrjardi and Tafreshi (2008) and Tafreshi and Khalaj (2008). Consequently, system failure at H/D=1.5 is governed by its pipe failure. In the other burial depths, the crown settlement was, 7.72 mm (3.86%), 5.18 mm (2.59%) and 3.84 mm (1.92%), respectively. For the 3rd loading phase, only the system of H/D=2.5 sustained this load, and the crown settlement was, 6.02 mm (3.01%). It is obvious that most of the settlement occurred in the first 300 cycles regardless the burial depth of the pipe. With load cycles increase, crown deformation deteriorates continuously until failure occurs. The transition

from one phase to another results in an increased rate of settlement, in particular in the first 300 cycles of each phase.

The inclusion of the pipe inside the soil under the application of static loading regime was investigated, as illustrated in Figure 4.9.

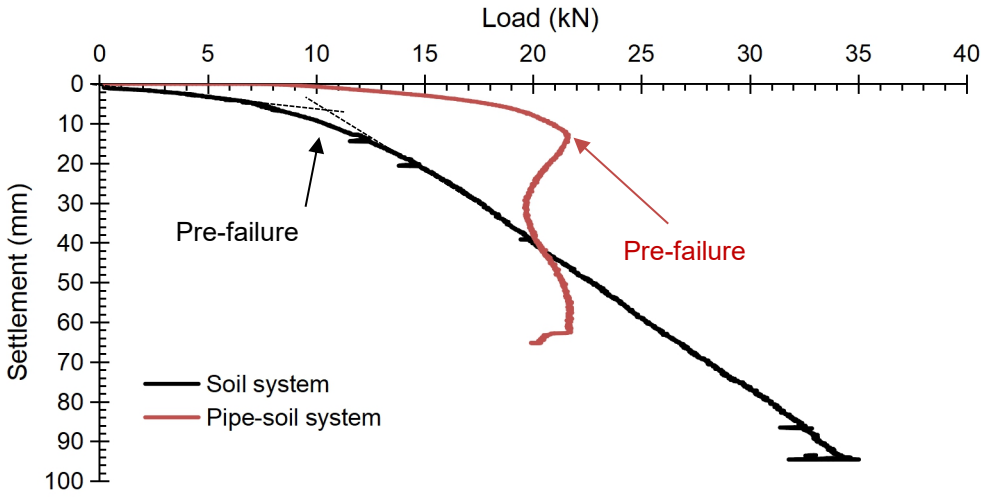

Figure 4.9 Comparison between soil and pipe-soil systems

It was concluded that, pipe inclusion in soil creates new composite system, which can sustain more loads compared with only soil. The behaviour of the composite system depends mainly on pipe burial depth. When the pipe is close to the surface, more pressure is transferred to it leading to excessive deformation in its crown followed by system failure, which occurred at *H/D*=1.5. Increasing this spacing will gradually reduce the transferred pressure to the crown of the pipe, and system will sustain more load phases with reduction in the footing settlement, which occurred at *H/D*=2 and 2.5. The results suggest that increasing spacing more than *H/D*=2.5 will lead to the creation of two zones, upper and lower zones. The upper zone can be considered only soil, which can sustain small amount of load; and the lower zone is a pipe-reinforced zone that can sustain more loads. However, since the load is transferred through both of them, settlement of the weak upper zone will be increased leading to system failure, as occurred at *H/D*=3. Consequently, increasing the burial depth of the pipe will reduce footing settlement until *H/D*=2.5, which is in agreement with the findings of Cao et al. (2016).

It is clear that, at the same loading phase, increasing burial depth significantly reduced pipe crown settlement, where the settlement slope is greatly reduced.

The reason of this behaviour is that increasing pipe burial depth will enable the existence of increased soil layer above the pipe, which will allow the formation of full arching mechanism leading to load mitigation. Consequently, reduced amount of the applied pressure will be transferred to the pipe, and enhanced value of lateral pressure will be applied to it.

4.4.1.4 Invert settlement

Normalised invert settlement, I_S/D, under variation of *H/D* is illustrated in Figure 4.10. It illustrates that increasing *H/D* plays a great role in decreasing pipe invert settlement. Figure 4.11 shows pipe invert settlement at the end of each loading phase with burial depth increase.

At the 1st loading phase, it is clear that maximum value for the invert settlement reached 0.51 mm (0.255%) at *H/D*=1.5, and this value started to decrease with the increase in the *H/D*. It reached, 0.36 mm (0.18%), 0.355 mm (0.178%) and 0.28 mm (0.14%) with an enhancement ratio of 29.4%, 30.4% and 45% at *H/D*=2, 2.5 and 3 respectively. With load increment until reaching the 2nd loading phase, failure occurred at *H/D*=1.5, due to pipe failure. The invert settlement value reached, 0.39 mm (0.195%), 0.355 mm (0.178%) and 0.32 mm (0.16%) at *H/D*=2, 2.5 and 3 respectively. The enhancement ratio reached 9% and 17.9% at *H/D*=2.5 and 3. At the 3rd loading phase, the only system that sustained this load is when the burial depth of the pipe reached *H/D*=2.5, and the settlement value was 0.38 mm (0.19%). Consequently, invert settlement is reduced with the increase in the pipe burial depth. In addition, invert settlement has minor contribution in system stability compared with crown settlement.

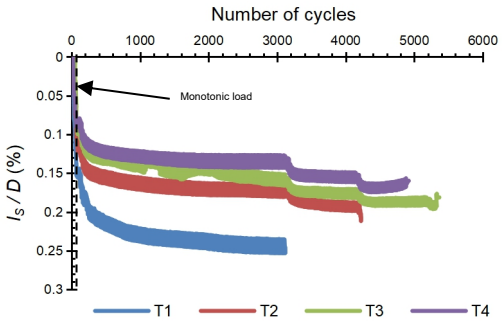

Figure 4.10 Invert settlement in Series A

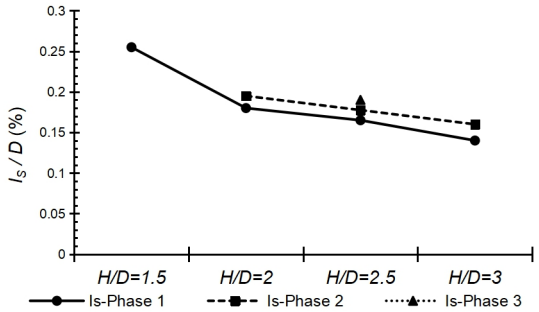

Figure 4.11 Pipe invert settlement with load phases increase

4.4.1.5 Vertical diametric change

Figure 4.12 illustrates the maximum pipe deformation shape just before failure occurs in different pipe burial depths. The vertical diameter of the pipe, ΔD, which equals to the difference between its crown and invert deformations, is changed due to the settlement of both the pipe crown and invert. Figure 4.13 illustrates the vertical diametric change with respect to the applied loading cycle's number. The vertical diameter change ratio with respect to the initial vertical diameter is significantly affected by the pipe crown deformation. That is why the pipe overall behaviour is governed by its crown state.

After applying load to the system, the load is transferred to the pipe deforming its circular cross section and converting it into either, elliptical or heart shape. The new formed cross section depends mainly on the density of the surrounding soil of the pipe, as well as the burial depth of the pipe (Rogers et al., 1996; Tafreshi and Khalaj, 2011). In the heart shape mode, the pipe crown and invert settle and its shoulders curvature increase. In the elliptical mode, the vertical diameter is shortened unlike the horizontal diameter, which tends to be extended. Medium soil density, that surrounds the pipe, will form elliptical cross section shape, and high soil density will create heart cross section shape. Visual inspection of the pipe deformation as well as measurements of the crown and invert suggest that the pipe cross section formed an elliptical shape; however, the used soil in this investigation has dense density.

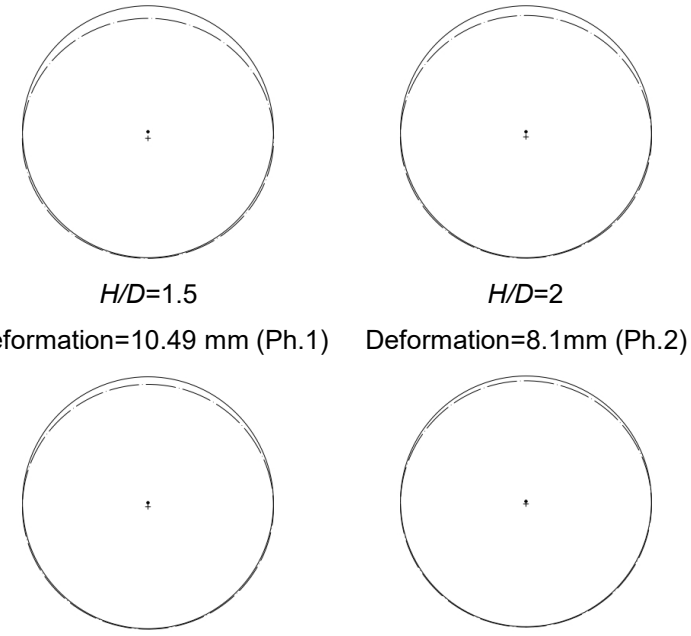

H/D=1.5 *H/D*=2

Deformation=10.49 mm (Ph.1) Deformation=8.1mm (Ph.2)

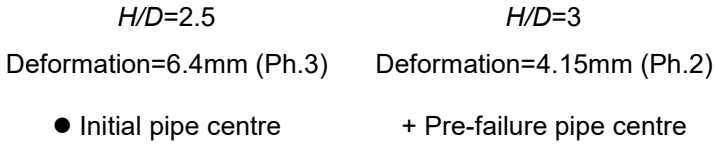

Figure 4.12 Pre-failure pipe deformation shape

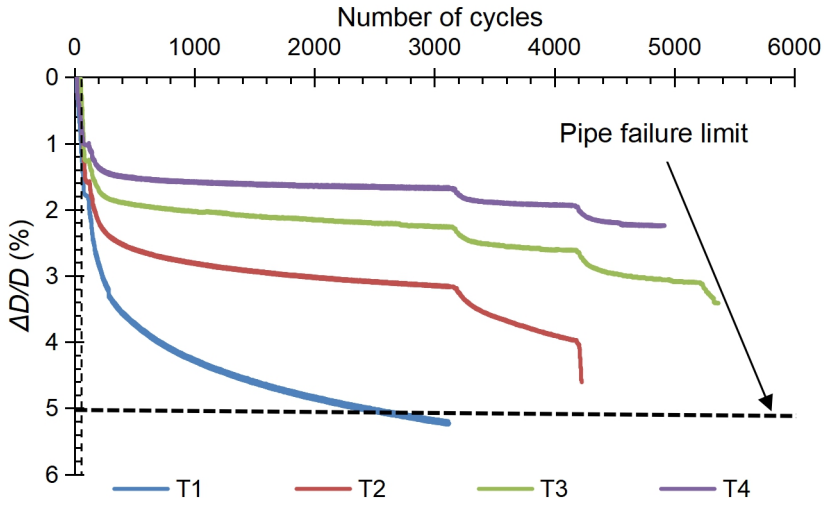

Figure 4.13 Vertical diametric change ratio of the pipe

4.4.1.6 Crown strain

The applied load to the pipe generates strain at its crown. Strain gauge is fastened on the pipe crown, as illustrated in Figure 3.27. The results of the measured crown strain are illustrated in Figure 4.14. It illustrates that, the burial depth of the pipe has significant effect on the generated strain at pipe crown. Figure 4.15 shows crown strain of the pipe under different loading phases with burial depth increase.

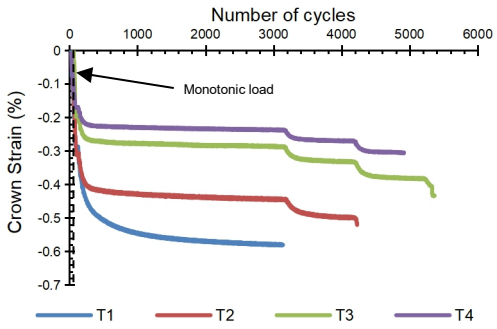

Figure 4.14 Crown strain in Series A

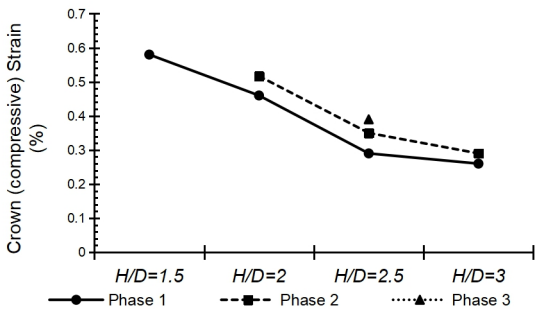

Figure 4.15 Pipe crown strain with load phases increase

It is clear that with the increase in the burial depth of the pipe, the generated compressive strain decreases, and after *H/D*=2.5 the strain decrease rate is

significantly reduced and tends to reach stability. At the 1st loading phase, strain values reached 0.58%, 0.46%, 0.29% and 0.26% at *H/D*=1.5, 2, 2.5 and 3 respectively. The enhancement ratio was 20.7%, 50% and 55.2% at *H/D*=2, 2.5 and 3 respectively. It is clear that the difference in the enhancement ratio at *H/D*=2.5 and 3 is only 5.2%, which gives an indication that after *H/D*=2.5, the improvement ratio in the strain reduction is insignificant. When the load increment reaches the 2nd loading phase, the first burial depth system, *H/D*=1.5, fails. The strain value reached 0.52%, 0.35% and 0.29% at *H/D*=2, 2.5 and 3 respectively. The improvement ratio reached 32.7% and 44.2% at *H/D*=2.5 and 3. At the 3rd loading phase, the strain reached 0.39% at *H/D*=2.5, while systems of other burial depths failed to sustain the applied loads. Consequently, increasing pipe burial depth positively contributes in enhancing the pipe performance, where, it reduces the generated compressive strains along its crown.

4.4.1.7 Spring line strain

Generated strains along pipe spring line are illustrated in Figure 4.16. The attached strain gauge to the pipe spring line is illustrated in Figure 3.27. The increase in the burial depth of the pipe has a vital role on increasing the lateral support of soil surrounding the pipe. Consequently, the generated strain along the pipe spring line is reduced with the increase in the burial depth of the pipe as shown in Figure 4.17.

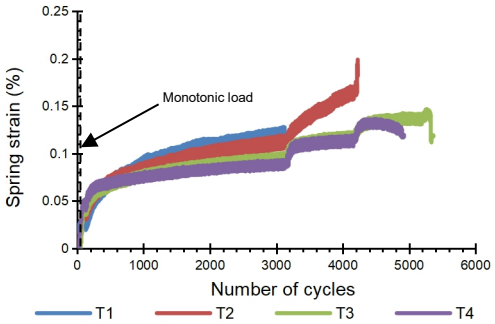

Figure 4.16 Spring line strain in Series A

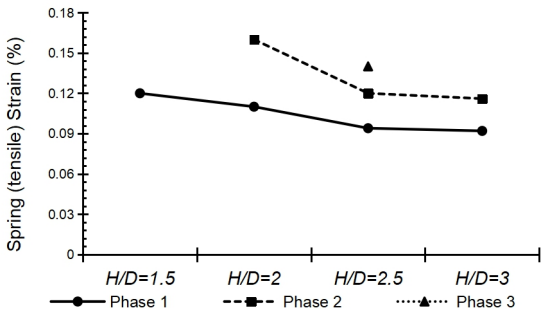

Figure 4.17 Pipe spring strain with load phases increase

As illustrated in the pipe crown strain, the increase in the burial depth of the pipe led to decrease in the generated tensile strain along the pipe spring line, and after *H/D*=2.5 the strain decrease rate is significantly reduced and tends to

reach stability. At the 1st loading phase, the strain values reached 0.12%, 0.11%, 0.09% and 0.09% at *H/D*=1.5, 2, 2.5 and 3 respectively. The improvement ratio reached 8.3%, 25% and 25% at *H/D*=2, 2.5 and 3 respectively. It is clear that there is no enhancement variation ratio at *H/D*=2.5 and 3, which gives an indication that pipe optimum burial depth is *H/D*=2.5. With load increment until reaching the 2nd loading phase, the first burial depth, *H/D*=1.5, fails. The strain value reached 0.16%, 0.12% and 0.116% at *H/D*=2, 2.5 and 3 respectively. The improvement ratio reached 25% and 27.5% at *H/D*=2.5 and 3. At the 3rd loading phase, the strain reached 0.14% at *H/D*=2.5, while the other burial depths failed to sustain the applied load, as the case in the pipe crown strain.

It can be noted that, the pipe strain measurements are in agreement with its deformation. The change in compressive strain that was measured at pipe crown is more remarkable than the tensile strain recorded at the spring line. This could be attributed to the counter effect of lateral pressure at the spring line.

4.4.1.8 Soil densification

Due to the applied cyclic loading profiles to the investigated systems, dynamic compaction process occurred in the soil, in which its density increased. Figure 4.18 illustrates the densification degree of each investigated system according to the applied loading phases. The densification degree was calculated according to Eq (4.1).

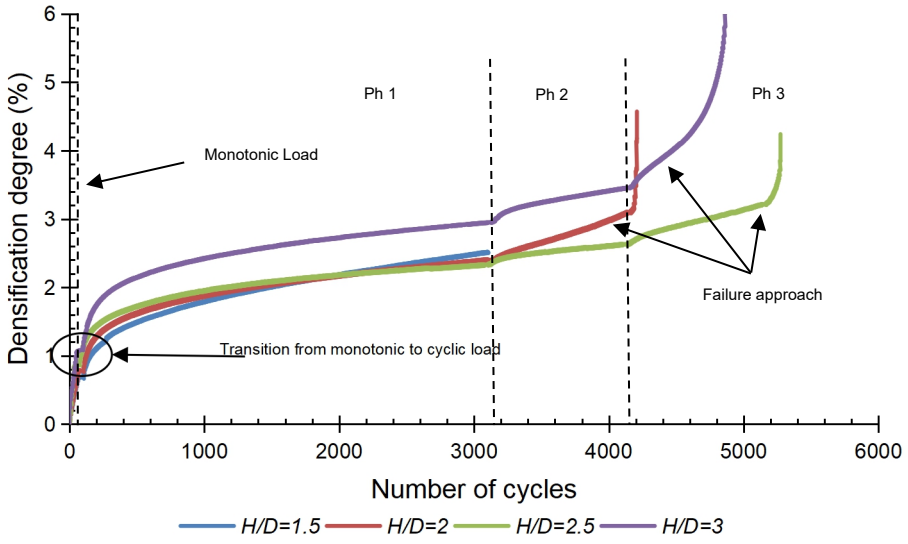

Figure 4.18 Soil densification degree due to cycles number increase

$$Densification\ degree\ (\%) = \frac{(Dc - Di)}{Di} 100 \qquad (4.1)$$

Where;

D_c: Sand density at certain cycle of the applied loading profile.

D_i: Sand density before applying loading profile (initial density).

Because of the applied loading cycles, both, footing and pipe crown settle, but with different vales. Consequently, the soil volume trapped between them was reduced leading to dynamic densification process in this trapped soil. It should be noted that the mass of the trapped soil is assumed to be constant during various phases of loading. Densification process depends not only on footing and on pipe crown settlement, but also, on the initial spacing between them, i.e. pipe burial depth, as illustrated in Figure 4.19. At lower burial depths, lower soil volume is available between the pipe and the footing. Consequently, lower air voids will be released out of soil volume leading to lower degree of densification, which is represented in the case at *H/D*=1.5. Increasing the burial depth leads to increased soil volume with increased air voids to be released, consequently, enhanced degree of densification will be achieved, as occurred at *H/D*=2 and 2.5. Results illustrated that, increasing pipe burial depth to reach *H/D*=3, will greatly increase the soil densification degree. Unfortunately, this enhanced soil densification degree will lead to increased footing settlement, which will cause system failure due to excessive footing settlement. This is in agreement with the unexpected behaviour of the footing settlement at *H/D*=3, as shown in Figure 4.4.

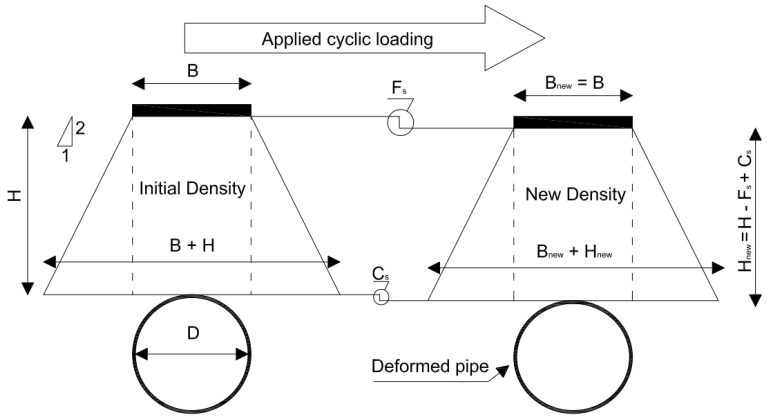

Figure 4.19 Dynamic densification process

Results demonstrate that, generally the highest densification degree occurs during the first 300 cycles of first loading phase regardless of the pipe burial depth. At *H/D*=1.5, densification degree of 1.3% was achieved during the first 300 cycles, which is approximately 52% of the overall occurred densification in this case. The maximum achieved densification degree at *H/D*=1.5 due to the applied cyclic loading was 2.5%. It is clear that, densification degree increased with pipe burial depth increase, in particular under the application of the first loading phase during the first 300 cycles. Further densification due to increased loading phases is incomparable with that occurred during the first loading phase. At higher burial depths, densification grading curves decrease, and with loading phases increase, this grading increase. It gives an indication to system failure approach. The densification led to a reduction in the soil volume followed by an increase in the footing settlement and reduction in the pipe deformation, where no soil heave was observed. This was followed by strain hardening which led to higher shear resistance.

4.4.1.9 Hysteresis response of the footing settlement

The applied loading profile to all of the tested systems consisted of two main steps, i. monotonic loading, where, footing settlement tended to be linear and ii. cyclic loading, where, footing settlement response depended on loading amplitude and number of cycles. In the cyclic loading step, dynamic compaction occurred in the soil and the footing settlement was represented by a hysteresis loop, where settlement varied during loading and unloading stages of the loading cycles. With the progression of loading cycles, soil particles were reorganized and realigned seeking equilibrium, which led to an enhanced degree of soil packing. Hence, the footing settlement showed the same hysteresis behaviour but with a significant reduction in the settlement rate and the system reached an elastic stability condition with a significant reduction in lost energy.

Figure 4.20 illustrates the hysteresis response of the footing settlement under the applied loading profile, at *H/D*=2. This illustrated the densification effect on the footing settlement due to the increase in the number of loading cycles.

In the initial loading cycles, for example, 0.25 mm of the footing settlement required approximately 15 loading cycles to occur, however, with the increase in loading cycles, the same settlement value required a significantly larger number of the applied loading cycles to occur. It is obvious that the settlement rate was significantly reduced with the increase in number of loading cycles. With the increase in the loading phase amplitude, the settlement rate started to increase once more leading to the system failure. This shows that the soil densification played a significant role in the system stability.

It should be noted that the initial portion of Figure 4.20 illustrates footing settlement due to its own weight. Moreover, to reach the exact value of the applied cyclic loading amplitude, the hydraulic actuator required approximately 100 seconds.

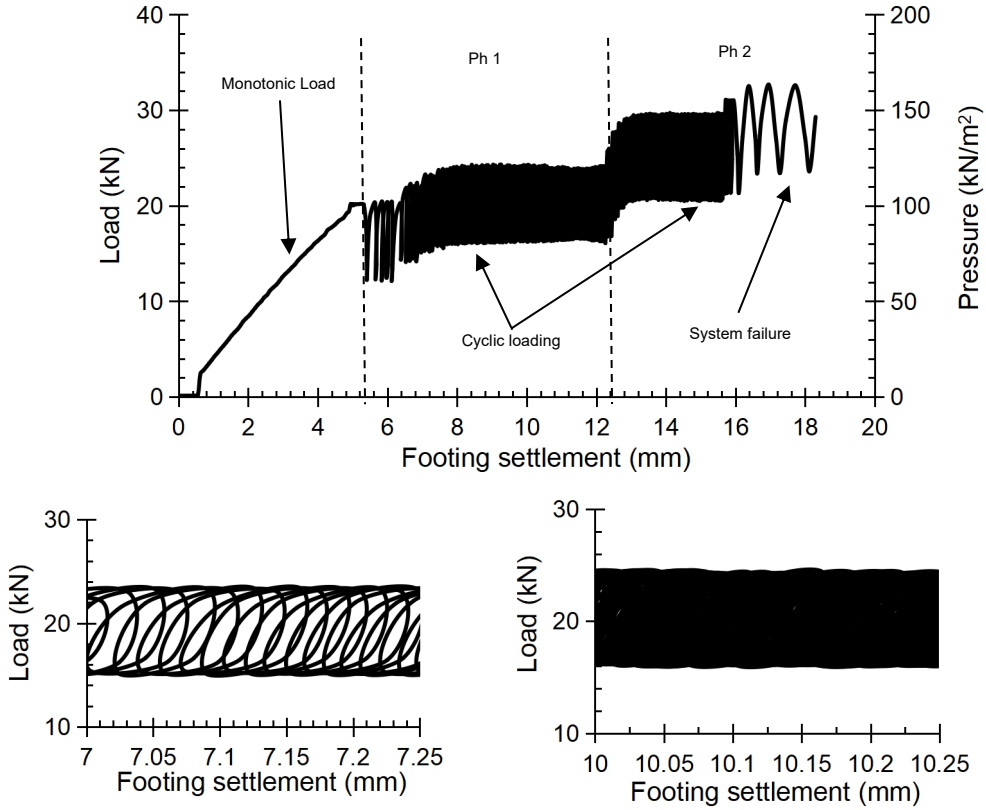

Figure 4.20 Hysteresis response of the footing settlement at *H/D*=2

4.4.2 Reinforced case

Two series, B and C, were conducted to investigate the influence of geogrid-reinforcement inclusion on load transfer and reinforced soil-pipe system load capacity. Table 4.1 illustrates the magnitude of the applied cyclic load in Series B and C, at different phases.

4.4.2.1 Footing settlement

Results for the footing settlement ratio, F_s/D, with loading cycles increase are presented in Figure 4.21. The settlement is normalized relative to the pipe diameter. It is clear that increasing the burial depth of the pipe significantly reduced the settlement of the footing, in addition, allowing pipe-soil system to sustain more load phases until reaching the failure point.

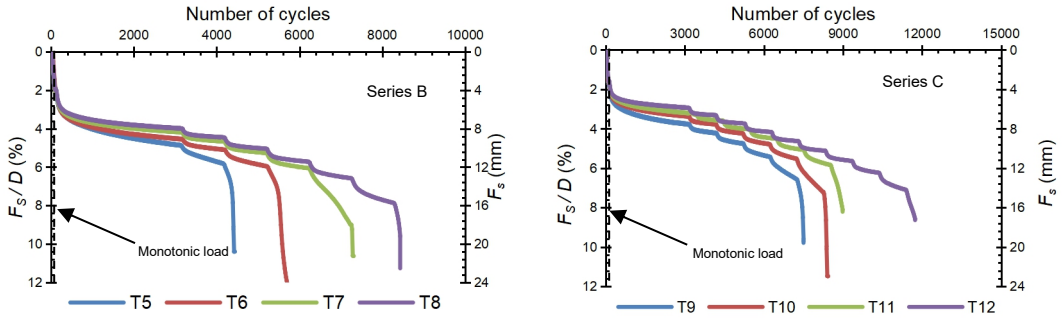

Figure 4.21 Footing settlement ratio against number of cycles

Table 4.2 and Table 4.3 demonstrate the footing settlement values due to increasing cyclic loading phases under the variation of pipe burial depth for Series B and C, respectively.

Table 4.2 Footing settlement due to cyclic loading application, Series B

Loading Phase	1				2				3			
H/D	1.5	2	2.5	3	1.5	2	2.5	3	1.5	2	2.5	3
F_S, mm	9.9	9.38	8.72	8.36	11.98	10.56	9.74	9.32	F	12.42	10.92	10.58
Enhancement ratio, %	-	5.25	11.92	15.55	-	11.85	18.69	22.2	-	-	12.1	14.81
Loading Phase	4				5				6			
H/D	1.5	2	2.5	3	1.5	2	2.5	3	1.5	2	2.5	3
F_S, mm	F	F	12.56	11.66	F	F	F	13.6	F	F	F	16.1
Enhancement ratio, %	-	-	-	7.16	-	-	-	-	-	-	-	-

Table 4.3 Footing settlement due to cyclic loading application, Series C

Loading Phase	1				2				3			
H/D	1.5	2	2.5	3	1.5	2	2.5	3	1.5	2	2.5	3
F_S, mm	7.72	6.98	6.72	6.2	8.74	7.76	7.48	6.98	9.74	8.66	8.3	7.72
Enhancement ratio, %	-	9.58	12.95	19.68	-	11.21	14.41	20.13	-	11.09	14.78	20.74
Loading Phase	4				5				6			
H/D	1.5	2	2.5	3	1.5	2	2.5	3	1.5	2	2.5	3
F_S, mm	10.88	9.74	9.36	8.74	13.42	11.38	10.38	9.9	F	14.72	12.14	10.4
Enhancement ratio, %	-	10.5	13.97	19.67	-	15.2	22.65	26.23	-	-	17.53	29.35
Loading Phase	7				8				9			
H/D	1.5	2	2.5	3	1.5	2	2.5	3	1.5	2	2.5	3
F_S, mm	F	F	F	11.64	F	F	F	12.84	F	F	F	14.54
Enhancement ratio %	-	-	-	-	-	-	-	-	-	-	-	-

Under the application of the 1st loading phase, the maximum footing settlement value was 9.9 mm (4.95%) for burial depth of *H/D*=1.5 in Series B, and 7.72 mm (3.86%) for the same burial depth in Series C. Increasing the pipe burial depth

led to reduction in the footing settlement value until it reached 8.36 mm (4.18%) and 6.2 mm (3.1%) with enhancement ratios of 15.55% and 19.68%, for a burial depth of *H/D*=3 in Series B and C, respectively. Increasing loading phase value increased the footing settlement value for all the burial depths, where the settlement rate rapidly increased at the shallowest burial depth declaring system failure approach. This behaviour dominated the tested systems response due to the increase of the applied loading phase value, until reaching the 6th loading phase, which was sustained at burial depth of *H/D*=3, in Series B, and the 9th loading phase, which was sustained at the same burial depth, in Series C.

Figure 4.22 illustrates normalised footing settlement to the pipe diameter at the end of the applied loading phases, with the burial depth increase for Series B and C with one layer and two layers of reinforcement respectively. It can be noted that at any loading phase the increase in the burial depth of the pipe provides a significant contribution in reducing the footing settlement. For example, at the 2nd loading phase in Series B, the footing settlement reached 11.98 mm (5.99%), 10.56 mm (5.28%), 9.74 mm (4.87%) and 9.32 mm (4.66%) at *H/D*=1.5, 2, 2.5 and 3 respectively. The enhancement ratio reached 11.85%, 18.69% and 22.2% at *H/D*=2, 2.5 and 3, compared with the case of *H/D*=1.5. It is obvious that the settlement rate was significantly reduced with the burial depth increase and after a burial depth of *H/D*=2.5, the settlement rate became slow with a difference in the enhancement ratio of only 3.5%. This indicates that the optimum burial depth of the pipe is at *H/D*=2.5, and there is no need to increase it.

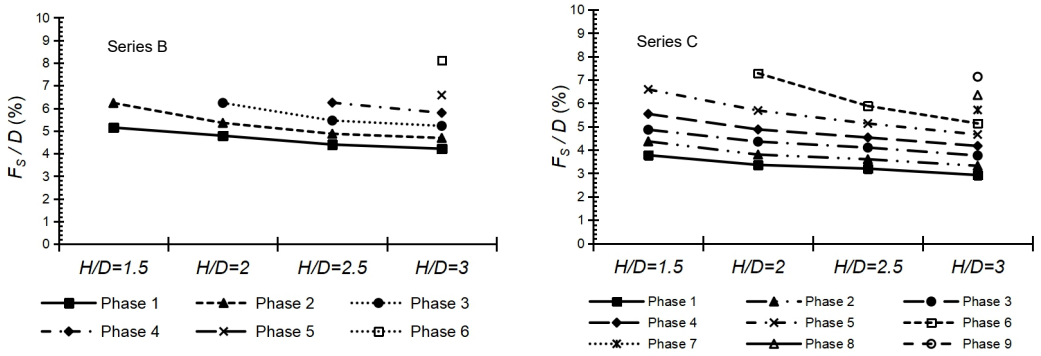

Figure 4.22 Footing settlement with loading phase increase

Data for the footing settlement in Series B and C are plotted against load phases to demonstrate the change in the settlement rate as cyclic loading progressed, as shown in Figure 4.23. As an example for system behaviour, the settlement rate increased from the 1st to the 2nd loading phases with 11.6%, and it significantly increased until it reached 23% from the 5th to the 6th phases at *H/D*=2, in Series C. This showed that the settlement rate was doubled. After this drastically increased settlement rate, the system could not sustain extra load phases and failure occurred. Similar patterns are observable at different *H/D* values. Consequently, at the same burial depth, the settlement rate increased slowly at the first loading phases and with further loading phases an increase in the settlement rate became faster and noticeable until failure occurred.

A maximum of three load phases were sustained in Series A for unreinforced sand, unlike Series B and C, where six and nine loading phases were sustained, respectively. The inclusion of reinforcing layers enabled the systems to sustain more load phases and slightly reduced footing settlement through enhancing the properties of the tested system, in particular its shearing resistance. The loads sustained by the tested systems in Series B and C were drastically increased compared with Series A. The trapped soil in-between the geogrid layer apertures created a passive earth resistance mechanism, by which the generated tensile stresses and strains were transferred from the soil to the reinforcing layers. When the number of reinforcing layers was increased, the trapped soil volume increased, and more applied load phases could be sustained.

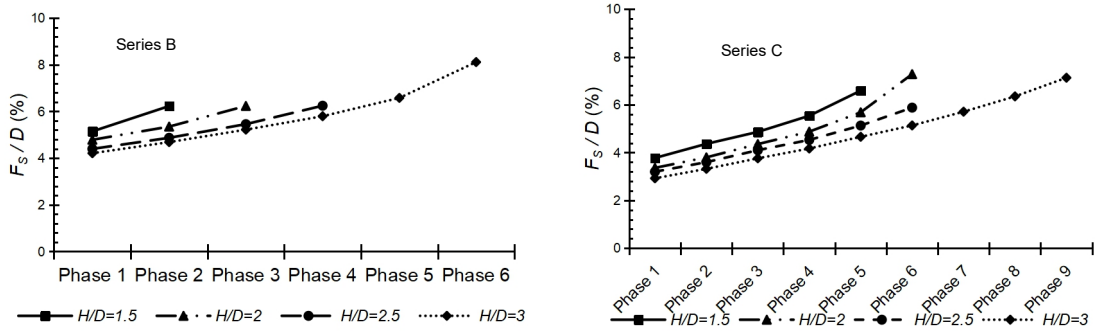

Figure 4.23 Change in footing settlement rate

4.4.2.2 Transferred pressure to the pipe

Figure 4.24 shows measured data for the soil pressure above the pipe crown at the mid-point of the pipe length. It is obvious that increasing the burial depth of the pipe significantly reduced the transferred pressure to the pipe, in addition, allowing pipe-soil system to sustain more load phases until reaching the failure point. These results show harmony between footing settlement and transferred pressure to the pipe.

Table 4.4 and Table 4.5 show the transferred pressure values to the pipe due to increasing cyclic loading phases under the variation of pipe burial depth for Series B and C, respectively.

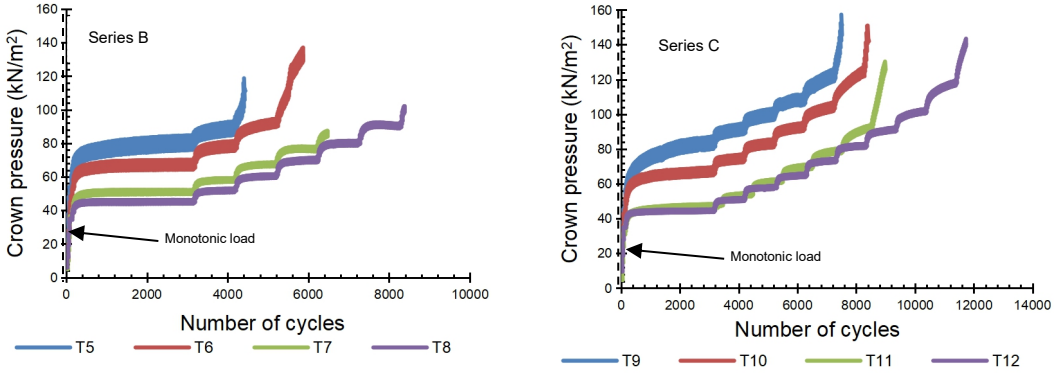

Figure 4.24 Transferred pressure to the pipe

Table 4.4 Transferred pressure due to cyclic loading application, Series B

Loading Phase	1				2				3			
H/D	1.5	2	2.5	3	1.5	2	2.5	3	1.5	2	2.5	3
Pressure, kPa	81	65.5	50.5	45.5	86.8	77	58.4	52.2	F	90.3	67.2	60.4
Enhancement ratio, %	-	15.9	35.2	42.7	-	11.3	32.7	39.8	-	-	24.5	33.1
Loading Phase	4				5				6			
H/D	1.5	2	2.5	3	1.5	2	2.5	3	1.5	2	2.5	3
Pressure, kPa	F	F	77.9	70.5	F	F	F	79.8	F	F	F	89.2
Enhancement ratio, %	-	-	-	9.5	-	-	-	-	-	-	-	-

Table 4.5 Transferred pressure due to cyclic loading application, Series C

Loading Phase	1				2				3			
H/D	1.5	2	2.5	3	1.5	2	2.5	3	1.5	2	2.5	3
Pressure, kPa	80.2	66	47.7	44.8	89.7	73.7	53.3	50.5	98.6	82.6	61.2	57.7
Enhancement ratio, %	-	17.7	40.5	44.1	-	17.8	40.6	43.7	-	16.2	37.9	41.5
Loading Phase	4				5				6			
H/D	1.5	2	2.5	3	1.5	2	2.5	3	1.5	2	2.5	3
Pressure, kPa	106.6	93.9	69.5	65	119.2	103.5	78.7	72.6	F	121.9	91.2	81.3
Enhancement ratio, %	-	11.9	34.8	39	-	13.2	34	39.1	-	-	25.2	33.3
Loading Phase	7				8				9			
H/D	1.5	2	2.5	3	1.5	2	2.5	3	1.5	2	2.5	3
Pressure, kPa	F	F	F	90.8	F	F	F	100.7	F	F	F	118.1
Enhancement ratio %	-	-	-	-	-	-	-	-	-	-	-	-

Under the application of the 1st loading phase, the maximum transferred pressure value to the pipe was 81 kN/m^2 for burial depth of *H/D*=1.5 in Series B,

and 80.2 kN/m^2 for the same burial depth in Series C. Increasing the pipe burial depth led to reduction in the transferred pressure value until it reached 45.5 kN/m^2 and 44.8 kN/m^2 with enhancement ratio of 42.7% and 44.1%, for burial depth of *H/D*=3 in Series B and C, respectively. Increasing loading phase value increased the transferred pressure value for all the burial depths, where the pressure rate rapidly increased at the shallowest burial depth declaring system failure approach. This behaviour dominated the tested systems response due to the increase of the applied loading phase value, until reaching the 6th loading phase, which was sustained at burial depth of *H/D*=3, in Series B, and the 9th loading phase, which was sustained at the same burial depth, in Series C.

Figure 4.25 illustrates the transferred pressure to the pipe at the end of the applied loading phases, with burial depth increase for Series B and C with one layer and two layers of reinforcement respectively.

It can be noted that at any loading phase the increase in the burial depth of the pipe provides a significant contribution in reducing the transferred pressure to the pipe. For example, at the 3rd loading phase in Series C, the transferred pressure reached 98.6 kN/m^2, 82.6 kN/m^2, 61.2 kN/m^2 and 57.7 kN/m^2 at *H/D*=1.5, 2, 2.5 and 3 respectively. The enhancement ratio reached 16.2%, 37.9% and 41.5% at *H/D*=2, 2.5 and 3, compared with the case of *H/D*=1.5. It is obvious that the pressure rate was significantly reduced with the burial depth increase and after a burial depth of *H/D*=2.5, the pressure rate became slow with a difference in the enhancement ratio of only 3.6%. This indicates that the optimum burial depth of the pipe is at *H/D*=2.5, which is identical to the optimum burial depth according to the footing settlement section.

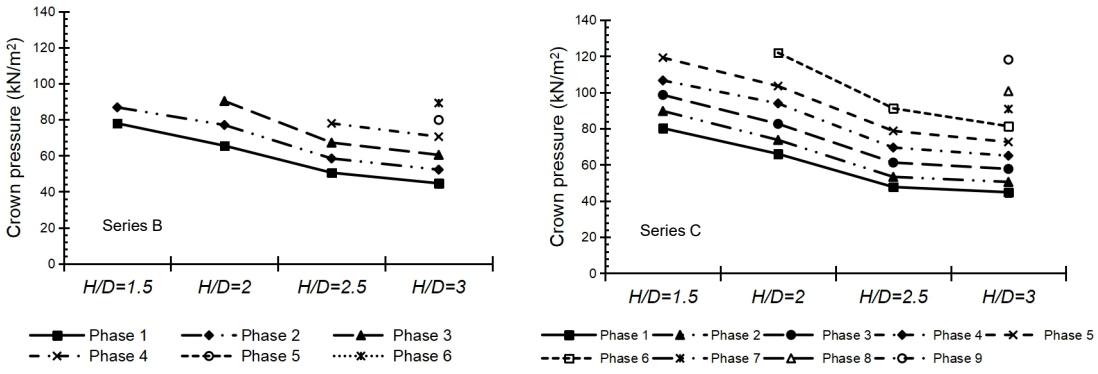

Figure 4.25 Transferred pressure to the pipe with loading phase increase

At the same pipe burial depth, the transferred pressure rate to the pipe is slow at the initial loading phases, and with loading phases increase, this rate is increased until failure occur, as illustrated in Figure 4.26. As an example for this behaviour, at *H/D*=2, in Series C, the pressure transfer rate increased from the 1st to the 2nd loading phases with 10.4%, and it significantly increased until it reached 15.1% from the 5th to the 6th phases. After this increased pressure transfer rate, the system could not sustain extra load phases and failure occurred. Similar patterns are observable at different *H/D* values. Consequently, at the same burial depth, the pressure transfer rate increased slowly at the first loading phases and with further loading phases an increase in the pressure transfer rate became faster and noticeable until failure occurred.

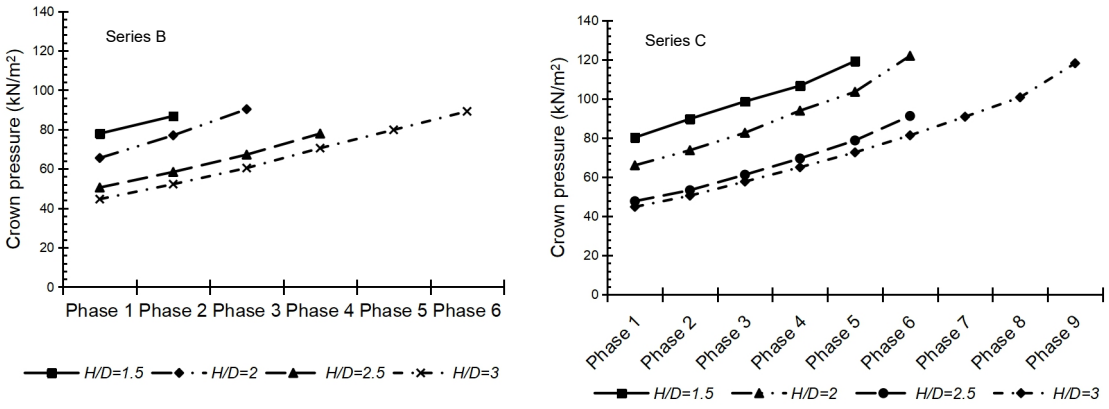

Figure 4.26 Change in transferred pressure rate

It is obvious that the inclusion of the reinforcing layers in the investigated soil-pipe systems enable these systems to sustain more loading phases compared with the unreinforced case. In the unreinforced systems, the application of loading phases generates tensile strain that forces the soil to move laterally, consequently, lower soil volume will be transferring the applied load to the pipe. In this case, higher pressure will affect the pipe leading to quicker system failure. The reinforcing layers inclusion allowed the creation of new composite material that has enhanced properties than the soil-pipe system alone. This composite material forced the soil to remain in its position even under the application of higher loading phases due to the generated passive earth resistance mechanism between the soil and the reinforcing layers, reinforcing layers membrane mechanism, in addition to soil arching.

4.4.2.3 Crown settlement

Normalised crown settlement, C_s/D, under variation of H/D is presented in Figure 4.27. It clearly illustrates that increasing the burial depth of the pipe has a great role in reducing settlement of pipe crown, as well as enabling the system to sustain more load phases until reaching the failure point.

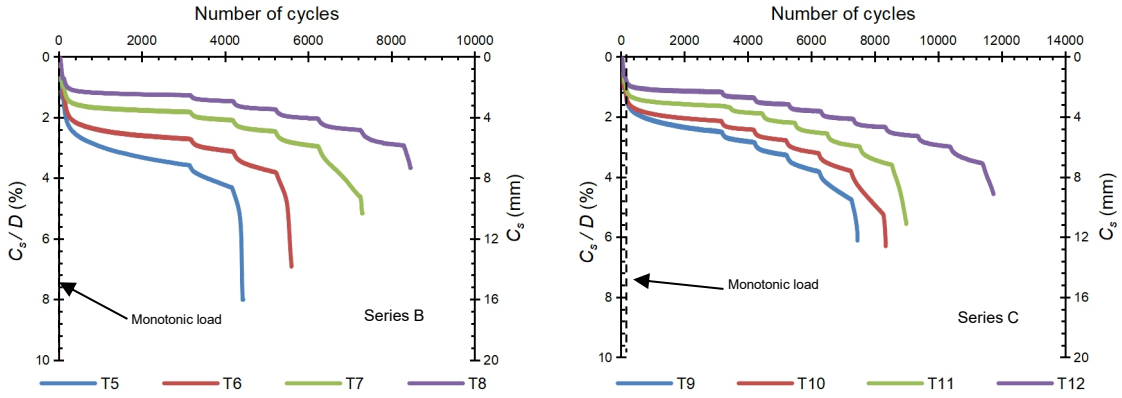

Figure 4.27 Crown settlement ratio against number of cycles

Table 4.6 and Table 4.7 show the crown settlement values due to increasing cyclic loading phases under the variation of pipe burial depth for Series B and C, respectively.

Table 4.6 Crown settlement due to cyclic loading application, Series B

Loading Phase	1				2				3			
H/D	1.5	2	2.5	3	1.5	2	2.5	3	1.5	2	2.5	3
C_S, mm	7.2	5.6	4	2.6	8.8	6.4	4.4	3	F	8	5	3.6
Enhancement ratio, %	-	22.2	44.4	63.9	-	27.3	50	65.9	-	-	37.5	55
Loading Phase	4				5				6			
H/D	1.5	2	2.5	3	1.5	2	2.5	3	1.5	2	2.5	3
C_S, mm	F	F	6.4	4.2	F	F	F	4.8	F	F	F	6.2
Enhancement ratio, %	-	-	-	34.4	-	-	-	-	-	-	-	-

Table 4.7 Crown settlement due to cyclic loading application, Series C

Loading Phase	1				2				3			
H/D	1.5	2	2.5	3	1.5	2	2.5	3	1.5	2	2.5	3
C_S, mm	5.2	4.4	3.4	2.4	6	5	4	2.8	6.8	5.6	4.4	3.2
Enhancement ratio, %	-	15.4	34.6	53.8	-	16.7	33.3	53.3	-	17.6	35.3	52.9
Loading Phase	4				5				6			
H/D	1.5	2	2.5	3	1.5	2	2.5	3	1.5	2	2.5	3
C_S, mm	8	6.6	5.2	3.8	9.8	7.8	6	4.2	F	10.6	7.4	4.8
Enhancement ratio, %	-	17.5	35	52.5	-	20.4	38.7	57.1	-	-	30.2	54.7
Loading Phase	7				8				9			
H/D	1.5	2	2.5	3	1.5	2	2.5	3	1.5	2	2.5	3
C_S, mm	F	F	F	5.4	F	F	F	6	F	F	F	7.2
Enhancement ratio %	-	-	-	-	-	-	-	-	-	-	-	-

Under the application of the 1st loading phase, the maximum crown settlement value was 7.2 mm (3.6%) for burial depth of H/D=1.5 in Series B, and 5.2 mm (2.6%) for the same burial depth in Series C. Increasing the pipe burial depth

led to reduction in the crown settlement value until it reached 2.6 mm (1.3%) and 2.4 mm (1.2%) with enhancement ratio of 63.9% and 53.8%, for burial depth of *H/D*=3 in Series B and C, respectively. Increasing loading phase value increased the crown settlement value for shallow burial depths, i.e. *H/D*=1.5 and 2, where the settlement rate rapidly increased and it controlled system failure. At higher burial depths, i.e. *H/D*=2.5 and 3, system failure was controlled by excessive footing settlement. This behaviour dominated the tested systems response due to the increase of the applied loading phase value, until reaching the 6th loading phase, which was sustained at burial depth of *H/D*=3, in Series B, and the 9th loading phase, which was sustained at the same burial depth, in Series C.

Figure 4.28 demonstrates normalised crown settlement to the pipe diameter at the end of the applied loading phases, with burial depth increase for Series B and C with one layer and two layers of reinforcement, respectively. It can be noted that at any loading phase the increase in the burial depth of the pipe provides a significant contribution in reducing the crown settlement. For example, at the 5th loading phase in Series C, the crown settlement reached 9.8 mm (4.9%), 7.8 mm (3.9%), 6 mm (3%) and 4.2 mm (2.1%) at *H/D*=1.5, 2, 2.5 and 3 respectively. The enhancement ratio reached 20.4%, 38.7% and 57.1% at *H/D*=2, 2.5 and 3, compared with the case of *H/D*=1.5.

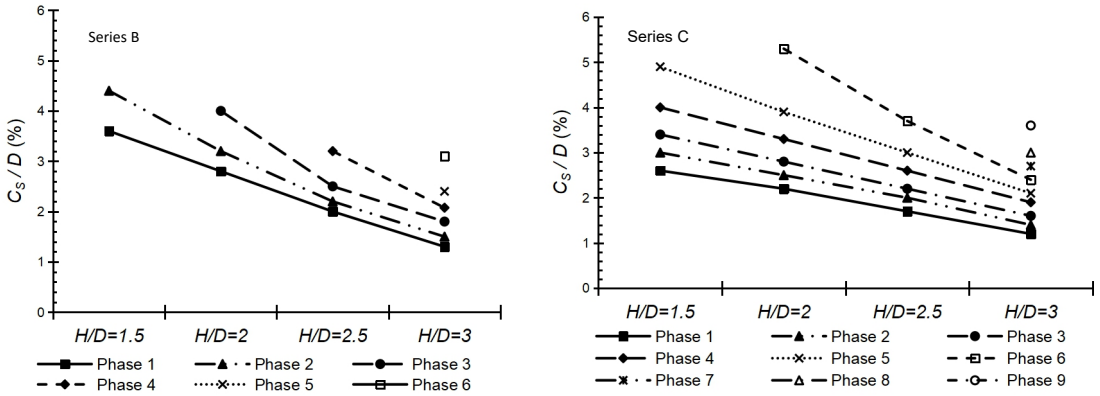

Figure 4.28 Crown settlement with loading phase increase

Data for the crown settlement in Series B and C are plotted against load phases to demonstrate the change in the settlement rate as cyclic loading progressed, as shown in Figure 4.29. It is obvious that the crown settlement rate at the same burial depth increased very slowly at the first loading phases, and with these

loading phases increase, the settlement rate starts to increase giving an indication to system failure approach. As an example for system behaviour, at *H/D*=2, in Series C, the crown settlement rate increased from the 1st to the 2nd loading phases with 12%, and it significantly increased until it reached 26.4% from the 5th to the 6th phases. This showed that the settlement rate was almost doubled. After this drastically increased settlement rate, the system could not sustain extra load phases and failure occurred. Similar patterns are observable at different *H/D* values. Consequently, at the same burial depth, the crown settlement rate increased slowly at the first loading phases and with further loading phases an increase in the settlement rate became faster and noticeable until failure occurred.

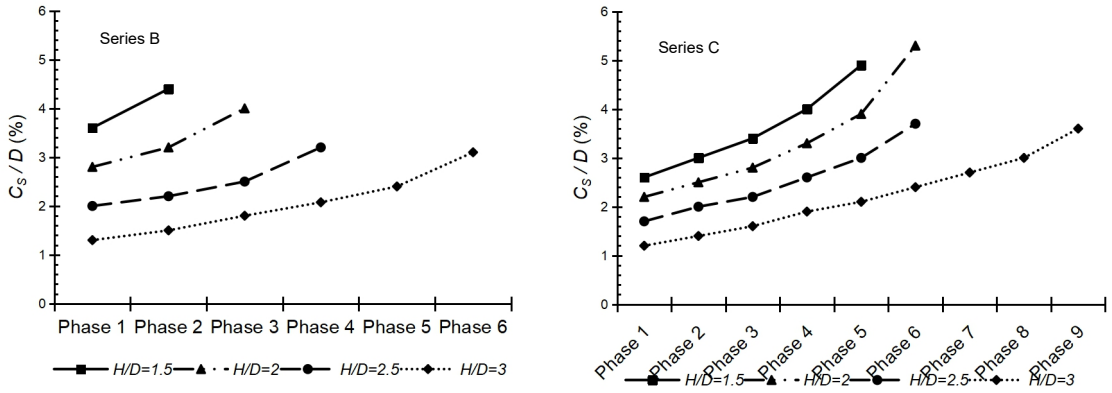

Figure 4.29 Change in crown settlement rate

It can be noted that the crown settlement in the unreinforced systems, i.e. Series A, is higher than its value in the reinforced systems, i.e. Series B and C. This can be attributed to the reduction in the transferred pressure to the pipe due to the inclusion of the reinforcing layers, which positively contributed in enhancing the system stability. The reduction in the transferred pressure to the pipe as well as the lateral support from the soil surrounding the pipe has vital influence on reducing its crown settlement. In both, reinforced and unreinforced systems, at shallow burial depths, i.e. *H/D*=1.5, crown settlement dominates the system stability, where higher-pressure value is transferred to it. At deep burial depths, i.e. *H/D*=3, footing response dominates the system stability, where lower pressure value is transferred to the pipe leading to insignificant crown settlement compared with the footing settlement.

4.4.2.4 Invert settlement

Normalised invert settlement, I_s/D, under variation of H/D is presented in Figure 4.30. It clearly illustrates that increasing the burial depth of the pipe has a great role in reducing settlement of pipe invert, as well as enabling the system to sustain more load phases until reaching the failure point. It is clear that the settlement value of the pipe invert is incomparable with the pipe crown or the footing settlement. However, it shows that the pipe burial depth increase has significant influence in controlling the system behaviour, where it reduced the pipe invert settlement value as occurred in the pipe crown and the footing settlement.

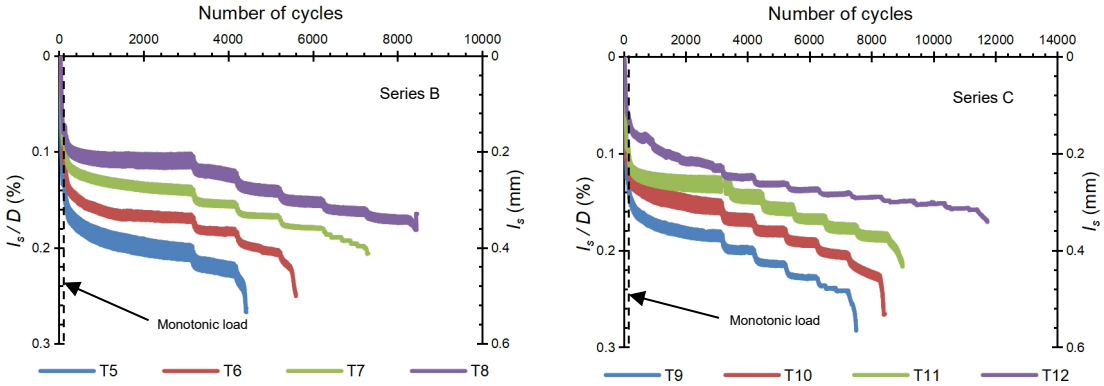

Figure 4.30 Invert settlement ratio against number of cycles

Table 4.8 and Table 4.9 show the invert settlement values due to increasing cyclic loading phases under the variation of pipe burial depth for Series B and C, respectively.

Table 4.8 Invert settlement due to cyclic loading application, Series B

Loading Phase	**1**				**2**				**3**			
H/D	1.5	2	2.5	3	1.5	2	2.5	3	1.5	2	2.5	3
I_S, mm	0.42	0.34	0.28	0.23	0.46	0.38	0.31	0.26	F	0.42	0.34	0.29
Enhancement ratio, %	-	19	33.3	45.2	-	17.4	39.1	43.5	-	-	19	31
Loading Phase	**4**				**5**				**6**			
H/D	1.5	2	2.5	3	1.5	2	2.5	3	1.5	2	2.5	3
I_S, mm	F	F	0.36	0.31	F	F	F	0.33	F	F	F	0.35
Enhancement ratio, %	-	-	-	13.9	-	-	-	-	-	-	-	-

Table 4.9 Invert settlement due to cyclic loading application, Series C

Loading Phase	**1**				**2**				**3**			
H/D	1.5	2	2.5	3	1.5	2	2.5	3	1.5	2	2.5	3
I_S, mm	0.38	0.33	0.28	0.24	0.41	0.35	0.3	0.25	0.44	0.37	0.32	0.26
Enhancement ratio, %	-	13.2	26.3	36.8	-	14.6	26.8	39	-	15.9	27.3	40.9
Loading Phase	**4**				**5**				**6**			
H/D	1.5	2	2.5	3	1.5	2	2.5	3	1.5	2	2.5	3
I_S, mm	0.46	0.39	0.34	0.28	0.48	0.42	0.36	0.29	F	0.46	0.38	0.3
Enhancement ratio, %	-	15.2	26.1	39.1	-	12.5	25	39.6	-	-	17.4	34.8
Loading Phase	**7**				**8**				**9**			
H/D	1.5	2	2.5	3	1.5	2	2.5	3	1.5	2	2.5	3
I_S, mm	F	F	F	0.3	F	F	F	0.31	F	F	F	0.32

Enhancement ratio %	-	-	-	-	-	-	-	-	-	-	-	-

Under the application of the 1st loading phase, the maximum invert settlement value was 0.42 mm for burial depth of *H/D*=1.5 in Series B, and 0.38 mm for the same burial depth in Series C. Increasing the pipe burial depth led to reduction in the invert settlement value until it reached 0.23 mm and 0.24 mm with enhancement ratio of 45.2% and 36.8%, for burial depth of *H/D*=3 in Series B and C, respectively. Increasing loading phase value increased the invert settlement value. It was noticed that the invert settlement rate was almost constant, where pipe deformation was dominated by its crown settlement. This behaviour dominated the tested systems response due to the increase of the applied loading phase value, until reaching the 6th loading phase, which was sustained at burial depth of *H/D*=3, in Series B, and the 9th loading phase, which was sustained at the same burial depth, in Series C.

Figure 4.31 illustrates normalised invert settlement to the pipe diameter at the end of the applied loading phases, with burial depth increase for Series B and C with one layer and two layers of reinforcement respectively.

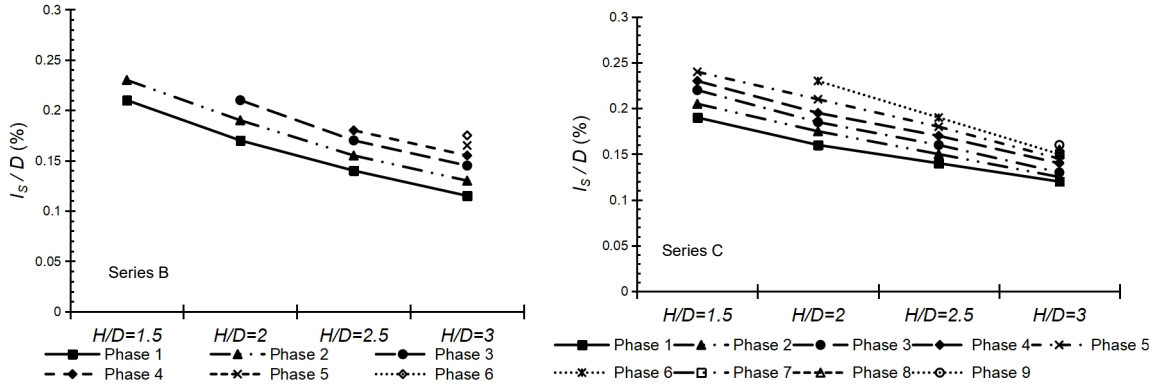

Figure 4.31 Invert settlement with loading phase increase

It is clear that at any loading phase the increase in the burial depth of the pipe provides a significant contribution in reducing the invert settlement. For example, at the 2nd loading phase in Series B, the invert settlement reached 0.46 mm, 0.38 mm, 0.31 mm and 0.26 mm at *H/D*=1.5, 2, 2.5 and 3 respectively. The enhancement ratio reached 17.4%, 39.1% and 43.5% at *H/D*=2, 2.5 and 3, compared with the case of *H/D*=1.5. It can be seen that the settlement rate was almost constant with the burial depth increase unlike the case of the footing settlement and the transferred pressure to the pipe. Consequently, according to

the findings of footing settlement and transfer pressure to the pipe, the optimum burial depth of the pipe is at *H/D*=2.5, and there is no need to increase it.

Figure 4.32 shows plotted data for the invert settlement in Series B and C against load phases to illustrate the change in the settlement rate as cyclic loading progressed. It can be noted that the invert settlement rate at the same burial depth increase almost constantly due to the increase in the applied loading cycles.

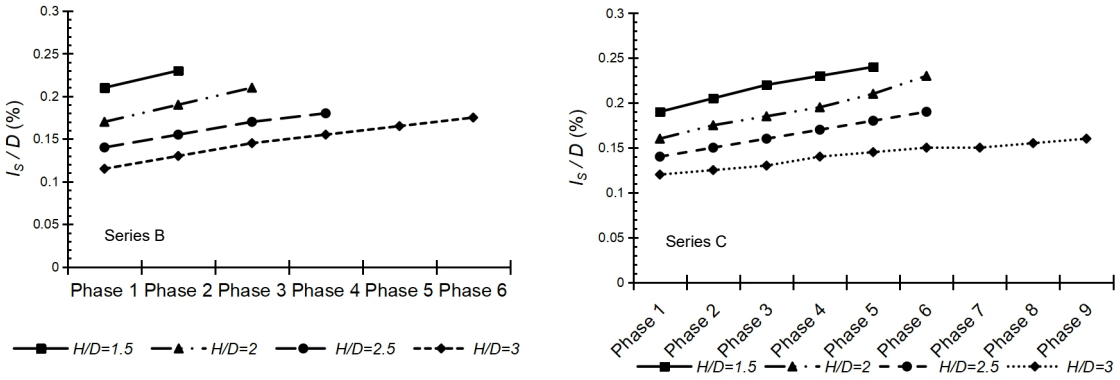

Figure 4.32 Change in invert settlement rate

It can be noted that the invert settlement in the unreinforced systems, i.e. Series A, is higher than its value in the reinforced systems, i.e. Series B and C. This can be attributed to the reduction in the transferred pressure to the pipe due to the inclusion of the reinforcing layers, which positively contributed in enhancing the system stability. In both, reinforced and unreinforced systems, invert settlement is reduced with the increase in the pipe burial depth. In addition, invert settlement has negligible contribution in system stability compared with crown settlement. Consequently, pipe deformation is governed by its crown deformation.

Generally, increasing the number of reinforcing layers led to a remarkable reduction in the crown deformation, which can be attributed to there being less pressure on the pipe crown. It is noted that in the unreinforced case, the pipe deformation value was higher than that in the reinforced case. The addition of the

reinforcing layers to the tested systems provided more stability to these systems. The reinforcing layer had the ability to restrain the generated tensile strains in

the soil. Consequently, the stress distribution differed above and underneath the reinforcing layer. The trapped soil in between the reinforcing layer apertures and the layer itself formed a stiff layer at which the generated stresses were redistributed. Therefore, the stresses transferred to the pipe were reduced, leading to a reduction in the pipe crown and invert deformation.

According to the findings of Figure 4.29 and Figure 4.32, it can be noted that the increase in the loading rate was slow at the initial loading phases, and with progression of loading phases, the settlement rate rapidly increased in the pipe until failure occurred. This indicated that the pipe started to settle as a whole body under small-applied load phases and, with later phases, the pipe significantly deformed changing its cross sectional shape until failure occurred, where the crown deformation dominated the overall deformation of the pipe. Despite the pipe deformation that occurred in Series B and C, the pipe was still practically in a usable condition, because the deformation led to a vertical diametric change of less than 5%.

4.4.2.5 Crown strain

The generated strain along the pipe crown due to the increase in the applied loading phases is illustrated in Figure 4.33. It should be noted that in all tests the generated strain along the pipe crown was compressive strain. The data show that with the increase in the burial depth of the pipe, the generated strain values along the crown were decreased.

Table 4.10 and Table 4.11 demonstrate the pipe crown compressive strain values due to increasing cyclic loading phases under the variation of pipe burial depth for Series B and C, respectively.

Figure 4.34 illustrates pipe crown strain at the end of the applied loading phases, with burial depth increase for Series B and C with one layer and two layers of reinforcement respectively.

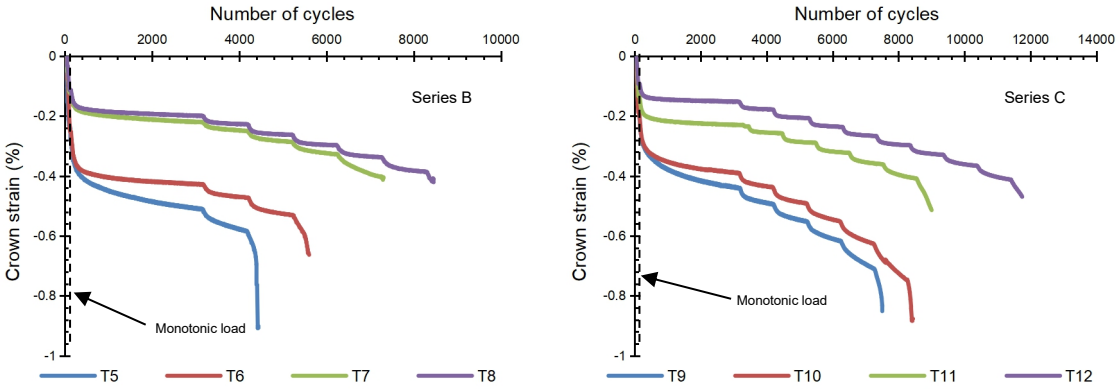

Figure 4.33 Pipe crown compressive strain against number of cycles

Table 4.10 Crown strain due to cyclic loading application, Series B

Loading Phase	1				2				3			
H/D	1.5	2	2.5	3	1.5	2	2.5	3	1.5	2	2.5	3
Strain, %	0.52	0.44	0.23	0.21	0.59	0.48	0.26	0.24	F	0.54	0.29	0.26
Enhancement ratio, %	-	15.4	55.8	59.6	-	18.6	55.9	59.3	-	-	46.3	51.9
Loading Phase	4				5				6			
H/D	1.5	2	2.5	3	1.5	2	2.5	3	1.5	2	2.5	3
Strain, %	F	F	0.33	0.3	F	F	F	0.34	F	F	F	0.39
Enhancement ratio, %	-	-	-	9.1	-	-	-	-	-	-	-	-

Table 4.11 Crown strain due to cyclic loading application, Series C

Loading Phase	1				2				3			
H/D	1.5	2	2.5	3	1.5	2	2.5	3	1.5	2	2.5	3
Strain, %	0.45	0.4	0.24	0.16	0.5	0.45	0.27	0.18	0.56	0.5	0.3	0.21
Enhancement ratio, %	-	11.1	46.7	64.4	-	10	46	64	-	10.7	46.4	62.5
Loading Phase	4				5				6			
H/D	1.5	2	2.5	3	1.5	2	2.5	3	1.5	2	2.5	3
Strain, %	0.62	0.56	0.33	0.24	0.71	0.63	0.37	0.27	F	0.75	0.41	0.3
Enhancement ratio, %	-	9.7	46.8	61.3	-	11.3	47.9	62	-	-	45.3	60
Loading Phase	7				8				9			
H/D	1.5	2	2.5	3	1.5	2	2.5	3	1.5	2	2.5	3
Strain, %	F	F	F	0.34	F	F	F	0.37	F	F	F	0.42
Enhancement ratio %	-	-	-	-	-	-	-	-	-	-	-	-

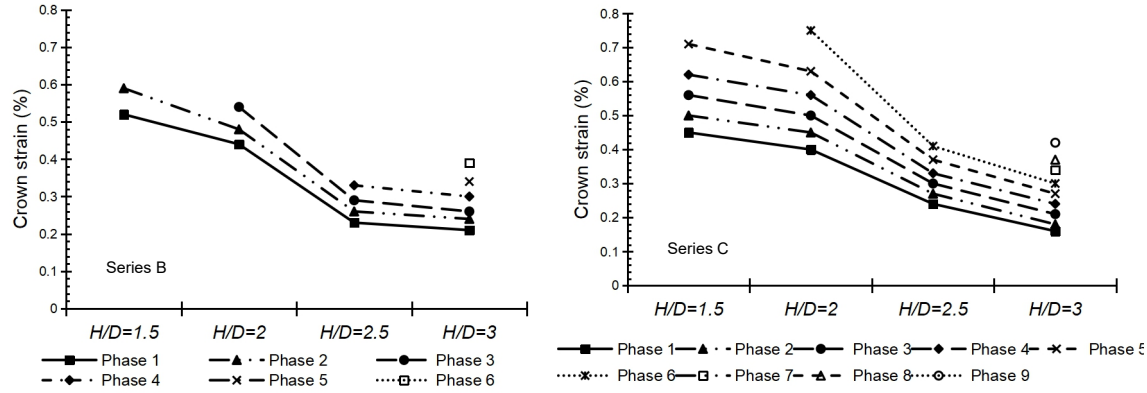

Figure 4.34 Pipe crown compressive strain with loading phase increase

It can be noted that at any loading phase the increase in the burial depth of the pipe provides a significant contribution in reducing the crown strain value. For example, at the 2nd loading phase in Series B, the crown strain reached 0.59%,

0.48%, 0.26% and 0.24% at *H/D*=1.5, 2, 2.5 and 3 respectively. The enhancement ratio reached 18.6%, 55.9% and 59.3% at *H/D*=2, 2.5 and 3, compared with the case of *H/D*=1.5. It is obvious that the strain rate was significantly reduced with the burial depth increase and after a burial depth of *H/D*=2.5, the strain rate became slow with a difference in the enhancement ratio of only 3.4%. This indicates that the optimum burial depth of the pipe is at *H/D*=2.5, and there is no need to increase it.

Data for the crown strain in Series B and C are plotted against load phases to demonstrate the change in the strain generation rate as cyclic loading progressed, as shown in Figure 4.35. It can be noted that the strain generation rate at shallow burial depths, i.e. *H/D*=1.5 and 2, increased almost constantly under the application of the initial loading cycles, and with loading cycles increase, the strain generation rate started to increase until failure occurred. This behaviour was obvious in Series C, where more loading phases were applied. As an example for system behaviour, at *H/D*=2, in Series C, the strain generation rate increased from the 1st to the 2nd loading phases with 11.1%, and it significantly increased until it reached 16% from the 5th to the 6th phases. On the other hand, at deep burial depths, i.e. *H/D*= 2.5 and 3, the strain generation rate was almost constant under the application of all the loading phases. As an example for system behaviour, at *H/D*=3, in Series C, the strain generation rate increase was 11.1%, 14.3%, 12.5%, 11.1%, 10%, 11.8%, 8.1% and 11.9% due to the transition from loading phase to the next one starting from the 1st to the 9th loading phases.

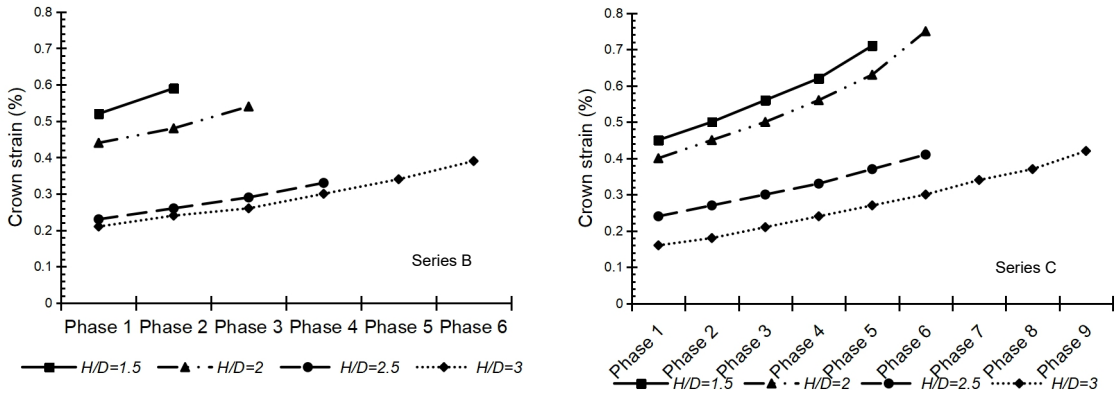

Figure 4.35 Change in pipe crown strain rate

As reported in the crown settlement section, the inclusion of the reinforcing layers reduced the stresses transferred to the pipe, regardless of the applied load phases and the burial depth. This led to a reduction in the pipe deformation. Consequently, the generated strain value of the pipe crown in the reinforced case was significantly lower than its value in the unreinforced case. In addition, at deep burial depths the transferred pressure to the pipe was significantly reduced because it was redistributed at the reinforcing layer level and then it was mitigated due to its transfer through the soil. This was the reason in the almost constant strain generation rate at deep burial depths. It is clear that the improvement in the system response is significantly increased at burial depth of *H/D*=2.5 and increasing this burial depth has minor contribution in enhancing the system stability.

4.4.2.6 Spring-line strain

The generated strain along the pipe spring-line due to the increase in the applied loading phases is illustrated in Figure 4.36. It should be noted that in all tests the generated strain along the pipe spring-line was tensile strain. The data show that with the increase in the burial depth of the pipe, the generated strain values decreased rapidly. It should be noted that the attached strain gauge along the pipe spring line at *H/D*=1.5 in Series B was broken, that is why its results are not reported.

Table 4.12 and Table 4.13 illustrate the pipe spring-line tensile strain values due to increasing cyclic loading phases under the variation of pipe burial depth for Series B and C, respectively.

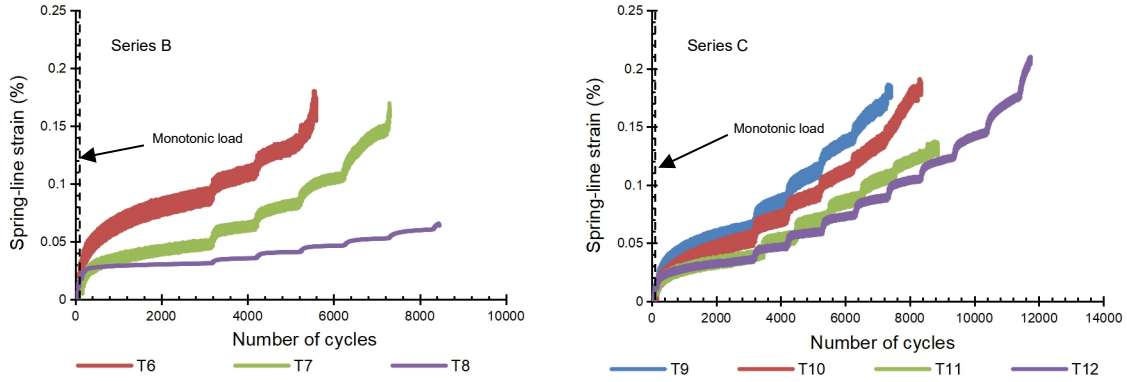

Figure 4.36 Pipe spring-line tensile strain against number of cycles

Table 4.12 Spring-line strain due to cyclic loading application, Series B

Loading Phase	1				2				3			
H/D	1.5	2	2.5	3	1.5	2	2.5	3	1.5	2	2.5	3
Strain, %	-	0.1	0.05	0.03	-	0.11	0.063	0.036	-	0.14	0.08	0.04
Enhancement ratio, %	-	-	50	70	-	-	42.7	67.3	-	-	42.8	71.4
Loading Phase	4				5				6			
H/D	1.5	2	2.5	3	1.5	2	2.5	3	1.5	2	2.5	3
Strain, %	-	F	0.11	0.047	-	F	F	0.053	-	F	F	0.07
Enhancement ratio, %	-	-	-	57.3	-	-	-	-	-	-	-	-

Table 4.13 Spring-line strain due to cyclic loading application, Series C

Loading Phase	1				2				3			
H/D	1.5	2	2.5	3	1.5	2	2.5	3	1.5	2	2.5	3
Strain, %	0.08	0.06	0.043	0.036	0.1	0.08	0.06	0.047	0.12	0.1	0.075	0.06
Enhancement ratio, %	-	25	46.25	55	-	20	40	53	-	16.7	37.5	50
Loading Phase	4				5				6			
H/D	1.5	2	2.5	3	1.5	2	2.5	3	1.5	2	2.5	3
Strain, %	0.14	0.115	0.09	0.074	0.17	0.14	0.108	0.09	F	0.18	0.135	0.108
Enhancement ratio, %	-	17.9	35.7	47.1	-	17.6	36.5	47.1	-	-	25	40
Loading Phase	7				8				9			
H/D	1.5	2	2.5	3	1.5	2	2.5	3	1.5	2	2.5	3
Strain, %	F	F	F	0.125	F	F	F	0.15	F	F	F	0.18
Enhancement ratio %	-	-	-	-	-	-	-	-	-	-	-	-

Figure 4.37 shows pipe spring-line strain at the end of the applied loading phases, with burial depth increase for Series B and C with one layer and two layers of reinforcement respectively.

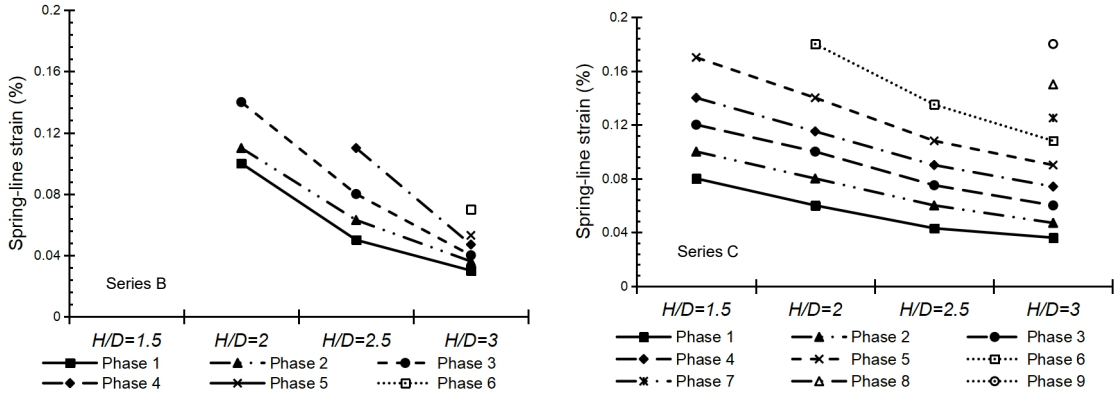

Figure 4.37 Pipe spring-line tensile strain with loading phase increase

It is clear that at any loading phase the increase in the burial depth of the pipe provides a significant contribution in reducing the spring-line strain value. For example, at the 5th loading phase in Series C, the spring-line strain reached 0.17%, 0.14%, 0.108% and 0.09% at *H/D*=1.5, 2, 2.5 and 3 respectively. The enhancement ratio reached 17.6%, 36.5% and 47.1% at *H/D*=2, 2.5 and 3, compared with the case of *H/D*=1.5. It is obvious that the strain rate was significantly reduced with the burial depth increase and after a burial depth of

H/D=2.5, the strain rate slightly decreased. This indicates that the optimum burial depth of the pipe is at *H/D*=2.5, and there is no need to increase it.

Data for the crown strain in Series B and C are plotted against load phases to demonstrate the change in the strain generation rate as cyclic loading progressed, as shown in Figure 4.38. It can be noted that the strain generation rate at the same burial depths, increased almost constantly under the application of the initial loading cycles, and with loading cycles increase, the strain generation rate started to increase until failure occurred. As an example for system behaviour, at *H/D*=3, in Series B, the strain generation rate increased from the 1st to the 2nd loading phases with 16.7%, and it significantly increased until it reached 24.3% from the 5th to the 6th phases. After this increased strain rate, the system could not sustain extra load phases and failure occurred. Similar patterns are observable at different *H/D* values. Consequently, at the same burial depth, the strain generation rate increased slowly at the first loading phases and with further loading phases an increase in the strain generation rate became faster and noticeable until failure occurred.

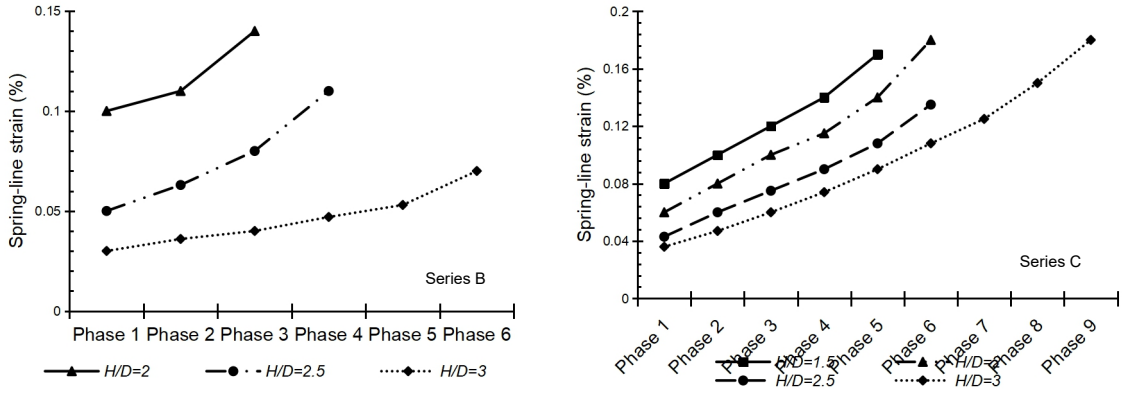

Figure 4.38 Change in pipe spring-line strain rate

The generated strain value of the pipe spring-line in the reinforced case was significantly lower than its value in the unreinforced case. On the other hand, the provided lateral support from the soil located at the pipe sides contributed to reducing the spring-line strain in particular at higher burial depths. This could be attributed to the increase in the vertical soil pressure at higher burial depths, which would lead to an increase in the generated horizontal pressure, enhancing the provided lateral support to the pipe particularly at its spring-line.

Generally, as reported in the crown and invert deformation sections, the inclusion of the reinforcing layers reduced the stresses transferred to the pipe, regardless of the applied load phases and the burial depth. This led to a reduction in the pipe deformation. Consequently, the generated strain value of the pipe crown and spring-lines in the reinforced case were significantly lower than its value in the unreinforced case. In addition, in both the reinforced and unreinforced investigated systems, measurements of tensile strain were recorded along the pipe spring-line. This indicated that the pipe deformation at the spring-line was outside, where horizontal diametric strain increasingly occurred.

4.4.2.7 Reinforcing layers strain

Due to the applied load to the tested systems, strains were generated in the soil, which may have led to soil failure. Inclusion of reinforcing layers played a significant role in preventing such failure. The inclusion of the reinforcing layers in soil creates a new composite material that can sustain higher load profiles and provide more system stability. It was noticed that in all tests the generated strain in the reinforcing layers was tensile strain.

4.4.2.7.1 Reinforcing layers strain in Series B

The generated strain in the reinforcing layers due to the increase in the applied loading phases is illustrated in Figure 4.39. Results illustrate that increasing the burial depth of the pipe had a negative effect on the generated strain in the reinforcing layers, where the reinforcing layer strain increased with the pipe burial depth increase. Figure 4.40 shows reinforcing layer strain at the end of the applied loading phases, with burial depth increase for Series B with one reinforcing layer. Table 4.14 shows the reinforcing layer tensile strain values due to increasing cyclic loading phases under the variation of pipe burial depth for Series B.

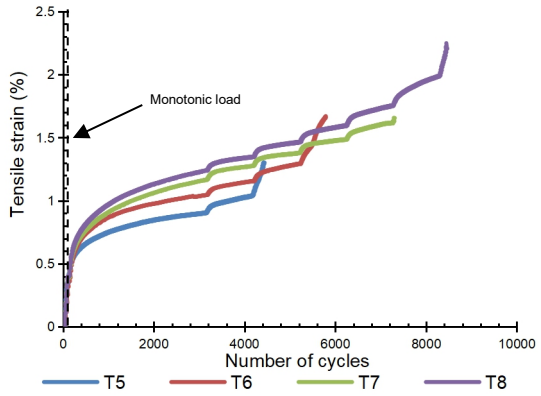

Figure 4.39 Generated strain in the reinforcing layer, Series B

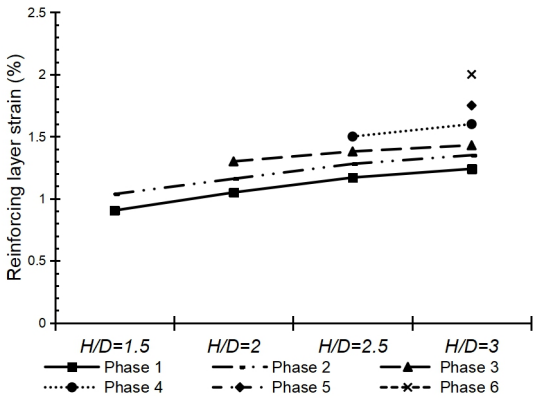

Figure 4.40 Reinforcing layer tensile strain with loading phase increase

Table 4.14 Reinforcing layer strain due to cyclic loading application, Series B

Loading Phase	**1**				**2**				**3**			
H/D	1.5	2	2.5	3	1.5	2	2.5	3	1.5	2	2.5	3
Strain, %	0.905	1.05	1.17	1.24	1.037	1.16	1.28	1.35	F	1.3	1.38	1.43
Increase ratio, %	-	16	29.3	37	-	11.9	23.4	30.2	-	-	6.2	10
Loading Phase	**4**				**5**				**6**			
H/D	1.5	2	2.5	3	1.5	2	2.5	3	1.5	2	2.5	3
Strain, %	F	F	1.5	1.6	F	F	F	1.75	F	F	F	2
Increase ratio, %	-	-	-	6.7	-	-	-	-	-	-	-	-

It is obvious that at the same loading phase, the increase of the pipe burial depth has significant contribution in increasing the generated strain in the reinforcing layer until reaching burial depth of *H/D*=2.5. After this burial depth, the generated strain rate in the reinforcing layer significantly decreases seeking stability. For example, at the 2nd loading phase, the strain generation rate was 11.9% due to increasing the burial depth from *H/D*=1.5 to 2, and 10.3% due to increasing the burial depth from *H/D*=2 to 2.5. Once the burial depth reached *H/D*=3, the strain generation rate was decreased where its value was 5.5%, which is approximately half the previously mentioned rates. This gives an indication that the optimum burial depth of the pipe is *H/D*=2.5.

With the pipe burial depth increase, its contribution in the system stability started to decrease slowly, where its deformation and the generated strain in it significantly decreased, and the reinforcing layer started gradually to dominate the system stability, where the generated strain in the reinforcing layers started to increase gradually. After *H/D*=2.5, the contribution of the reinforcing layer was no longer dependent on the burial depth of the pipe, while the pipe contribution was significantly reduced, and the increase in the sustained strain by the reinforcing layer was significantly decreased. As illustrated in the crown

settlement of the unreinforced system section, the distance between the pipe and the soil surface was divided into two zones, upper and lower zones. The pipe itself reinforced the lower zone, and contributed to the upper zone stability. When the spacing between the soil surface and the pipe exceeded a certain limit, i.e. *H/D*=2.5, the stability of the upper zone was primarily dominated by the soil properties, as shown in Figure 4.4. Here comes the role of the reinforcing layer, which has a minor contribution in the upper zone stability when it is close to the pipe and vice versa.

In the beginning of the first loading phase application, in particular the first 300 cycles, the generated strain rate was very fast, and with the increase in cycles, this rate started to decrease, as indicated in Figure 4.39. This phenomenon was caused by the slack effect that occurred in the reinforcing layer (Chenggang, 2004; Sieira et al., 2009; Tran et al., 2013).

In general, the slack effect can be defined as, in accordance with the extensible nature of the reinforcing layer, it experiences stretching and deformation before contributing to the system stability. At low settlement levels, the friction generated between soil particles and the reinforcing layer initiates the stretching process to the layer, where its contribution during this stage is minimum. With the increase in settlement, the stretching process gradually decreases until the layer is fully stretched, declaring the end of the slack effect of the layer (Abu-Farsakh et al., 2013). Once the slack effect ended, the strain generation rate decreased. It was also obvious that the strain increased gradually according to the applied load, and once the system started to fail, the strain value increased rapidly, regardless of the burial depth of the pipe or the applied load phases. Visual inspection of the reinforcing layers demonstrated that no damage occurred in the layers, where only permanent deformation occurred. Consequently, the increase in the pipe burial depth enhanced the reinforced system stability, however, the spacing between the reinforcing layer and the pipe increased, leading to more generated tensile strain to be resisted by the reinforcing layer.

4.4.2.7.2 Reinforcing layers strain in Series C

The generated strain in the reinforcing layers due to the increase in the applied loading phases is illustrated in Figure 4.41. As illustrated in Series B, increasing the burial depth of the pipe had a negative effect on the generated strain in the reinforcing layers, where the reinforcing layer strain increased with the pipe burial depth increase. In addition, the generated strain in the lower reinforcing layer is usually higher than the generated strain in the upper reinforcing layer.

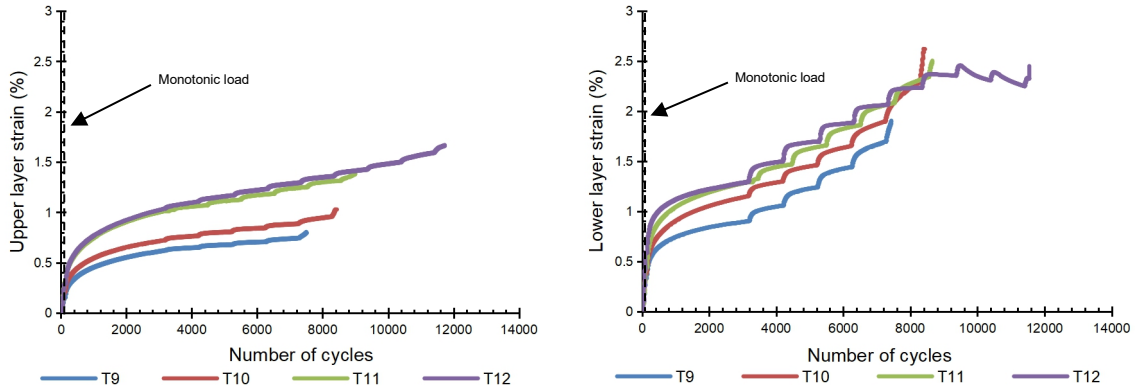

Figure 4.41 Generated strain in the reinforcing layer, Series C

Table 4.15 and Table 4.16 show upper and lower reinforcing layer tensile strain values, respectively, due to increasing cyclic loading phases under the variation of pipe burial depth for Series C.

Table 4.15 Upper layer strain due to cyclic loading application, Series C

Loading Phase	1				2				3			
H/D	1.5	2	2.5	3	1.5	2	2.5	3	1.5	2	2.5	3
Strain, %	0.62	0.72	1.02	1.04	0.65	0.76	1.07	1.1	0.68	0.8	1.125	1.17
Increase ratio, %	-	16.1	64.5	67.7	-	16.9	64.6	69.2	-	17.6	65.4	72.1
Loading Phase	4				5				6			
H/D	1.5	2	2.5	3	1.5	2	2.5	3	1.5	2	2.5	3
Strain, %	0.71	0.85	1.186	1.23	0.74	0.88	1.25	1.29	F	0.96	1.31	1.36
Increase ratio, %	-	18.3	67	73.2	-	18.9	68.9	74.3	-	-	36.5	41.7
Loading Phase	7				8				9			
H/D	1.5	2	2.5	3	1.5	2	2.5	3	1.5	2	2.5	3
Strain, %	F	F	F	1.42	F	F	F	1.5	F	F	F	1.59
Increase ratio, %	-	-	-	-	-	-	-	-	-	-	-	-

Table 4.16 Lower layer strain due to cyclic loading application, Series C

Loading Phase	1				2				3			
H/D	1.5	2	2.5	3	1.5	2	2.5	3	1.5	2	2.5	3
Strain, %	0.9	1.16	1.29	1.3	1.054	1.3	1.465	1.5	1.24	1.46	1.66	1.7
Increase ratio, %	-	28.9	43.3	44.4	-	23.34	39	42.3	-	17.7	33.9	37.1
Loading Phase	4				5				6			
H/D	1.5	2	2.5	3	1.5	2	2.5	3	1.5	2	2.5	3
Strain, %	1.44	1.67	1.86	1.9	1.7	1.9	2.08	2.063	F	2.2	2.33	2.23
Increase ratio, %	-	16	29.2	31.9	-	11.8	22.4	21.4	-	-	5.9	1.4
Loading Phase	7				8				9			
H/D	1.5	2	2.5	3	1.5	2	2.5	3	1.5	2	2.5	3
Strain, %	F	F	F	2.35	F	F	F	2.38	F	F	F	2.34
Increase ratio, %	-	-	-	-	-	-	-	-	-	-	-	-

Figure 4.42 shows reinforcing layer strain at the end of the applied loading phases, with burial depth increase for Series C with two reinforcing layer.

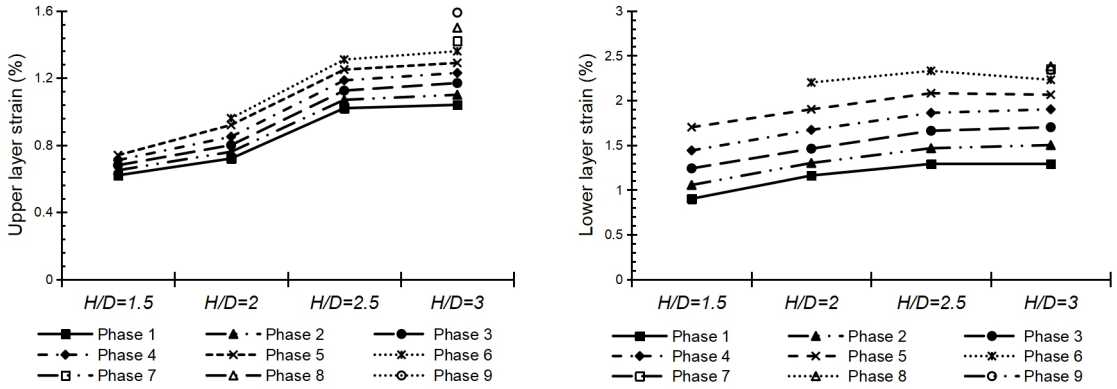

Figure 4.42 Reinforcing layer tensile strain with loading phase increase

It is obvious that at the same loading phase, the increase of the pipe burial depth has significant contribution in increasing the generated strain in the upper and lower reinforcing layers until reaching burial depth of *H/D*=2.5. After this burial depth, the generated strain rate in the reinforcing layers significantly decreases seeking stability, which is similar to the reinforcing layers behaviour in Series B. For example, at the 3rd loading phase in the lower reinforcing layer, the strain generation rate was 17.7% due to increasing the burial depth from *H/D*=1.5 to 2, and 13.7% due to increasing the burial depth from *H/D*=2 to 2.5.

Once the burial depth reached *H/D*=3, the strain generation rate was significantly decreased where its value was 2.4%. This gives an indication that the optimum burial depth of the pipe is *H/D*=2.5.

In Series C, a two layer reinforced system resisted the generated tensile strain in the soil, and the contribution of each of them depended on the generated tensile force as well as the deformation that occurred in each of them. At the end of all tests, the soil was excavated carefully and the deformation and deformed shape of the reinforcing layers were inspected. It was always recorded that the upper layer underwent large deformation in comparison with that recorded for the lower reinforcing layer. This could be attributed to there being less soil cover above the upper reinforcing layer leading to transferring higher-pressure value to it, where the pressure was redistributed and lower pressure value was transferred to the lower reinforcing layer. However, Figure 4.43 illustrates that, generally the lower layer sustained more strain than the upper layer did, regardless of the pipe burial depth or the loading phase, which is in good agreement with Jones and Cooper (2005). The maximum recorded strain in the lower layer was higher than the strain in the upper layer by 56.47%, 43.6%, 56.2% and 67.9% for *H/D*=1.5, 2, 2.5 and 3, respectively.

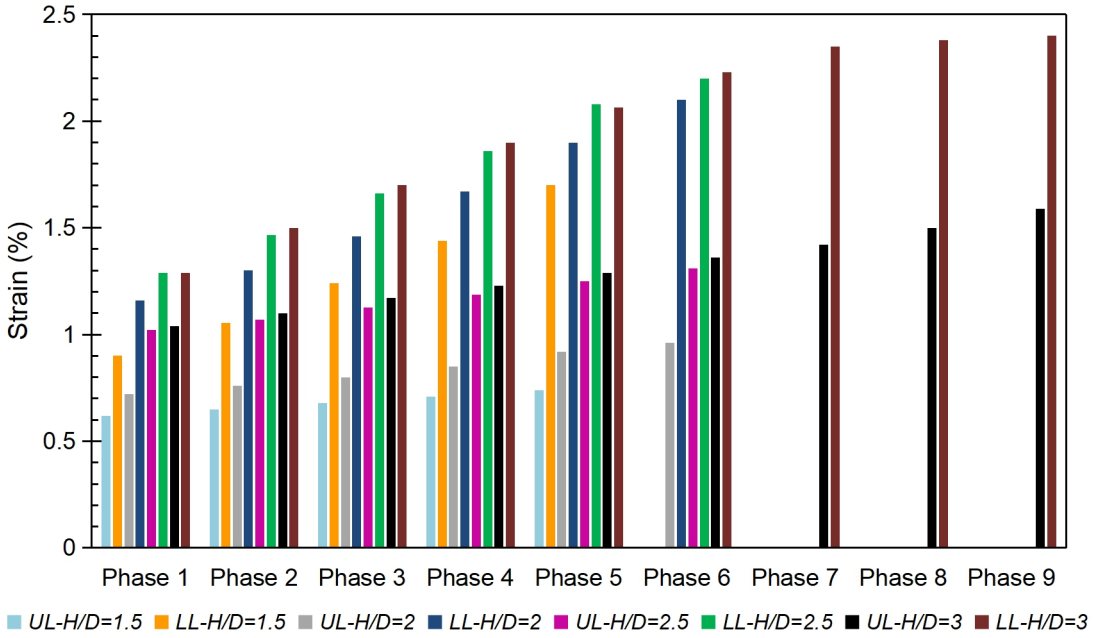

Figure 4.43 Difference between upper and lower layers strain, Series C

This indicated that, the two reinforcing layers and the trapped sand layer between them formed a stiff platform, which behaved as if it was a flexible reinforced slab as illustrated in Figure 4.44, which was in good agreement with Mohamed (2010). In this case, the reinforced zone was subjected to bending stresses that highly affected the lower reinforcing layer. In addition, once the load was applied to this platform, its lower surface suffered tensile strain unlike its upper surface, which might have suffered compressive strain. Consequently, the generated tensile strain in the lower reinforcing layer governed the behaviour and stability of the whole system. In addition, the reinforcing layer failure was governed by the sustained strain value rather than its deformation. It was taken into consideration that there was no prolonged loading; consequently, no creep deformation was observed in the reinforcing layers.

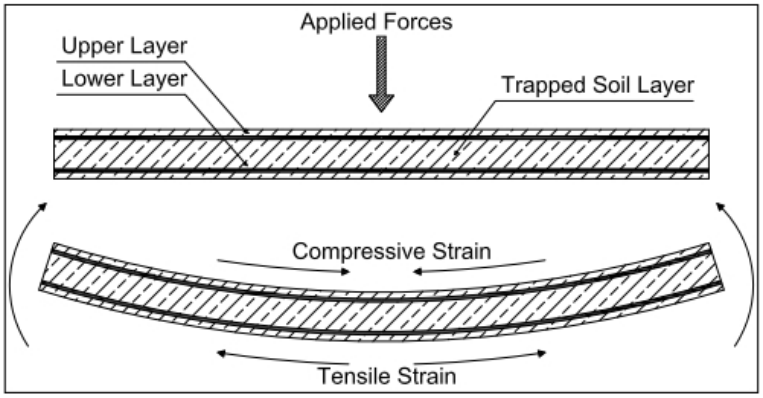

Figure 4.44 Formed stiff platform

4.5 Repeatability

To assure the accuracy of research findings, one of the tests was repeated two times under the same conditions, as illustrated in Series D. The same loading profile is applied in the two tests. Figure 4.45 illustrates the footing and the pipe crown settlement, comparisons. Careful inspection of results of multiple tests illustrated that, there is a very slight variation between the results of the two tests, where variation reached at most 1.75% in footing settlement and 2.2% in crown settlement. It is obvious that the variation ratio increased once failure occurred. This provides confidence in the reliability of the testing technique and that the attained results are of high quality and accurate.

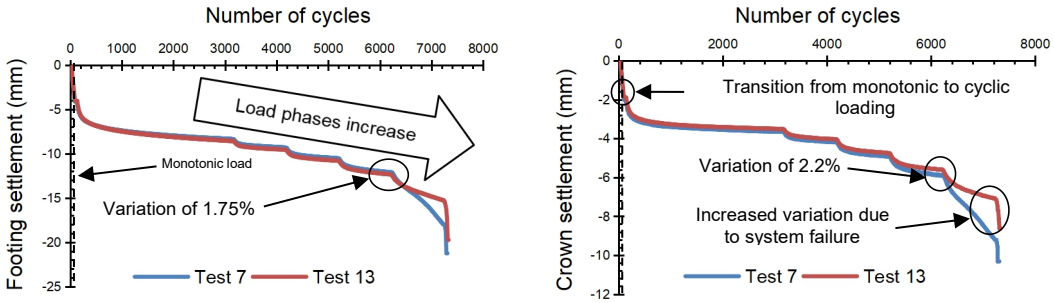

Figure 4.45 Footing and crown settlement comparisons

4.6 Summary

In this chapter, large-scale physical models were tested to investigate the behaviour of buried flexible pipes in unreinforced and geogrid-reinforced soil under the application of incrementally increasing cyclic loading. Four different burial depths were investigated, in unreinforced, and one-layer and two-layer geogrid-reinforced soil. Based on the findings of these physical models, the following conclusions can be drawn;

1- The maximum rate and value of the generated settlement and strain in each tested system occurred during the first 300 cycles of the first loading phase, and with further loading cycles, these rates and values decreased significantly until reaching an almost stable state, at the end of the loading phase. Application of further loading phases resulted in similar behaviour with significantly reduced values.

2- The transition from one loading phase to another led to an increase in the recorded settlements and strains, but with a significantly reduced scale compared with the initial loading phase. This was not the case in the loading phase, where system failure occurred.

3- In the unreinforced case, increasing the burial depth of the pipe had a significant contribution in decreasing the pipe deformation and strain, and it has situational contribution to the footing settlement.

4- In the unreinforced case, after burial depth of H/D=2.5, the footing settlement started to increase compared with lower burial depths due to the enhanced degree of soil densification which allows more volume to the footing to settle in. Moreover, the pipe contribution in enhancing the system stability is significantly reduced, where it was too far from the

upper soil zone. The results suggest that the behaviour of the whole system relied on pipe location, where it could provide stability according to its stiffness.

5- In the reinforced case, increasing the burial depth of the pipe had a significant contribution in decreasing the pipe deformation and strain in addition to the footing settlement. The existence of the reinforcing layers forces the soil to remain in its position under the generated tensile strains as a result of the passive earth resistance mechanism generation between the reinforcing layers and the trapped soil in between its apertures. This action plays a great role in decreasing the footing settlement even at deep burial depths.

6- The increase in the loading cycle number led to a soil densification process, which had significant contribution in reducing the deformation rate of the pipe. The densification process allowed the formation of stiffer soil around the pipe, which provided more lateral support to the pipe leading to reduction in the pipe deformation. The reduced pipe deformation significantly contributed in decreasing the generated strain in the pipe crown and spring-line.

7- The inclusion of the reinforcing layers created a new composite material, which had enhanced properties in comparison with the soil alone. This material had the ability to sustain more loading phases, and provide more protection to the buried pipe.

8- The inclusion of the reinforcing layers had significant contribution in decreasing the generated deformation and strain in the pipe.

9- At the initial loading phases, where the applied load was relatively small, the pipe tended to settle as a whole body with an almost constant settlement rate along its crown and invert. Once the value of the loading phases increased, the crown deformation rate significantly increased compared with the invert increase rate, leading to distortion in the pipe original circular cross-sectional shape.

10- Although sand beds prepared in this experimental investigation were dense, the new formed shape of the pipe cross section after applying loading phases was elliptical.

11- In the case of using multiple-reinforcing layers, the generated strain in the lower layer was always the highest. However, the settlement of the upper layer was remarkably higher than that of the lower layer. The formed flexible slab governed this behaviour. This slab was subjected to bending stresses; consequently, it suffered tensile and compressive strains along its lower and upper surfaces, respectively.

CHAPTER 5

BEHAVIOUR EVALUATION OF BURIED RIGID PIPES

5.1 Introduction

Rigid pipes have been used for a long time in various engineering purposes, e.g. minerals transfer, because of their high circumferential and flexural stiffness. They can resist several types of loading profiles, where insignificant deformation occurs unlike the generated strain, which causes cracks in its walls. Because of the recent worldwide expansion, new roads and buildings could be built over already existing infrastructures, which would apply additional loads and stresses threatening their safety. In this chapter, fully instrumented laboratory tests were conducted to investigate the behaviour of buried concrete pipes in unreinforced and geogrid-reinforced sand beds, where incrementally increasing cyclic loading was applied, which represented different vehicle capacities or load increase with passing time.

5.2 System components

The systems investigated in this chapter were prepared using three main components:

1- Silica sand (beds and backfill).
2- Geogrid reinforcing layers (Tensar *SS20*).
3- Rigid concrete pipes (cast in laboratory).

The influence of the pipe burial depth variation relative to its diameter, *H/D*, and the number of the inserted geogrid-reinforcing layers in the backfill cover above the pipe was investigated. A total of 10 tests were experimentally performed and discussed. An illustrative schematical diagram describing the tested systems is shown in Figure 3.16-B.

Concrete pipes of 230 mm outer diameter, 14 mm wall thickness and 990 mm length were cast in the laboratory. A thickness difference of 1 mm at most, was measured in the concrete pipe due to the corrugation of the mould tubes.

5.3 Loading profile

The applied loading profile to the investigated systems in this chapter is similar to that adopted in Chapter 4, however; the value of the monotonic loading was not the same. To determine a realistic value for the monotonic loading, the behaviour of a buried concrete pipe in unreinforced sand bed was investigated, as presented in Figure 5.1.

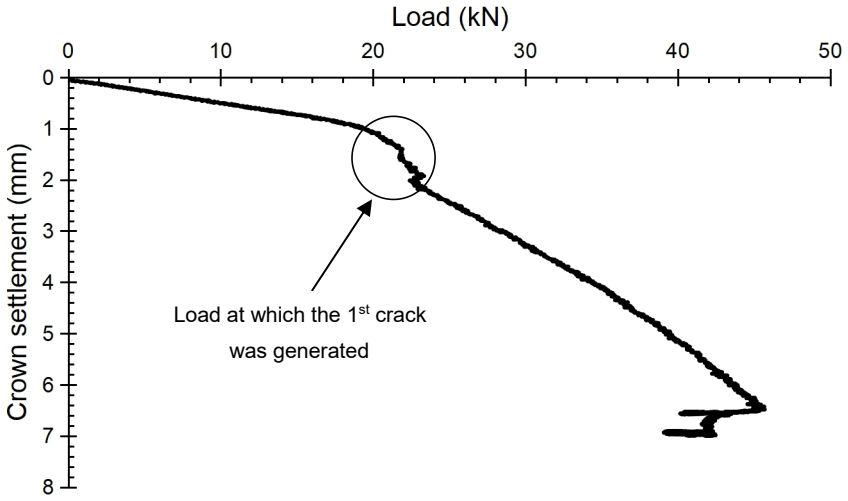

Figure 5.1 Deformation of the crown of the concrete pipe

The monotonic load amplitude was chosen to be less than the failure load to ensure that no cracks were formed in the pipe before applying cyclic loading phases, where its value was 13 kN. Figure 5.2 illustrated the applied loading profile, where its values are presented in Table 5.1.

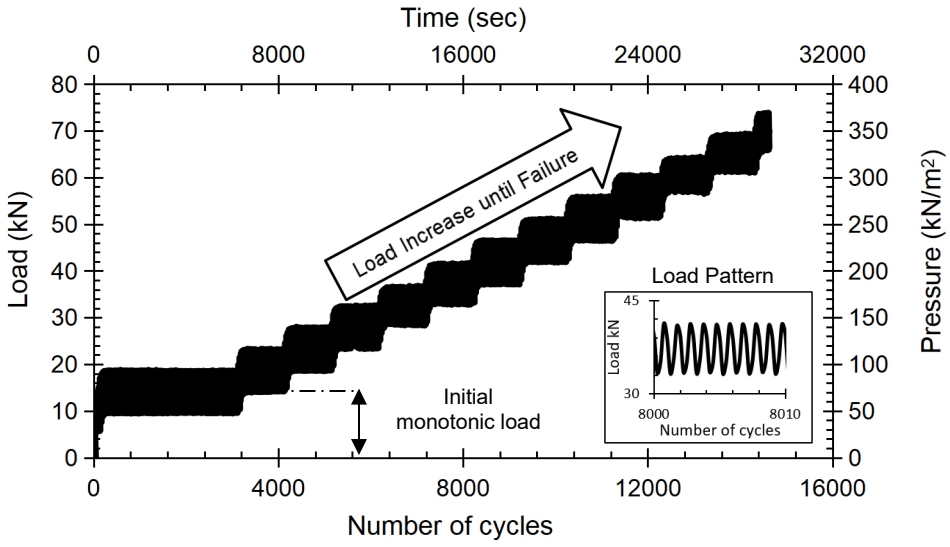

Figure 5.2 Applied loading profile

Table 5.1 Value of the applied cyclic loading phases

Test series			Load phase	Mean load (kN)	Load range (kN)		Amplitude (kN)
					Min.	Max.	
Series C	Series B	Series A	Phase 1	13	8	18	5
			Phase 2	18	13	23	5
			Phase 3	23	18	28	5
			Phase 4	28	23	33	5
			Phase 5	33	28	38	5
			Phase 6	38	33	43	5
			Phase 7	43	38	48	5
			Phase 8	48	43	53	5
			Phase 9	53	48	58	5
			Phase 10	58	53	63	5
			Phase 11	63	58	68	5
			Phase 12	68	63	73	5

5.4 Results and discussions

In this section, the influences of pipe burial depth and number of reinforcing layers on the behaviour of unreinforced and geogrid-reinforced systems were assessed and discussed. Measurements of footing and pipe deformation, pipe and reinforcement generated strain as well as transferred pressure to the pipe crown are presented and discussed. The followed testing scheme in this chapter is illustrated in Table 3.10. It should be noted that the settlement of the pipe and footing is presented as a normalised ratio of the pipe diameter.

5.4.1 Unreinforced case

Series A of the testing scheme examined the contribution of *H/D* variation on the behaviour of buried rigid pipes in unreinforced sand. The tested systems sustained a maximum of five loading phases, as illustrated in Table 5.1, until failure occurred.

5.4.1.1 Footing settlement

The variation of the footing settlement ratio, F_s/D, with the number of loading cycles was presented in Figure 5.3. It is clear that increasing the burial depth of the pipe reduced the settlement of the footing. In addition, increasing the burial depth allowed the pipe-soil system to sustain more load phases until reaching the failure point.

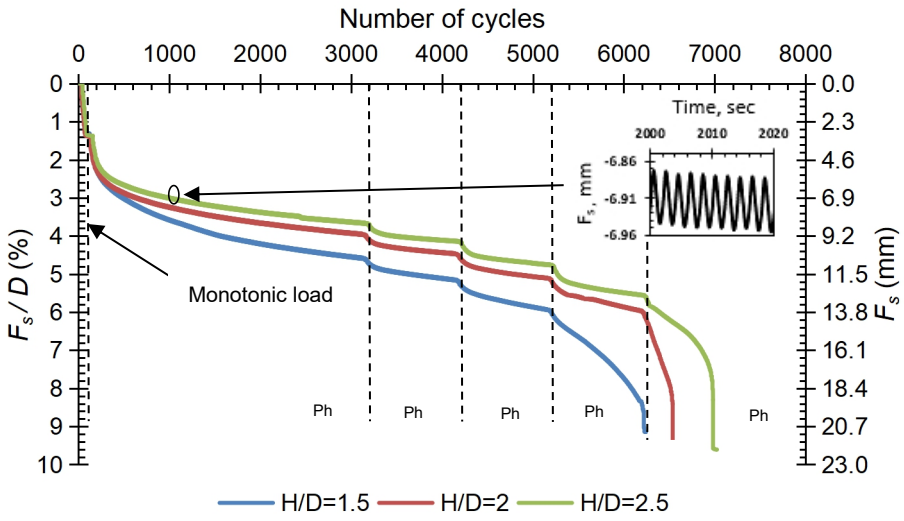

Figure 5.3 Footing settlement ratio against number of cycles

It was observed that during the application of the monotonic loading, footing settlement at the three burial depths was approximately equal, where insignificant variation in the normalised footing settlement value, F_s/D, was observed, where it approximately equalled 1.33%. Under the application of the 1st loading phase, footing settlement increased, where it reached its maximum increasing rate during the 1st 300 cycles, where slight footing settlement variation was observed between the three burial depths. The normalised footing settlement was 2.74%, 2.66% and 2.48% for *H/D*=1.5, 2 and 2.5, respectively. With applying further loading cycles, the footing settlement difference between the three tests became more obvious. The maximum footing settlement occurred at *H/D*=1.5, i.e. T1, where the normalised footing settlement value reached 4.7%. With the increase of the burial depth, the footing settlement rate and values were reduced, where its normalised value reached 4.1% and 3.8%, with enhancement ratios of 12.77% and 19.15%, at *H/D*=2 and 2.5 respectively. With the increase in the applied loading phases, the systems kept the same behaviour with slight increase in the settlement rate in T2 and T3, and significant increase in T1, until reaching the 3rd loading phase. At the 3rd loading phase, normalised footing settlement value reached 6.13% at *H/D*=1.5, and system failure occurred after this phase as illustrated in Figure 5.3. The increase in the burial depths in the other two systems, T2 and T3, enabled them to sustain more loading phases, where the normalised settlement value was 5.2% and 4.9%, respectively at the end of the 4th loading phase. Due to the

application of the 5th loading phase, excessive footing settlement occurred in T2 and T3, declaring systems failure. It was noticed that after the 1st loading phase, settlement difference between each constitutive loading phases was constant, in particular at *H/D*=2 and 2.5. This could be attributed to the pipe itself, where it behaved as a system support, which attracted applied loads while suffering small deformation. Sudden significant increase in the settlement difference was observed once the pipe fail to attract applied loads, i.e. cracks were formed.

Figure 5.4 illustrated normalised footing settlement at the end of each loading phase due to the variation of the burial depth of the pipe.

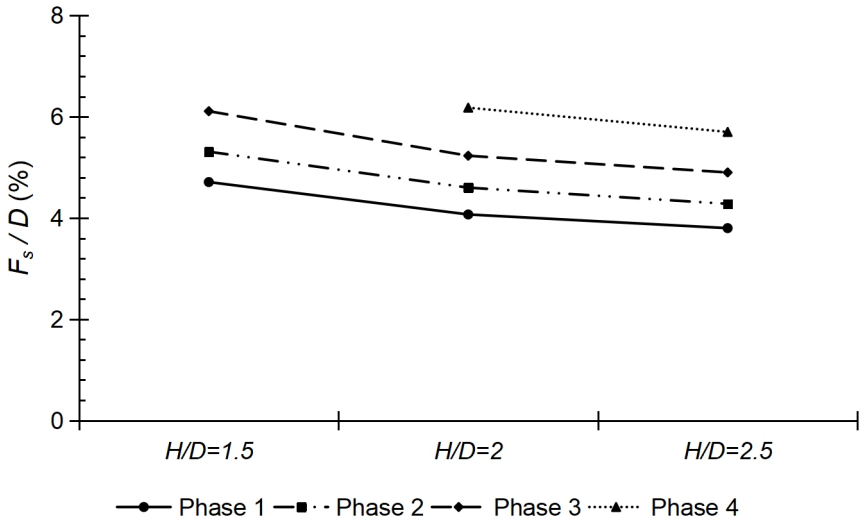

Figure 5.4 Normalised footing settlement at the end of load phases

It is obvious that the reduction in the footing settlement is governed by the increase in the pipe burial depth, regardless of the value of the applied cyclic load. The results suggested that a *H/D*=2 was an optimum value for the system behaviour. This can be attributed to the reduction in the settlement rate at burial depth of *H/D*=2.

5.4.1.2 Hysteresis response of the footing settlement

Due to the application of cyclic loading, footing settlement varied during loading and unloading stages of the loading cycles. With the progression of loading cycles, soil particles were reorganized and realigned seeking equilibrium, which led to an enhanced degree of soil packing, and the footing settlement showed a hysteresis behaviour.

Figure 5.5-A illustrated the hysteresis response of the footing settlement under the applied loading profile, at *H/D*=2.

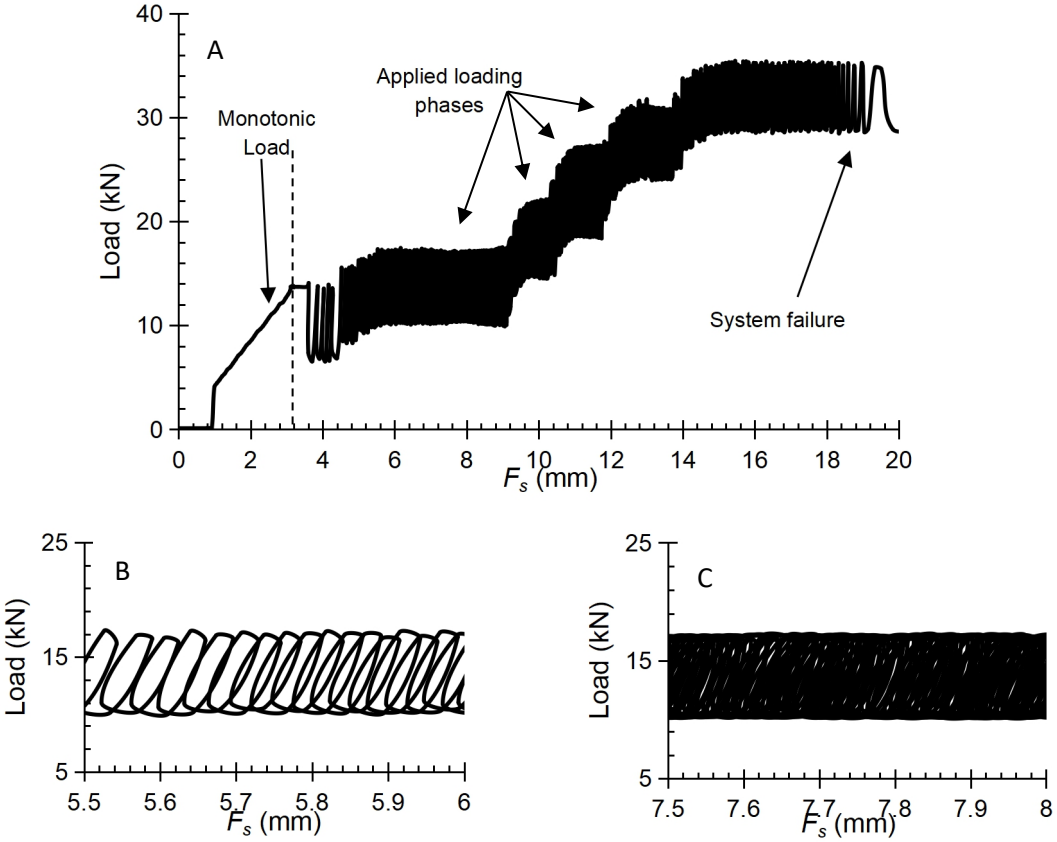

Figure 5.5 Hysteresis response of the footing settlement at *H/D*=2
A: Overall response. B: Response at initial stages. C: Response under increased cycles

This illustrated the densification effect on the footing settlement due to the increase in the number of loading cycles. In the initial loading cycles, Figure 5.5-B, for example, 0.5 mm of the footing settlement required approximately 17 loading cycles to occur, however, with the increase in loading cycles, the same settlement value required a significantly larger number of the applied loading cycles to occur, as shown in Figure 5.5-C. It is obvious that the settlement rate was significantly reduced with the increase in the number of loading cycles. With the increase in the loading phases, the settlement rate started to increase once more declaring system failure. This illustrated that the soil densification played a significant role in the system stability. It should be noted that the initial portion of Figure 5.5-A illustrated footing settlement due its own weight. In

addition, to reach the exact value of the applied cyclic loading amplitude, the hydraulic actuator required approximately 100 seconds.

5.4.1.3 Transferred pressure to the pipe

Figure 5.6 demonstrated measured data for the soil pressure above the pipe crown at the mid-point of the pipe length.

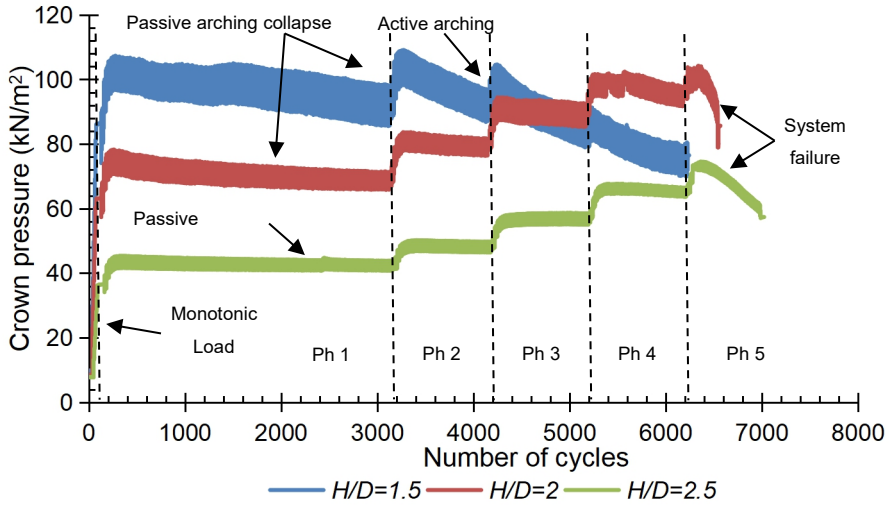

Figure 5.6 Transferred pressure to the pipe against number of cycles

In T1, where *H/D*=1.5, under the application of the monotonic loading step, pressure value of 86 kPa was recorded above the crown of the pipe, where 65 kPa was applied to the footing. With the application of the 1st cyclic loading phase, the pressure value increased until reaching 106 kPa at the 300 cycle, where 90 kPa was applied to the footing. The increase in the recorded pressure values over the crown can be attributed to the generated passive arching mechanism, which attracted generated pressure over the adjacent soil portions surrounding the soil prism above the pipe. In addition, since the pipe is close to the footing, it interacted with the slip surfaces, which led to direct transfer of pressure to the crown, which would weaken the resistance of the pipe to external loading.

At this stage, hair cracks were visually observed along the invert and the crown of the pipe, which led to collapse in the passive arching mechanism. Consequently, recorded pressure value over the crown of the pipe decreased to be 103 kPa at the 600 cycle. In between the 600 and the 1500 loading cycles, pressure values were almost of constant value. With applying further loading

cycles, recorded pressure value decreased again, where it reached 97.5 kPa at the end of the 1st loading phase with a reduction rate of 5.3%, and the crack became more obvious. It was an obvious sign that the pipe ability to attract pressure was reduced due to cracks formation, and the dominating passive arching mechanism is gradually collapsing. The pressure reduction rate was determined based on change of pressure values between particular number of loading cycles. During the 2nd loading phase, pressure value increased to be 108 kPa at the 300 cycle as a result of the increase of the applied pressure value to the footing, where it was 115 kPa. At the end of the 2nd loading phase, pressure value decreased to be 96 kPa with a reduction rate of 11.1%, without any change in the pressure behaviour such as that observed during the 1st loading phase. It should be noted that a sudden significant decrease of the rate and value of the pressure curve on the pipe occurred, which could be considered as a clear sign that the passive arching mechanism was collapsed and turning the pressure transfer mechanism into an active one. This behaviour was continued during the 3rd loading phase with more deterioration in the pressure reduction rate, until system failed during the 4th loading phase.

In T2, the recorded pressure value due to the application of the monotonic loading was less than that applied to the footing by 3.1%. In addition, the recorded pressure value above the crown of the pipe at the 300 cycle was 76.7 kPa, whereas it was 90 kPa at the footing, which indicated a decrease in the transferred pressure to the crown with 14.8%, despite the formation of a passive arching mechanism. Unlike visual observations of T1, no hair cracks were generated at the 300th cycle of the 1st loading phase, despite a slight reduction of pressure value along the crown of the pipe that was observed between the 300th and the final loading cycles of the 1st loading phase, where the reduction rate was 7%. This slight reduction in the measured pressure illustrated a slight collapse in the passive arching mechanism. With applying further loading phases, recorded pressure value above the crown was increased until the 300 cycle of each phase, and then it almost remained constant until reaching the end of this phase. This behaviour continued until system failure. It should be noted that with the increase in the burial depth of the pipe, the volume of the interacted soil in load mitigation between the footing and the pipe was increased.

This was the reason in the formation of load mitigation mechanism, which positively contributed in reducing the transferred pressure value to the pipe.

It was observed that the behaviour of pressure transfer in T3 was similar to that observed in T2, except the pressure transfer during 1st loading phase, where pressure value was almost constant during this phase. In addition, the measured pressure values during the applied loading profile was lower than those captured in T2. This can be attributed to the enhanced contribution of the load mitigation mechanism due to the increase in the existing volume of soil between the pipe and the footing, which enabled the passive arching mechanism to maintain its strength.

In general, the applied load on the footing led to the formation of differential settlement between the immediate soil beneath the footing and the adjacent soil portions. This differential settlement caused the generation of shear stresses between these soil zones, which can be defined as an arching effect (Terzaghi and Peck, 1967). The used pipe in this investigation is a rigid one, consequently it had high ability to attract the applied load to the system, since it had higher stiffness than the soil, and it behaved as a support for the system. This led to the formation of passive arching mechanism (Young and Trott, 1984; Peter et al., 2018). The transferred pressure to the pipe was the summation of two mechanisms, namely i. passive arching and ii. load mitigation. At lower burial depths, i.e. T1, the negative contribution of the passive arching mechanism controlled the transferred pressure value, where lower soil layer was allowed to interact in the load mitigation mechanism, decreasing its contribution. That is why rapid cracks were formed in T1. On the contrary, at higher burial depths, i.e. T2 and T3, the positive contribution of the load mitigation mechanism dominated the system, where increased soil layer was allowed to interact in the pressure mitigation above the pipe leading to a reduction of measured pressure at the pipe crown, which is in a good match with the findings of Arockiasamy et al. (2006) and Rakitin and Xu (2013). This led to the formation of bearable tensile strain, where no cracks were formed at the initial loading phases. It was obvious that system failure initiation could be predicted from the sharp inclination of the pressure curve, where an increased tensile strain formed cracks in the pipe, which weakened its ability to bear additional loads.

5.4.1.4 Crown settlement

Normalised crown settlements, C_s/D, under the variation of H/D were presented in Figure 5.7. Results clearly illustrated that distinctive relationships were obtained as a function of burial depth. Increasing the burial depth of the pipe had a great role in reducing the settlement of the pipe crown, as well as enabling the system to sustain more load phases.

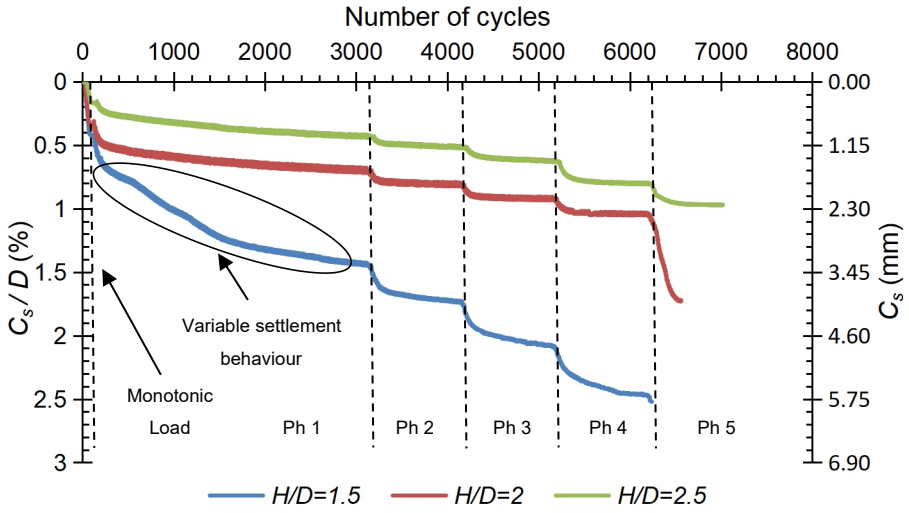

Figure 5.7 Crown deformation ratio against number of cycles

Crown settlement in T1, during the application of the monotonic loading and the 1st loading phase was an ideal reflection to the measured pressure above the crown. Because of the application of the monotonic loading, crown settlement occurred, where its normalised value was 0.43%. Once the 1st loading phase was applied, rapid increased rate of 39.4% in the crown settlement occurred until reaching the 300 cycle, where the normalised settlement value was 0.71%, and hair crack was visually observed. Since the measured pressure above the crown of the pipe was reduced in between the 300 and the 600 cycles, it was noticed that the crown settlement rate was decreased to be 14%, where the normalised settlement value was 0.826% at the 600 cycle.

At this loading cycle, constant pressure value was measured above the crown until reaching the 1500 cycle. As a result, crown settlement rate increased again with a rate of 32.8%, where its normalised value was 1.23% at the 1500 cycle. Until the end of the 1st loading phase, measured pressure value was reduced, consequently, crown settlement rate decreased with 15.7%, where normalised settlement value was 1.46%. With applying further loading phases, it was

noticed that the crown settlement rate rapidly increased during the first 300 cycles of each loading phase, and this rate was significantly decreased with further loading cycles, because of the measured reduction in the transferred pressure to the crown of the pipe, where the normalised settlement value was 2.1% at the end of the 3rd loading phase. With the application of the 4th loading phase, system failure occurred due to excessive footing settlement, as shown in Figure 5.3.

With the increase of the burial depth, T2 and T3, the crown settlement rate and values were reduced, where its normalised values reached 0.75% and 0.478%, with enhancement ratios of 48.6% and 67.26%, for *H/D*=2 and 2.5, respectively, at the end of the 1st loading phase compared with the case of *H/D*=1.5. With the increase in the applied loading phases values, the systems kept the same behaviour with slightly increasing settlement rate, where normalised settlement values were 0.97% and 0.83% for *H/D*=2 and 2.5, respectively, at the end of the 4th loading phase. With the application of the 5th loading phase, T2 and T3 failed due to excessive footing settlement.

Data illustrated that the crown settlement value and rate at shallow burial depths were significantly higher than those measured at deeper burial depths. This can be attributed to the minor contribution of the shallow soil cover in mitigating the transferred pressure to the pipe.

Figure 5.8 illustrated the normalised settlement of the pipe crown at the end of each loading phase with the increase in the burial depth.

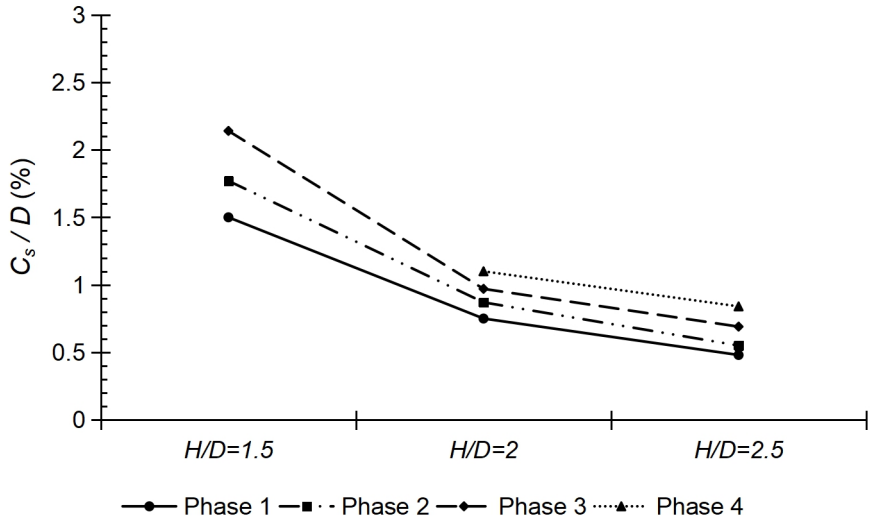

Figure 5.8 Normalised crown settlement at the end of load phases

It is clear that, at the same loading phase, increasing the burial depth reduced the pipe crown settlement, where the settlement slope was reduced, which could be attributed to the positive contribution of the improved load mitigation mechanism, however a full passive arching mechanism was generated (Aqoub et al., 2018). According to the results, the contribution of load mitigation mechanism is higher than the passive arching one at deep burial depths.

5.4.1.5 Invert settlement

Normalised invert settlement, I_S/D, under the variation of H/D was illustrated in Figure 5.9.

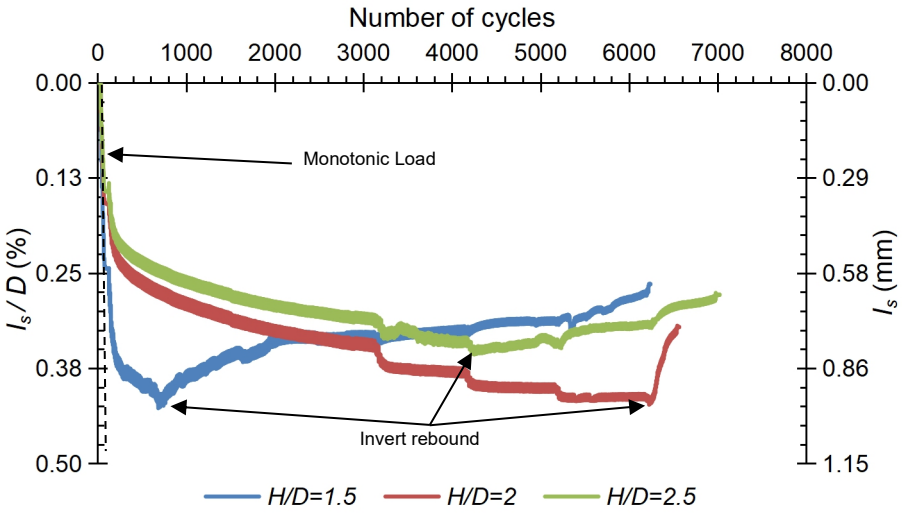

Figure 5.9 Invert settlement ratio against number of cycles

It is clear that under the application of loading phases, the pipe invert settled until reaching certain value, which was dependent upon the pipe burial depth and the applied loading phase. There after a rebound in the invert movement was observed as clearly indicated in Figure 5.9.

Invert settlement in T1 was varied according to the transferred pressure to the crown of the pipe, where the pressure was transferred to the pipe invert through its walls. During the application of the monotonic loading, invert settled where its normalised value was 0.24%. During the 1st cyclic loading phase, the invert settlement behaviour was changed. It was observed that the invert rapidly settled with a rate of 38.5% until reaching the 300 cycle, where the normalised settlement value was 0.39%.

At this stage, hair crack was visually observed along the inner invert, consequently measured transferred pressure to the pipe crown gradually started to decrease. This led to the reduction in the invert settlement rate, where it decreased with a rate of 5.8% until reaching the 600 cycle. In between the 300 and the 600 cycles, the pipe was pressurised by gradually decreasing rate pressure, and more pressure was transferred to the soil portions surrounding the pipe as a result of the initiated passive arching mechanism collapse, which would cause further confinement to the pipe. Due to the applied cyclic loading, the stiffness of the bedding layer increased because of the occurred soil densification. This led to an increase in the reaction forces value between the bedding layer and the invert of the pipe, which by turn increased the upward applied pressure along the invert of the pipe. The findings of Lay and Brachman (2014) illustrated that using a thick loose bedding layer generated reduced value of reaction forces between the bedding layer and the invert of the pipe. On the other hand, Abolmaali and Kararam (2009) indicated that using compacted bedding layer generated increased value of the reaction forces between them. Consequently, with the application of cyclic loading, the density of the bedding layer gradually increase, leading to an increase in the applied reaction forces between the bedding layer and the invert of the pipe, contributing in the invert rebound occurrence. Starting from the 600 cycle until reaching the 1500 cycle, the measured pressure value above the crown of the pipe became almost constant. Consequently, invert settlement should has been increased again. The formed crack and the applied upward pressure along the invert contributed in converting the downward movement of the invert into an upward one, initiating invert rebound, after reaching normalised settlement of 0.42%, where the upward movement rate increased to be 11.5%. By reaching the 1500 cycle, measured pressure value along the crown was decreased; consequently, the invert rebound rate was decreased to be 7.8% until reaching the end of the 1st loading phase. Applying further cyclic loading phases resulted in an increase in the rebound that occurred with slow rate, where it was 3.5% and 3.7% for the 2nd and the 3rd loading phases, respectively. System failure occurred at the 4th loading phase due to excessive footing settlement.

At deeper burial depths, i.e. T2 and T3, it was observed that the rebound occurred at advanced loading phases, unlike the case in T1, where the reduced value of the reaction forces were applied along the invert because of the decrease in the bedding layer stiffness with the increase in the burial depth, i.e. lower degree of densification. Due to the application of the monotonic loading, the invert settled until its normalised value reached 0.158% and 0.143% for T2 and T3, respectively. The maximum settlement rate was recorded at the 300 cycle of the 1st loading cycle, where the normalised value was 0.253% and 0.228% and the settlement rate reached 37.5% and 37.3% for T2 and T3, respectively. As further loading cycles were applied until reaching the end of the 1st loading phase, the normalised settlement value was 0.35% and 0.31%, respectively, where the settlement rate was reduced to be 27.7% and 26.4%. With the application of further loading phases the settlement rate decreased until reaching the 3rd loading phase, where a smooth rebound was observed in T3. In T2 the rebound did not occur until reaching the beginning of the 5th loading phase, where it was very sharp as system failure occurred. The earlier occurred invert rebound in T3 could be attributed to the increased generated strain along the spring-line of the pipe, which will be illustrated in the spring-line strain section.

5.4.1.6 Soil densification

Figure 5.10 illustrated the densification degree of each investigated system according to the applied loading phases.

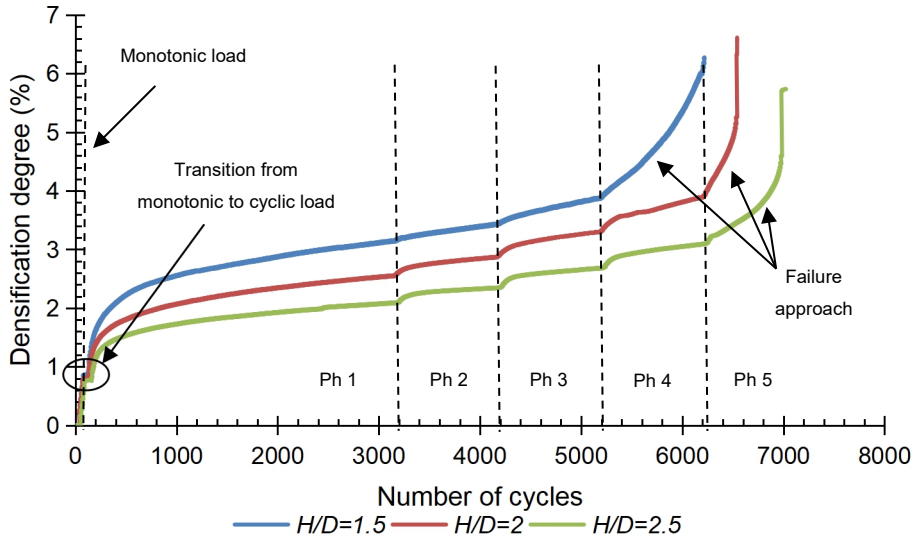

Figure 5.10 Soil densification due to the increase in the number of cycles

Densification degree was analytically calculated assuming a constant trapped trapezoidal soil mass in between the footing and the pipe, and its variable volume due to footing and pipe crown deformations with the application of loading cycles. The densification degree was calculated according to Eq (4.1).

As an example, at *H/D*=1.5, under the application of the 1st loading phase, the densification degree during the first 300 cycles was 1.9%, which represented 61.6% of the overall densification that occurred in this loading phase. At the end of the 1st loading phase, the densification degree was 3.1%. The increase in the applied cyclic loading phases, led to an increase in the densification degree, where the increase rate was 7.7%, 11.2% and 29% until reaching the 4th loading phase. The densification rate increase is governed by the relatively remarkable value of the footing settlement and the small value of the crown settlement.

It is clear that the densification degree decreased with pipe burial depth increase. Further densification due to increased loading phases is incomparable with that occurred during the first loading phase. At higher burial depths, the rate of change in the densification curves was decreased, and with loading phase progression, this rate increased, indicating system failure approach. In general, the densification led to a reduction in the soil volume followed by a reduction in footing and pipe settlement rates. In this investigation, this concept was achieved until reaching the 4th loading phase in T1 and the 5th loading

phase in T2 and T3, where densification rates were rapidly increased declaring failure approach.

5.4.1.7 Pipe cross-section during test and at failure

According to the illustrated data for pipe crown settlement, Figure 5.7, and invert settlement, Figure 5.9, it is clear that the pipe crown settled downward regardless of the pipe burial depth, unlike the pipe invert that experienced downward settlement followed by upward movement depending upon the loading value and the pipe burial depth. These two opposite reactions played a vital role in decreasing the vertical diameter of the pipe, as illustrated in Figure 5.11.

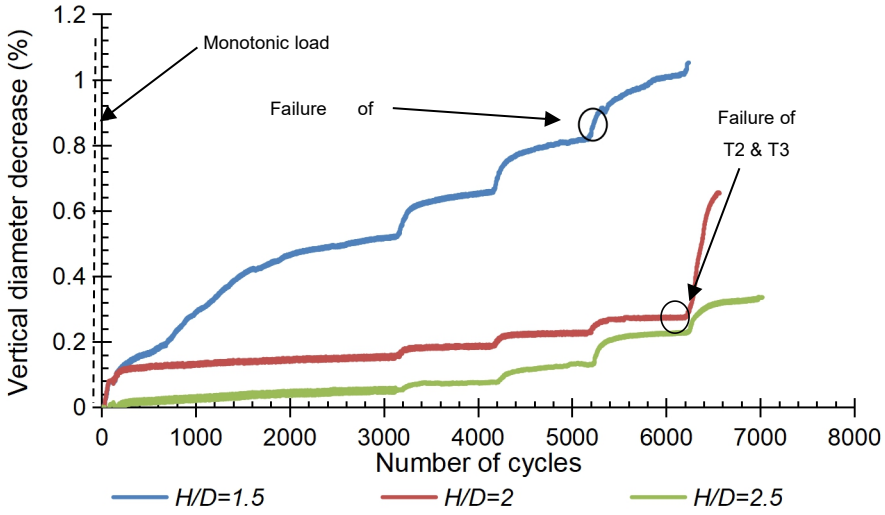

Figure 5.11 The decrease in the vertical diameter of the pipe against number of cycles

It is obvious that at a shallow burial depth, *H/D*=1.5, the decrease in the vertical diameter value and rate were significantly increasing, where the diameter reduction ratio was 0.85% at failure. At deeper burial depths, *H/D*=2 and 2.5, the decrease ratio significantly reduced, where it was 0.28% and 0.25% at failure, respectively. According to these data, it is obvious that the optimum burial depth of the pipe is at *H/D*=2. Figure 5.12 showed the deformed shape of the pipe at different burial depths, after loading. It was observed that at shallow burial depth, i.e. *H/D*=1.5, the cross-section of the pipe was deformed due to the generated cracks into four segments forming an elliptical shape. However, at deep burial depths, i.e. *H/D*=2 and 2.5, the cross-section of the pipe was

slightly deformed, where it kept its circularity; however cracks were formed along the invert, crown and spring-lines.

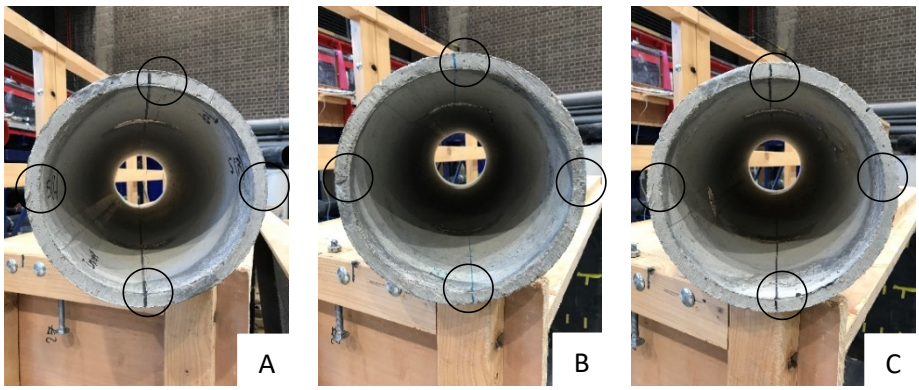

Figure 5.12 Deformed shape of the pipe after loading
A: H/D=1.5. B: H/D=2. C: H/D=2.5.

5.4.1.8 Pipe strain

When applied load was transferred through the soil to the pipe, it generated strain. Due to the pipe geometry and type, pipe would experience tensile strains along its inner crown and invert, and its outer spring-line. Consequently, strain gauges were attached at these specific locations. Formation of cracks was expected along these locations once the generated tensile strain exceeded the tensile strength of the pipe material.

Invert strain

The strain generated along the pipe invert was illustrated in Figure 5.13. It demonstrated that increasing the burial depth of the pipe had a significant effect in reducing the generated strain along the pipe invert, which matched the findings of Lay and Brachman (2014).

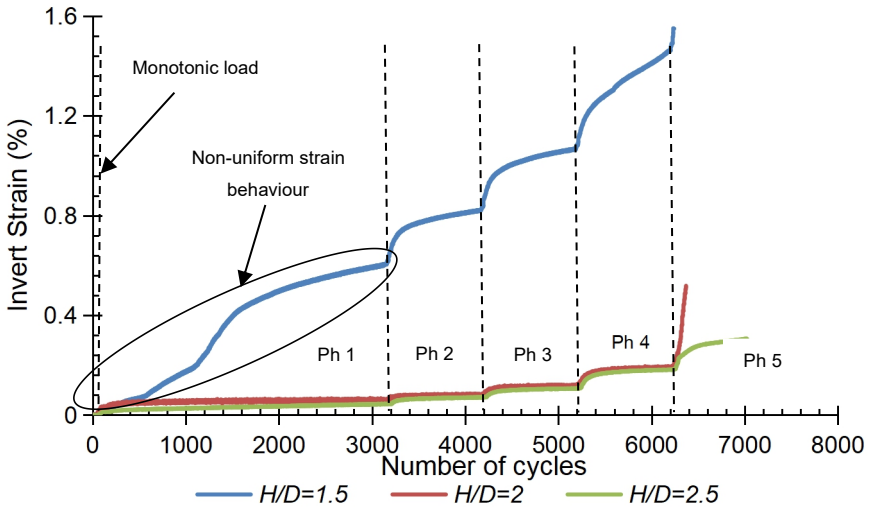

Figure 5.13 Invert strain against number of cycles

In T1, where *H/D*=1.5, it was observed that the generated strain along the invert of the pipe experienced a non-uniform behaviour during the 1st cyclic loading phase, where it varied according to the transferred pressure to the pipe, reflecting transferred pressure to the pipe. Because of the application of the monotonic loading, a tensile strain of 0.02% value was generated. At the 300 cycle of the 1st loading phase, strain value was tripled, where it reached 0.06% and a hair-line crack was visually observed at this stage. Until reaching the 600 cycle, strain value increased to 0.077% with a reduced strain rate, where the transferred pressure value to the pipe was reduced. After the 600 cycle and until reaching the 1500 cycle, the transferred pressure value to the pipe was almost constant, however; the strain generated along the invert varied. It increased to 0.2% and 0.39% at the 1100 cycle and the 1500 cycle, respectively, where strain rate from the 1100 to the 1500 cycle was faster. This change in the strain rate can be attributed to the increase in the applied stresses at the pipe invert as a result of the increase in the applied bedding layer reaction, which matched the findings of Abolmaali and Kararam (2009), and supported the occurrence of the invert rebound. At the end of the 1st loading phase, the strain value increased to be 0.6% but with a reduced strain rate, where the transferred pressure to the pipe was significantly decreased, because of the collapse that occurred in the passive arching mechanism. As further loading phases were applied, strain rate was increased until failure occurred at the beginning of the 4th loading phase, where rapid strain rate was observed.

In T2 and T3, burial depth of the pipe was increased leading to a decrease in the strain value due to the application of the monotonic loading, where its value was 0.015% and 0.011%, respectively. Due to the application of the cyclic loading, the soil was densified as shown in Figure 5.10, which provided more support to the pipe, in addition to the decrease in the transferred pressure to the pipe. This led to a reduction in the generated strain along the invert, where its value was 0.053% and 0.045% at the end of the 1st loading phase. This behaviour dominated the strain generation along the invert until failure occurred at the beginning of the 5th loading phase.

Figure 5.14 showed the invert strain of the pipe at the end of each loading phase with burial depth increase. It is obvious that, increasing the burial depth of the pipe under the application of the same cyclic loading phase had a great influence on decreasing the generated strain value and rate along the pipe invert, which is clear at *H/D*=2. This supported the claim which indicated that the optimum burial depth of the pipe is at *H/D*=2.

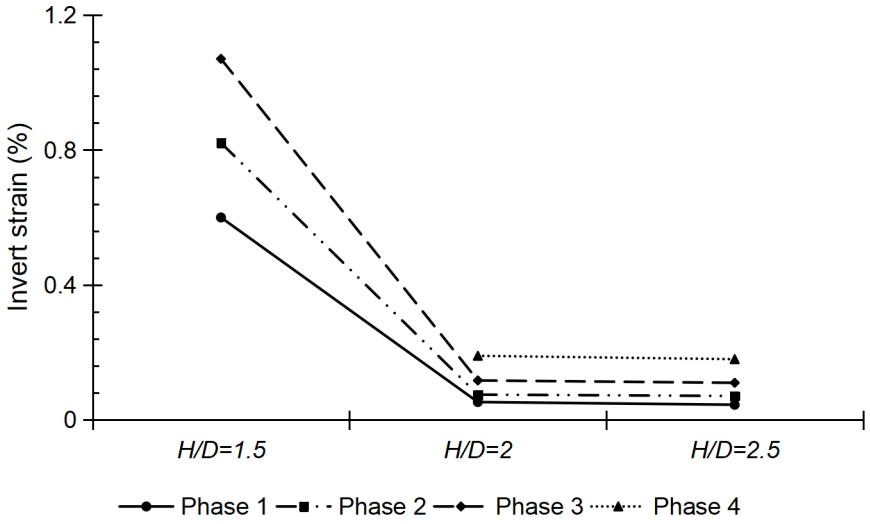

Figure 5.14 Invert strain at the end of loading phases

Crown strain

The results of the measured strain along the crown of the pipe are shown in Figure 5.15.

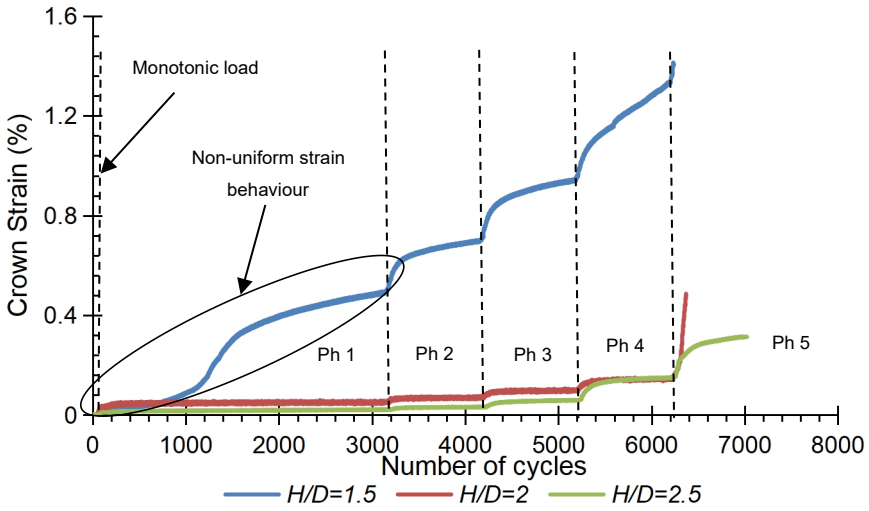

Figure 5.15 Crown strain against number of cycles

It demonstrated that the increase in the burial depth of the pipe significantly decreased the generated strain along the pipe crown. Figure 5.13 and Figure 5.15 provided strain measurements, which indicated that the generated tensile strain along the inner invert and crown experienced similar behaviour, however the invert experienced more strain than the crown did, which is in agreement with Abolmaali and Kararam (2009). This can be attributed to the low deformable nature of the pipe material, where it behaved as a rigid support to the tested systems, in addition to the relatively compacted bedding layer as a result of the applied cyclic loading. Consequently, all applied loads were transferred to the invert of the pipe, generating additional strain.

At the 1st loading phase, strain values reached 0.49%, 0.049% and 0.021% at *H/D*=1.5, 2 and 2.5 respectively. The strain reduction ratio was 90% and 95.7% at *H/D*=2 and 2.5 respectively. It is clear that the difference in the enhancement ratio at *H/D*=2 and 2.5 was only 5.7%, which gave an indication that after *H/D*=2, the improvement ratio in the strain reduction was insignificant. This behaviour dominated the generated strain along the pipe crown with the increase of the applied loading phases until reaching the 3rd loading phase. Once the 3rd loading phase was ended and the tested systems were subjected to the 4th loading phase, the first burial depth system, T1, failed, where the generated strain value and rate were rapidly increased. The strain value reached 0.163% and 0.153% at *H/D*=2 and 2.5, respectively. The improvement ratio reached 6.1% at *H/D*=2.5. Applying more loading phases to T2 and T3 resulted in

system failure due to excessive footing settlement, where rapid strain rate was observed at failure. Data illustrated that, the strain generation rate reached its maximum value in each loading phase during the 1st 300 cycles, except the 1st loading phase in T1, where maximum strain rate was observed between the 1100 and the 1500 cycles, and then it was significantly reduced until the application of the following loading phase. In addition, the transition from loading phase to the following one led to an increase in the strain generation rate until failure occurred. For example, in T2, the transition from the end of the 1st loading phase until reaching the 300 cycle of the 2nd loading phase generated strain rate of 26.6%. This value increased due to the transition from the 2nd and 3rd loading phases into the 3rd and 4th loading phases where it was 29.3% and 33.1%, respectively until failure occurred due to more applied loading phases.

Figure 5.16 showed the crown strain of the pipe at the end of each loading phase with burial depth increase. At the same loading phase and due to increasing the pipe burial depth, the strain generation value and rate significantly reduced, in particular at a burial depth of *H/D*=2. This indicated that the optimum burial depth of the pipe is *H/D*=2.

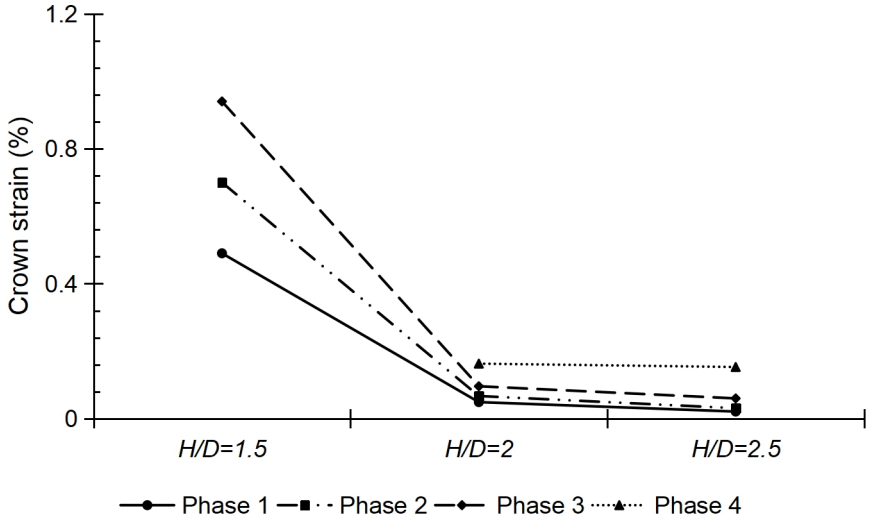

Figure 5.16 Crown strain at the end of loading phases

Spring-line strain

Figure 5.17 presented the generated strains along the spring-line of the pipe. The increase in the burial depth of the pipe had a vital role in increasing the

lateral support of the soil surrounding the pipe. Consequently, the generated strain along the spring-line was reduced with the increase in the burial depth of the pipe.

It can be noted that the spring-line strain pattern is similar to the crown and invert strains with a significantly reduced scale. Spring-line strain was related to the transferred pressure pattern to the pipe.

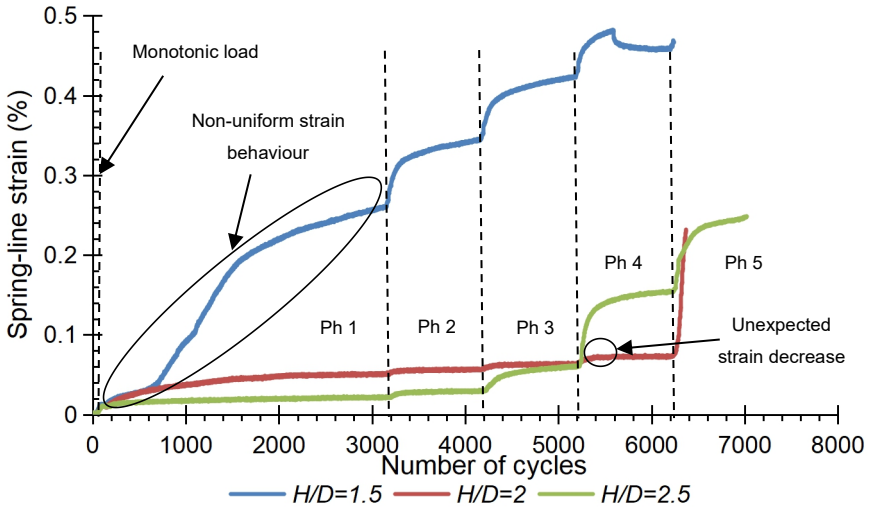

Figure 5.17 Crown strain against number of cycles

In T1, under the application of the monotonic loading, strain value reached 0.012%, which was less than that observed along the invert with 40%. Under applying the 1st loading phase, particularly at the 300 cycle, pressure value was increasing leading to the generation of spring-line strain of 0.02%, which is only one third of the measured invert strain at this cycle. By reaching the 600 cycle, it was observed that strain value was increased to be 0.03% with reduced rate, where pressure value along the pipe was decreased. As observed in the invert strain, the strain generation rate along the spring-line between the 600 and the 1500 cycles was changed at the 1100 cycle, where it was faster in between the 1100 and the 1500 cycles, however the measured pressure had an almost constant value. This can be attributed to the additional applied pressure to the invert of the pipe due to bedding layer reactions, which contributed in adding more stresses along the spring-line of the pipe. As more cycles were applied until reaching the end of the 1st loading phase, the pressure value was decreasing, consequently the spring-line strain was increased with an obviously reduced rate, where its value was 0.26%, which was less than that observed

along the invert by 56.7%. With the application of more loading phases, spring-line strain behaviour became uniform, where it was increasing during the 1st 300 cycles of the loading phase, and then its rate decreased until reaching the end of the loading phase. This behaviour was continued until reaching failure.

In T1, under the application of the 1st loading phase, it was observed that the crack was generated along the invert of the pipe leading to stress redistribution inside the soil, where stresses were reduced over the pipe, as shown in Figure 5.6, and were forced to be transferred to the soil portions surrounding the pipe. The collapse in the passive arching mechanism caused some changes in the stress redistribution. The confined soil portions around the pipe applied additional lateral support to it, and provided the pipe with additional resistance against the horizontal deformation, which is in agreement with Tan and Moore (2007). This explained the significant reduction in the strain generated between the spring-line and the invert of the pipe.

At deeper burial depths, T2 and T3, measured strain along the spring-line due to the applied monotonic loading was 0.01% and 0.0098% respectively. With the application of the 1st loading cycle, it was observed that the strain rate was increased until reaching the 300 cycle, where the strain value reached 0.022% and 0.014%, respectively. After this cycle, strain rate became steady and no change was observed until reaching the end of the 1st loading phase, where strain value was 0.05% and 0.021%, respectively. With applying further loading phases, the strain rate was slightly increasing during the 1st 300 cycles of each loading phase, and then it became stable again, but its value became higher in T3, during the 4th loading phase. This behaviour was continued until failure occurred, which was indicated by very rapid strain rate. At the end of each test, the pipe was visually inspected out of the tank.

Figure 5.18 illustrated that the generated crack along the spring-line of the pipe in T2 was split into two cracks, where only one of them intersected with the strain gauge.

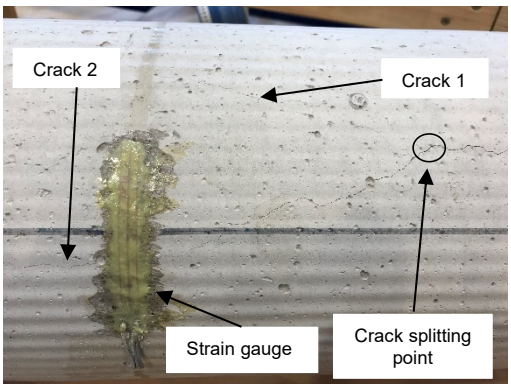

Figure 5.18 Splitted crack along the spring-line in T2

This can explain the lower strain value in T2 compared with T3, during the 4th loading phase. The splitted cracks in T2 resulted in forming narrower cracks compared with those observed in T3, which could have provided additional resistance to the invert rebound, hindering its occurrence.

In T2 and T3, the burial depth of the pipe was relatively high, compared with T1, which led to additional horizontal supporting stresses along the spring-lines of the pipe because of the additional self-weight of the soil. In addition, a reduced pressure value was transferred to the pipe because of the positive contribution of the load mitigation mechanism. These were the reasons in the reduced tensile stresses along the spring-line of the pipe compared with those measured along the invert and the crown.

It was noticed that the strain reduction rate between the spring-line and the invert of the pipe in T1 was significantly higher than its value in T2 and T3, as shown in Figure 5.19.

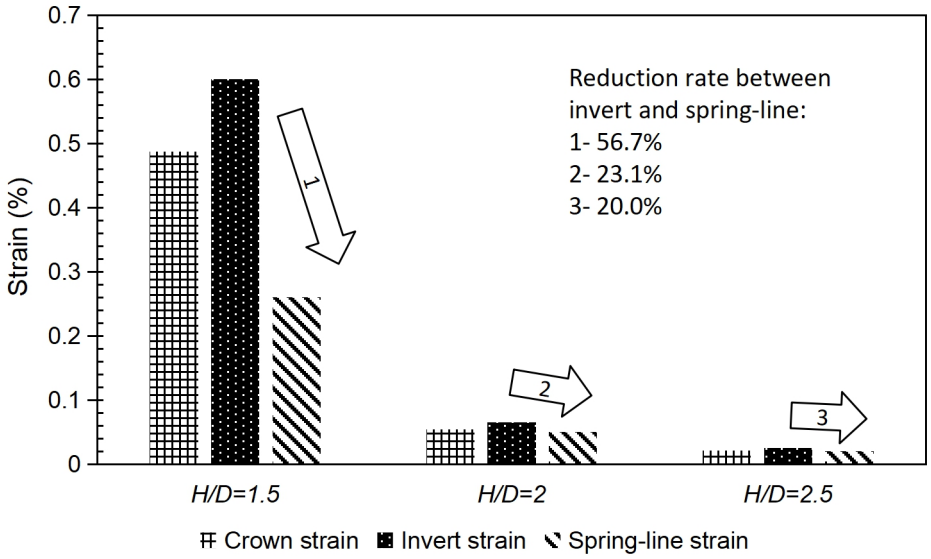

Figure 5.19 Pipe strain at the end of the 1st loading phase

This could be attributed to the quick rebound of the invert which illustrated the generation of significant tensile strain along the invert, and the occurred collapse in the passive arching mechanism, which provided enhanced lateral support to the spring-line. This did not occur in T2 and T3, where a late smooth invert rebound occurred.

5.4.2 Reinforced case

Two series, B and C, were conducted to investigate the influence of geogrid-reinforcement inclusion on load transfer and reinforced soil-pipe system load capacity. Table 5.1 illustrated the magnitude of the applied cyclic load in Series B and C, at different phases. Variation of the reinforcing layers number and the burial depth of the pipe is discussed in this section.

5.4.2.1 Footing settlement

The variation of the footing settlement ratio (F_s/D) with the number of loading cycles is presented in Figure 5.20. It was clear that increasing the burial depth of the pipe and the number of the reinforcing layers significantly contributed in reducing the settlement of the footing, and allowed the tested systems to sustain more load phases until reaching the failure point.

Table 5.2 and Table 5.3 illustrate the normalised footing settlement value due to increasing the cyclic loading phases under the variation of the burial depth of the pipe for Series B and C, respectively.

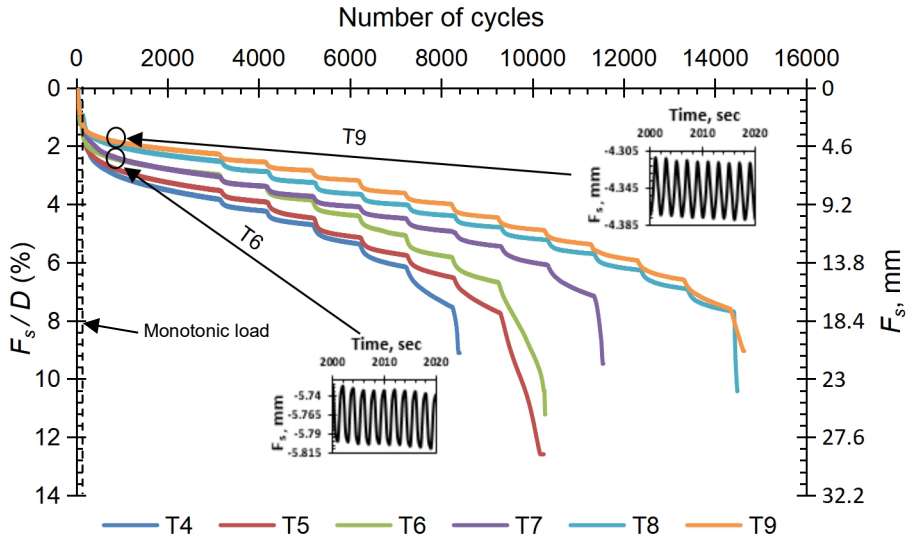

Figure 5.20 Footing settlement ratio against number of cycles, Series B and C

Table 5.2 Normalised footing settlement due to cyclic loading, Series B

Loading Phase	**1**			**2**			**3**			**4**		
H/D	1.5	2	2.5	1.5	2	2.5	1.5	2	2.5	1.5	2	2.5
F_s/D (%)	3.92	3.64	3.1	4.36	4.07	3.55	4.88	4.59	4.07	6.27	5.71	5.24
Enhancement ratio (%)	-	7.14	20.9	-	6.65	18.58	-	5.94	16.6	-	4.14	19.29
Loading Phase	**5**			**6**			**7**					
H/D	1.5	2	2.5	1.5	2	2.5	1.5	2	2.5			
F_s/D (%)	6.27	5.71	5.24	7.68	6.73	5.98	F	7.9	6.92			
Enhancement ratio (%)	-	8.93	16.42	-	12.37	22.13	-	-	12.41			

Table 5.3 Normalised footing settlement due to cyclic loading, Series C

Loading Phase	**1**			**2**			**3**			**4**		
H/D	1.5	2	2.5	1.5	2	2.5	1.5	2	2.5	1.5	2	2.5
F_s/D (%)	3.14	2.63	2.37	3.48	3	2.62	3.82	3.36	2.94	4.19	3.75	3.18
Enhancement ratio (%)	-	16.22	24.63	-	13.71	24.66	-	12.04	23.12	-	10.44	24.03
Loading Phase	**5**			**6**			**7**			**8**		
H/D	1.5	2	2.5	1.5	2	2.5	1.5	2	2.5	1.5	2	2.5
F_s/D (%)	4.53	4.16	3.71	5.04	4.5	4.07	5.55	4.88	4.55	6.17	5.35	4.97
Enhancement ratio (%)	-	8.31	18.22	-	10.71	19.27	-	12.2	18.04	-	13.29	19.45
Loading Phase	**9**			**10**			**11**			**12**		
H/D	1.5	2	2.5	1.5	2	2.5	1.5	2	2.5	1.5	2	2.5
F_s/D (%)	7.26	5.83	5.43	F	6.24	6	F	7.02	6.66	F	7.81	7.63
Enhancement ratio (%)	-	19.67	25.19	-	-	3.88	-	-	5.07	-	-	2.27

It was observed that during the application of the monotonic loading; footing settlement in the three burial depths in Series B and C, were approximately equal. Insignificant variation in the normalised footing settlement value was

observed, where the average value was 1.18% and 0.9% for Series B and C, respectively, with enhancement ratio of 23.73% in Series C, compared with Series B. Due to the application of the 1st loading phase, the footing settlement variation became obvious, where the maximum settlement rate was observed during the 1st 300 cycles in each test. The maximum normalised settlement value occurred in *T4*, where its value was 2.46%, while the minimum value occurred in *T9* with a value of 1.6%. With further loading cycles, settlement rate significantly decreased until reaching a stable rate at the end of the loading phase, where the normalised settlement value reached 3.92% and 2.37% for *T4* and *T9*, respectively. With the increase in the applied loading phases, the systems kept the same behaviour with slight increase in the deep burial depths, i.e. *H/D*=2 and 2.5, and significant increase in shallow burial depths, i.e. *H/D*=1.5, until failure occurred, which was indicated by the sudden increase in the settlement rate of the footing.

Figure 5.21 showed normalised footing settlement at the end of the applied loading phases, with burial depth increase for Series C, where two reinforcing layers were utilised.

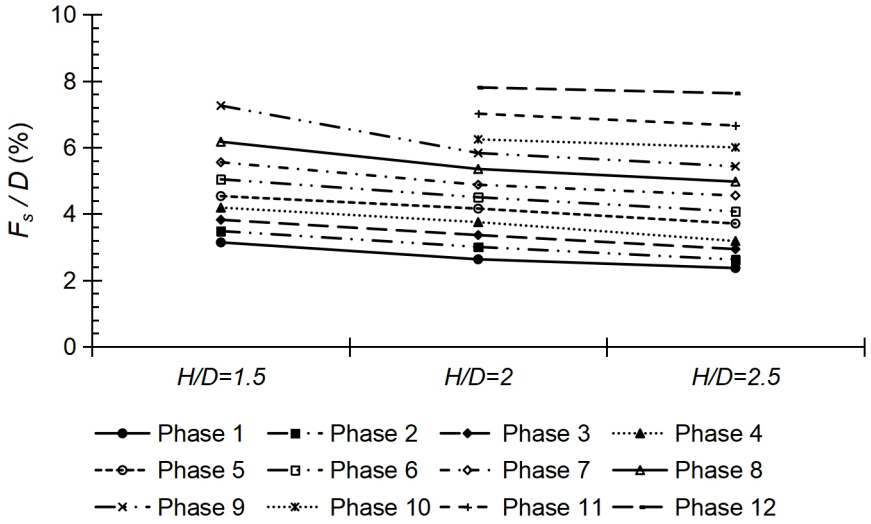

Figure 5.21 Footing settlement with loading phases increase, Series C

It can be noted that at any loading phase the increase in the burial depth of the pipe contributed in reducing the footing settlement. For example, at the 9th loading phase, the normalised footing settlement reached 7.26%, 5.83% and 5.43% at *H/D*=1.5, 2 and 2.5 respectively. The enhancement ratio reached

19.67% and 25.19% at *H/D*=2 and 2.5, compared with the case of *H/D*=1.5. It is obvious that the settlement rate slightly reduced at the initial loading phases, and with the increase in the loading phases, the settlement reduction rate increased.

Data for the normalised footing settlement in Series C are plotted against load phases to demonstrate the change in the settlement rate as cyclic loading progressed, as shown in Figure 5.22. In *T7*, where *H/D*=1.5, the settlement rate increased from the 1st to the 2nd loading phases with 9.8%, and it increased until reaching 15% from the 8th to the 9th phases. After this increased settlement rate, the system could not sustain extra load phases and failure occurred. Similar patterns were observed at different *H/D* values. Consequently, at the same burial depth, the settlement rate increased slowly at the initial loading phases and with the application of further loading phases, an increase in the settlement rate became faster and noticeable until failure occurred.

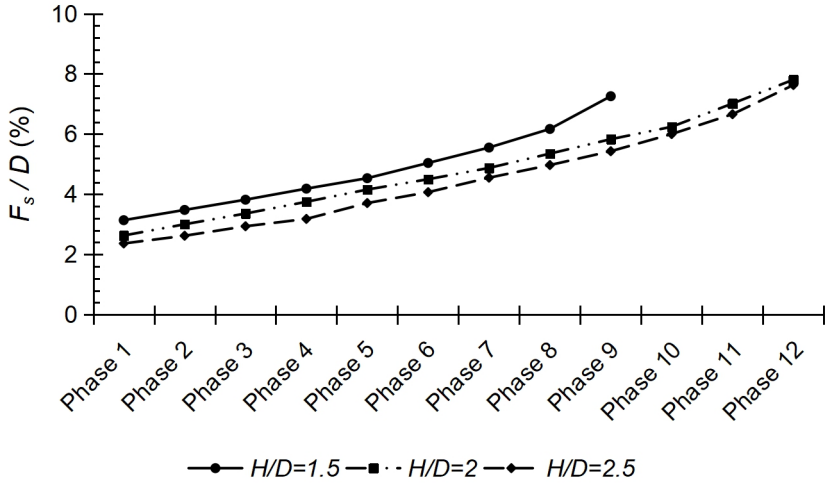

Figure 5.22 Change in footing settlement rate, Series C

It was obvious that footing settlement decreased gradually with the inclusion of the reinforcing layers, where new composite system with enhanced properties was formed, in particular its shearing resistance. The number of loading cycles sustained by the tested systems in Series B and C were drastically increased compared with Series A. The trapped soil in-between the geogrid layer apertures created a passive earth resistance mechanism, by which the generated tensile stresses and strains were transferred from the soil to the reinforcing layers, where lateral soil movement significantly decreased. This

behaviour kept the volume, at which the footing could settle, filled with soil, leading to a reduction in footing settlement. When the number of reinforcing layers was increased, the trapped soil volume increased, and more applied load phases could be sustained, as observed in Series C. It was noted that during the first 300 cycles of the 1st loading phase, settlement rate and value were the highest. This could be attributed to the slack effect of the reinforcing layers, where the layers were stretched due to the applied loads before they contributed in the system stability. Settlement rate rapidly increased once more at the loading phase, where failure occurred.

5.4.2.2 Transferred pressure to the pipe

Figure 5.23 illustrated measured data for the soil pressure above the pipe crown at the mid-point of the pipe length due to burial depth increase in Series B, where one reinforcing layer was used.

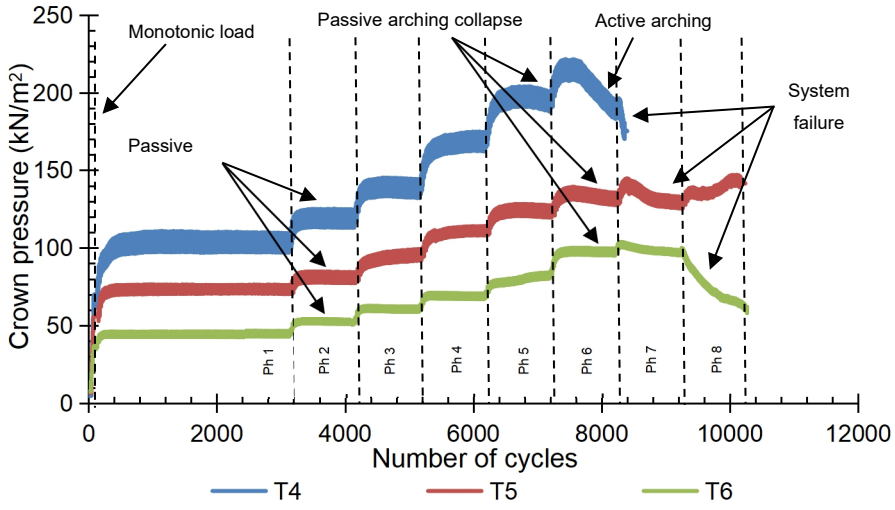

Figure 5.23 Transferred pressure to the pipe against loading cycles, Series B

Table 5.4 illustrates the transferred pressure values to the crown of the pipe due to increasing the cyclic loading phases under the variation of the burial depth of the pipe for Series B.

Table 5.4 Transferred pressure values due to cyclic loading, Series B

Loading Phase	**1**			**2**			**3**			**4**		
H/D	1.5	2	2.5	1.5	2	2.5	1.5	2	2.5	1.5	2	2.5
Pressure (kPa)	107.3	75	45.8	125	84	53	143.6	99	60.6	174.3	113	73.2
Enhancement ratio (%)	-	30.1	57.3	-	32.8	57.6	-	31.1	57.8	-	35.2	58
Loading Phase	**5**			**6**			**7**					
H/D	1.5	2	2.5	1.5	2	2.5	1.5	2	2.5			

Pressure (kPa)	200.2	127	83.8	195	135.3	99.4	F	132.6	97.5			
Enhancement ratio (%)	-	36.6	58.1	-	30.6	49	-	-	26.5			

Increasing the burial depth of the pipe significantly reduced the transferred pressure to its crown. The application of the monotonic loading generated pressure of 69 kPa, 53.5 kPa and 35.4 kPa in *T4*, *T5* and *T6*, respectively, along the crown of the pipe, whilst the footing pressure was 65 kPa. The pressure reduction ratio reached 22.5% and 48.7% for *T5* and *T6*, respectively, compared with *T4*. The generated pressure in *T4* was slightly higher than that applied to the footing with 5.8%. This could be attributed to i, self-weight of the soil above the pipe and ii, generated passive arching mechanism due to the difference in stiffness between the soil and the pipe, which attracted the generated pressure in the adjacent soil portions to the pipe. Visual observation at this stage illustrated no crack formation along the pipe, despite the increased pressure generated in *T4*. In the 1st cyclic loading phase, in particular after applying the first 300 cycles, the maximum generated pressure rate on the crown was observed, where the pressure value was 101 kPa, 73.2 kPa and 42.5 kPa for *T4*, *T5* and *T6*, respectively, however the applied pressure to the footing was 90 kPa. The generated pressure value in *T4* was higher than that applied to the footing with 10.9%; however, the pressure curve illustrated no crack formation, as pressure value and rate were stable without any variation. With further loading cycles during the 1st loading phase, the pressure generation rate was significantly decreased, where the pressure value remained almost constant until reaching the end of the 1st loading phase. It was an obvious sign that the pipe still attracting the generated pressure without the formation of any cracks. The inclusion of the reinforcing layer distributed the applied pressure along its plane, where pressure of a lower value over a wider area was transferred underneath the layer. Due to this pressure distribution, additional pressure was applied to the soil regions surrounding the pipe, which provided additional lateral support, and enhanced the confinement of the pipe, which in turn allowed the pipe to sustain higher transferred pressure without the formation of cracks.

With the application of further cyclic loading phases, the transferred pressure value increased until reaching the 5th loading phase in *T4* and the 6th loading

phase in *T5* and *T6*. In *T4*, and during the 5th loading phase, it was observed that the pressure value and rate were slightly decreased, however the pressure value at the end of the 5th loading phase was 203 kPa, which is still higher than that applied to the footing by 6.4%. This illustrated the initiation of the passive arching mechanism collapse, where cracks were visually observed at this stage. For *T5* and *T6*, a similar collapse in the passive arching mechanism was observed during the 6th loading phase, where the pressure transfer rate slightly decreased, and hairline cracks were observed. After these loading phases, it was observed that the transferred pressure rate and value significantly decreased, which was a clear sign that the pipe could not sustain any additional pressure, which could be attributed to the loss of its strength due to the formed cracks.

In *T4*, and during the 6th loading phase, the pressure transfer rate was significantly decreased, where its values were 220 kPa and 194 kPa at the 300th and the last cycles of the 6th loading phase. The pressure value at the end of the loading phase was less than the applied pressure by 9.8%, which can be considered as evidence of the collapsed passive arching mechanism and the initiation of active arching. In *T5* and *T6*, the collapse that occurred in the passive arching became more obvious due to the application of further loading phases, where the reduction rate of the pressure transfer curves increased until the occurrence of system failure.

Figure 5.24 illustrated measured data for the soil pressure above the pipe crown at the mid-point of the pipe length due to burial depth increase in Series C, where two reinforcing layers were used.

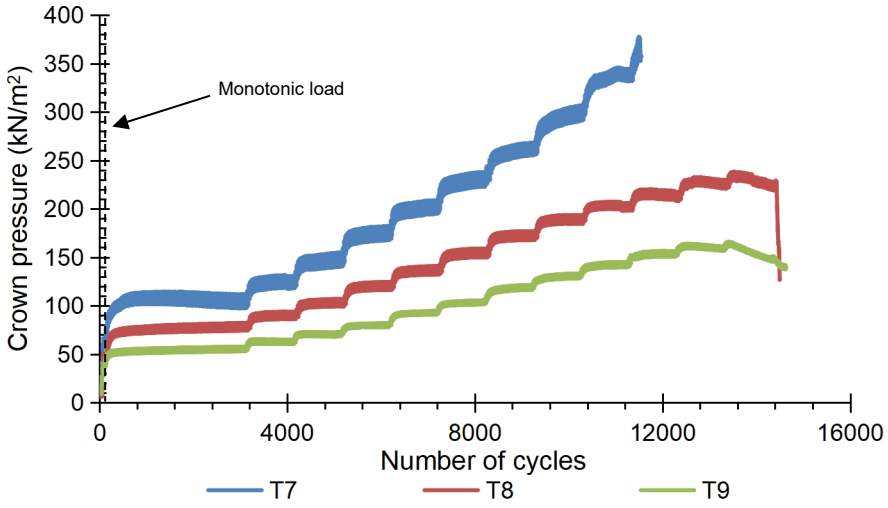

Figure 5.24 Transferred pressure to the pipe against loading cycles, Series C

Table 5.5 illustrates the transferred pressure values to the crown of the pipe due to increasing the cyclic loading phases under the variation of the burial depth of the pipe for Series C.

In Series C, the pressure transfer behaviour was similar to that adopted in Series B; however, the tested systems sustained additional loading phases due to the inclusion of two reinforcing layers, which enhanced the provided lateral support to the pipe allowing it to withstand additional loading phases.

Table 5.5 Transferred pressure values due to cyclic loading, Series C

Loading Phase	**1**			**2**			**3**			**4**		
H/D	1.5	2	2.5	1.5	2	2.5	1.5	2	2.5	1.5	2	2.5
Pressure (kPa)	109	80.5	57	128.4	92.5	64.5	152.8	105	71.6	181.2	123	80
Enhancement ratio (%)	-	26.15	47.7	-	28	49.8	-	31.3	53.1	-	32.1	55.9
Loading Phase	**5**			**6**			**7**			**8**		
H/D	1.5	2	2.5	1.5	2	2.5	1.5	2	2.5	1.5	2	2.5
Pressure (kPa)	204.2	138.4	92.8	234	158.6	104.7	267.6	176.6	121.2	304.5	190.9	133
Enhancement ratio (%)	-	32.2	54.6	-	32.2	55.3	-	34	54.7	-	37.3	56.3
Loading Phase	**9**			**10**			**11**			**12**		
H/D	1.5	2	2.5	1.5	2	2.5	1.5	2	2.5	1.5	2	2.5
Pressure (kPa)	343	204	145	F	218	154	F	225	161	F	223	150
Enhancement ratio (%)	-	40.7	57.8	-	-	29.4	-	-	28.7	-	-	32.9

Due to the applied load on the footing, differential settlement between the immediate soil beneath the footing and adjacent soils was formed. Consequently, shear stresses between these soil zones were generated

forming an arching effect (Terzaghi and Peck, 1967). Since the pipe is a rigid one, it had higher stiffness than the soil, consequently, its ability to attract load was increased. This behaviour led to the formation of passive arching mechanism (Young and Trott, 1984; Vaslestad et al., 1993; Peter et al., 2018). Unlike the unreinforced case, the transferred pressure to the pipe in the reinforced case was the summation of three mechanisms, namely i. passive arching, ii. load mitigation and iii. distributed load over reinforcing layer. Distributed load over reinforcing layer mechanism was generated due to the inclusion of the reinforcing layers. In this mechanism, the reinforcing layer and the trapped soil in-between its apertures formed a stiff composite layer, where transferred pressure was distributed along its plane generating a wider loaded area with lower pressure value underneath it. This mechanism depended on the generated passive earth resistance between the soil and the reinforcing layer. Increasing number of the reinforcing layers increase the contribution of this mechanism. At lower burial depths, the negative contribution of the passive arching mechanism controlled the transferred pressure value to the pipe, where lower soil layer was allowed to interact in the load mitigation mechanism, decreasing its contribution. On the contrary, at deeper burial depths the positive contribution of the load mitigation mechanism dominated the system, where increased soil layer was allowed to interact in the pressure mitigation above the pipe leading to a significant reduction of measured pressure at the pipe crown, which is in a good match with the results of Arockiasamy et al. (2006). It could be considered that the intensively occurring inclination in the pressure curve is clear evidence that the tested pipe-soil systems were in the failure phase, where the increase in the tensile strain values contributed to the formation of cracks along the pipe leading to stress redistribution and system failure.

Figure 5.25 showed measured data for the soil pressure above the pipe crown due to the inclusion of the reinforcing layers at burial depth of H/D=1.5. Due to the application of the monotonic loading, the generated pressure above the crown reached 86 kPa, 69 kPa and 62 kPa for *T1*, *T4* and *T7* respectively, with a reduction ratio of 19.8% for *T4* and 27.9% for *T7* relative to *T1*. With the application of the 1st cyclic loading phase, at the 300 cycle pressure values were 106.8 kPa, 101 kPa and 96 kPa, respectively. With the application of

further cycles, it was observed that the pressure value in *T4* and *T7* remained almost constant until reaching the end of the 1st loading phase, which indicated that the pipe was able to attract loads to it without forming any cracks. In *T1*, unreinforced case, it was observed that the pressure value along the crown followed a non-uniform behaviour, as described in section *5.4.1.3*. Visual inspection illustrated the formation of cracks in *T1* during the 1st loading phase, which indicated that the pipe cannot attract load anymore and the controlling passive arching mechanism started to collapse, where the transferred pressure value was still higher than the applied one.

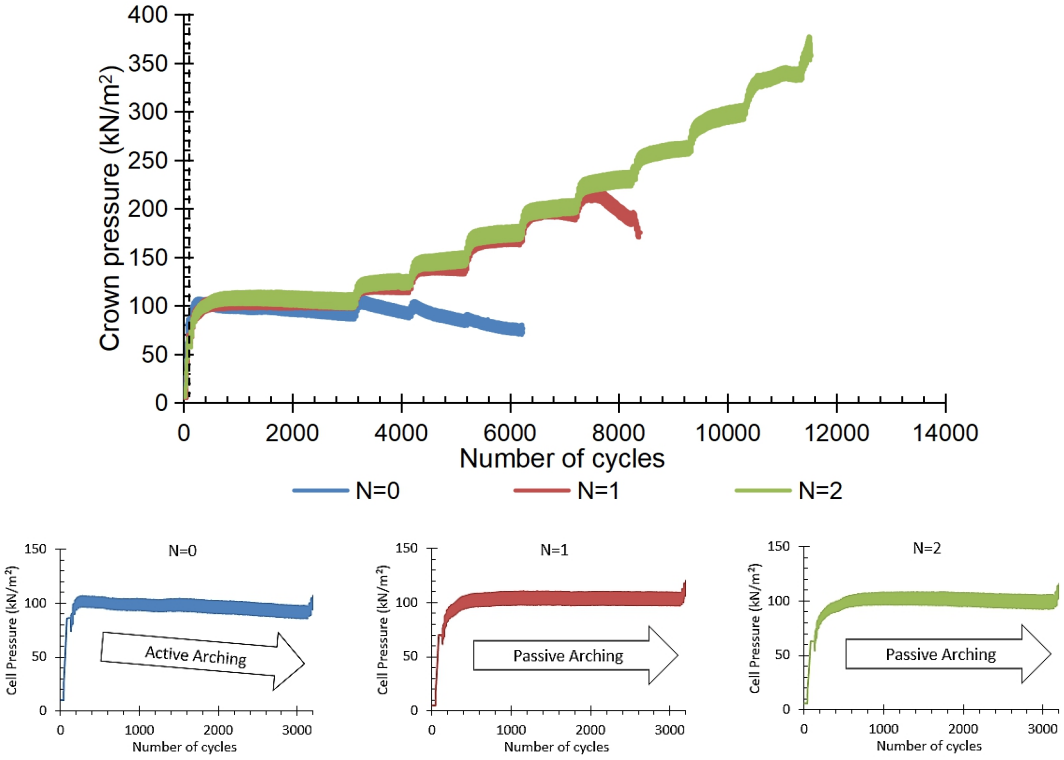

Figure 5.25 RFT layers inclusion effect on pressure transfer at H/D=1.5

It was observed that the inclusion of the reinforcing layers slightly decreased the transferred pressure to the pipe; however, it provided significant lateral support to it, through the redistribution of stresses along the reinforcing layer plane, which allowed the system to sustain additional loading phases. In *T1*, pipe failure, i.e. cracks formation, was noticed during the 1st loading phase, where in *T4* and *T7* failure occurred in the 5th and 10th loading phases, respectively. Consequently, it is obvious that the increase in the burial depth of the pipe significantly reduced the transferred pressure to the crown of the pipe. On the other hand, the inclusion of the reinforcing layers provided the system with

enhanced lateral support, where additional loading phases were sustained safely.

5.4.2.3 Crown settlement

Normalised crown settlements (C_s/D) under variation of H/D, for Series B and C are presented in Figure 5.26. It was clear that the inclusion of the reinforcing layers under the increase in the burial depth of the pipe had a significant effect on decreasing the crown settlement. Pipe burial depth and number of the reinforcing layers governed reduction rate of the crown settlement.

Table 5.6 and Table 5.7 illustrate the normalised crown settlement value due to increasing the cyclic loading phases under the variation of the burial depth of the pipe for Series B and C, respectively.

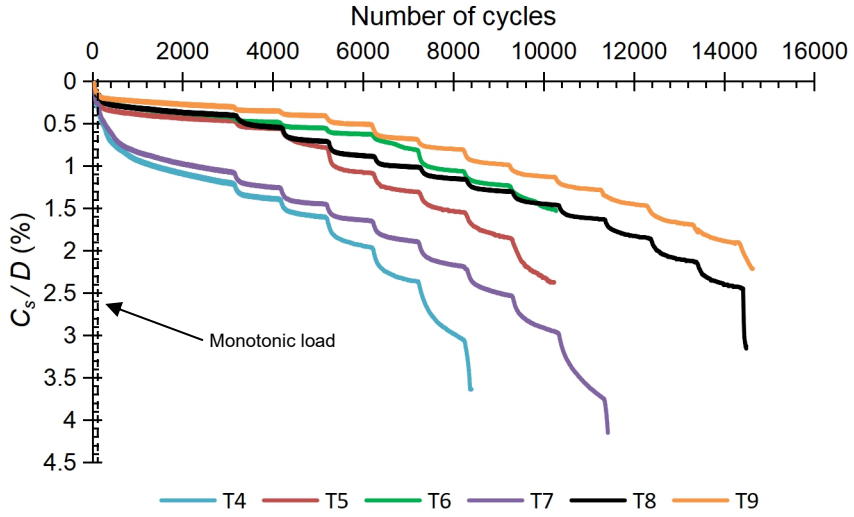

Figure 5.26 Normalised crown settlement with loading phase increase

Table 5.6 Normalised crown settlement due to cyclic loading, Series B

Loading Phase	**1**			**2**			**3**			**4**		
H/D	1.5	2	2.5	1.5	2	2.5	1.5	2	2.5	1.5	2	2.5
C_s/D (%)	1.25	0.49	0.45	1.45	0.6	0.53	1.67	0.83	0.59	2.1	1.15	0.68
Enhancement ratio (%)	-	60.8	64	-	58.6	63.3	-	50.6	64.7	-	43.9	66.8
Loading Phase	**5**			**6**			**7**					
H/D	1.5	2	2.5	1.5	2	2.5	1.5	2	2.5			
C_s/D (%)	2.43	1.35	0.89	3.1	1.61	1.1	F	1.9	1.29			
Enhancement ratio (%)	-	44.4	63.4	-	48.1	64.5	-	-	32.1			

Table 5.7 Normalised crown settlement due to cyclic loading, Series C

Loading Phase	**1**			**2**			**3**			**4**		
H/D	1.5	2	2.5	1.5	2	2.5	1.5	2	2.5	1.5	2	2.5
C_s/D (%)	1.12	0.44	0.33	1.31	0.58	0.37	1.5	0.73	0.43	1.71	0.91	0.51
Enhancement ratio (%)	-	60.9	70.7	-	55.6	71.4	-	51.2	71.2	-	46.8	70.2

Loading Phase	**5**			**6**			**7**			**8**		
H/D	1.5	2	2.5	1.5	2	2.5	1.5	2	2.5	1.5	2	2.5
C_s/D (%)	1.95	1.05	0.71	2.22	1.19	0.84	2.61	1.34	1.01	3.02	1.49	1.15
Enhancement ratio (%)	-	46.2	63.6	-	46.3	62.3	-	48.8	61.2	-	50.6	61.8
Loading Phase	**9**			**10**			**11**			**12**		
H/D	1.5	2	2.5	1.5	2	2.5	1.5	2	2.5	1.5	2	2.5
C_s/D (%)	3.8	1.66	1.31	F	1.89	1.48	F	2.15	1.71	F	2.45	1.93
Enhancement ratio (%)	-	56.3	65.5	-	-	21.4	-	-	20.3	-	-	21.1

It was clear that, the maximum settlement rate of the crown occurred at the shallowest burial depths, *T4* and *T7*, during the 1st 300 cycles of the 1st loading phase, where the normalised settlement value reached 0.67% and 0.57% respectively, which was lower than that measured in *T1* with 8.2% and 21.9%. With the progression of loading cycles, the settlement rate decreased smoothly until reaching a steady rate in *T4* and *T7* by reaching the end of the 1st loading phase, where the normalised settlement value was 1.25% and 1.12%, respectively, with a reduction ratio of 16.1% and 24.8% compared with *T1*. With the application of further loading phases, it was observed that the crown settlement increased during the 1st 300 cycles of each loading phase and then the rate was decreased at the end of the phase, where a slight increase in the settlement rate was observed at deeper burial depths, while at shallow burial depths the rate was significant.

It was noted that the crown settlement rate at shallow burial depths was very rapid until reaching the 300 cycle of the 1st loading phase, where the reinforcing layers were in the stretching phase, known as the slack effect (Chenggang, 2004; Sieira et al., 2009; Abu-Farsakh et al., 2013; Tran et al., 2013). Once the slack effect was ended, the reinforcing layers contribution in decreasing the crown settlement was initiated through the formation of the membrane and the distributed load over reinforcing layer mechanisms. It was observed that the crown settlement rate decreased smoothly until reaching a steady rate forming a uniform settlement pattern. A non-uniform settlement pattern was observed in *T1*, where cracks were generated due to the lower lateral support, leading to stresses fluctuation along the pipe with loading cycle's application, as observed in Figure 5.6.

At deeper burial depths, it was observed that the maximum settlement rate occurred at an earlier cycle compared with the shallow burial depths, where the

settlement value was significantly lower in the deep burial depths. The increase in the burial depth of the pipe contributed in providing more lateral support to it, due to the increased soil own-weight. In addition, the inclusion of the reinforcing layers resulted in a pressure distribution along wider area. This led to a pressurizing process for the soil portions around the pipe, which increased the provided lateral support for the pipe contributing in the decrease of its crown settlement rate and value.

Data illustrated that the highest settlement rate occurred within the first 300 cycles of the 1st loading phase, regardless of the burial depth of the pipe and the number of the reinforcing layers. With the increase in the applied loading cycles, the crown deformation deteriorated until system failure.

The relation between pipe crown settlement at the end of each loading phase with the increase in the burial depth for Series C was shown in Figure 5.27.

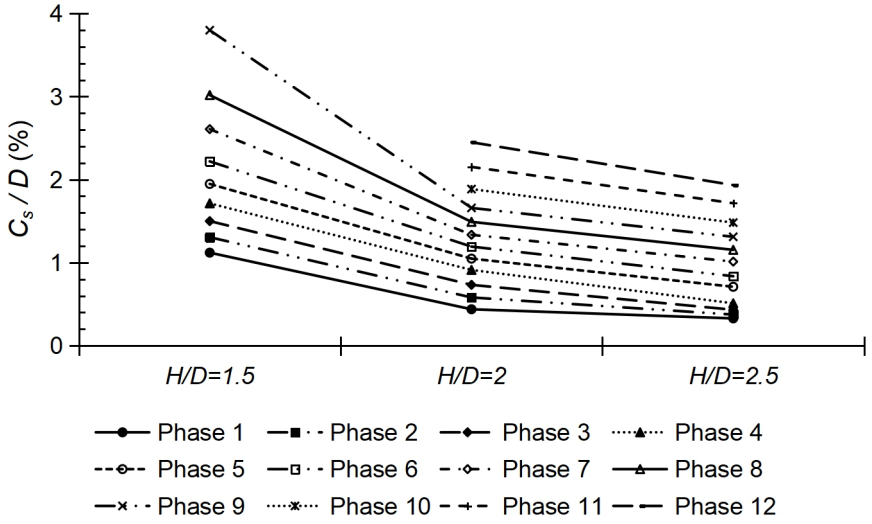

Figure 5.27 Normalised crown settlement at the end of each phase, Series C

It is clear that, at the same loading phase, increasing the burial depth significantly reduced the pipe crown settlement, where the settlement slope was reduced. This can be attributed to the higher soil cover above the pipe, which contributed in mitigating the transferred load, in addition to the reinforcing layers which redistributed the pressure providing more lateral support to the pipe, however a full passive arching mechanism could be generated (Aqoub et al., 2018). According to the results, the contribution of load mitigation and distributed load over reinforcing layer mechanisms was higher than the passive

arching one at deep burial depths, as measured pressure values along the crown of the pipe decreased with burial depth increase.

Similar behaviour was observed in Series B, as shown in Figure 5.28, however, normalised settlement values were relatively higher, compared with Series C, due to the relatively lower lateral support as a result of the inclusion of one reinforcing layer in Series B. Moreover, lower number of loading phases was sustained in Series B.

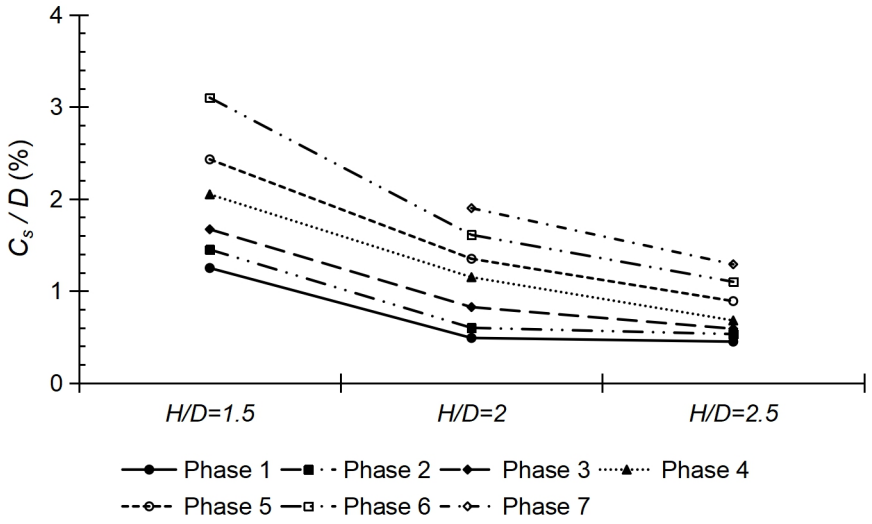

Figure 5.28 Normalised crown settlement at the end of each phase, Series B

5.4.2.4 Invert settlement

Normalised invert settlement, I_S/D, under variation of H/D for Series B and C were illustrated in Figure 5.29 and Figure 5.30, respectively. It is clear that under the application of loading phases, pipe invert settled until reaching a certain value then a rebound occurred, where its upward movement was initiated. Applied load, pipe burial depth and number of the reinforcing layers governed the occurrence of this behaviour.

Table 5.8 and Table 5.9 illustrated the normalised invert settlement value due to increasing the cyclic loading phases under the variation of the burial depth of the pipe for Series B and C, respectively.

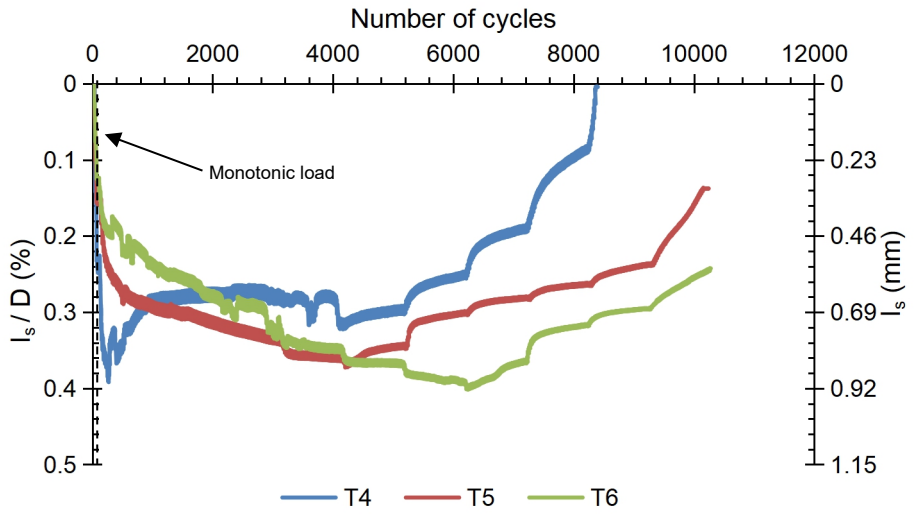

Figure 5.29 Invert deformation due to loading phases increase, Series B

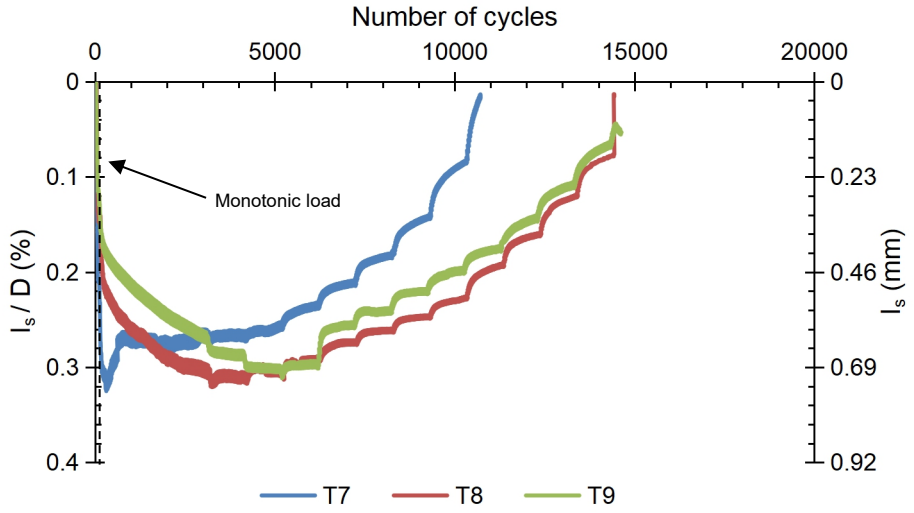

Figure 5.30 Invert deformation due to loading phases increase, Series C

Table 5.8 Normalised invert settlement due to cyclic loading, Series B

Loading Phase	**1**			**2**			**3**			**4**		
H/D	1.5	2	2.5	1.5	2	2.5	1.5	2	2.5	1.5	2	2.5
I_s/D (%)	0.28	0.34	0.32	0.31	0.36	0.34	0.29	0.34	0.37	0.24	0.3	0.39
Loading Phase	**5**			**6**			**7**					
H/D	1.5	2	2.5	1.5	2	2.5	1.5	2	2.5			
I_s/D (%)	0.19	0.28	0.36	0.08	0.26	0.31	F	0.23	0.29			

Table 5.9 Normalised invert settlement due to cyclic loading, Series C

Loading Phase	**1**			**2**			**3**			**4**		
H/D	1.5	2	2.5	1.5	2	2.5	1.5	2	2.5	1.5	2	2.5
I_s/D (%)	0.26	0.3	0.26	0.26	0.3	0.29	0.25	0.3	0.3	0.23	0.29	0.28
Loading Phase	**5**			**6**			**7**			**8**		
H/D	1.5	2	2.5	1.5	2	2.5	1.5	2	2.5	1.5	2	2.5
I_s/D (%)	0.21	0.27	0.25	0.18	0.26	0.24	0.14	0.24	0.22	0.1	0.23	0.2

Loading Phase	9			10			11			12		
H/D	1.5	2	2.5	1.5	2	2.5	1.5	2	2.5	1.5	2	2.5
I_s/D (%)	0.02	0.19	0.17	-	0.16	0.14	-	0.12	0.11	-	0.08	0.07

At shallow burial depth, i.e. *T4* and *T7*, the rebound occurred during the 1st loading phase once the normalised invert settlement reached 0.39% and 0.32%, respectively, which was lower than that measure in *T1* with 8.47% and 24.9%. Increasing the burial depth and the number of reinforcing layers hindered the rebound occurrence.

In *T1*, it was observed that the rebound occurred due to the formed crack along the invert of the pipe and the increased pressure from the underneath of the pipe. In *T4* and *T7*, no cracks were formed along the invert of the pipe during the 1st loading phase, however the rebound occurred. The concrete pipe behaved as a rigid support that attracted the applied loads because of its high stiffness. Consequently, its invert behaved as a support to the pipe itself, where its main function was to transfer load to the bidding layer underneath it. Stiffness variation between the invert and the bidding layer formed a stress concentration zone between them. With the progression of the loading cycles, the density of the soil was increased, i.e. soil densification, consequently, increased stresses were generated between the bedding layer and the invert (Abolmaali and Kararam, 2009). Moreover, the upward reaction forces between them increased as well, initiating the invert rebound. In addition, the enhanced confinement effect of the soil portions surrounding the pipe due to the existence of the reinforcing layer provided more resistance to the pipe against deformation forcing its invert settlement to rebound under the applied upward stresses along its invert.

At deeper burial depths, smooth invert rebound occurred at further loading phases, where it occurred at the 3rd and 4th loading phases for *T8* and *T9*, respectively. This can be attributed to the enhanced provided lateral support to the pipe because of the reinforcing layers existence and the reduced pressure value influencing the pipe. Consequently, the system required an increased number of loading cycles to increase the stiffness of the bedding layer, which would generate feasible upward pressure along the invert of the pipe, initiating its rebound.

In reinforced and unreinforced cases, the invert rebound was very sharp at shallow burial depth and occurred during the 1st loading phase. With the increase in the burial depth of the pipe, the rebound occurred gradually under the application of further cyclic loading phases.

5.4.2.5 Pipe cross-section deformed shape

Figure 5.31 illustrated the deformed shape of the pipe due to the applied loading profile for Series B. According to the findings of the pipe crown and invert settlements, it was clear that under all loading phases the pipe crown settled downward, regardless of the pipe burial depth and the number of the reinforcing layers.

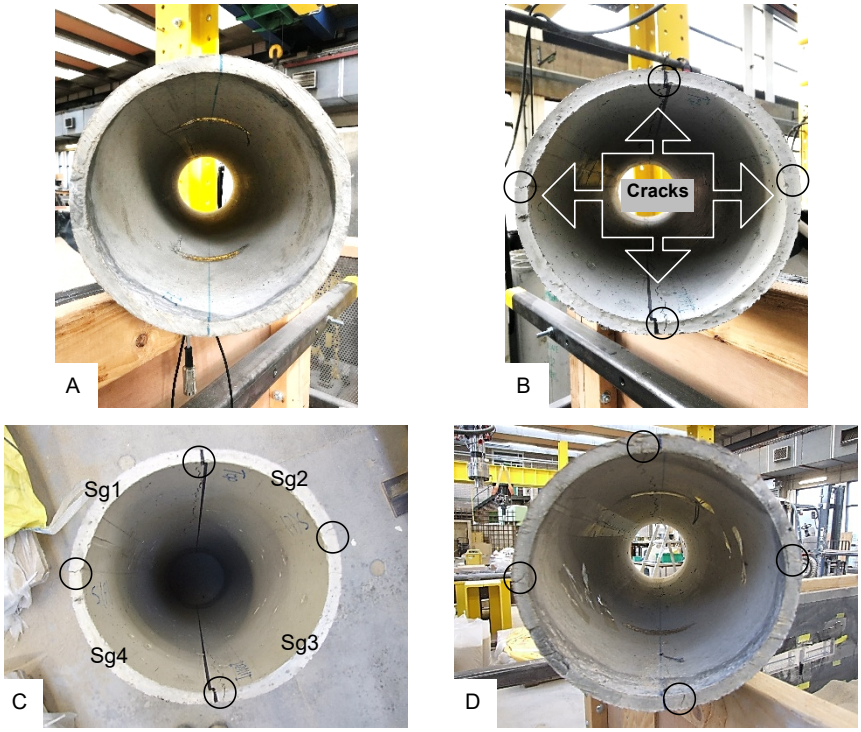

Figure 5.31 Deformed cross-section of the pipe, Series B
A: Original. B: *H/D*=1.5. C: *H/D*=2. D: *H/D*=2.5. (Sg: segment)

On the other hand, the pipe invert experienced downward settlement followed by upward movement depending upon the cyclic loading phase, burial depth and the number of the reinforcing layers. These two opposite responses played a vital role in the new formed pipe cross-section, which depended on the reduction in the vertical diameter and the increase in the horizontal one. It was observed that the initial circular cross-section of the pipe was deformed due to the generated cracks into four segments, between the formed cracks, forming

an elliptical shape, as shown in Figure 5.31. The inclusion of the reinforcing layers and the burial depth increase in the tested systems hindered and controlled the crack formation and propagation; moreover, they contributed in enhancing the systems performance and allowed them to sustain more loading phases, until failure occurred.

5.4.2.6 Pipe strain

Due to the transferred pressure from the soil to the pipe, tensile and compressive strains were generated in the pipe. Strain gauges were fastened at three controlling locations, inner crown, invert and outer spring-line, where the pipe experienced tensile strain along these lines. Formation of cracks was expected along these locations once the generated tensile strain exceeded the tensile strength of the pipe material.

Invert strain

Generated strain along the invert of the pipe for Series B and C was illustrated in Figure 5.32.

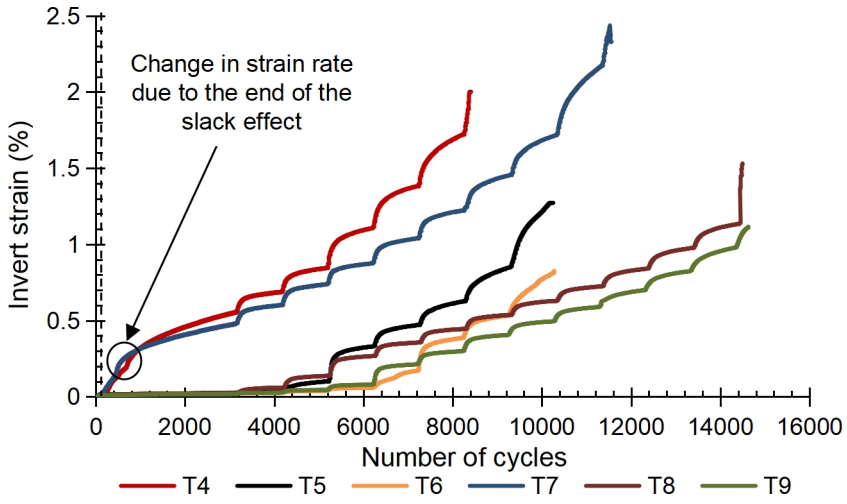

Figure 5.32 Invert strain against number of cycles, Series B and C

Table 5.10 and Table 5.11 illustrated the strain value of the invert due to increasing the cyclic loading phases under the variation of the burial depth of the pipe for Series B and C, respectively.

Table 5.10 Invert strain due to cyclic loading, Series B

Loading Phase	1			2			3			4		
H/D	1.5	2	2.5	1.5	2	2.5	1.5	2	2.5	1.5	2	2.5

I_{st} (%)	0.56	0.026	0.019	0.7	0.041	0.027	0.845	0.1	0.042	1.164	0.336	0.064
Enhancement ratio (%)	-	95.4	96.6	-	94.1	96.1	-	88.2	95	-	71.1	94.5
Loading Phase	**5**			**6**			**7**					
H/D	1.5	2	2.5	1.5	2	2.5	1.5	2	2.5			
I_{st} (%)	1.38	0.47	0.169	1.725	0.626	0.38	F	0.85	0.53			
Enhancement ratio (%)	-	65.9	87.8	-	63.7	78	-	-	37.6			

Table 5.11 Invert strain due to cyclic loading, Series C

Loading Phase	**1**			**2**			**3**			**4**		
H/D	1.5	2	2.5	1.5	2	2.5	1.5	2	2.5	1.5	2	2.5
I_{st} (%)	0.48	0.028	0.02	0.6	0.063	0.028	0.74	0.136	0.045	0.91	0.27	0.079
Enhancement ratio (%)	-	94.3	96.5	-	89.6	95.4	-	81.6	94	-	70.6	91.3
Loading Phase	**5**			**6**			**7**			**8**		
H/D	1.5	2	2.5	1.5	2	2.5	1.5	2	2.5	1.5	2	2.5
I_{st} (%)	1.04	0.36	0.21	1.22	0.45	0.3	1.46	0.54	0.3	1.46	0.54	0.41
Enhancement ratio (%)	-	65.8	79.6	-	63.2	75.6	-	63.1	72.2	-	63.5	71.3
Loading Phase	**9**			**10**			**11**			**12**		
H/D	1.5	2	2.5	1.5	2	2.5	1.5	2	2.5	1.5	2	2.5
I_{st} (%)	2.17	0.72	0.59	F	0.84	0.7	F	0.98	0.82	F	1.13	0.98
Enhancement ratio (%)	-	66.7	72.9	-	-	16.7	-	-	15.7	-	-	13.6

It demonstrated that a significant reduction in the generated strain rate and value was observed due to the increase of the pipe burial depth and the inclusion of the reinforcing layers. At shallow burial depth, *T1*, *T4* and *T7*, it was observed that the strain generation rate due to the application of the monotonic loading was very rapid, where the strain value was 0.02%, 0.016% and 0.012%, respectively. With the application of the 1st loading phase, it was observed that the generated strain in *T1* followed a non-uniform pattern, which was related to the transferred pressure to the pipe and the early formed cracks. In *T4* and *T7*, no cracks were formed during the 1st loading phase, and an average rapid strain rate of 85% was observed until reaching the 300 cycle, which was more rapid than that observed in *T1*. With further loading cycles until reaching the end of the 1st loading phase, the strain rate was decreased to be 67.6% and 77.5% for

T4 and *T7*, respectively, where strain value was less than that measured in *T1* with 7.5% for *T4* and 20.2% for *T7*. This decrease in the strain rate could be attributed to the end of the slack effect of the reinforcing layers, where their contribution in enhancing the system behaviour was initiated. With the progression of loading phases, strain rate increased during the 1st 300 cycles and then it decreased, where a stable rate controlled the strain pattern until reaching the end of the loading phase. Failure was observed once the strain rate was rapidly increased without a following decrease due to further loading cycles.

At deeper burial depths, *H/D*=2 and 2.5, a uniform strain pattern was observed, where strain rate increased during the 1st 300 cycles of each loading phase, and then it decreased to follow a more stable rate until reaching the end of the loading phase. The increase in the burial depth and the inclusion of the reinforcing layers positively influenced the generated strain along the invert, where its value was decreased. In *T9*, where two layers were used, generated strain value at the end of the 1st loading phase was 0.02%, where it was lower than that measured in *T6* (one layer) and *T3* (unreinforced) with 4% and 55.5%, respectively. This illustrated that the contribution of inserting a reinforcing layer is obvious at the initial loading phases; however, the number of the reinforcing layers insignificantly influenced the system behaviour, which could be attributed to the relatively low value of the applied loads. At the 6th loading phase, *T3* failed to sustain the applied loads. On the other hand, the generated strain along the invert in *T9* was lower than that measured in *T6* by 18.5%. This illustrated that increasing the number of the reinforcing layers increased their contribution in enhancing the system performance with the progression of the applied loading phases. At relatively higher value of applied loads, the lower reinforcing layer suffered more deformation, relative to the 1st loading phase, leading to enhancing the contribution of the membrane mechanism, which by turn enhanced the behaviour of the reinforced soil above the pipe leading to more reduction in the generated strain in the pipe. In general, in the unreinforced series the pipe experienced significantly increased strain value along its invert compared with the reinforced series, where a low-confined soil zone surrounded the pipe and no membrane mechanism enhanced the

performance of the backfill cover because of the absence of the reinforcing layers. The reinforcing layers allowed the tested systems to sustain additional loading phases safely, where lower strain values were applied along the pipe, particularly during advanced loading phases.

Crown strain

The strain generated along the crown of the pipe for Series B and C was illustrated in Figure 5.33.

According to Figure 5.32 and Figure 5.33, strain generation pattern along the crown of the pipe was similar to that observed along its invert.

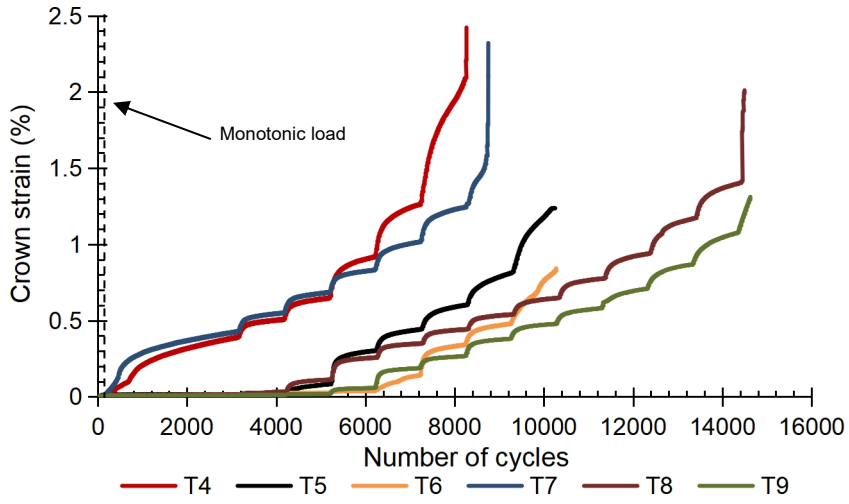

Figure 5.33 Crown strain against number of cycles, Series B and C

However, it experienced lower values due to the stress concentration zone between the invert and the bedding layer, in addition to the insignificant deformable nature of the pipe material. This behaviour demonstrated that burial depth of the pipe and number of the reinforcing layers significantly influenced the strain generation rate and value of pipe crown. Moreover, slight increase in the strain values of T7 was observed compared with T4 during the initial loading phases, where the opposite should have been occurred. This could be attributed to the slight variation between the compressive strength of the concrete pipe in both tests.

Table 5.12 and Table 5.13 illustrated the strain value of the crown due to increasing the cyclic loading phases under the variation of the burial depth of the pipe for Series B and C, respectively.

Table 5.12 Crown strain due to cyclic loading, Series B

Loading Phase	**1**			**2**			**3**			**4**		
H/D	1.5	2	2.5	1.5	2	2.5	1.5	2	2.5	1.5	2	2.5
C_{st} (%)	0.397	0.02	0.014	0.51	0.027	0.02	0.65	0.083	0.025	0.97	0.31	0.045
Enhancement ratio (%)	-	95	96.4	-	94.7	95.7	-	87.2	96.1	-	59.04	95.4
Loading Phase	**5**			**6**			**7**					
H/D	1.5	2	2.5	1.5	2	2.5	1.5	2	2.5			
C_{st} (%)	1.26	0.44	0.139	2.06	0.61	0.34	F	0.814	0.477			
Enhancement ratio (%)	-	62.1	89	-	70.4	83.5	-	-	41.4			

Table 5.13 Crown strain due to cyclic loading, Series C

Loading Phase	**1**			**2**			**3**			**4**		
H/D	1.5	2	2.5	1.5	2	2.5	1.5	2	2.5	1.5	2	2.5
C_{st} (%)	0.43	0.014	0.007	0.55	0.036	0.011	0.69	0.11	0.017	0.83	0.26	0.058
Enhancement ratio (%)	-	96.7	98.2	-	93.5	98	-	83.8	97.6	-	69	93
Loading Phase	**5**			**6**			**7**			**8**		
H/D	1.5	2	2.5	1.5	2	2.5	1.5	2	2.5	1.5	2	2.5
C_{st} (%)	1.02	0.35	0.19	1.25	0.45	0.265	1.5	0.54	0.38	F	0.65	0.48
Enhancement ratio (%)	-	65.7	81.7	-	64.3	78.8	-	64.1	74.7	-	-	26.3
Loading Phase	**9**			**10**			**11**			**12**		
H/D	1.5	2	2.5	1.5	2	2.5	1.5	2	2.5	1.5	2	2.5
C_{st} (%)	F	0.78	0.58	F	0.94	0.71	F	1.17	0.87	F	1.41	1.07
Enhancement ratio (%)	-	-	24.9	-	-	24.9	-	-	26.1	-	-	23.5

Figure 5.34 showed the crown strain of the pipe at the end of the applied loading phases with the burial depth increase in Series B. During the 1st loading phase, the measured strain values were 0.397%, 0.02% and 0.014% at burial depths of 1.5, 2 and 2.5, respectively. Reduction ratios of 94.96% and 96.37% was observed at *H/D*=2 and 2.5, respectively, compared with *H/D*=1.5.

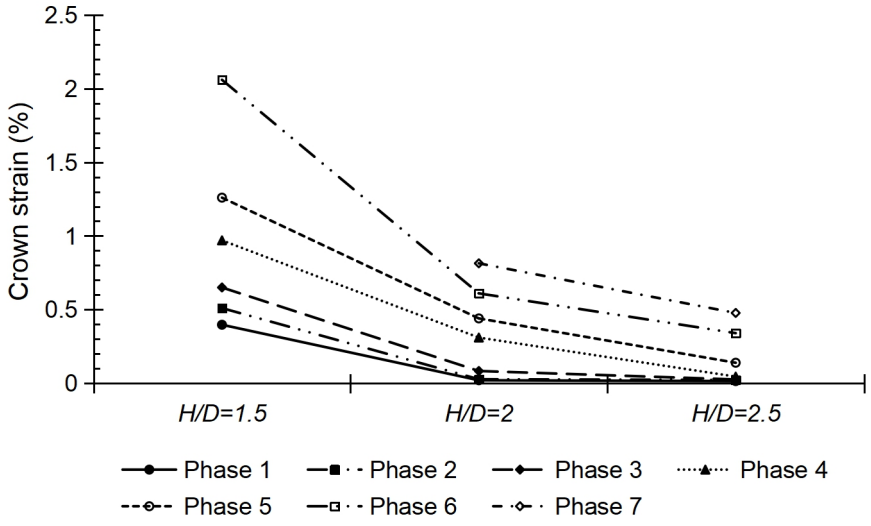

Figure 5.34 Crown strain at the end of each loading phase, Series B

It should be noted that insignificant reduction ratio was observed due to the increase in the burial depth from *H/D*=2 to 2.5, only 1.4%, which indicated that the optimum burial depth of the pipe is at *H/D*=2. This behaviour controlled the generated strain along the pipe crown until reaching the 5th phase for *H/D*=1.5, and the 7th phase for *H/D*=2 and 2.5, respectively, where failure occurred due to excessive footing settlement as illustrated in Figure 5.3. With the increase in the applied loading phases, it was noted that the strain reduction rate became more obvious while increasing the burial depth, where the load mitigation mechanism would have enhanced contribution. It was noted that the strain reduction curve between H/D=1.5 and 2 is steeper in the 6th loading phase compared with the 1st one.

As observed in the generated strain along the pipe invert, the generated strain pattern along the pipe crown during the 1st loading phase at a shallow burial depth experienced two different rates, particularly at the 300 cycle. This could be attributed to the ending of the reinforcing layer slack effect.

In Series C, similar behaviour was recorded for the generated strain along the pipe crown, but with reduced values as shown in Figure 5.35. This could be attributed to the inclusion of two reinforcing layers, which enabled the generation of an enhanced membrane mechanism and an improved degree of the provided lateral support to the pipe. Consequently, the increase in the burial

depth of the pipe and the number of the reinforcing layers significantly decreased the generated strain along the pipe crown.

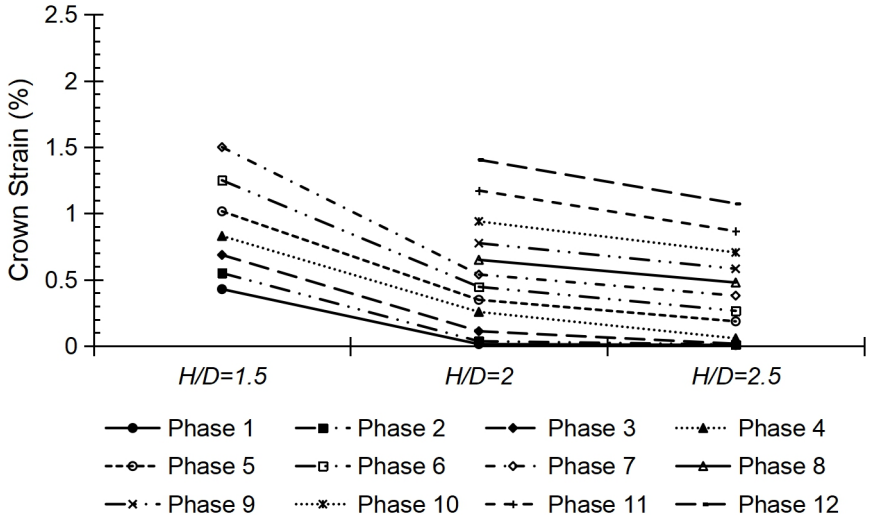

Figure 5.35 Crown strain at the end of each loading phase, Series C

Spring-line strain

Figure 5.36 demonstrated the generated strain along the pipe spring-line with the increase in the applied loading phases, for Series B and C.

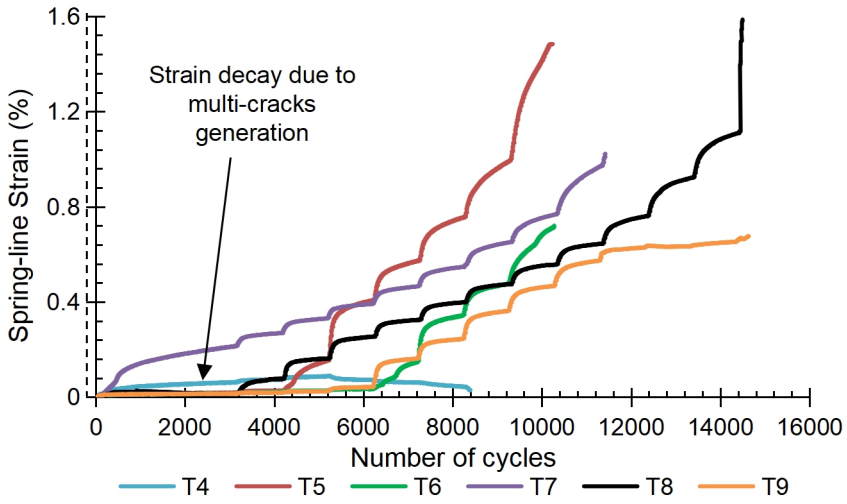

Figure 5.36 Spring-line strain due to the increase in loading phases, Series B and C

It is obvious that the spring-line strain pattern is similar to that generated along the pipe crown and invert but with a significantly reduced scale. This can be attributed to the inclusion of the reinforcing layers, which led to a pressure redistribution process over the adjacent soil portions to the pipe, allowing an

increase in the provided lateral support to the pipe, particularly its spring-line, i.e. formation of confined zone. On the other hand, the increased burial depth enabled the existence of larger soil volume with larger own-weight, providing extra lateral support.

An unexpected decay in the spring-line strain behaviour during *T4* was observed. Visual inspection of the pipe, after testing, indicated the generation of two cracks along the pipe spring-line, where the 1st intersected with the strain gauge and the 2nd did not, as presented in Figure 5.37.

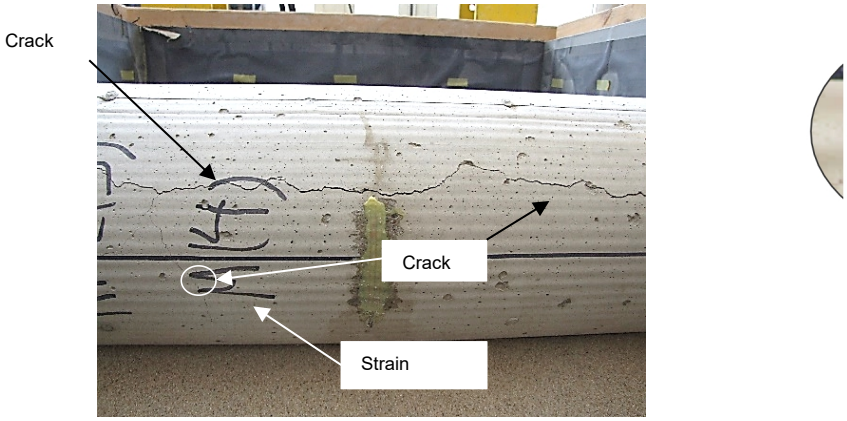

Figure 5.37 Generated cracks along the pipe spring-line in T4

Concrete tensile failure can be defined by cracks formation, where higher value of tensile strain was represented by wider crack. It was noticed that the 2nd crack was wider than the 1st one. Consequently, the actual generated tensile strain along the pipe spring-line was not recorded, since the 2nd crack did not intersect with the strain gauge. This explained the obvious decay in the strain value along the pipe spring-line in *T4*.

Table 5.14 and Table 5.15 illustrated the strain value of the spring-line due to increasing the cyclic loading phases under the variation of the burial depth of the pipe for Series B and C, respectively.

Table 5.14 Spring-line strain due to cyclic loading, Series B

Loading Phase	**1**			**2**			**3**			**4**		
H/D	1.5	2	2.5	1.5	2	2.5	1.5	2	2.5	1.5	2	2.5
SL_{st} (%)	-	0.0194	0.0182	-	0..026	0.022	-	0.155	0.026	-	0.416	0.039
Enhancement ratio (%)	-	-	6.19	-	-	15.71	-	-	83.1	-	-	90.63
Loading Phase	**5**			**6**			**7**					
H/D	1.5	2	2.5	1.5	2	2.5	1.5	2	2.5			
SL_{st} (%)	-	0.57	0.147	-	0.763	0.34	-	0.993	0.476			
Enhancement ratio	-	-	74.25	-	-	55.44	-	-	52.1			

(%)												

Table 5.15 Spring-line strain due to cyclic loading, Series C

Loading Phase	**1**			**2**			**3**			**4**		
H/D	1.5	2	2.5	1.5	2	2.5	1.5	2	2.5	1.5	2	2.5
SL_{st} (%)	0.21	0.02	0.017	0.27	0.08	0.028	0.332	0.162	0.045	0.41	0.24	0.079
Enhancement ratio (%)	-	91.6	92.1	-	71.4	89.7	-	52.2	56.6	-	41.5	80.8
Loading Phase	**5**			**6**			**7**			**8**		
H/D	1.5	2	2.5	1.5	2	2.5	1.5	2	2.5	1.5	2	2.5
SL_{st} (%)	0.464	0.325	0.212	0.557	0.4	0.3	0.65	0.475	0.41	0.77	0.556	0.5
Enhancement ratio (%)	-	29.9	54.3	-	28.5	46.5	-	27.1	37.8	-	27.6	35.7
Loading Phase	**9**			**10**			**11**			**12**		
H/D	1.5	2	2.5	1.5	2	2.5	1.5	2	2.5	1.5	2	2.5
SL_{st} (%)	0.97	0.64	0.59	F	0.76	0.7	F	0.92	0.82	F	1.13	1.12
Enhancement ratio (%)	-	33.8	39.5	-	-	7.76	-	-	10.74	-	-	1.63

5.4.2.7 Reinforcing layers strain

Soil failure is governed by the tensile strain generated due to applied loading profiles. Consequently, the inclusion of reinforcing layers is required. Figure 5.38 illustrated the generated strain in the reinforcing layer according to the increase in the applied cyclic loading phases, in Series B, where one reinforcing layer was utilised to enhance the backfill performance.

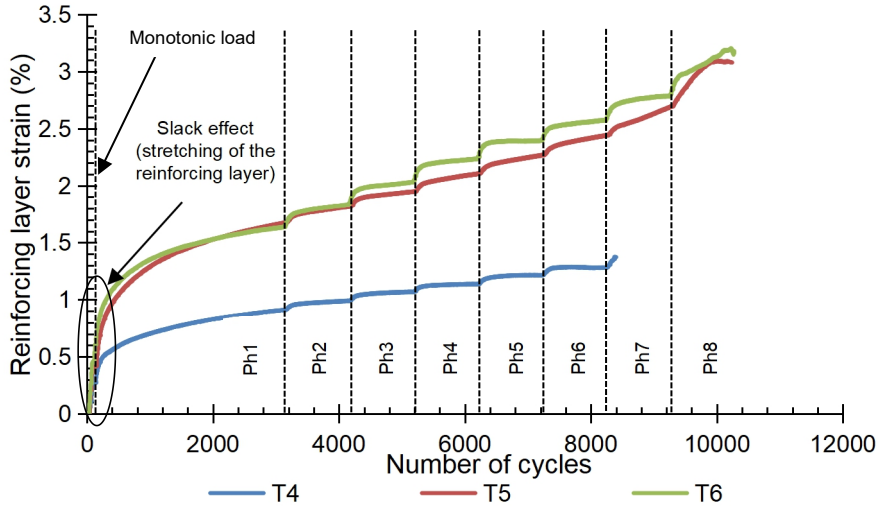

Figure 5.38 Strain generated in the reinforcing layers, Series B

At the same cyclic load, it was observed that the increase in the burial depth of the pipe negatively influenced the generated strain in the reinforcing layer, where its value increase, as presented in Figure 5.39.

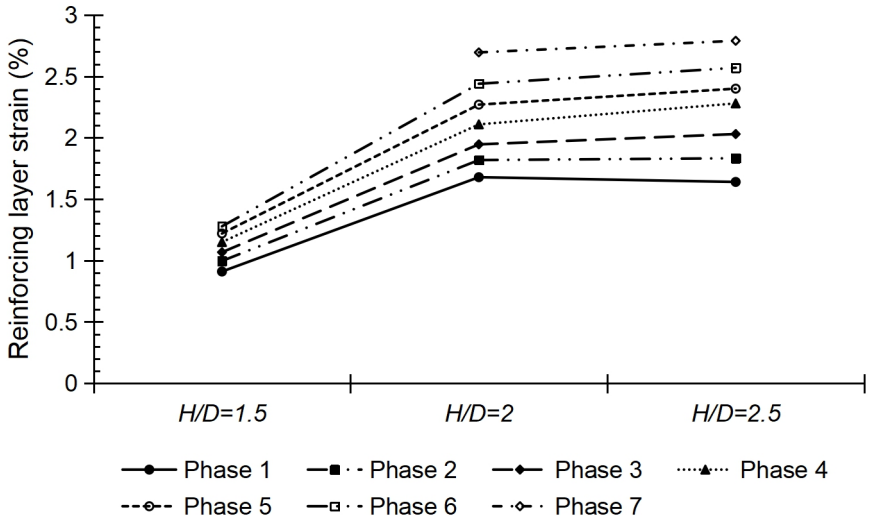

Figure 5.39 Strain generated in the reinforcing layers at the end of each loading phase, Series B

Location of the pipe contributed to the system stability, where system stability became less dependent on the pipe at deep burial depths, where generated strain along the wall of the pipe significantly reduced, as shown in Figure 5.32, Figure 5.33 and Figure 5.36. At this stage, the reinforcing layer started gradually to dominate the system stability, which was obvious at and after a burial depth of *H/D*=2, as strain value significantly increased. The distance between the pipe and the soil surface was divided into two zones, upper and lower zones. According to the high stiffness of the pipe, it reinforced the lower zone, and contributed to the upper zone stability. At deep burial depths, the stability of the upper zone was dominated by the soil properties, where tensile strain value increased and the reinforcing layer existence to sustain the tensile strains became crucial. Consequently, the inclusion of reinforcing layers maintained the upper zone stability, where it had a minor contribution in the upper zone stability when it is close to the pipe, i.e. at shallow burial depth, and vice versa.

Strain generation rate was dependent on the slack effect of the reinforcing layers, as shown in Figure 5.38. During the first 300 cycles of the 1st loading phase, strain generation rate was fast as slack effect progressed, and with the increase in loading cycles, this rate significantly decreased as no more slack effect occurred (Chenggang, 2004; Sieira et al., 2009; Tran et al., 2013). It was also obvious that the strain increased gradually according to the applied load, and once the system started to fail, the strain value increased rapidly,

regardless of the burial depth of the pipe or the applied loading phases. Visual inspection of the reinforcing layers illustrated permanent deformation, however no damage was observed. Eventually, increasing the pipe burial depth enhanced the reinforced system stability, where the reinforcing layer endured the generated tensile strain.

In Series C, two reinforcing layers were used to increase the system stability and provide more protection to the buried pipe. Figure 5.40 illustrated the strain generated in the two reinforcing layers according to both burial depth and applied loading cycles.

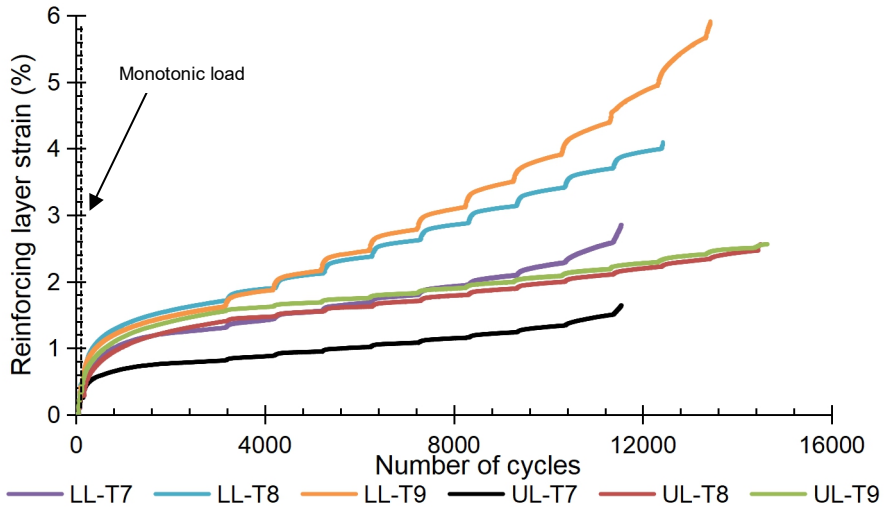

Figure 5.40 Generated strain in the reinforcing layers, Series C

Figure 5.41 demonstrates a comparison between the generated strains in the two reinforcing layers with respect to the applied loading phases.

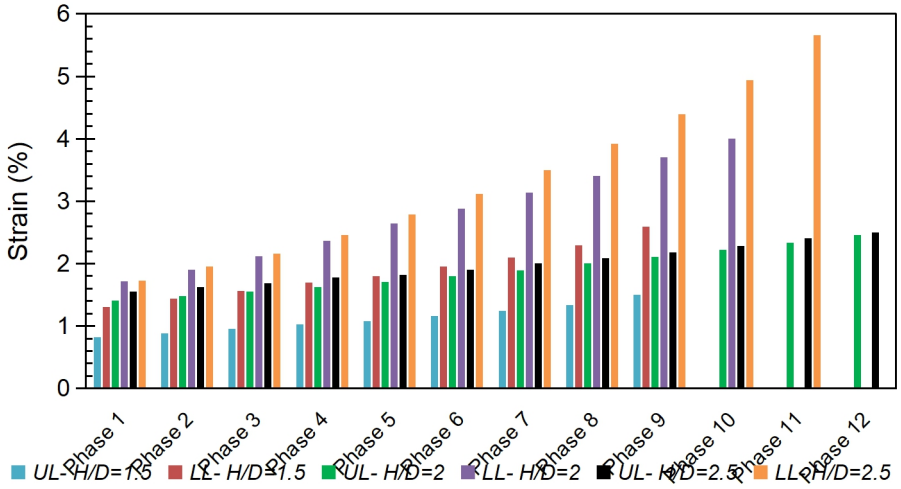

Figure 5.41 Comparison between upper and lower layers strain, Series C

In this case, the layers endured the generated tensile strain in the soil, where the contribution of each of them depended on the generated tensile force and the occurred deformation. After testing, the soil was excavated carefully, and the deformation and deformed shape of the reinforcing layers were inspected. Usually, the upper layer deformation was higher than the lower one. Since the upper layer is closer to the footing, a high-pressure value transferred to it, where a lower value was transferred to the lower layer.

However, Figure 5.41 illustrated that, generally the sustained strain value by the lower layer is higher than that sustained by the upper one, regardless of the pipe burial depth or the loading phase, which was in agreement with the findings of Jones and Cooper (2005). The maximum measured strain in the lower layer was higher than that measured in the upper one by 42%, 44.4% and 57.5% for *H/D*=1.5, 2 and 2.5, respectively.

This behaviour illustrated that, a stiff platform was formed out of the two reinforcing layers and the trapped soil layer between them, which behaved as a flexible reinforced slab, which was in good agreement with Mohamed (2010). Due to the applied load, the formed stiff platform was subjected to bending stresses, where the lower reinforcing layer was highly influenced as shown in Figure 4.44. Consequently, tensile strain was generated along its lower surface unlike its upper surface, which suffered compressive strain. Therefore, the generated tensile strain in the lower reinforcing layer governed the behaviour and stability of the whole system. It should be noted that, the reinforcing layer failure was governed by the sustained strain value rather than its deformation. It was taken into consideration that there was no prolonged loading; consequently, no creep deformation was observed in the reinforcing layers.

5.5 Repeatability

Series D represented the repetition of one test under the same conditions two times; T4 and T10, to make sure that the used instruments and devices are well calibrated and properly used. A comparison between the footing and pipe crown settlement of the two tests is demonstrated in Figure 5.42.

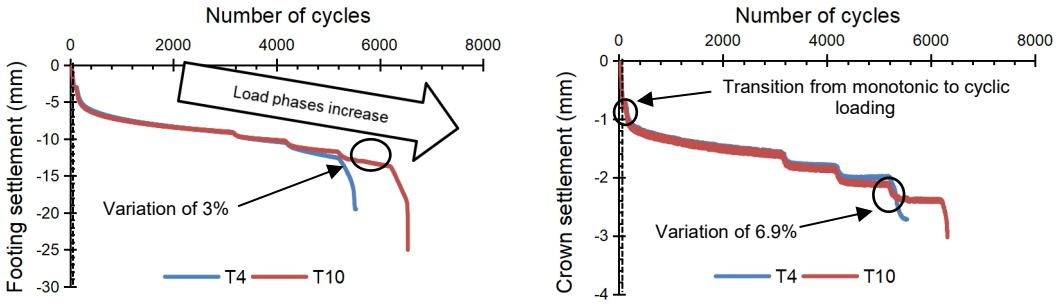

Figure 5.42 Footing and crown settlement comparisons

Careful inspection illustrated that there is slight variation between the findings of the two tests, where variation of 3% and 6.9% was reached in the footing and the crown settlement, respectively. This variation increased once failure occurred. It was noticed that T10 sustained four loading phases; however, T4 sustained three loading phases. This could be attributed to the slight variation in the compressive strength of the concrete pipe.

5.6 Summary

In this chapter, fully instrumented physical models were tested to investigate the behaviour of buried rigid pipes in unreinforced and geogrid-reinforced sand beds under the application of incrementally increasing cyclic loading. Based on the findings of these physical models, the following conclusions can be drawn;

1- Maximum rate and value of deformations and strains occurred during the first 300 cycles of the 1st loading phase. With further loading cycles' application, measured rates and values significantly decreased until reaching almost stable values at the end of the loading phase. With the progression of loading phases, same behaviour is repeated with significant reduced values.

2- Progression of the loading cycles led to a soil densification process, which contributed in reducing the deformation rate of the pipe, and the settlement of the footing.

3- In the unreinforced case, at shallow burial depth, generated cracks along the pipe were observed during the 1st loading phase, where a collapse in the passive arching mechanism was occurred, decreasing the transferred pressure to the pipe, and providing additional lateral support to it. At deeper burial depths, generated cracks along the pipe were

observed at further loading phases, as a result of the positive contribution of the load mitigation mechanism.

4- In the unreinforced case, at *H/D*=1.5, during the 1st loading phase, generated deformations and strains of the pipe experienced a non-uniform behaviour, which was matched with the transferred pressure to the pipe.

5- The generated strain patterns along the pipe were similar; however, the generated strains along the invert and the crown of the pipe were much higher than those measured along its spring-line.

6- The densification process of the soil vitally contributed in increasing the stiffness of the soil, in particular the bedding layer, which allowed for more reaction forces to be generated between the bedding layer and the invert of the pipe. These reaction forces applied upward pressure, initiating an invert rebound.

7- At shallow burial depths, the invert rebound occurred faster than those measured at deep burial depths due to the faster densification of the bedding layer. At deep burial depths, the densification of the bedding layer required more loading phases to occur hindering the rebound of the invert.

8- Increasing the burial depth of the pipe had a significant contribution in decreasing its deformations and strains, decreasing transferred pressure to it, decreasing the rates and the values of the footing settlement, and increasing the generated strains in the reinforcing layers. The results suggested that the behaviour of the whole system relied on the pipe location, where it could provide stability to the system according to its stiffness.

9- Due to the crown and invert deformations, cracks were formed along the wall of the pipe distorting its cross-section, where the new formed cross-section consisted of four segments between the formed cracks, seeking to form an elliptical shape, which was more obvious at shallow burial depths. The inclusion of the reinforcing layers and the increase in the burial depth of the pipe hindered and controlled the generation and propagation of the cracks.

10- In the unreinforced case, pressure transfer inside the soil was governed by two mechanisms; i. passive arching and ii. Load mitigation mechanisms. The inclusion of the reinforcing layers provided one more mechanism, i.e. distributed load over reinforcing layer plane, which depended upon the soil-reinforcement interaction mechanisms, particularly the passive earth resistance.

11- The reinforcing layers inclusion decreased the generated strains and deformations of the pipe and the footing settlement because of the pressure redistribution process. Moreover, it allowed the systems to sustain additional loading.

12- At initial loading phases, the inclusion of the reinforcing layers had obvious influence in decreasing the generated strain in the pipe. However, the increase in the layers number had significant contribution in decreasing the generated strains, while applying advanced loading phases.

13- In Series C, the generated strain in the lower layer was usually higher than that measured in the upper layer, despite the increased deformation of the upper layer. This could be attributed to the formed flexible slab, which suffered tensile and compressive strains along its lower and upper surfaces, respectively.

14- The inclusion of the reinforcing layers achieved the *ITM* concept, where reduced deformations and strains influenced the buried rigid pipe and more loading phases were sustained safely.

CHAPTER 6

FINITE ELEMENT IMPLEMENTATION

6.1 Introduction

Finite element analysis (*FEA*) is used to obtain a numerical solution to many of the engineering problems. *FEA* is a method for simulating loading conditions on a system that is represented by elements. It is used to solve structural problems such as stress, buckling, reactions calculations, settlement values, impact, explosion, vibration analysis and non-structural problems as heat transfer, fluid flow, and distribution of electric or magnetic potential. *FEA* serves to reduce product testing, hence reducing its development time and cost, also gives the ability to make parametric study on any engineering system, which gives clearer investigation of the system behaviour as well as prediction of its failure. The finite element method of structural analysis enables the designer to detect stress, vibration, and thermal problems during the design process and to evaluate design changes before the construction of a possible prototype. This will enable the reduction in cost and number of created prototypes used to solve the problem (Logan, 2011).

Commercial finite element package ABAQUS/CAE version 6.14 is used in this research, and the following section refers extensively to the associated manuals. This software has been used in many different engineering fields throughout the world. It can solve problems ranging from relatively simple linear analysis to the most challenging nonlinear simulations. The software contains an extensive library of elements that can model virtually any geometry, and an extensive material models enable it to simulate the behaviour of most typical engineering materials, e.g. metals, rubber, reinforced concrete, geosynthetics and geotechnical materials such as soils and rocks, (Abaqus, 2014). ABAQUS finite element system includes:

1- ABAQUS/Standard, a general-purpose finite element program.
2- ABAQUS/Explicit, an explicit dynamics finite element program.

3- ABAQUS/CAE, an interactive environment used to create finite element models, submit ABAQUS analyses, monitor and diagnose jobs, and evaluate results.
4- ABAQUS/Viewer, a subset of ABAQUS/CAE that contains only the post processing capabilities of the visualization module.

Since finite element analysis has been chosen to investigate the research problem, then, two main challenges are to be considered.

1- Geometry:

The geometry problem includes the dimensions of the elements forming the problem, the boundary conditions, the element type choice and the solution mode.

2- Material model:

The material model is considered the constitutive model that defines the behaviour of each involved element in the problem. Material models are most likely to be nonlinear elasto-plastic. Wide range of constitutive models may be used to identify certain element, but, each one of them has its own advantages and disadvantages, and the choice process is based on achieving the most benefit from the material model (Nagy, 2007).

6.2 Utilization of FEA

FEA method is very suitable for practical engineering problems of complex geometries. To obtain good accuracy in regions of rapidly changing variables, a large number of small elements must be used. The use of FE simulation has many advantages as follows (Logan, 2011):

1- Simulation of complex designs of engineering components and structures.
2- Comprehensive information regarding the distribution of stresses and strains inside a structure.
3- Better understanding of the effect of geometric features on the stress/strain state.
4- Model irregularly shaped bodies quite easily.
5- Handle different load conditions easily.
6- Model bodies composed of several different materials.

7- Handle unlimited number of boundary conditions.
8- Vary the size of the elements to make it possible to use small elements where necessary.
9- Changing the finite element model is relatively easy.
10- Include various dynamic effects.
11- Handle nonlinear behaviour existing with large deformations and nonlinear materials.

Although there are many benefits of using finite element simulation, there are also risks. Before using finite element method to simulate any problem, the theory behind this methodology must be well understood. On the other hand, the input data must be accurately describing the tested materials to get reasonable results. The greater the number of elements that define a certain component, the more accurate the result, but that will influence the solution time.

6.3 Problem modelling

To be able to investigate the behaviour of any problem by using *FEA*, the following steps should be followed:

1- Material model definition.
   a- Defining the constitutive model describing the behaviour of each element in the problem, either it was elastic, plastic or combination of them (elasto-plastic).
2- Geometrical definition of the problem.
   a- Dimensions of each element.
   b- Boundary conditions definition.
   c- Proper meshing.
   d- Choosing appropriate element type.
   e- Defining steps at which different loads are applied.
3- Interaction between different elements forming the problem.
4- Load definition.
5- Output definition.

6.4 General plasticity

The behaviour of the material under loading and unloading conditions is the main concept, which defines if its representation depends on the elastic or

plastic theory. Generally, because of the variation in the soil's response due to loading and unloading conditions (recoverable and irrecoverable deformations), soil behaves as elasto-plastic material. If an elasticity-based model is used to represents the soil's behaviour under general loading conditions, then, special loading criterion must be defined for both cases, loading and unloading, which is known as deformation theory of plasticity. Each theory has its own limitations. This concept is applied to the deformation theory of plasticity, and to be able to overcome these limitations, the flow (incremental) theory of plasticity should be considered. The flow theory of plasticity relies on three fundamental concepts (Chen and Mizuno, 1990). These concepts are as follows:

1- Yield function.
2- Flow rule.
3- Hardening rule.

Flow theory of plasticity can be described as, according to the development of stress-strain increment relationship, the total increase in the strain, $d\mathcal{E}_{ij}$, can be considered as the summation of both the elastic strain increment, $d\mathcal{E}_{ij}^{e}$, and the plastic strain increment, $d\mathcal{E}_{ij}^{p}$, as shown in Eq (6.1).

$$d\mathcal{E}_{ij} = d\mathcal{E}_{ij}^{e} + d\mathcal{E}_{ij}^{p} \qquad (6.1)$$

The elastic strain increment, $d\mathcal{E}_{ij}^{e}$, is governed by Hook's law, where the material properties such, elastic, bulk and shear moduli remain constant. On the other hand, the estimation process of the plastic strain increment, $d\mathcal{E}_{ij}^{p}$, requires the identification of a yield surface and a flow rule at which the stress corresponding to the increment of plastic strain, $d\mathcal{E}_{ij}^{p}$, can be identified.

6.4.1 Yield function

It is important to identify the separation point between the elastic and plastic behaviour of any material. Under the application of uniaxial test, for example, tension or compression test, the separation point between the elastic and plastic behaviour of the material can be easily identified from the stress-strain curve, and it is considered the yield point at which the behaviour of the material converts from linearity to non-linearity. In the case of combined tests, under biaxial stress conditions, the yielding point becomes a yielding curve, which should be identified. Furthermore, under the application of three-dimensional

test, the yield curve becomes a yield surface, which can be represented mathematically as a yield criterion (Chen and Mizuno, 1990).

The yield surface can help in the determination of the stress state by which the material will behave as plastic manner, furthermore, to separate elastic and plastic behaviour zones of the material. Stress paths located within the yielding surface produce recoverable deformation as a result of being in the elastic domain. Contrarily, stress paths that intersect the yielding surface produce a combination of recoverable and irrecoverable deformation due to the existence in the plastic domain. The yielding surface can be expressed as an initial yielding function, F, as follows in Eq (6.2):

$$F(\sigma_{ij}) = F_c \qquad (6.2)$$

Where;

$F_c \rightarrow$ is a constant value for perfectly plastic material and in the case of strain hardening material, it can be considered of variable value.

In the case of biaxial stress space, the yielding surface can be as shown in Figure 6.1-A. Considering a perfectly plastic material, the yielding surface is fixed in stress space and the plastic deformation will occur once the stress path moves on the yield surface or intersects it. For strain hardening material, the generated stresses will intersect the yielding surface and go beyond it as shown in Figure 6.1-B.

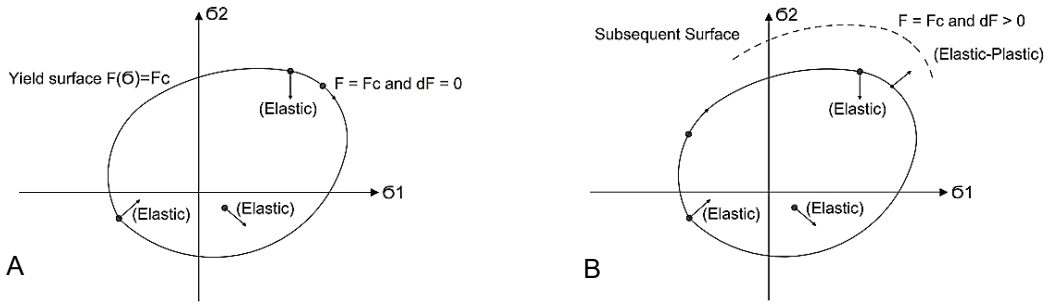

Figure 6.1 Yield surfaces in perfectly plastic and hardening materials, (Chen and Mizuno, 1990)

A: perfectly plastic material. B: Hardening material.

6.4.2 Flow rule

The main function of the flow rule is to define the relation between the current state of stress σ_{ij}, and the next increment of the plastic strain $\mathcal{E}_{ij}^{p}$ for a yielded material subjected to further loading. The concept of plastic potential function (g)

is used to establish the flow rule. According to the plasticity theory, the plastic potential function can define the direction of the plastic strain increment according to Eq (6.3) (Chen and Mizuno, 1990):

$$d\mathcal{E}_{ij}^{p} = d\lambda \frac{\partial g}{\partial \sigma ij} \qquad (6.3)$$

Where;

$d\lambda \rightarrow$ is a positive scalar, which depends on the state of stress and load history.

According to the coincidence between the plastic potential function and yield surface, the flow rule can be one of the following:

a- Associated flow rule in case the potential and yield surfaces coincide with each other ($F = g$).

b- Non-associated flow rule if they did not coincide with each other ($F \neq g$).

The surface of the plastic potential function (g) and the vector describing the direction of the plastic strain increment $\mathcal{E}_{ij}^{p}$, are intersected at the current stress point σ_{ij} and they form a right angle as show in Figure 6.2.

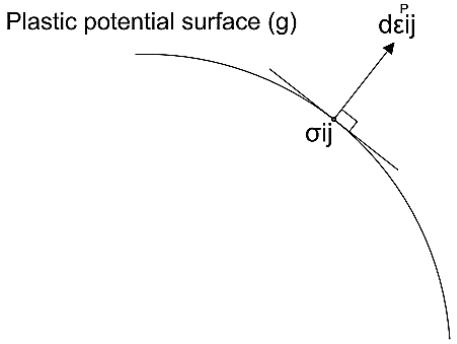

Figure 6.2 Plastic strain increment direction

6.4.3 Hardening rule

The flow theory of plasticity depends on three main assumptions:

1- The shape of initial yield surface.

2- Evolution of the subsequent loading surface (hardening rule).

3- Formation of an appropriate flow rule.

According to the perfect plasticity theory, the yield surface is fixed in the stress space, but according to the hardening plasticity theory, the yield surface is not fixed, and the stress state of the material can move outside the yield surface.

Consequently, the motion of the yield surface during plastic loading can be defined according to the hardening rule.

Variable hardening rules can be followed according to the loading nature (Chen and Mizuno, 1990). For example:

1- Isotropic hardening rule.
2- Kinematic hardening rule.
3- Mixed hardening rule.

The isotropic hardening rule enables the loading surface to expand/contract uniformly without distortion as plastic flow continues as shown in Figure 6.3, while the kinematic hardening rule allows the loading surface to translate as a rigid body in the stress space without rotation keeping the size and shape of the initial yield surface as shown in Figure 6.3. The mixed hardening rule is the more general hardening rule, and it combines the advantages of the previous two hardening rules, allowing the loading surface to expand/contract uniformly in all directions, as well as translating as a rigid body in the stress space. The plasticity models that follow the kinematic and mixed hardening rules are generally known as anisotropic hardening models.

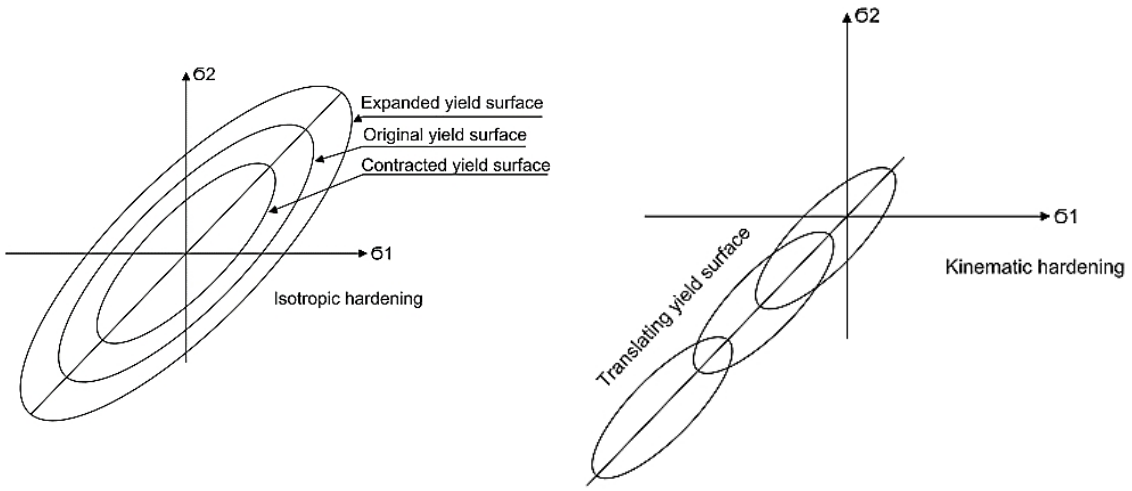

Figure 6.3 Isotropic and kinematic hardening

The model that follows the isotropic hardening rule can simulate the material under the application of only monotonic loading, while the models that follows either the kinematic or mixed hardening rule enable the application of cyclic and dynamic loading.

The loading function can be expressed in terms of stress state σ_{ij}, plastic strain ε_{ij}^{p} and the hardening parameter k as follow, Eq (6.4):

$$F = F(\sigma_{ij}, \varepsilon_{ij}^{p}, k) \quad (6.4)$$

The hardening parameter (k) is often a function of the plastic trajectory or the total plastic work in the case of metallic materials. On the other hand, in the case of soils, the hardening parameter (k) depends on the amount of plastic compaction. The difference between the perfect and hardening plasticity theories is illustrated in Table 6.1.

Table 6.1 Difference between the perfect and hardening plasticity theories

Perfect Plasticity Theory	Hardening Plasticity Theory
Non-deformed material	Deformed material
Yield function (surface)	Loading function (surface) (subsequent yield surface)
Fixed in the stress space	Not fixed in the stress space and varies according to the hardening rule type
The yield function can be determined according to the flow rule	The loading function changes its geometry according to the flow rule

6.5 Material model (constitutive model)

The research is about investigating the behaviour of buried structure while using geogrid-reinforcing layers to enhance the backfill soil behaviour. Consequently, the model will consist of the following elements:

1- Soil.
2- Geogrid reinforcements.
3- Buried structure.

Each of them has different behaviour; consequently, different material models will be assigned to each element of them.

6.5.1 Soil constitutive model

Soil behaves as an elasto-plastic material because of the variation between its behaviour before and after load application. To simulate the soil, both elastic and plastic models should be used to form elasto-plastic model that truly describes the soil's behaviour. Three plasticity models are provided by ABAQUS to simulate the sandy soil's plasticity (Abaqus, 2014).

1- Extended Mohr-Coulomb plasticity model.
2- Extended Drucker-Prager model.
3- Drucker-Prager/Cap model.

6.5.1.1 Extended Mohr-Coulomb plasticity model

Extended Mohr-Coulomb (*EMC*) is an extension of the classical *MC* failure criterion. It is an elastoplastic model that uses the yield function of the Mohr-Coulomb form in addition to a hardening law and a flow rule. The yield function includes isotropic cohesion hardening/softening. However, the model uses a flow potential that has a hyperbolic shape in the meridional stress plane and an elliptic shape (with no corners) in the deviatoric stress space. Therefore, *EMC* can be considered a combination of:

a- Classical Mohr-Coulomb (*MC*).
b- Hardening/softening yield function.
c- Flow rule.

Classical Mohr-Coulomb model (MC)

The *MC* criterion is one of the most widely used theories for describing the failure of soil materials. This is because of its mathematical simplicity, and the physical meaning of the material parameters.

The MC theory can be thought of as a set of linear equations in principal stress space that represent a shear failure surface for an isotropic material, with no effect from the intermediate principal stress (σ_{II}). It assumes that failure occurs when shear stress on any point in a material reaches a limit value that depends linearly on the normal stress in the same plane. The classical formulation of the MC model can be identified as illustrated in Eq (6.5).

$$\tau = c + \sigma \tan \Phi \qquad (6.5)$$

Where; τ and σ are the shear and normal stresses on the failure plan respectively, c is the cohesion, Φ is the angle of internal friction.

Figure 6.4 illustrates a representation of the *MC* failure criterion on a Mohr circle diagram. The criterion states that the larger the normal stress σ, the more shear the material can sustain (Helwany, 2007; Abaqus, 2014).

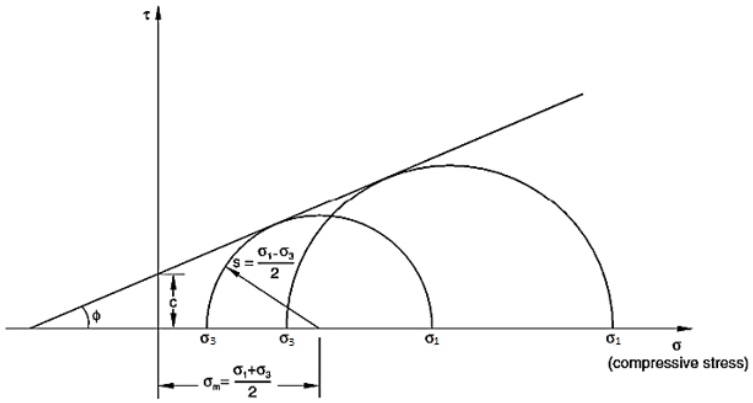

Figure 6.4 Mohr-Coulomb failure criterion

Hardening/softening yield function

For general state of stress, the yield function of the *EMC* is expressed in terms of three stress invariants, where they can be described as follows:

1- Equivalent stress/hydrostatic pressure (*p*):

$$p = -\frac{1}{3}\,trace\,(\sigma) = -\frac{1}{3}(\sigma_1 + \sigma_2 + \sigma_3) \qquad (6.6)$$

2- The Mises equivalent stress (*q*), (Du et al., 2009):

$$q = \sqrt{\frac{3}{2}(s:s)} = \frac{1}{\sqrt{2}}\sqrt{(\sigma 1-\sigma 2)^2+(\sigma 2-\sigma 3)^2+(\sigma 3-\sigma 1)^2} \qquad (6.7)$$

3- The third invariant of deviatoric stress (r):

$$r = \left(\frac{9}{2}s\cdot s:s\right)^{1/3} \qquad (6.8)$$

Where;

S is the stress deviator and (*:*) is the scalar product.

The variables *q* and *p* are commonly defined in soil mechanics as the deviatoric stress and the effective mean stress, respectively and they both define the meridional stress plane.

Consequently, the yield surface (*F*) can be expressed as:

$$F = R_{mc}q - p\tan\Phi - c = 0 \qquad (6.9)$$

Where:

Φ is the classical friction angle of the material, ranging from 0 to 90 degrees.

c is the evolution of the cohesion of the material in the form of isotropic hardening (or softening) and it is a function of the equivalent plastic strain ε_{ij}^{p}.

R_{mc} is a measure of the shape of the yield surface in the deviatoric stress.

Flow rule (flow theory of plasticity)

The meaning of the flow rule is that there must be an extension of the elastic stress-strain relation in the elastic zone into the plastic zone, at which permanent plastic strain is possible in addition to the elastic strain. This plastic strain remains even after the removal of the stresses and applied loads. Consequently, the strain in plastic material can be described as the summation of the recoverable elastic strain and the irrecoverable plastic strain (Chen and Mizuno, 1990).

The flow potential, *g*, used for the *EMC* model has a hyperbolic function in the meridional stress plane and is described by the smooth elliptic function in the deviatoric stress plan, as shown in Eq (6.10):

$$g=\sqrt{(\in c|o\ tan\psi)^2+(Rmwq)^2}-(p\ tan\psi) \qquad (6.10)$$

Where:

R_{mw} → is the polar radius and it is a function of *Θ* (the deviatoric polar angle) and *e*, as described below. It controls the shape of g in the deviatoric plane, (p-q).

ψ → is the dilatancy angle measured in the p-$R_{mw}q$ plane at high confining pressure.

$c|o$ → is the initial cohesion yield stress that is corresponding to zero plastic strain, $c|o = c(\mathcal{E}_{ij}^{p}=0)$.

$\in$ → is a parameter referred to as the meridional eccentricity (with default value of 0.1), which controls the shape of g in the meridional plane.

e → is a parameter referred to the deviatoric eccentricity, that describes the "out-of-roundness" of the deviatoric section ($0<\Theta<\frac{\pi}{3}$) . The default value of the deviatoric eccentricity is equal to ($\frac{3-sin\varphi}{3+\sin\varphi}$), and allows the ABAQUS Mohr-Coulomb model to match the behaviour of the classical Mohr-Coulomb model in triaxial compression and tension. It may have a range of $0.5<e<1$.

Summary of EMC model

1- It is used in combination with the linear elastic material model.
2- It is used to model materials with the classical Mohr-Coulomb yield criterion.

3- The yield behaviour depends on the hydrostatic pressure, which may lead to stronger material under increased confining pressure.
4- It allows the material to harden and/or soften isotropically.
5- The plastic behaviour will generally be accompanied by some volume change.
6- It uses a smooth flow potential that has a hyperbolic shape in the meridional stress plane and an elliptic shape in the deviatoric stress surface which is generally non-associated (plastic potential function and yield surface does not coincide, $F \neq g$).

The use of the *EMC* model to describe the soil backfill requires the identification of five main parameters as illustrated in Table 6.2:

Table 6.2 EMC model parameters

Φ	Slope of the failure curve in p-R_{mc}q plane (classical soil friction angle)	Defining plasticity
ψ	Soil dilation angle	
$c\|o$	Initial cohesion stress, corresponding to zero plastic strain (soil's cohesion)	
E	Young's modulus	Defining elasticity
υ	Poisson's ratio	

To be able to identify the required inputs experimentally, triaxial and direct shear tests should be performed.

6.5.1.2 Extended Drucker-Prager model

The extended Drucker-Prager model is used to model frictional materials, which are typically granular-like soils and rock, and exhibit pressure-dependent yield (the material becomes stronger as the pressure increases). It can be used to model materials in which the compressive yield strength is greater than the tensile yield strength, such as those commonly found in composite and polymeric materials (Abaqus, 2014).

On the other hand, it allows the material to harden and/or soften isotropically. Generally, it allows volumetric change with inelastic behaviour, which can be defined as the flow rule, defining the inelastic straining, allows simultaneous

inelastic dilation (volume increase) and inelastic shearing. It can include creep, if the material exhibits long-term inelastic deformations. It can be used with the elastic material model, in order to define the material plasticity. It can simulate material response under monotonic loading.

The model is written in terms of the three-stress invariants. It provides for a possibly circular yield surface in the deviatoric plane to match different yield values in triaxial tension and compression, associated inelastic flow in the deviatoric plane, and separate dilation and friction angles.

The model is a generalization of the MC model in the sense that the hexagonal form of the failure contour in the principal stress space has been replaced by a simple circular cone with symmetry about the hydrostatic axis. This overcomes the shortcoming of complications with the treatment of plastic at corners, i.e. singularity (Chen and Baladi, 1985), as shown in Figure 6.5.

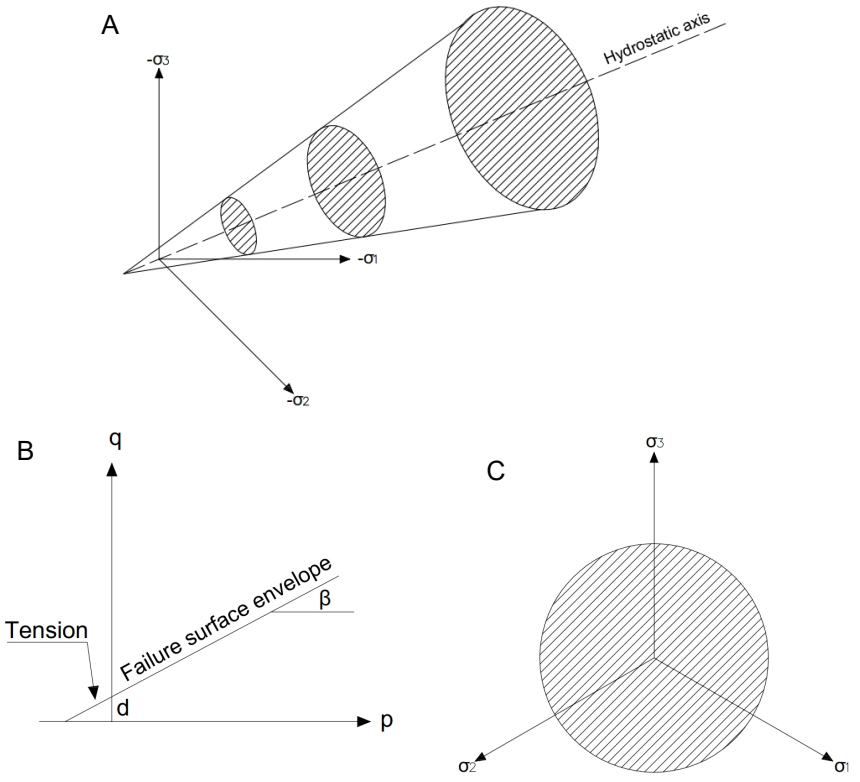

Figure 6.5 Drucker-Prager model
A: Deviatoric space. B: Meridional plane. C: *π*-plane.

Summary of EMC model:

1- The extended Drucker-Prager model is used to model frictional materials, which are typically granular-like soils and rock, and

exhibit pressure-dependent yield (the material becomes stronger as the pressure increases).

2- It can be used to model materials in which the compressive yield strength is greater than the tensile yield strength, such as those commonly found in composite and polymeric materials.
3- It can be used in combination with the linear elastic material model.
4- The yield behaviour depends on the value of the material stress parameter (K) as well as the relation between both, the internal friction angle and the dilation angle.

The major disadvantage in the extended Drucker-Prager model is its inability to model compressive plastic strains and it is restricted to the modelling of dense sand and highly over consolidated clays. Consequently, it can't model loose sands (Nagy, 2007; Abaqus, 2014).

The use of the extended Drucker-Prager model to describe the soil backfill requires the identification of the following parameters:

1- Soil's friction angle in the p-q plane (β).
2- Dilation angle of the soil (ψ).
3- Material stress parameter (K).

In order to describe the soil's hardening, the triaxial test should be performed to identify the yield stress of the soil as a function of its plastic strain.

6.5.1.3 Drucker-Prager / Cap model

A proper modelling of soils requires the consideration of strain or work-hardening theory of plasticity. Consequently, soil might be modelled as an elastic-plastic hardening material (Drucker et al., 1957). The use of a cap model can clearly identify the soil's behaviour, in particular after its shear failure. The Drucker-Prager/Cap model was originally developed to overcome the problem of the Drucker-Prager model, and predict the plastic deformation of soils under compression (Chen and Mizuno, 1990). The addition of a spherical end-cap to the Drucker-Prager yield surface will allow the control of the plastic volumetric change of the soil, i.e. dilatancy, when the material yields in shear as shown in Figure 6.6 (Drucker et al., 1957; Abaqus, 2014):

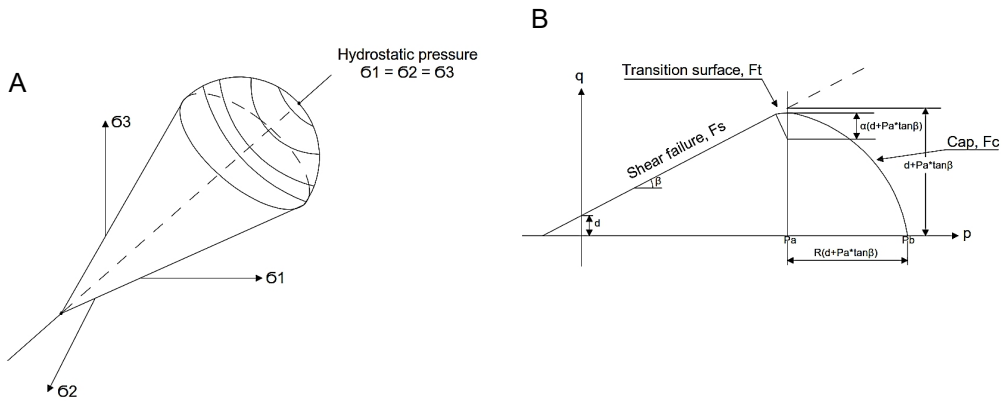

Figure 6.6 Drucker-Prager/Cap model
A: Deviatoric space. B: Meridional plane.

The yield surface of the cap model consists mainly of two intersecting segments:

1- Shear failure surface, F_s.

2- Cap surface, F_c.

The shear failure segment provides dominantly shearing flow, and the cap segment provides an inelastic hardening mechanism to account for plastic compaction and helps in controlling the volumetric dilatancy when the material yields in shear (Abaqus, 2014). A transition surface, F_t, is introduced in between the shear failure surface and the cap surface to provide a smooth transition between them.

The cap serves two main purposes as follows:

- It bounds the yield surface in hydrostatic compression, thus providing an inelastic hardening mechanism to represent plastic compaction.
- It helps to control volume dilatancy when the material yields in shear by providing softening as a function of the inelastic volume increase created as the material yields on the Drucker-Prager shear failure and transition yield surface (Abaqus, 2014).

Drucker-Prager / Cap model summary:

1- It satisfies the theoretical requirements of stability.

2- It provides control of excessive dilatancy unlike Dracker-Prager model.

3- It is applicable to several materials.

4- Its parameters are generated from experimental tests.

Required parameter for modelling material using the Cap model are illustrated in Table 6.3:

Table 6.3 Parameters of Cap model

Elastic properties	Cap plasticity	Cap hardening / softening
• Modulus of elasticity. • Poisson's ratio. • Density.	• Cohesion. • Friction angle. • Cap eccentricity. • Initial yielding surface position. • Transition surface. • Flow stress ratio.	• Yielding stress. • Volumetric plastic strain.

The previous parameters can be identified according to the triaxial, direct shear and compaction tests. The values of the rest of the parameters have ranges to their values (Abaqus, 2014).

The direct shear test provides the internal friction angle and the soil's cohesion according to Mohr-Coulomb criteria; consequently, these data must be converted. Eqs (6.11) and (6.12) illustrate the conversion equations (Helwany, 2007; Nagy, 2007; Moayed et al., 2012; Pistrol et al., 2012; Hsuan et al., 2013):

$$(tan\,\beta) = \frac{6\,sin\,\Phi}{3 - sin\,\Phi} \qquad (6.11)$$

$$(d) = \frac{18\,c\,cos\,\Phi}{3 - sin\,\Phi} \qquad (6.12)$$

Where, β and *d* are the friction angle and the cohesion in the meridional plane (*p*-*q*).

6.5.1.4 Soil constitutive model choice

The choice process for which constitutive model will be used to simulate the soil numerically depends mainly on the model simplicity, the ease with which its parameters can be defined, the number of required iterations to achieve solution convergence and its accuracy. From the previous constitutive models, it is clear that the *EMC* is the simplest model that can simulate the soil. On the other hand, the Cap model has the highest accuracy in adopting the solution but requires high computational efforts and iterations to reach a stable solution (convergence). The required parameters to define the *EMC* are simple and can be determined easily by using simple experimental tests. On the other hand, the required parameters to define the Cap model are more than those in the *EMC* and determining them requires special experimental testing (Triaxial test for fully

saturated sand). Consequently, to simulate the behaviour of soil, *EMC* model will be used.

6.5.2 Geogrid reinforcement constitutive model

Earth reinforcing by using geosynthetic-reinforcing layers is known to be an effective method to enhance the performance and service life of different earth structures (e.g. embankments, pavements, foundations and retaining walls). Reinforced soil structures are usually designed using limit equilibrium methods. These methods do not generally provide sufficient information on the failure load, displacements and strains developing in the reinforcement during loading conditions (Alagiyawanna et al., 2001).

Many researchers have studied the effect of using geogrid reinforcing layers to enhance structures behaviour. Most of these researches focused on the overall response of the reinforced structure while adopting simplifying assumptions related to either the details of the geogrid geometry or the constitutive model of the geogrid material.

The nonlinear stress-strain response of geogrid polymeric material is recognized as an important characteristic that needs to be captured in both analytical and numerical modelling of reinforced-soil applications. It is therefore, necessary to develop a nonlinear constitutive model for the geogrid material to improve the accuracy of the numerical analysis defining both the reinforcement elasticity and plasticity. This model should contain sufficient components to characterize the unconfined response, i.e. in air, and captures the important geometric features of the geogrid before it interacts with the backfill material. In addition, the model has to be relatively simple, with respect to the number of required parameters, to facilitate implementation into existing numerical codes.

Some researchers considered the constitutive model representing the geogrid reinforcement behaviour as a linear elastic model, and considered the geogrid geometry as if it was a planer sheet, ignoring the apertures between its longitudinal and transverse ribs (Wathugala et al., 1996; Leng, 2003; Zhuang, 2009; Ibrahim et al., 2014; AlAbdullah and Taresh, 2016). The missing plastic behaviour of the geogrid reinforcement will not define its actual performance. On the other hand, ignoring the apertures of the geogrid will prevent the

confinement effect of the geogrid reinforcement because of the lack of the passive earth resistance mechanism generated through the interaction between the backfill and the geogrid's ribs. Consequently, the need for a proper geogrid model considering both its plasticity and its three-dimensional geometry becomes necessary.

6.5.2.1 Constitutive behaviour

The ABAQUS package is used to build the constitutive model that can simulate the nonlinear elasto-plastic behaviour with isotropic hardening (Hussein and Meguid, 2016). The followed method to model the geogrid reinforcement behaviour requires the conversion from the experimental stress-strain data (engineering/nominal data) into true stress-strain data that can be considered as an input data in the software. This is achieved by decomposing the total strain values into elastic and plastic strains to cover the entire range of the geogrid response. The model's components are as follows:

a- Elasticity.

b- Plasticity (Isotropic yielding – Isotropic hardening rule).

An elastic isotropic model describes the elasticity component, where the stress-strain relation follows the elasticity matrix (Hook's Law). The plasticity is modelled using von Mises yield criterion with isotropic hardening and associated flow rule. The isotropic yielding is defined by expressing the uniaxial yield stress as a function of the equivalent uniaxial plastic strain. The isotropic hardening rule is expressed in ABAQUS using a tabular data of yield stress as a function of plastic strains. All these data can be extracted from the engineering data resulting from the experimental tensile test.

ABAQUS requires true stress and true strain data to define the geogrid plasticity, and this conversion process can be achieved according to Eqs (6.13) and (6.14) (Abaqus, 2014).

$$\varepsilon_{true} = ln\ (1 + \varepsilon_{nom}) \qquad (6.13)$$

$$\sigma_{true} = \sigma_{nom}\ (1 + \varepsilon_{nom}) \qquad (6.14)$$

Where; ε_{nom} and σ_{nom} are the resulting strain and stress from the geogrid tensile test, and ε_{true} and σ_{true} are the true strain and stress required by the software to define the geogrid plasticity.

After calculating the value of the true strain, ε_{true}, it should be decomposed into true elastic strain, ε^{el} and true plastic strain, ε^{pl}, where:

$$\varepsilon_{true} = \varepsilon^{el} + \varepsilon^{pl} \qquad (6.15)$$

The value of the true elastic strain, ε^{el}, can be calculated from Hooke's law, considering the geogrid elastic modulus, E, and the true stress value, σ_{true}, at which the material's behaviour is converted from being linear into nonlinear, i.e. the end of the elastic zone. However, at first the value of the elastic modulus of the geogrid material, E, should be identified from the elastic zone of the stress-strain curve (test data). In some cases, the elastic zone is very small / limited, consequently, the initial tangent modulus (slope of the first portion of the curve) is considered the elastic modulus of the geogrid reinforcement.

Finally, by subtracting the true elastic strain value from the total true strain, the value of the true plastic strain is available and can be used to define the geogrid plasticity. The illustrated flowchart in Figure 6.7 can clearly present the followed steps to identify the plasticity inputs required by ABAQUS (Abaqus, 2014; Hussein and Meguid, 2016).

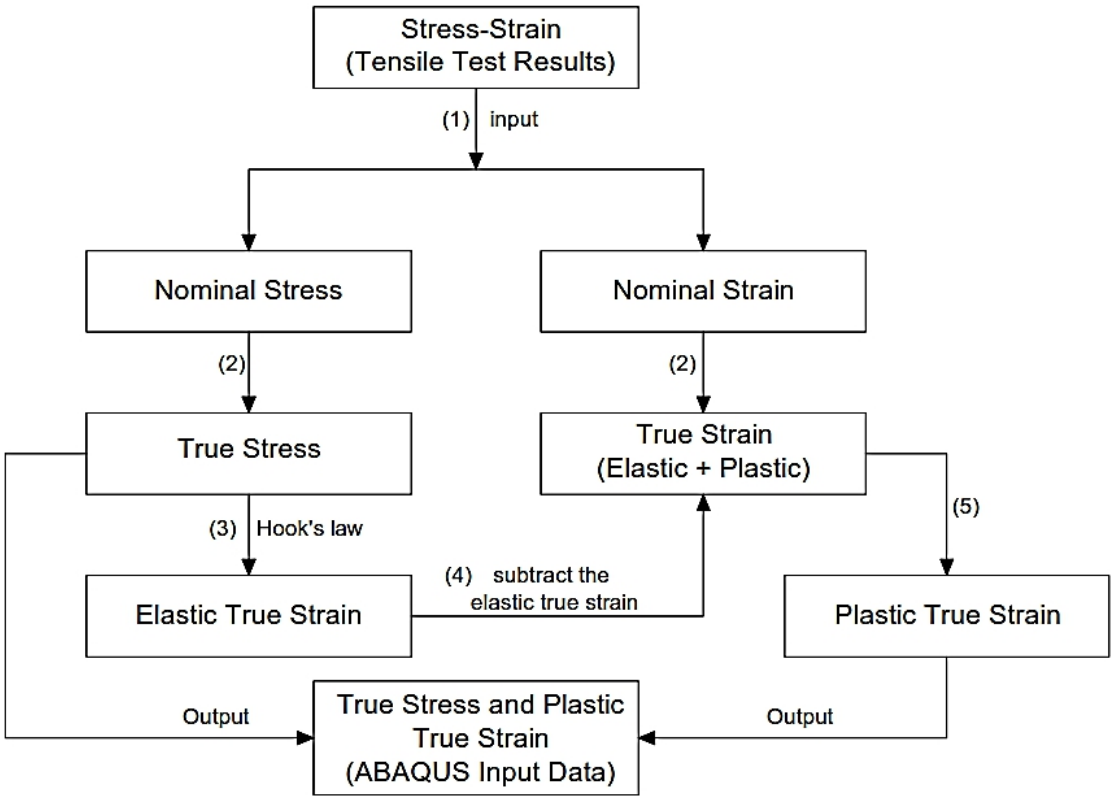

Figure 6.7 Plastic behaviour identification of geogrid reinforcement

6.5.3 Flexible pipe constitutive model

Flexible pipes are mainly manufactured from polymer and plastic materials such Polymeric un-plasticized (*uPVC*), High-density Polyethylene (*HDPE*), Poly-vinyl chloride (*PVC*) and in some cases, it may be of steel material.

Many researchers used a linear elastic constitutive model to simulate the behaviour of flexible pipe numerically (Brachman et al., 2000; McGrath, 2005; Nobahar et al., 2007; Kang et al., 2009; Keatley, 2009; Lee, 2010; Elshesheny et al., 2014; Cao et al., 2016). The model mainly required the identification of the elastic modulus, E, and the Poisson's ratio of the material of the pipe.

Experimental testing of buried flexible pipes provided data, which illustrated that the deformed shape of the pipe after the applied loading profile is either a heart shape or elliptical shape, depending on the compaction degree of the backfill soil (Mehrjardi and Tafreshi, 2008; Tafreshi and Khalaj, 2011; Elshesheny et al., 2019). Consequently, it can be concluded that the pipe experienced plastic deformation, where its original circular cross-section was deformed into a heart or elliptical cross-section. Therefore, using a linear elastic constitutive model to

simulate the flexible pipe performance is not correct, and the addition of plastic model defining the plasticity of the pipe is essential to simulate the behaviour of the pipe numerically.

A similar model to that used to simulate the geogrid reinforcing layers was used to simulate the flexible pipe behaviour. A tensile test was performed on a specimen from the pipe, and the resulting engineering stress-strain data were converted into true stress and true plastic strain data by following the illustrated steps in Figure 6.7. The linear portion of the used constitutive model was defined using the elastic modulus of the pipe's material, *E*, and its Poisson's ratio. In addition, the yielding stress of the pipe's material should be identified to define the stress value at which the pipe will be damaged (Alamatian et al., 2013). The flexible pipe is considered undamaged until the deformation of its diameter reaches 5% of its original length, and after this value the pipe is considered damaged and the applied loads above it must be reduced (Tafreshi and Khalaj, 2008).

6.6 Interaction mechanism

The interaction is an important property to describe the relative motion and stress transfer between different elements forming the problem. The simulation of the soil-geogrid interaction is considered one of the most difficult tasks while modelling the reinforced soil system, especially if the model was a three-dimensional one. The test involves large deformations that lead to relative movements between the geogrid and the surrounding soil. This generates severe nonlinearities at the contact between the soil and the geogrid, in addition to the other sources of nonlinearity from the geogrid and soil materials. ABAQUS has the ability to provide a master-slave contact pair technique which can be used to model the interaction between different elements in the model (Abaqus, 2014; Hussein and Meguid, 2016).

6.6.1 Master-slave contact pair

The master-slave contact pair approach is a surface-based contact simulation, which depends mainly on the definition of the surfaces which are already in contact (footing on a soil), or those who will contact each other as a result of the applied loads in the model (bullet penetrating plate). Consequently, there must

be an interaction property model that governs the relationship between the contacted bodies, i.e. mechanical contact property. These defined surfaces are divided into two main categories, masters and slaves. The master surface has a coarser mesh and higher elastic modulus than the slave one, which has a finer mesh and lower elastic modulus, allowing the master surface to penetrate the slave one without any distortion in the formed mesh. Combining the master and slave surfaces form one-contact pair (Abaqus, 2014).

6.6.2 Main features of a contact pair

The definition of any contact pair requires the following steps:

1- Contact pair discretization.
2- Contact pair enforcement.
3- Constraints evolution upon sliding.

6.6.2.1 Contact pair discretization

The definition of a contact pair in ABAQUS is based on one of the following types, as illustrated in Figure 6.8 (Abaqus, 2014):

a- Surface-to-surface.
b- Node-to-surface.

In surface-to-surface type, the contact between the two surfaces is a contact between the areas located between the generated nodes, where, the node is centred inside the contacted area. This means that each contact constraint is formulated based on an integral over the region surrounding a slave node. Consequently, all nodes will be participating in the contact surface. On the other hand, in node-to-surface type, each contact condition involves a single slave node and a group of nearby master nodes. Therefore, some nodes along the master surface might not participate in the formed contact surface.

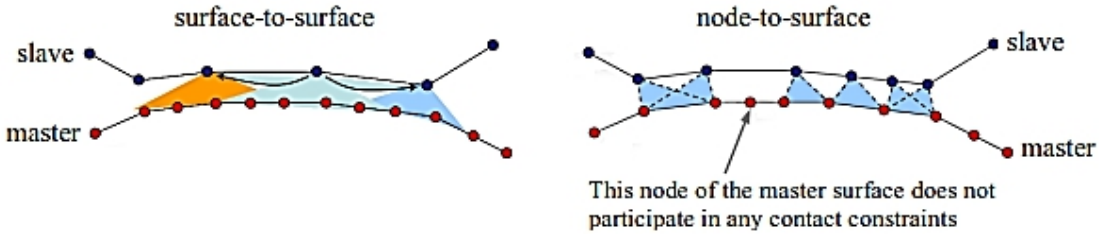

Figure 6.8 Contact pair discretization

The use of node-to-surface type requires a complete match between the generated nodes on the two contact surfaces to make sure that all the generated nodes along the two surfaces are participating in the formed contact pair, i.e. slave surface nodes coincide with the master surface nodes. On the contrary, the surface-to-surface type allows the interaction between two surfaces with different mesh densities, as the interaction occurs between the formed surfaces between the nodes along the two surfaces.

6.6.2.2 Contact pair enforcement (constitutive model)

The function of a contact pair is to transfer forces between its two surfaces (master and slave). ABAQUS can identify this transmitted force by two main components, shear force through tangential behaviour and normal force through normal behaviour. There is generally a relationship between these two force components.

In a mechanical contact property, the interaction between contacting surfaces is defined by assigning a contact property model to a contact pair. This contact property can be defined as the constitutive model of the contact pair. Two constitutive models are used in this research to identify the interaction between the two surfaces as follows:

a- Friction model.

b- Contact pressure-overclosure (penetration/clearance).

The friction model is used to induce frictional stresses to resist sliding, while the contact pressure-overclosure model controls the contact pressure that resists penetration in the normal direction (Abaqus, 2014). Both models are used simultaneously for contact pair involved in the analysis.

Friction model

To define the force resisting the relative tangential motions of the contacting surfaces, ABAQUS introduce a frictional model. This frictional model is a subroutine in the tangential behaviour, which can describe the stick/slip discontinuity (frictional behaviour/penalty) condition in the tangential direction. The coulomb friction model is used to define the frictional model, which depends on the friction coefficient between the interacted bodies, μ, as well as the elastic slip between them, E_{slip}, (Tang, 2011; Abaqus, 2014).

The coulomb frictional model considers that every two contacting surfaces are describing one contact pair, and these surfaces can resist shearing stress up to a certain value, $\tau_{critical}$. Once this value is reached, sliding between the two surfaces will occur, which can be defined as sticking phenomenon as shown in Figure 6.9. This frictional model follows the Mohr-Coulomb failure criterion, which can be defined as shown in Eq (6.16):

$$\tau_{critical} = c + \sigma_n \tan\delta \qquad (6.16)$$

Where:

$\tau_{critical}$→ is the shear strength at which the slip occurs for the first time.

c→ is the cohesion.

σ_n→ is the normal stress.

δ→ is the interface friction angle between soil and geogrid.

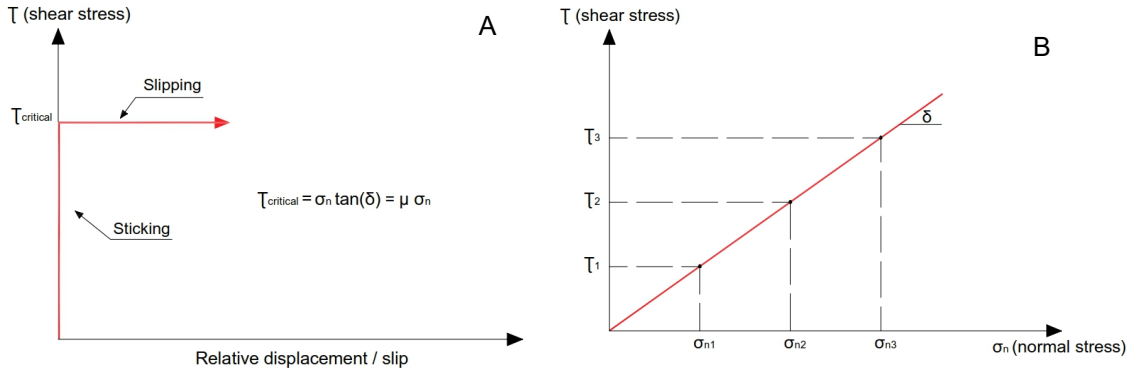

Figure 6.9 Coulomb frictional model
A: Sticking phenomena. B: Geogrid-soil friction angle.

The interface friction angle (δ) between the sand and the geogrid can be obtained experimentally by using a large direct shear test as shown in Figure 6.9. Hence, the value of the coefficient of friction can be determined (μ = tan δ), which is approximately two thirds of the soil's frictional angle, Φ, (Latha and Somwanshi, 2009; Mehdipour et al., 2013).

ABAQUS provides two methods to enforce the sticking constraints in Coulomb friction model (Abaqus, 2014):

1- Lagrange multiplier contact algorithm.
2- Penalty/stiffness method.

In the Lagrange multiplier method, the slip between any two contacted surfaces occurs only when the shear stress between the both exceeds the value of $\tau_{critical}$. However, the Lagrange multipliers increase the computational cost of the

analysis by adding more degrees of freedom to the model and often by increasing the number of iterations required to obtain a converged solution.

On the other hand, the penalty function method (stiffness method) permits some relative motion between the surfaces, when they should be sticking, an elastic slip, as shown in Figure 6.10. While the surfaces are sticking (i.e., $\tau < \tau_{critical}$), the magnitude of sliding is limited to this elastic slip (E_{slip}). Within this elastic stick condition, if the tangential load is removed, the body returns to its original state with complete sticking between the two interacted surfaces (Tang, 2011; Lei et al., 2013; Abaqus, 2014; Hussein and Meguid, 2016).

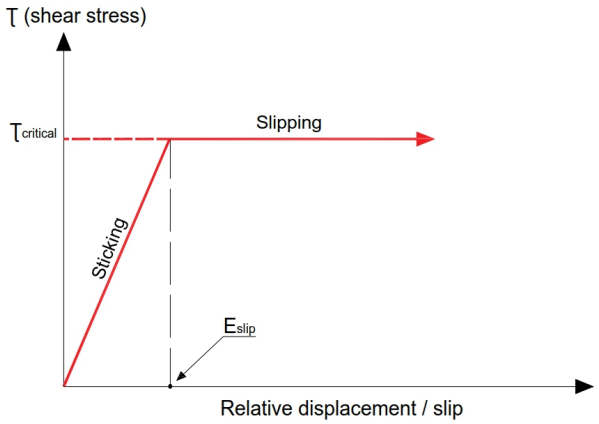

Figure 6.10 Coulomb friction enforced by penalty / stiffness method

Using the penalty method is better than the Lagrange multiplier method because, it is easy to implement, and does not require solving a nonlinear system of equations in every time step, i.e. a time saving method. The Coulomb friction model used in this research follows the penalty/stiffness method and it contains two components, a friction coefficient (μ), and a tolerance parameter to calculate the elastic slip (E_{slip}).

Contact pressure-overclosure (penetration/clearance)

The contact-pressure overclosure model is used in order to identify the contact pressure that resists penetration between the two interacted surfaces. Open/closed discontinuity in the normal direction is similar to the stick/slip discontinuity in the friction model. The most common used contact pressure-overclosure models are (Abaqus, 2014; Hussein and Meguid, 2016):

a- The hard contact model.

b- The softened contact model.

In the hard contact model, no contact pressure occurs until nodes are in contact, and once the contact has been established between the contacting surfaces, unlimited contact pressure can be transmitted between them without penetration between the two surfaces. The surfaces start to separate if the contact pressure reduces to zero or if the normal stress becomes tensile (negative value) and they can come into contact again when the clearance between them reduces to zero.

On the other hand, in the softened contact model, the contact pressure is a linear function of the penetration between the interacted surfaces. The surfaces transmit contact pressure when the overclosure/penetration between them, measured in the contact (normal direction), is greater than zero. As in the case of hard contact, the surfaces start to separate if the contact pressure reduces to zero or if the normal stress becomes tensile (negative value).

6.6.2.3 Constraints evolution upon sliding

The relative motion between two interacted surfaces in ABAQUS can be defined in the mechanical contact simulation by using one of the following methods (Abaqus, 2014):

a- Small sliding.

b- Finite sliding.

Small sliding contact is an approximate formulation, which assumes that there will be relatively little sliding between the two surfaces, and it is based on linearized approximations of the master surface per constraint. Because of the assumption that the relative tangential motion between the two surfaces should be small, the usage of this method is very limited, few nonlinearity problems will be generated, and the solution will be achieved within few iterations.

On the other hand, the finite-sliding contact method is the most general tracking approach and allows for arbitrary relative separation, sliding, and rotation of the interacted surfaces. It includes nonlinear geometric effects that can help in simulations that involve large deformations and rotations, which represents the common case of relative motion between two interacted surfaces.

6.7 Summary

Finite element analysis is a powerful and reliable tool to predict the behaviour of various engineering problems. It can investigate the occurred deformation, stresses, strains and reaction forces due to the application of various loading profiles. Geometry and material models defining each element in the problem are the main challenges in the finite element modelling. In this research, the behaviour of buried pipes under geogrid-reinforced and unreinforced sand beds is investigated, which presents three main elements to be simulated namely, i. soil, ii. pipe, and iii. geogrid-reinforcing layers. The behaviour of these elements should be simulated using an elasto-plastic model, which has the ability to predict both the elastic and the plastic response. The used model for each element must provide relatively accurate results while using relatively reduced number of parameters to define the model.

Extended Mohr-Coulomb, *EMC*, model was used to represent the behaviour of the used sandy soil, where it has the ability to represent its plasticity using the cohesion, internal friction angle and dilation angle of the soil. An elastic model was added to the *EMC* model to define the elasticity of the soil using its elastic modulus, Poisson's ratio and density. For both the pipe and the geogrid-reinforcing layers, an elasto-plastic model was used to represent their behaviour. The model was a combination of two models, elastic and plastic models. In the elastic model, the elastic modulus, Poisson's ratio and density of the modelled element was used. In the plastic model, the extracted true stress-strain curve out of the experimental/engineering stress-strain curve of each element was used.

A proper interaction between the modelled elements would predict the real response of the integrated system due to the applied loads. Contact pairs were generated to define the interaction between the contacted surfaces, where surface-to-surface discretization was used. The contact pairs were enforced by defining interaction property combining both frictional and contact pressure-overclosure properties. In the frictional property, the penalty/stiffness method was used to define the occurred slip between the two interacted surfaces. In the contact pressure-overclosure property, the hard contact method was used to control the penetration between the two interacted surfaces. In addition, finite

sliding between the two interacted surfaces was used as a constraint evolution upon sliding, where it represents the common case unlike the small sliding, which assumes the occurrence of relatively small sliding between the interacted surfaces in the contact pair.

CHAPTER 7

FINITE ELEMENT PARAMETRIC STUDY

7.1 Introduction

The finite element method is an effective tool to predict the response of several engineering problems under the application of different loading conditions. Usually, experimental testing provides accurate results, however; FE method can be considered an easy and relatively accurate method compared with experimental testing, where it saves effort and time. In this chapter, the performance of buried pipes in geogrid-reinforced and unreinforced sand beds while applying cyclic loading is numerically investigated. Three-dimensional, 3D, finite element models will be generated to simulate the experimentally investigated cases in Chapter 4, for validation. Subsequently a parametric study will be performed to investigate the influence of variable parameters on the overall performance of the pipe-reinforced-soil system. The geogrid reinforcing layers will be simulated as a planer sheet (membrane), and as 3D solid elements (brick elements), where the variation between both of them will be clearly defined. In the parametric study, the number of reinforcing layers, burial depth of the pipe, unit-weight of the soil and the applied loading amplitude will be varied. Based on the outcomes of this parametric study the optimum values of the burial depth of the pipe and the number of the reinforcing layers could be predicted.

7.2 Numerical modelling

According to the adopted technique for modelling the geogrid layers, either it was planer or 3D, the modelling method of the soil will be entirely changed. However, the simulation of both the pipe and the footing will be the same.

7.2.1 Modelling of the footing

A rigid rectangular steel strip footing of 1000 mm in length, 200 mm in width and 30 mm in depth was used. Eight node continuum brick elements with reduced integration (*C3D8R*) were used to simulate the footing, as illustrated in Figure 7.1. Linear properties were assigned to the footing, as shown in Table 7.1, as it

was a rigid footing and the applied loads to it would not generate plastic deformation.

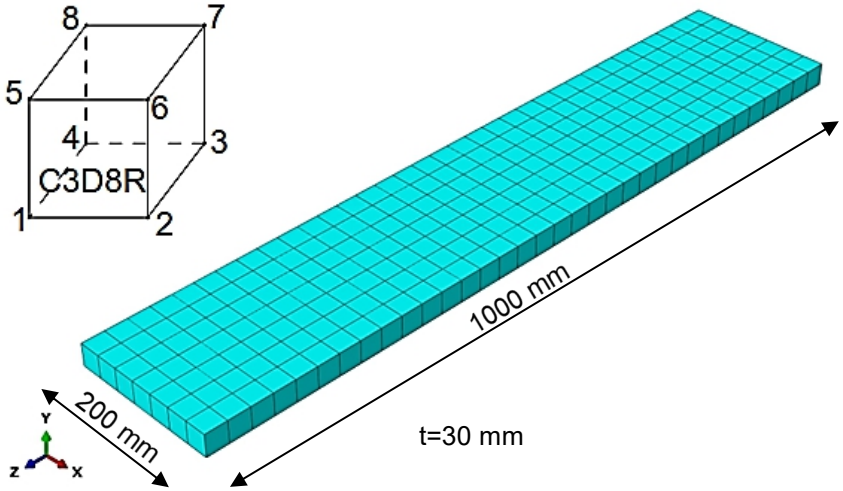

Figure 7.1 Strip footing model, *C3D8R*

Table 7.1 Linear properties of the strip footing

Property	*E* (MPa)	Poisson's ratio	Density (kg/cm^3)
Value	2.1e5	0.3	0.0079

7.2.2 Pipe modelling

A 200 mm *HDPE* pipe with 5 mm wall thickness and 1000 mm length was used in this investigation. To consider the thickness deformation of the pipe, three-dimensional elements were used to simulate the pipe. Eight node continuum brick elements with reduced integration (*C3D8R*) were used to simulate the pipe, as presented in Figure 7.2. According to the British Standard specifications, BS EN ISO 527-1:2012, (BS, 2012), tensile tests were performed on specimens formed out of the pipe material. The stress-strain behaviour of the specimen, presented in Figure 3.10, illustrated that the pipe material experienced both, elastic and plastic behaviours. Consequently, the plastic behaviour of the pipe material must be combined with the elastic behaviour to represent a model, which can represent the real behaviour of the pipe. The flowchart presented in Figure 6.7 was used to convert the experimental stress-strain behaviour of the pipe into true stress-plastic strain behaviour (input data in ABAQUS), defining its plasticity. The model used to simulate the pipe behaviour can be considered to be a combination between Table 7.2, representing linear properties, and Figure 7.3, representing the plastic behaviour.

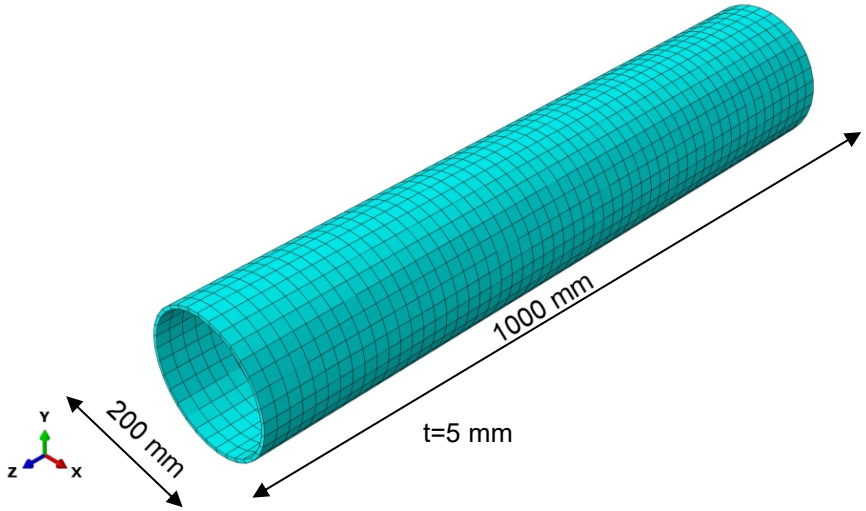

Figure 7.2 HDPE pipe model, *C3D8R*

Table 7.2 Linear properties of the HDPE pipe

Property	*E* (MPa)	Poisson's ratio	Density (kg/cm^3)
Value	700	0.46	0.0009226

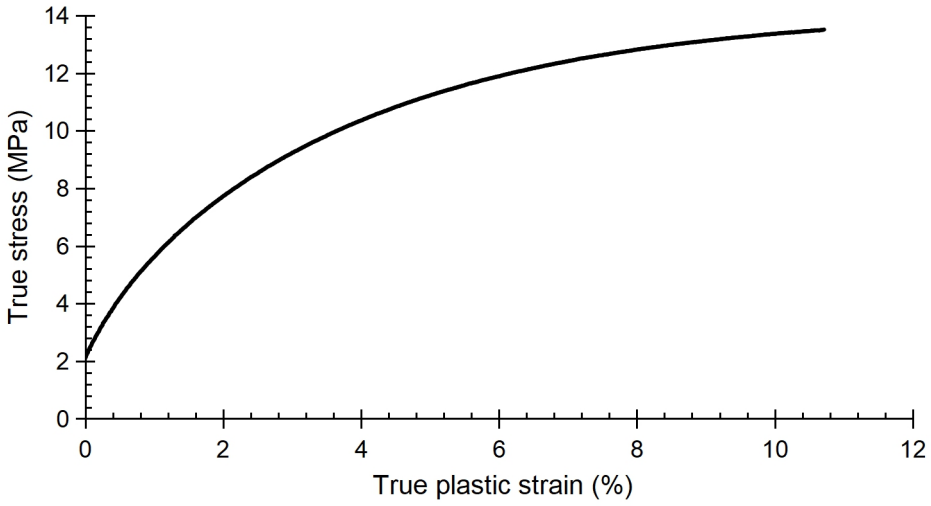

Figure 7.3 True stress-plastic strain of the pipe material.

7.2.3 Geogrid reinforcement modelling

The geogrid reinforcing layers can be modelled using completely different methods in ABAQUS, either a planer sheet or a three-dimensional model. Each simulation method requires specific modelling of the soil and the interaction mechanisms controlling the load and stress transfer between the soil and the geogrid reinforcing layers. As an initial step, the dimensions of the

experimentally used biaxial geogrid layer was measured using a digital calibre. A layer of one square meter area was extracted from the reinforcing sheet, where the thickness of each longitudinal and transverse rib, dimensions of each aperture, and the thickness of the sheet at several locations were measured and the average value of each measured distance was considered in the numerical modelling. The average dimensions of the numerically simulated geogrid layer are illustrated in Table 7.3.

Table 7.3 Average dimensions of the numerically modelled geogrid layer

Thickness of longitudinal rib (mm)	Thickness of transverse rib (mm)	Average thickness of entire layer (mm)	Aperture dimensions (mm)
2.7	2.4	1.27	37*37

It was noted that the experimentally tested geogrid reinforcing layer had 25 apertures in both, the machine and the cross-machine directions. Consequently, the calculated length and the width of the numerically modelled layer was 995.2 mm and 987.4 mm, respectively. To simplify the geometry of the geogrid layers and the nonlinear contact analysis, the local increase in thickness of the formed junctions between the longitudinal and the transverse ribs was not modelled. This approximation is expected to cause a slight reduction in the bearing resistance that would develop at these locations on the transverse ribs.

7.2.3.1 Planer geogrid layer (membrane)

In the case of simulating the geogrid layers as a planer sheet, membrane, the reinforcing layer is drawn as a whole sheet and then the existing apertures, 25 apertures in each direction, between the longitudinal and the transverse ribs are removed from the sheet, as illustrated in Figure 7.4. It should be noted that the membrane sheet in ABAQUS has zero geometrical thickness; however, the exact thickness of the geogrid layer was defined in the used membrane model as a property, *Thickness: Membrane thickness: Value: 1.27*. Three-node triangular elements, *M3D3*, were used to simulate the geogrid reinforcing layer.

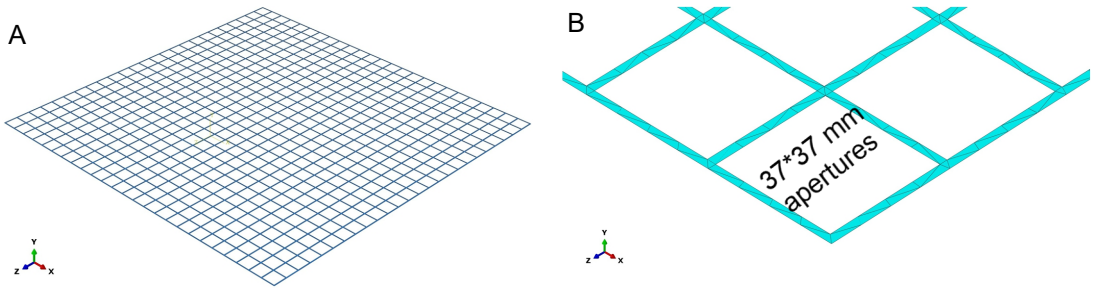

Figure 7.4 Planer geogrid layer (membrane)
A: Entire layer. B: Meshed zero geometrical thickness layer.

According to the British Standard specifications on multi rib geogrid specimens, BS EN ISO 10319:2015, (BS, 2015), tensile specimens were taken out of the geogrid reinforcing sheet and tested in tension. Figure 3.7 illustrated the experimental stress-strain behaviour of the reinforcing layer material. It is clear that the reinforcing layer material experienced elastic and plastic behaviours. Consequently, using a linear model to represent the properties of the reinforcing layer is unfavourable, where adding a plastic model to the linear one is necessary to represent the real behaviour of the reinforcing layer. As the case in the pipe, the flowchart presented in Figure 6.7 was used to convert the experimental stress-strain behaviour of the pipe into true stress-plastic strain behaviour (input data in ABAQUS), defining its plasticity. The model used to simulate the reinforcing layer behaviour can be considered a combination between Figure 7.5 and Table 7.4, which represent its plastic and elastic behaviours, respectively.

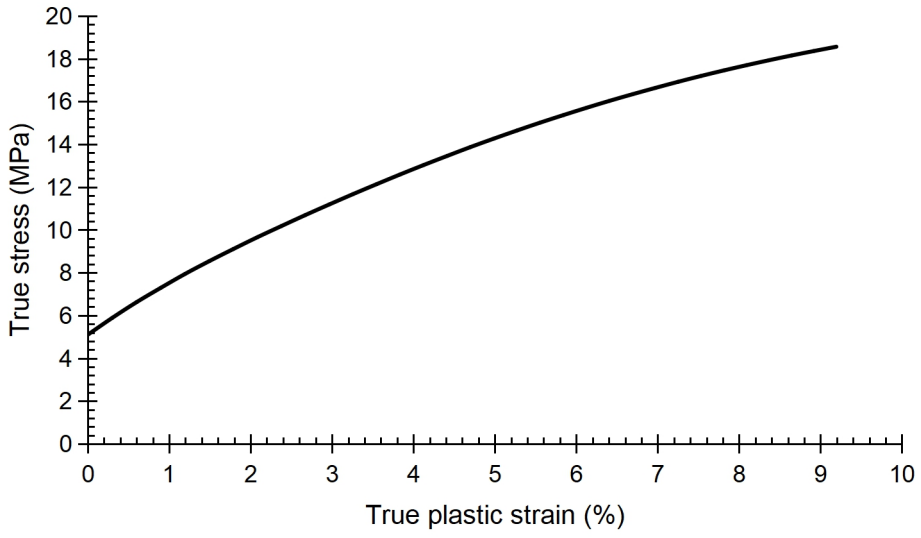

Figure 7.5 True stress-plastic strain of the reinforcing layer

Table 7.4 Linear properties of the reinforcing layer

Property	*E* (MPa)	Poisson's ratio	Density (kg/cm^3)
Value	300	0.3	0.000268

7.2.3.2 Three-dimensional geogrid layer (brick elements)

The inclusion of the reinforcing layers in the soil has the ability to form a new composite material, which has enhanced properties compared with soil. The properties of the formed material depend mainly on the load transfer mechanisms between the soil and the reinforcing layers, in particular the passive earth resistance mechanism. This mechanism depends on the contact generated between the trapped soil in-between the geogrid apertures and the transverse ribs. Consequently, the three-dimensional modelling of the geogrid layer will allow such this type of interaction, representing the real behaviour of the reinforced soil system. Eight node continuum brick elements with reduced integration (*C3D8R*) were used to simulate the geogrid layers, as presented in Figure 7.6.

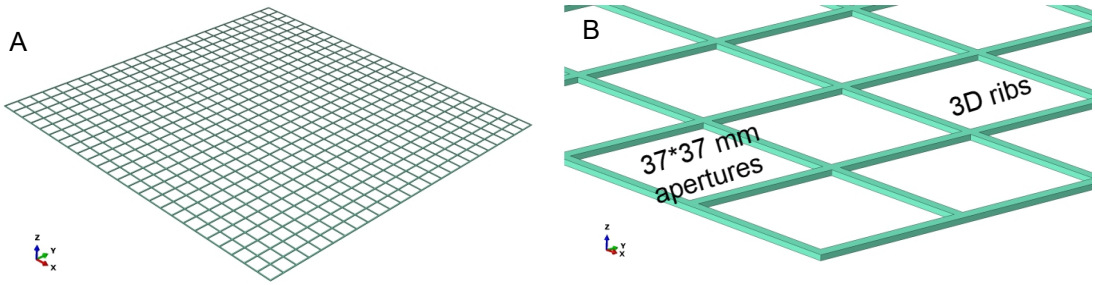

Figure 7.6 3D geogrid layer (brick elements)
A: Entire layer. B: Non-zero geometrical thickness layer.

Initially, a solid block representing the geogrid layer was drawn using ABAQUS. This block had a thickness representing the average thickness of the geogrid layer. Then, the calculated number of apertures, 25 apertures in each direction, were removed from the block using a special tool in the software, *Create Cut: Extrude*. It should be noted that the same material model that was used for the reinforcing layers in the membrane modelling was used in the 3D modelling, where the linear behaviour was represented by Table 7.4, and the plastic behaviour was represented by Figure 7.5. The membrane and the 3D modelling

represent the geometry of the modelled element and they do not affect the material model.

7.2.4 Soil modelling

The geometrical modelling process of the soil was dependent on the technique by which the reinforcing layers were modelled. In general, the silica sand was modelled using an elasto-plastic Mohr-Coulomb failure criteria (Mohr-Coulomb plasticity model) and its domain was discretized using 8-node linear brick elements (*C3D8R*). Table 7.5 illustrates the input parameters for the soil, following Table 6.2.

Table 7.5 Soil input parameters in the FE modelling

Elastic properties			Plastic properties		
E (MPa)	Poisson's ratio	Density (kg/cm^3)	$\Phi°$	$\psi°$	*c* (MPa)
55	0.35	0.001632	36.5	6.5	1e-5

where; Ψ= Φ-30, (Rajkumar and Ilamparuthi, 2008)

7.2.4.1 Geometrical modelling while using planar reinforcement

In this case, the soil was modelled as one part, where the planar reinforcing layers (membrane) had zero volume since its geometrical thickness was set to zero. A 3D block was drawn using ABAQUS, and then a cylindrical part was removed from it to allow the insertion of the pipe in its predesigned position, as illustrated in Figure 7.7.

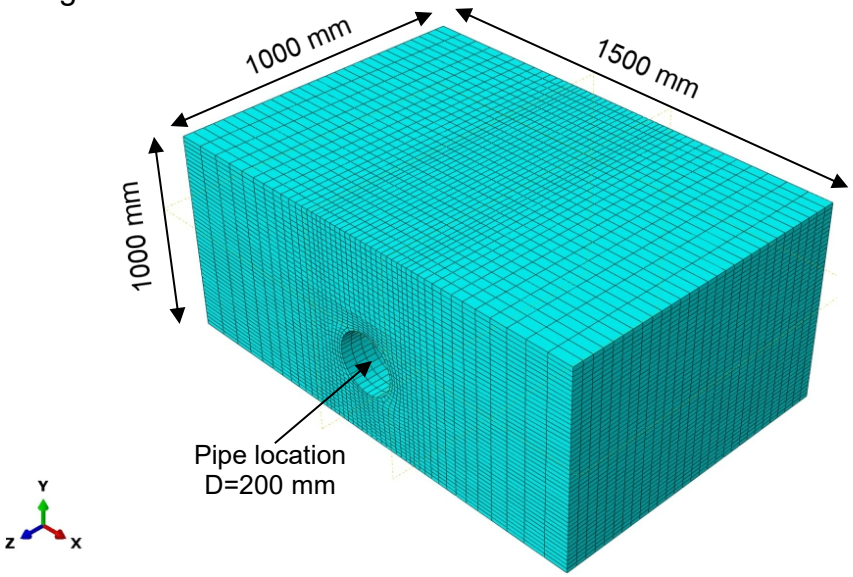

Figure 7.7 Soil modelling for membrane reinforcement

7.2.4.2 Geometrical modelling while using 3D reinforcement

In this case, the thickness of the reinforcing layer, t=1.27 mm, was modelled, consequently, the reinforcing layer had a specific volume. As a result, the volume, which the reinforcing layer will occupy, must be free of soil. This led to dividing the soil part into a number of smaller parts depending on the number of the inserted reinforcing layers in the soil.

For example, the use of one reinforcing layer will require the following formation of the soil, i, upper soil, ii, lower soil, and iii, fill soil, as shown in Figure 7.8. The upper and lower soil parts are considered full blocks. The fill soil is mainly used to fill the formed apertures between the longitudinal and the transverse ribs of the reinforcing layer (interlocked soil). Consequently, the interaction between the fill soil and the reinforcing layer could simulate the real case of the reinforced soil system, where the passive earth resistance and the frictional mechanisms can be easily modelled. In case of inserting (N) number of the reinforcing layers in the soil, the soil part will be divided into, upper and lower soils, (N) number of the fill soils and (N-1) soil blocks between the fill soils.

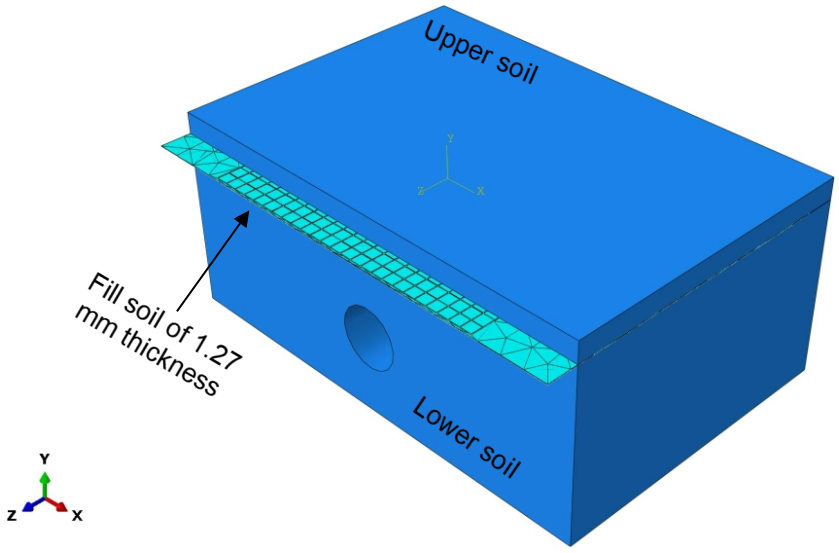

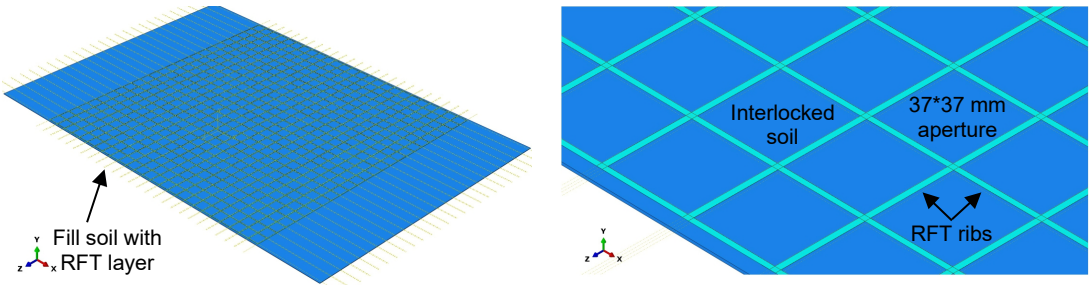

Figure 7.8 Modelled soil parts

7.2.5 Interaction property

The reinforced soil system behaviour depends mainly on the interaction between the ribs of the reinforcing layers and the soil particles. Two main mechanisms should be simulated to clearly define the loads and stress transfer between them, passive earth resistance and frictional mechanisms. Generally, surface-to-surface interaction as discussed in section *6.6.2.1* was used in this study. It is recommended that the material of higher elastic modulus should be defined as a master surface and have a coarser mesh (Abaqus, 2014). Consequently, the reinforcing layer surfaces were assigned as master and the soil surfaces were assigned as slave.

An interaction property, which consists of two behaviours, was used to define the soil-geogrid interaction, tangential behaviour (penalty) and normal behaviour (hard contact). The main function of the tangential behaviour is to define the generated friction in the contact pair. This can be achieved through defining the friction coefficient between the soil and the reinforcing layer material (equals 0.4522), which was experimentally determined using a large shear box test, and an elastic slip factor to simplify the interaction non-linearity (E_{slip} = 0.005). On the other hand, the normal behaviour (hard contact) was used to identify the contact pressure that resists penetration between the two interacted surfaces in the contact pair.

The used interaction property should be assigned to each two interacting surfaces (contact pair), which is impossible to be achieved manually. ABAQUS has the ability to detect each contact pair in the model by using the option of: *Find Contact Pairs*. The detected contact pairs are completely controllable, where the type of interaction can be executed using either a contact property or tie constraints. Moreover, the sliding that occurred between the two surfaces in each contact pair can be either small or finite sliding according to the nature of

interacted surfaces. In this study, the type of interaction was executed by assigning the pre-defined contact property, where finite sliding was used. Table 7.6 illustrates the number of the generated contact pairs relative to the number of the inserted geogrid reinforcing layers.

Table 7.6 Number of the generated contact pairs

Number of geogrid layers	1 layer	2 layers	3 layers	4 layers
Number of contact pairs	2504	5008	7512	10016

Since the soil was formed out of multiple parts depending on the number of the reinforcing layers, an interaction between each two parts should be defined to allow loads and stresses transfer between each of them. As long as each one of these soil parts has the same properties, ABAQUS has the ability to merge these parts to form a new part allowing stress and deformation continuity without the need for defining interaction between the variable soil parts. This can be achieved by using: *Merge/Cut Instances*.

7.2.6 Boundary conditions definition

The boundary conditions were defined as roller supports at the outer four edges of the model, which prevent the translation of the surface along its perpendicular direction and allow translation in other directions. The base of the model was subjected to a fixed boundary condition that prevented translation in all directions. The upper surface was left free with no boundary conditions. Figure 7.9 represents the assigned boundary conditions in the finite element models.

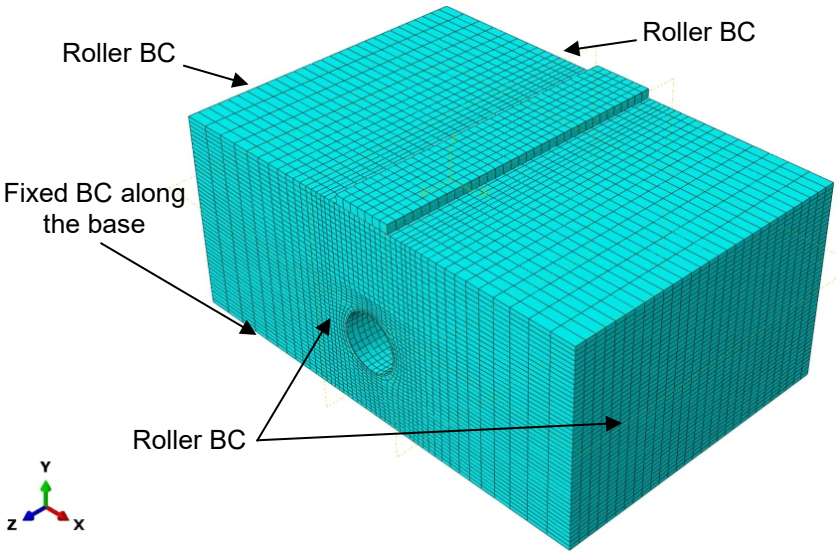

Figure 7.9 Boundary conditions of the model

7.2.7 Criteria of element selection

Variable elements are available in ABAQUS to mesh the different parts forming the whole model; however, the selection of the most appropriate element should be based on the following criteria:

1- Hexahedral and tetrahedral elements.
2- First and second order elements.
3- Reduced and full integration.

7.2.7.1 Hexahedral and tetrahedral elements

The meshing process in the finite element analysis is considered an important stage, where the mesh choice and its density significantly control the accuracy of the results of the model and the computational time efforts. Since the used finite element models are three-dimensional models, then two options of mesh type are allowed, hexahedral and tetrahedral meshes, as illustrated in Figure 7.10, (Benzley et al., 1995; Wang et al., 2004).

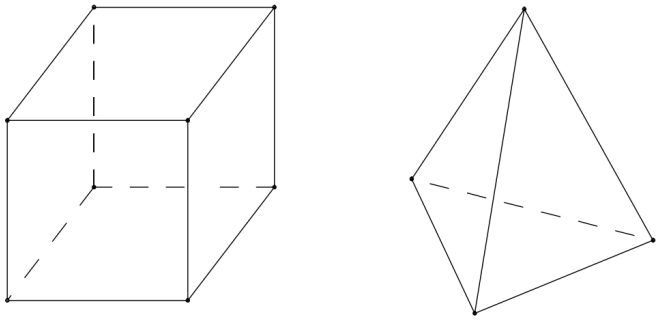

Figure 7.10 Continuum brick elements, hexahedral and tetrahedral

The tetrahedral elements have the ability to mesh any geometry even the complex geometries. Very complex steps should be followed to allow the meshing process for complex geometries if hexahedral elements would be used, where the complex geometry should be divided into simple geometries using partitions, usable tool in ABAQUS. On the other hand, the tetrahedral elements are considered time-consuming, as those models meshed by such elements require more computational time efforts to be executed compared with those meshed by hexahedral elements. Since numerous contact pairs were generated, much interest was paid for the computational time efforts. Consequently, hexahedral elements were used in this study, where solution accuracy was considered.

7.2.7.2 First and second order elements

ABAQUS provides two main orders of the hexahedral elements, first-order (linear) interpolation elements and second-order (quadratic) interpolation elements. A linear hexahedral element has nodes only at the corners of its edges. However, a quadratic one has mid-side nodes in addition to those at the corners, as shown in Figure 7.11.

In FEA, the behaviour representation of any element requires the assigning process of a polynomial equation to it, where the order of the equation depends mainly on the number of nodes per edge in the element. Consequently, a linear/first order and a quadratic/second order polynomial equations are assigned for linear and quadratic elements, respectively. In general, order of an element is the same as that of the polynomial equation used to represent its behaviour. Using higher order of polynomial equations results in higher

accuracy, however this accuracy will be achieved at the cost of increased computational time. Hence, it is better to have balance between degree of accuracy and computational time.

In problems involving contact, first-order elements are more favourable compared with second-order ones, where lower number of nodes and surfaces would be generated. On the contrary, in problems involving curvatures, bending, non-severe distortion or incompressibility, second-order elements perform much better than the first-order elements, where they allow mesh over-constraining/locking. For incompressible materials, the volumetric strain of elements should be constant. Consequently, in second-order elements, all the 20-nodes must remain almost constant/non-deformable, where 20-constraints would be used per one element to restrain three degrees of freedom, which results in mesh over-constraining/locking. On the other hand, in first-order elements, the strain operator provides constant volumetric strain throughout the element, preventing mesh locking and reducing the computational time efforts (Abaqus, 2014).

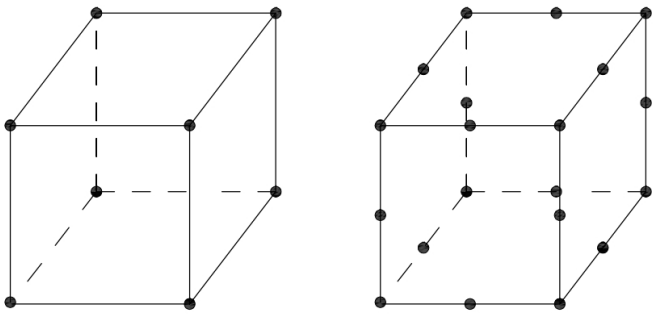

Figure 7.11 Linear and quadratic hexahedral elements

In the current study, numerous contact pairs were generated, mainly between the geogrid reinforcing layers and the soil, and severe elements deformation was expected in the model; consequently, linear/first-order hexahedral elements were used. Moreover, in the Abaqus/Explicit analysis v.14, only first-order elements are allowed and second-order elements are not applicable.

7.2.7.3 Reduced and full integration

To represent the material behaviour, Abaqus evaluates its response at each integration point in each element representing the material. Some continuum

elements in Abaqus can use full or reduced integration, a choice that could have a significant effect on the accuracy of the element for a given problem, in addition to the required solving time.

In Abaqus/Explicit, it is allowable to choose between full or reduced integration for linear/first-order hexahedral elements, where reduced integration elements are referred to as uniform strain elements. The full integration grants higher accuracy compared with the reduced integration, however; it requires significantly more computational time and elements tend to be more stiff in bending (Abaqus, 2014). For example, element type *C3D8* has 8-integration points, while *C3D8R* has only one, as illustrated in Figure 7.12. Therefore, element assembly is eight times more costly for *C3D8* than for *C3D8R*. Since the reduced integrated hexahedral element (*C3D8R*) has one integration point in its centre, it is crucial to use small elements/fine mesh to capture a stress concentration in the model. Reduced integration might lead to element distortion/hourglass, which would be avoided by using: *Hourglass control* option in Abaqus.

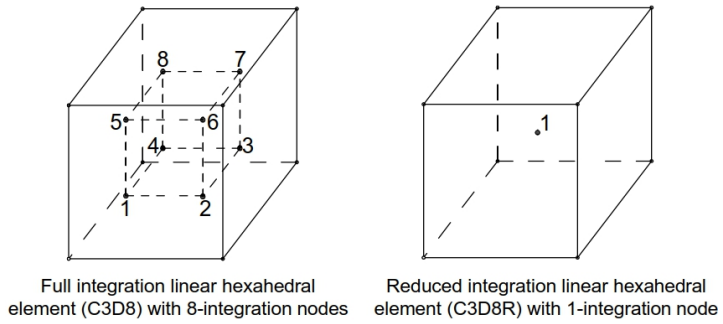

Figure 7.12 Full and reduced integration hexahedral elements

In the current study, the geogrid reinforcing layers had a thickness of 1.27 mm, which massively contributed in increasing the number of the generated elements. Consequently, reduced integrated linear hexahedral elements (*C3D8R*) were used to control the required computational time, while maintaining high solution accuracy.

7.2.8 Meshing of the entire model

The meshing of the model was selected to maintain sufficient mesh density, which would represent the laboratory test successfully. In addition, the mesh has to minimize the computational time.

The process of mesh size selection for the geogrid and the pipe models using continuum elements (*C3D8R*) is governed by their thickness. Sensitivity analysis was conducted using different mesh sizes to determine a suitable mesh for both the geogrid layers and the pipe that achieves a balance between accuracy and computational time efforts. The 3D mesh for both the pipe and the geogrid reinforcing layer is shown in Figure 7.13. The pipe and the geogrid reinforcing layer were meshed using 1728 and 1976 elements, respectively.

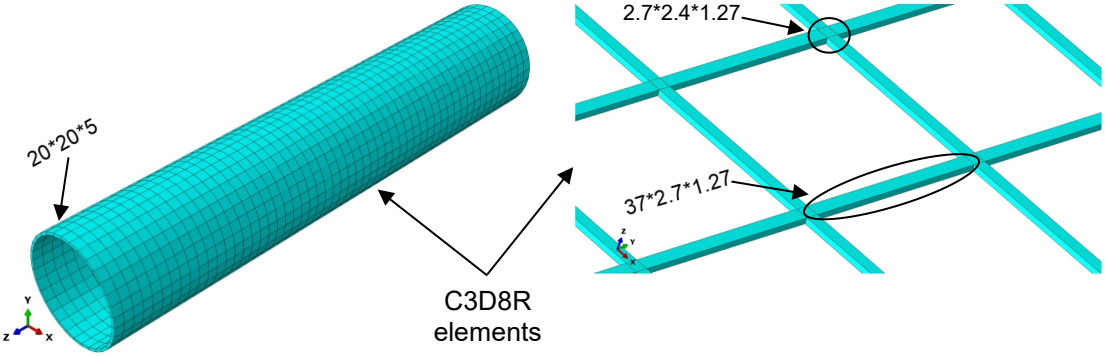

Figure 7.13 Mesh of the pipe and the geogrid layer

The process of soil meshing depended mainly on the created partitions, which allowed for the formation of soil parts that can be meshed using the available techniques in Abaqus: Structured and Sweep, as illustrated in Figure 7.14.

The number of the used elements to mesh the soil ranged between 63161 and 140814 elements, according to the burial depth of the pipe and the number of the used reinforcing layers, as illustrated in Figure 7.15. Based on the number of the elements for each of the model's components, the number of the used elements in the entire model ranged between 67103 and 150684 elements. It should be noted that a mesh sensitivity study was carried out to determine the most appropriate element size for each element, where the currently used mesh sizes provided both optimum solution accuracy and solution time.

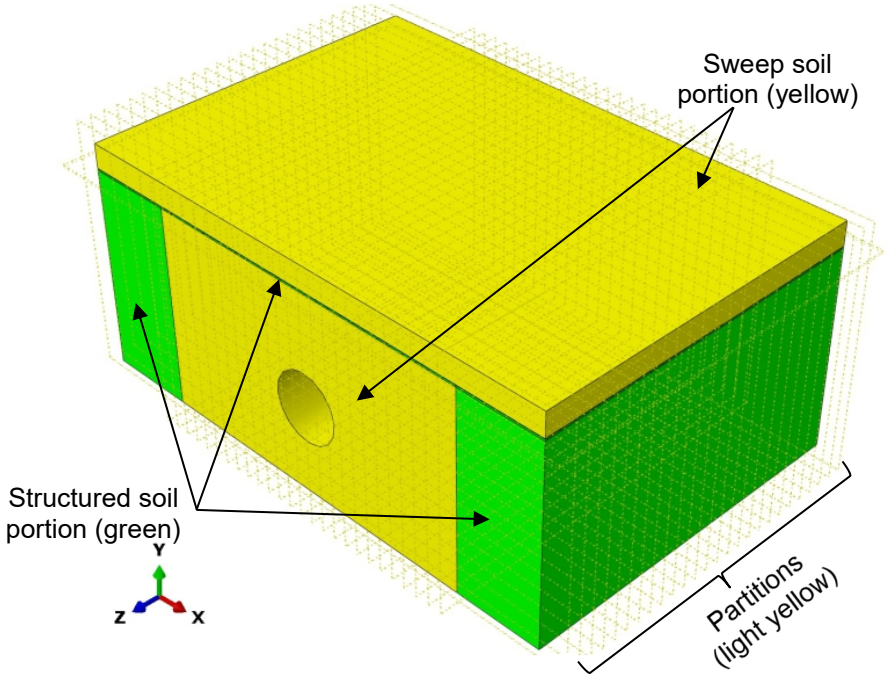

Figure 7.14 Used techniques for soil meshing

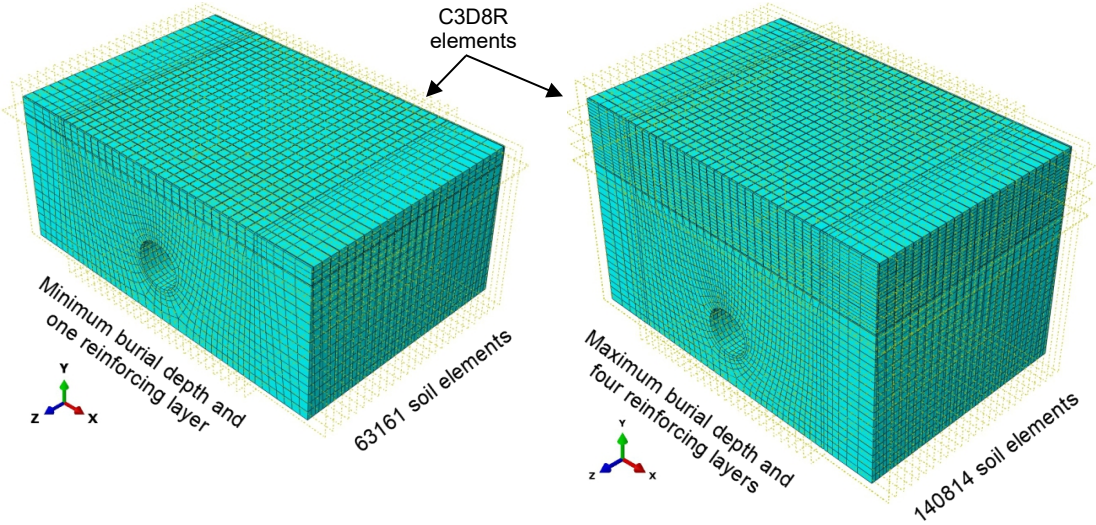

Figure 7.15 Meshing of soil at different conditions

7.2.9 Applied loading

Similar loading profile to that in the experimental testing was applied in the finite element modelling, where a monotonic load of 18 kN and load amplitude of 5 kN were selected, as illustrated in Figure 7.16. The monotonic loading was applied until reaching the mean value of the cyclic loading, and then the cyclic loading was applied to the footing for 200 cycles. The frequency of the cyclic loading was selected to be 0.5 Hz.

It should be noted that, the loading was applied on two phases/steps. In the first step, the geostatic pressure was applied to the whole system, where the second step was utilized to apply the pre-defined loading profile. According to the generated contact pairs between the 3D modelled geogrid reinforcing layers and the soil, the required time for solving each model was varied. The required time for solution ranged between ten and fifteen days per one model, despite using a computer of 16 GB RAM memory. Hence, the applied number of cycles in the finite element analysis was reduced compared with the experimental number of cycles, where applying the first loading phase of the experimental loading profile, 3000 cycles, in the finite element analysis would take months to solve only one model.

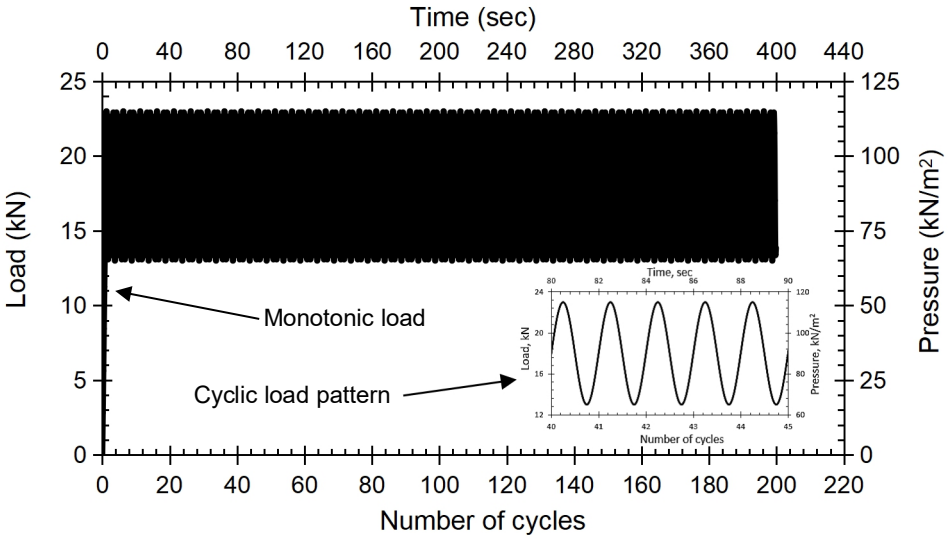

Figure 7.16 Loading profile in the finite element analysis

7.3 Model validation

The validation stage is considered an essential step to prove that the model discretization, selected material models, selected elements type, interaction criteria, properties of the different elements forming the model and the boundary conditions are correct and matched the real case with an accepted range. In this chapter, the validation stage was executed by comparing the results of the finite element model with those of the experimental testing in Chapter 4. Two validation stages were performed as follows:

1- Unreinforced case, to ensure that the modelling of the soil, pipe, footing and loading is correct.

2- Reinforced case using one geogrid-reinforcing layer modelled as continuum brick elements (3D with defined geometrical thickness) and planer sheet (membrane of zero geometrical thickness), to illustrate the importance of modelling the thickness of the reinforcing layer.

In the two stages, the validation was performed by comparing the experimental and numerical deformations of both the footing and the crown of the pipe.

7.3.1 Stage one of validation, unreinforced case

In this validation stage, a pipe was buried under unreinforced sand, where its burial depth was *H/D*=1.5. Consequently, the sand dimensions were 1500 mm in length, 1000 mm in depth, and 650 mm in height. To validate the suggested models, the results of the finite element analysis were compared with the experimental data. Relations between the number of loading cycles and the settlement of both, the footing and the crown of the pipe are illustrated in Figure 7.17.

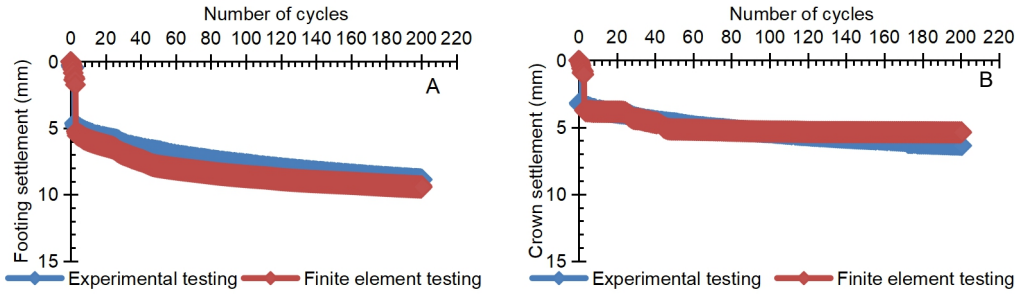

Figure 7.17 Stage one of validation, unreinforced soil
A: Footing settlement. B: Crown settlement.

The comparison between the results obtained using the developed finite element model agreed reasonably well with the experiment data, where accuracy of maximum 93.6% and 88.71% (maximum variation of reading reached 6.4% and 11.29%) was achieved for the footing and the crown settlements, respectively. This illustrated that the adopted technique for modelling soil, pipe and footing is correct and dependent data on this model are reliable. Moreover, the detrimental effect of the boundary conditions interference was successfully avoided.

7.3.2 Stage two of validation, geogrid-reinforced case

In this stage, the inclusion technique of one geogrid-reinforcing layer was validated. The layer was modelled using two different techniques, continuum brick elements (3D) and planer sheet (membrane). Figure 7.18 illustrated the relations between the number of loading cycles and the settlement of both, the footing and the crown of the pipe while varying the modelling technique of the geogrid layer.

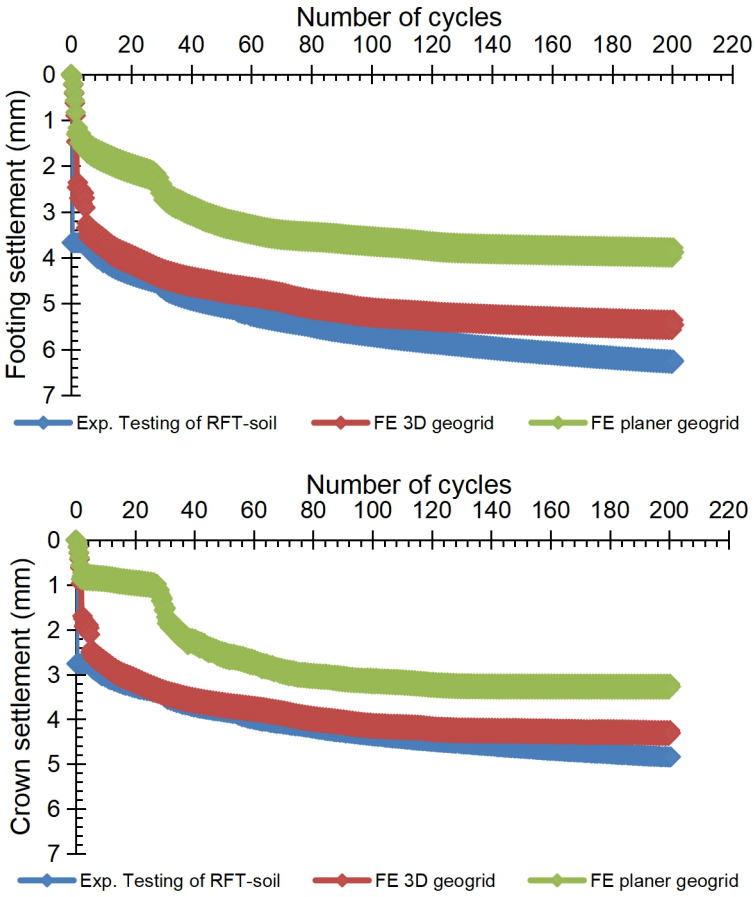

Figure 7.18 Stage two of validation, geogrid-reinforced soil

In the case where the geogrid-reinforcing layer was modelled as continuum brick elements (3D), both the numerical footing and crown settlements agreed reasonably well with the experiment data, where accuracies of 90.3% and 91.7% (maximum variation of readings reached 9.7% and 8.3%) were achieved, respectively. On the contrary, the geogrid-reinforcing layer modelling as planar sheet (membrane) resulted in significant variation in the obtained finite element outcomes compared with those obtain from the experimental testing. The achieved accuracy reached only 61.6% and 68.8% (results variation of 38.4%

and 31.2%) for the numerical settlements of the footing and the crown, respectively, which is clearly not acceptable.

In the planer modelling technique, the adopted interaction mechanism between the geogrid layer and the soil was selected as embedded region/perfect bond, neglecting the friction mechanism between them. Such this interaction mechanism significantly enhanced the soil performance resulting in underestimated finite element results compared with those obtained experimentally. Moreover, since the planar sheet has zero geometrical thickness, the passive earth resistance mechanism, which is considered the main load transfer mechanism between geogrids and soil, was ignored. On the other hand, the three-dimensional modelling of the geogrid layer allowed the proper modelling of the interaction criteria between the geogrid and the soil, where frictional and passive earth resistance mechanisms were numerically modelled.

Based on the finite element outcomes, it is clear that the planer (membrane) modelling technique of the geogrid layer underestimated the footing and the crown settlement responses compared with the experimental results, unlike the three-dimensional modelling technique, which accurately predicted the real performance of the reinforced-system. Consequently, in the following numerical parametric study, the geogrid reinforcing layers were modelled using the continuum brick technique, where (*C3D8R*) elements were used.

7.4 Parametric study

In this chapter, a parametric study was performed on two steps. In the first step, the contribution of varying the burial depth of the pipe and the number of the reinforcing layers was investigated, while fixing the value of the unit weight of the soil and the value of the applied loading, Figure 7.16, in addition to the reinforcing layers configuration, as illustrated in Table 7.7.

After determining the optimum burial depth of the pipe due to the outcomes of the first step, the second step of the parametric study was performed. In this step, the contribution of varying both the unit weight of the soil and the number of the reinforcing layers on the overall behaviour of the system was investigated, while fixing the value of the burial depth of the pipe to be equal to the optimum

value obtained from the first step, as presented in Table 7.8. It should be noted that the applied cyclic loading profile in the second step had higher amplitude compared with the first step.

Table 7.7 First step of the parametric study

Test type	Unit weight of the sand	Series	Tests	Test configuration					Tests No.
				RFT. No. (*N*)	*u/B*	*h/B*	*L/B*	*H/D*	
Unreinforced	16.01 kN/m^3	A	T1-T4	-	-	-	-	1.5-2-2.5-3	4
Reinforced		B	T5-T8	1	0.35	0.35	5		4
		C	T9-12	2					4
		D	T13-16	3					4
		E	T17-20	4					4

Where; *u* represents the spacing between the reinforcing layers, *h* refers to the spacing between the topmost layer and the footing and *L* represents the length of the reinforcing layer.

Table 7.8 Second step of the parametric study

Unit weight of the soil (kN/m^3)	Series	Test	Test configuration					Tests No.
			RFT. No.	*u/B*	*h/B*	*L/B*	*H/D*	
15.1 (Loose)	F	T21-T25	0-1-2-3-4	0.35	0.35	5	2.5	5
16.01 (Medium)	G	T26-T30						5
16.82 (Dense)	H	T31-T35						5

7.4.1 First step of the parametric study

In this step, the burial depth of the pipe and the number of the geogrid-reinforcing layers were varying. Consequently, the dimensions of the investigated models in this step were as presented in Table 7.9:

Table 7.9 Dimensions of the investigated parameters in the first step of FE

Pipe		Soil			RFT	
H/D	Burial depth (mm)	Height (mm)	Length (mm)	Width (mm)	*u=h* (mm)	*L* (mm)
1.5	300	650	1500	1000	70	1000

2	400	750				
2.5	500	850				
3	600	950				

7.4.1.1 Unreinforced case, Series A

In this series, the contribution of varying the burial depth of the pipe in unreinforced soil was investigated.

Settlement of the footing

Results for the normalised footing settlement (F_s/D) while increasing the number of the applied loading cycles is presented in Figure 7.19. The settlement is normalized relative to the pipe diameter.

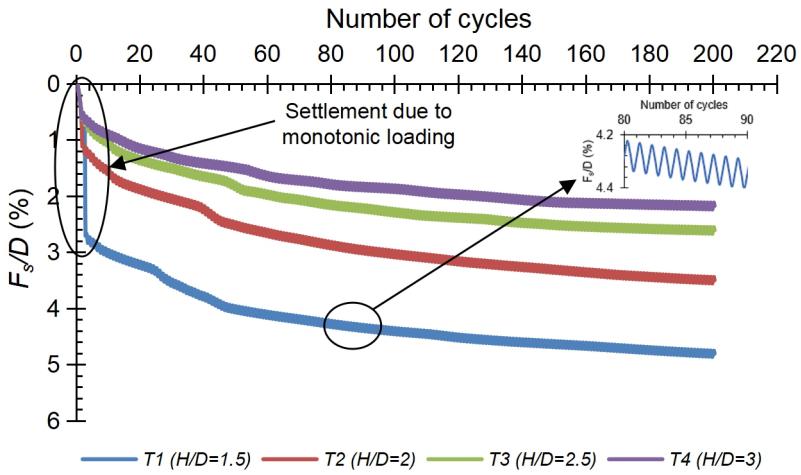

Figure 7.19 Normalised footing settlement due to loading cycles progression, N=0

Results illustrated that the increase in the burial depth of the pipe significantly reduced the settlement of the footing. At the shallowest burial depth, i.e. H/D=1.5, the normalised settlement ratio of the footing reached 4.81%, and with the increase in the burial depth of the pipe this ratio decreased, where it reached 3.5%, 2.61% and 2.17% for H/D=2, 2.5 and 3, respectively. The enhancement ratio in the footing settlement was 27.2%, 45.7% and 54.9% for H/D=2, 2.5 and 3, respectively, compared with the shallowest burial depth of the pipe, H/D=1.5.

To further inspect the relationship for footing settlement, Figure 7.20 was plotted to illustrate the footing settlement at the end of the loading profile relative to the burial depth of the pipe.

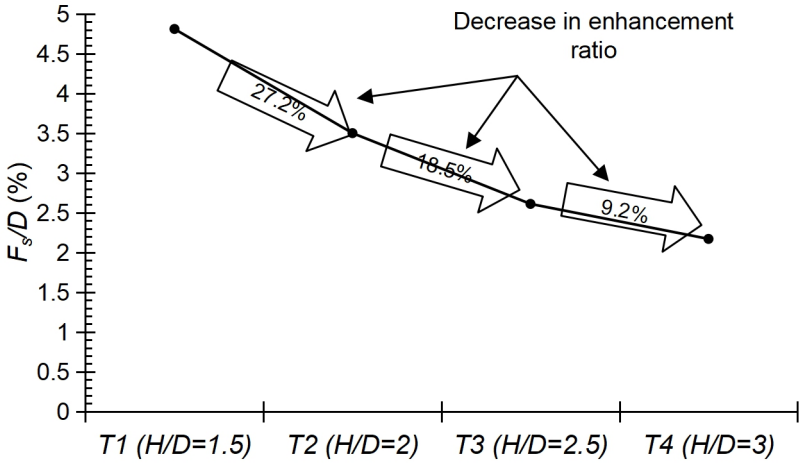

Figure 7.20 Normalised footing settlement at the end of the loading profile

The enhancement ratio in the settlement of the footing decreased with the increase in the burial depth of the pipe, where an enhancement of 27.2% occurred due to increasing the burial depth from *H/D*=1.5 to 2, and only 9.2% occurred while increasing *H/D* from 2.5 to 3. The results suggested that *H/D* of 2.5 was an optimum value for the footing settlement, where small ratio of enhancement in the settlement was achieved for burial depths more than 2.5. The settlement of the footing and the deformed shape of the whole model due to the variation in the burial depth of the pipe is shown in Figure 7.21.

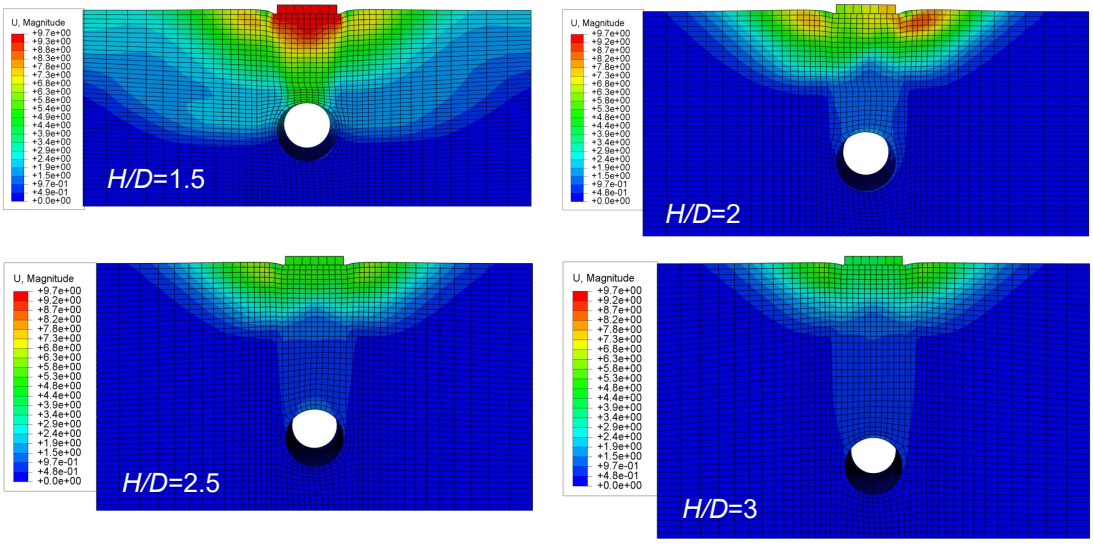

Figure 7.21 Footing settlement due to burial depth increase (mm)

Deformation of the pipe

The normalised crown settlement of the pipe at the end of the loading profile due to the variation in its burial depth is presented in Figure 7.22.

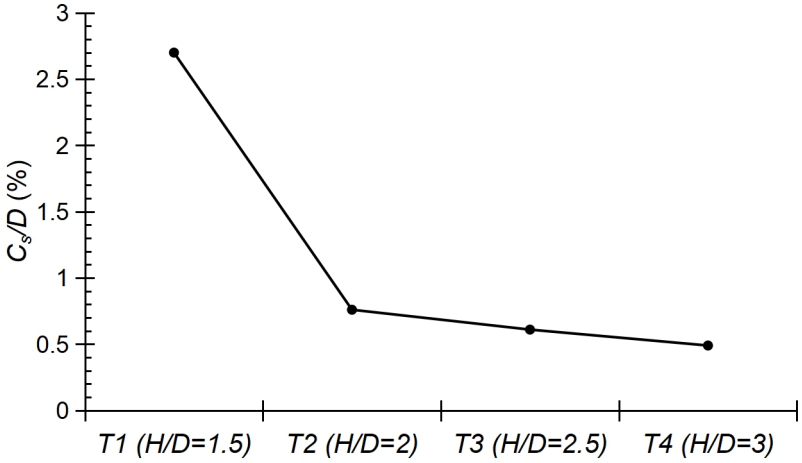

Figure 7.22 Normalised crown settlement at the end of the loading profile

At H/D=1.5, the pipe was in close vicinity to the footing, where small layer of soil interacted in the pressure mitigation. Moreover, the pipe interacted with the slip surface of the soil. Consequently, high value of pressure was transferred directly to the pipe, resulting in significant settlement on the crown of the pipe, as shown in Figure 7.23. With the increase in the burial depth of the pipe, more soil volume was located between the pipe and the footing, which kept the pipe far from the slip surface of the soil and reduced the value of the transferred pressure to the pipe. Consequently, the settlement of the crown of the pipe was reduced, as illustrated in Figure 7.23.

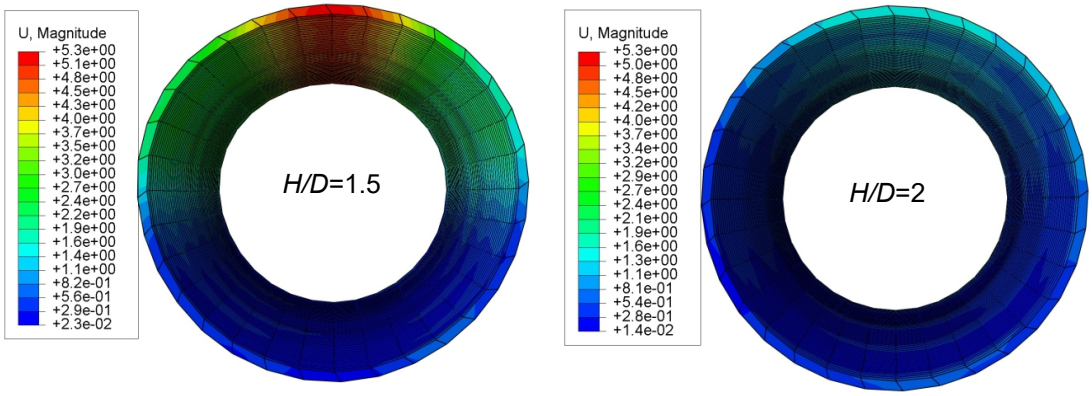

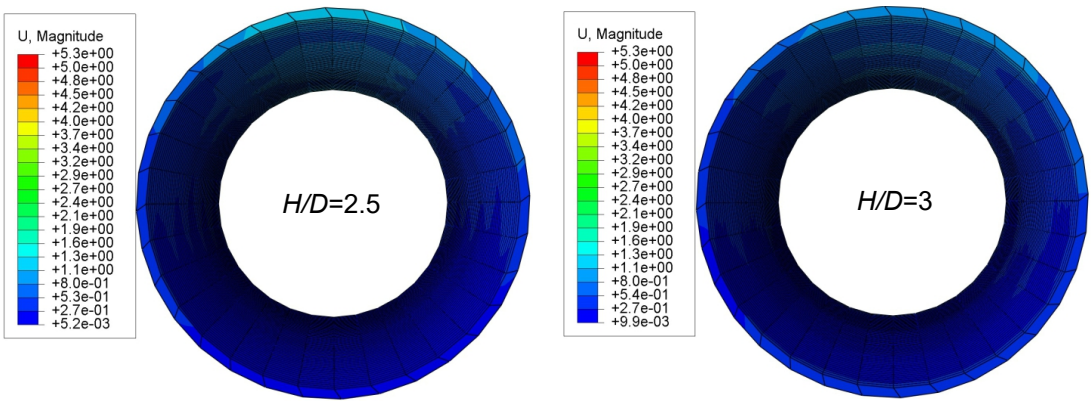

Figure 7.23 Pipe deformation due to burial depth increase (mm)

Transferred pressure to the pipe

The value of the transferred pressure to the pipe is governed by its location relative to the footing, i.e. its burial depth. Figure 7.24 illustrated the relation between the burial depth of the pipe and the transferred pressure to its crown at the end of the applied loading profile. Increasing the burial depth of the pipe contributed in decreasing the value of the transferred pressure to the pipe. At the shallowest burial depth, *H/D*=1.5, the measured pressure on the crown was 87.3 kPa. With the increase in the burial depth, the transferred pressure to the crown of the pipe was reduced to be 74.6 kPa, 63.1 kPa and 61.2 kPa for *H/D*=2, 2.5 and 3, respectively. The achieved enhancement ratio due to the burial depth increase was 14.5%, 27.7% and 29.8%, respectively, relative to the shallowest burial depth.

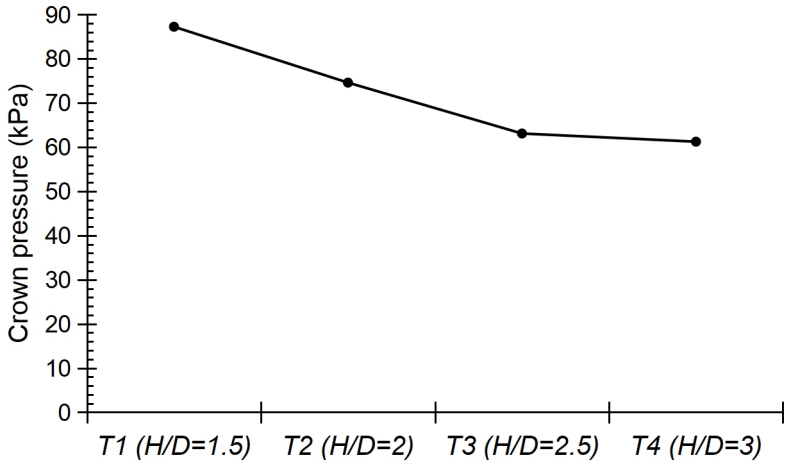

Figure 7.24 Transferred pressure to the crown of the pipe

According to the pressure measurements and the achieved enhancement ratios, it is worth noting that, increasing the burial depth of the pipe from *H/D*=1.5 to 2 resulted in a reduction in the transferred pressure to the pipe by 14.5%. This value was approximately doubled to be 27.7% due to increasing the burial depth of the pipe to *H/D*=2.5. Moreover, additional increase in the burial depth, *H/D*=3, resulted in a pressure reduction of 29.8%. The variation between the reduced pressure values due to increasing the burial depth of the pipe to *H/D*=2.5 and 3 was only 2.1%, which illustrated that in terms of pressure reduction, the optimum burial depth of the pipe is *H/D*=2.5.

According to the applied pressure to the footing, as shown in Figure 7.16, the maximum applied pressure value was 115 kPa. On the other hand, the measured pressure values along the crown of the pipe at variable burial depths were less than 115 kPa as illustrated in Figure 7.24. Consequently, a pressure reduction mechanism was formed inside the soil mass. Figure 7.21 illustrated a relative settlement between the directly located soil portion underneath the footing and the adjacent soil portions to it. This led to the formation of shear stresses between these portions of soils and the generation of an active arching mechanism, (Terzaghi and Peck, 1967), which redistributed the pressure inside the soil mass and reduced the transferred pressure to the crown of the pipe. Figure 7.25 showed the pressure distribution inside the soil mass at different burial depths of the pipe at the end of the loading profile.

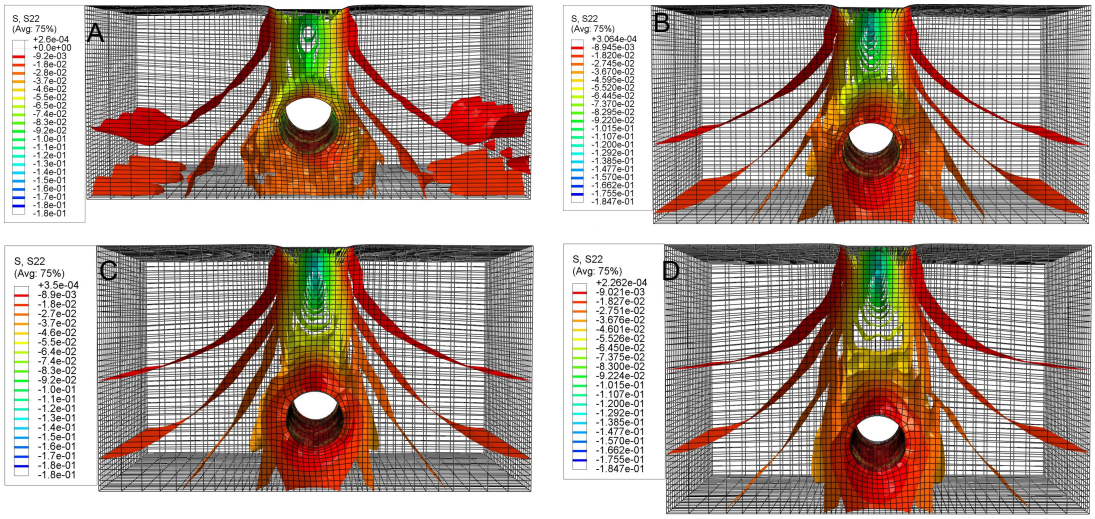

Figure 7.25 Pressure distribution due to burial depth increase (MPa)
A: *H/D*=1.5, B: *H/D*=2, C: *H/D*=2.5 and D: *H/D*=3

The contribution of the formed active arching mechanism depended mainly on the height of the soil layer located between the footing and the pipe, where lower height of this soil layer resulted in the formation of partial arching mechanism. At the shallowest burial depth, *H/D*=1.5, it is obvious that most of the applied pressure on the footing was directly transferred to the crown of the pipe, where partial arching mechanism contributed in the pressure redistribution process. With the increase in the burial depth of the pipe to reach *H/D*=2, an enhancement in the arching mechanism contribution occurred, where lower pressure value was transferred to the pipe. At *H/D*=2.5 it was obvious that a full arching mechanism was formed, where significant decrease in the transferred pressure to the pipe was recorded and the additional increase in the burial depth, *H/D*=3, resulted in insignificant additional decrease in the transferred pressure to the pipe. This supported the claim of selecting *H/D*=2.5 as an optimum burial depth of the pipe according to the pressure reduction point of view.

7.4.1.2 Reinforced case

In the reinforced case, four series were performed to investigate the contribution of varying the value of the burial depth of the pipe from *H/D*=1.5 to 3, in reinforced soil, where one, two, three and four geogrid reinforcing layers were utilized to reinforce the soil in series B, C, D and E, respectively.

Settlement of the footing

Figure 7.26 showed the normalised footing settlement (F_s/D) due to the progression of the loading cycles, while increasing the burial depth of the pipe in series B, where one reinforcing layer was utilised.

Results illustrated that the increase in the burial depth of the pipe reduced the settlement of the footing. At the shallowest burial depth, i.e. *H/D*=1.5, the normalised settlement ratio of the footing reached 2.73%, and with the increase in the burial depth of the pipe this ratio decreased, where it reached 1.17%, 0.99% and 0.89% for *H/D*=2, 2.5 and 3, respectively.

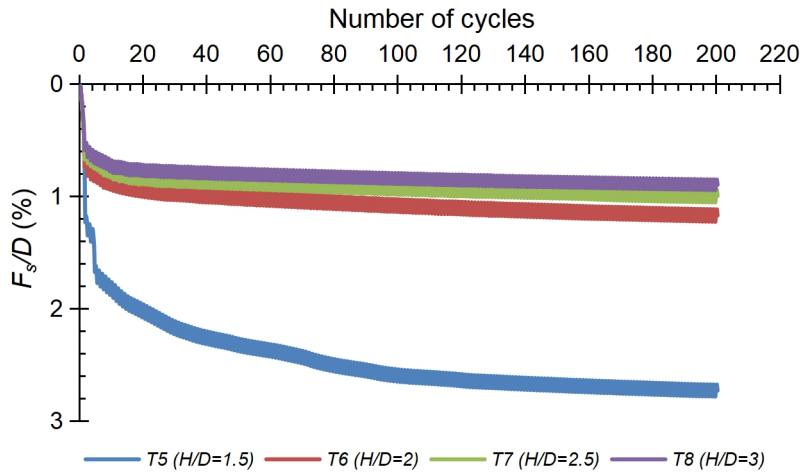

Figure 7.26 Normalised footing settlement due to burial depth variation, *N*=1

The reduction ratio in the footing settlement was 57.1%, 63.7% and 67.4% for *H/D*=2, 2.5 and 3, respectively, compared with the shallowest burial depth of the pipe, *H/D*=1.5. The settlement of the footing is dependent on the position of the pipe in the system. When the pipe is close to the footing, significant pressure is transferred to it leading to obvious deformation in the pipe followed by more footing settlement. On the other hand, if the pipe is located far from the footing, it suffers lower deformation leading to a reduction in the footing settlement. The inclusion of the geogrid reinforcing layer in the pipe-soil system contributed in decreasing the settlement of the footing through the generated load transfer mechanisms between the soil and the geogrid reinforcing layer. Measurements of the footing settlement in series A and B illustrated that the inclusion of one reinforcing layer in the pipe-soil system enhanced its performance, where the footing settlements in the reinforced system were lower than those measured in the unreinforced system by 43.2%, 66.5%, 61.7% and 58.6% for *H/D*=1.5, 2, 2.5 and 3, respectively.

Figure 7.27 represented a comparison between the normalised footing settlement in the four reinforced cases, i.e. series B, C, D and E, where it illustrated the normalised footing settlement at the end of the loading profile while increasing the burial depth of the pipe.

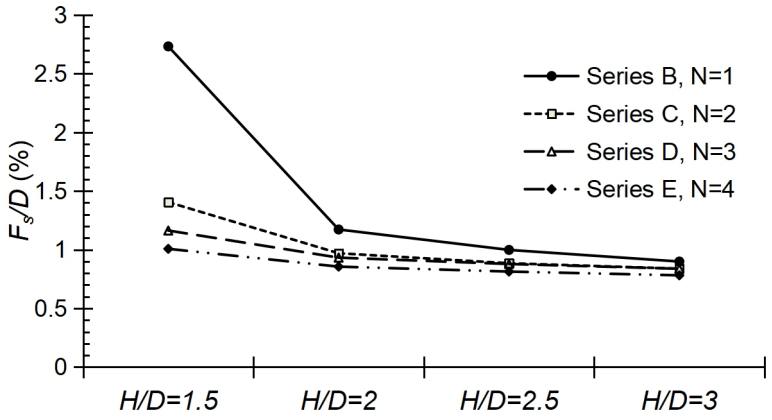

Figure 7.27 Normalised footing settlement in reinforced soil

The increase in the burial depth of the pipe allowed the formation of thicker layer of soil between the pipe and the footing. This layer has the ability to mitigate the generated pressure inside the soil and reduce the transferred pressure to the pipe, which positively reduced the deformation of both the pipe and the footing. On the other hand, the inclusion of the reinforcing layers in the soil generates a new composite material, reinforced soil, which has enhanced properties compared with unreinforced soil, in particular its shearing strength. The enhancement in the reinforced soil properties resulted from the soil-reinforcement interaction mechanisms, frictional, membrane and passive earth resistance mechanisms. Consequently, the inclusion of higher number of the reinforcing layers in the soil results in enhanced load transfer mechanisms, higher resistance to the applied load on the reinforced pipe-soil system, and reduction in the footing settlement. Table 7.10 demonstrated the normalised footing settlement values and the achieved reduction ratios, relative to the shallowest burial depth, due to increasing the burial depth of the pipe in series B, C, D and E, respectively.

Table 7.10 Reduction ratio in the footing settlement in series B, C, D and E

Series	B, (N=1)				C, (N=2)			
H/D	1.5	2	2.5	3	1.5	2	2.5	3
F_s/D (%)	2.73	1.17	0.99	0.89	1.41	0.97	0.88	0.83
Reduction ratio (%)	-	57.1	63.7	67.4	-	31.2	37.6	40.1
Series	D, (N=3)				E, (N=4)			
H/D	1.5	2	2.5	3	1.5	2	2.5	3
F_s/D (%)	1.16	0.93	0.87	0.83	1	0.86	0.81	0.78

Reduction ratio (%)	-	19.8	25	28.4	-	14	19	22

Figure 7.28 showed the relation between the normalised footing settlement and the increase in the number of the reinforcing layers at different burial depths of the pipe. It is obvious that at any burial depth of the pipe, increasing the number of the reinforcing layers decreased the value of the normalised footing settlement.

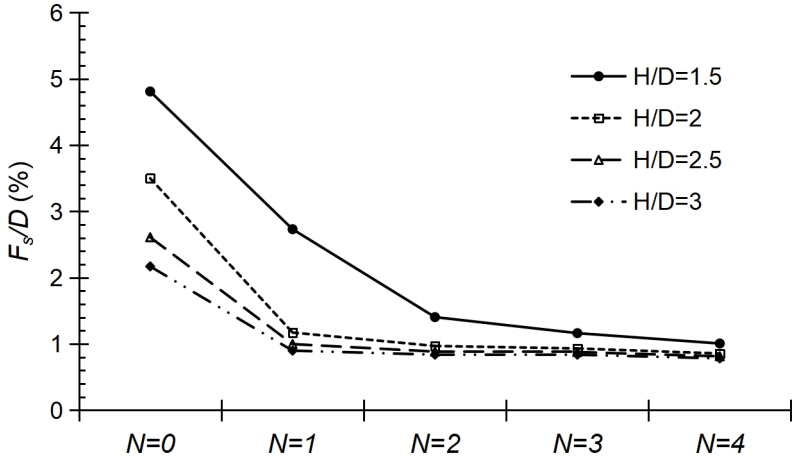

Figure 7.28 Normalised footing settlement due to layers number increase

The use of two reinforcing layers allowed the formation of a stiff platform, which was formed out of the two-geogrid layers and the trapped soil layer between them (Mohamed, 2010). This stiff platform behaved as if it was a flexible reinforced slab, which contributed in decreasing the footing settlement. Increasing the number of the reinforcing layers increased the stiffness of the formed platform leading to convergence in the reduction ratios in the footing settlement at any burial depth, which is in good agreement with the findings of Tafreshi and Khalaj (2008). However, insignificant reduction values in the footing settlement were observed while using three and four reinforcing layers compared with series C, where two layers of reinforcement were used. This could illustrate that the optimum reduction in the settlement of the footing was achieved while using two geogrid-layers of reinforcement and more layers did not achieve feasible enhancement.

Transferred pressure to the pipe

Figure 7.29 showed measured data for the transferred soil pressure to the crown of the pipe due to the variation in the burial depth of the pipe at the end of the loading profile for the four reinforced series, i.e. Series B, C, D and E.

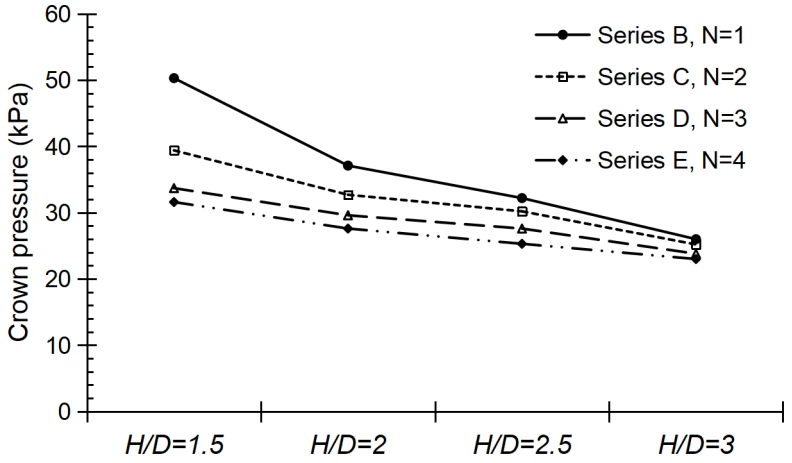

Figure 7.29 Values of crown pressure at variable burial depths

According to the measured pressure data, it is clear that increasing the burial depth of the pipe in the reinforced pipe-soil systems resulted in a reduction in the values of the transferred pressure to the crown of the pipe. For example, in series B where one geogrid-reinforcing layer was used, the transferred pressure value to the crown reached 50.3 kPa at the shallowest burial depth. This value decreased where it was 37.1 kPa, 32.2 kPa and 26 kPa for *H/D*=2, 2.5 and 3, respectively. In addition, these values of pressure were lower than those measured in series A, unreinforced case, with 42.4%, 50.3%, 49% and 57.6% for *H/D*=1.5, 2, 2.5 and 3, respectively.

It should be noted that the measured values of the crown pressure in Figure 7.29 are lower than those measured experimentally in Figure 4.24. This could be attributed to the non-modelling of the junctions of the reinforcing layers, which could negatively influence the soil-reinforcement interaction i.e. the passive earth resistance mechanism. In addition, the experimentally used pressure cell was located 3 cm above the crown of the pipe, where in the finite element analysis the pressure measuring process occurred exactly at the crown of the pipe.

Table 7.11 represents the values of the transferred pressure to the crown of the pipe and the achieved reduction rations, relative to both the shallowest burial

depth and series A, due to increasing the burial depth of the pipe in series B, C, D and E, respectively.

Table 7.11 Reduction ratio in the crown pressure in series B, C, D and E

Series	B, (*N*=1)				C, (*N*=2)			
H/D	1.5	2	2.5	3	1.5	2	2.5	3
Pressure value (kPa)	50.3	37.1	32.2	26	39.4	32.7	30.2	25.2
Reduction ratio w.r.t. *H/D*=1.5 (%)	-	26.2	35.9	48.3	-	17	23.4	36
Reduction ratio w.r.t. series A (%)	42.4	50.3	48.9	57.6	54.8	56.2	52.1	58.8
Series	D, (*N*=3)				E, (*N*=4)			
H/D	1.5	2	2.5	3	1.5	2	2.5	3
Pressure value (kPa)	33.7	29.6	27.6	23.8	31.6	27.6	25.3	23
Reduction ratio w.r.t. *H/D*=1.5 (%)	-	12.2	18	29.4	-	12.7	19.9	27.2
Reduction ratio w.r.t. series A (%)	61.4	60.3	56.3	61.1	63.8	63	59.9	62.4

In general, the inclusion of the reinforcing layers in the investigated pipe-soil systems generated load transfer mechanisms between the ribs of the layers and the particles of the sand, which enabled the soil cover above the pipe to mitigate the generated pressure and transfer lower pressure value to the pipe. In the reinforced series, the transferred pressure to the pipe was the summation of the arching mechanism and the distributed load over the reinforcing layer mechanism, which was generated due to the inclusion of the reinforcing layers. As illustrated in series A, the contribution of the arching mechanism was enhanced with the increase in the burial depth of the pipe. The friction and the generated passive earth resistance between the ribs of the reinforcing layer and the trapped soil inside its apertures contributed in forming a stiff composite layer, where the transferred pressure was distributed along its plane generating a wider loaded area with a lower pressure value underneath it, as shown in Figure 7.30.

Moreover, the distributed vertical pressure contributed in forming a horizontally pressurised zone surrounding the spring-lines of the pipe creating a confined zone around it. This confined zone allowed the pipe to sustain the transferred pressure to it while suffering lower deformation due to the laterally provided

support. Increasing the number of the reinforcing layers enhanced the contribution of the distributed load over the reinforcing layer mechanism, where more soil volume was interacted with the reinforcing layers and the distributed load over the first layer was redistributed along the following layers.

Figure 7.31 showed the transferred pressure values to the crown of the pipe at the end of the loading profile at variable burial depths due to increasing the number of the inserted geogrid-reinforcing layers in the investigated pipe-soil systems.

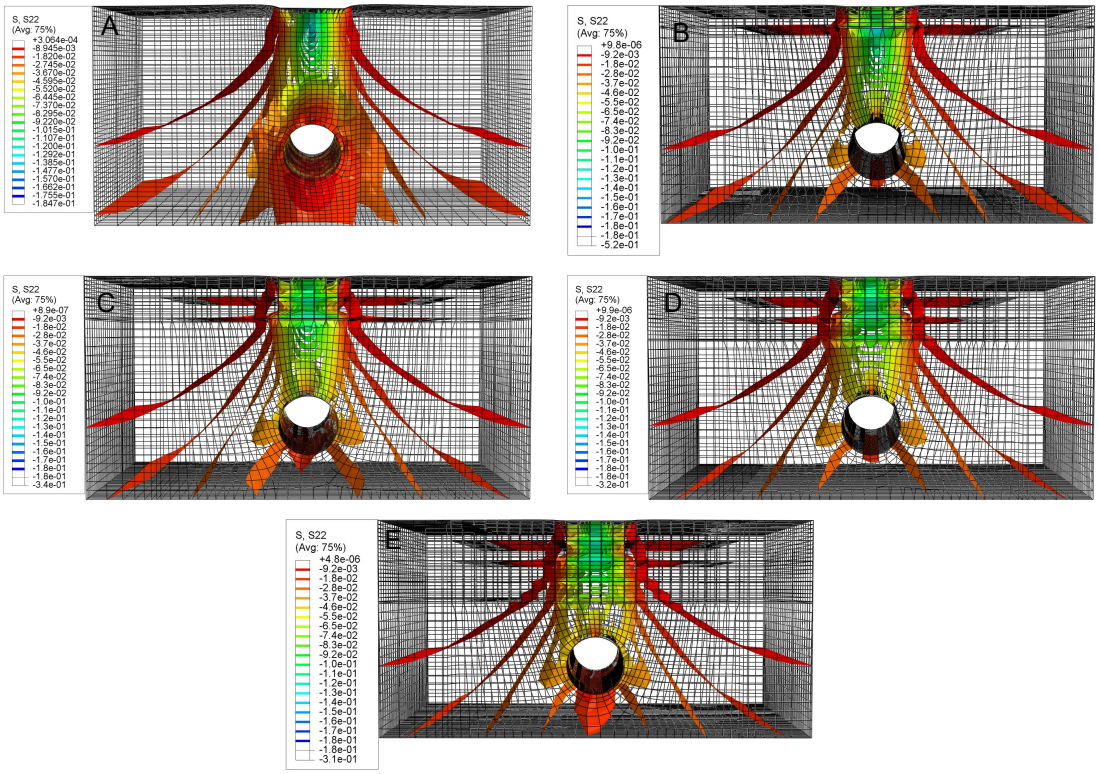

Figure 7.30 Pressure distribution in geogrid-reinforced systems, *H/D*=2 (MPa)
A: *N*=0, B: *N*=1, C: *N*=2, D: *N*=3 and E: *N*=4

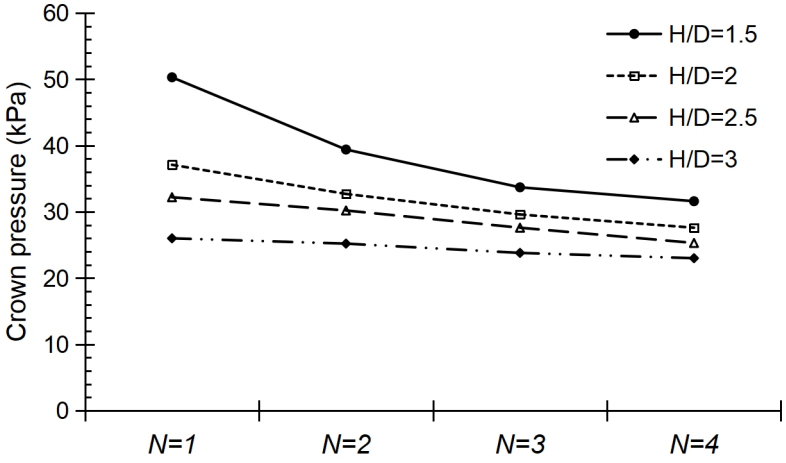

Figure 7.31 Values of crown pressure with different number of geogrid layers

At shallow burial depth, *H/D*=1.5, the measured pressure value at the crown of the pipe reduced with obviously variable rates due to increasing the number of the geogrid-reinforcing layers. The reduction rate due to increasing the layers' number from one to two layers was 10.9%, however, this rate decreased to be approximately one-fifth the initial rate due to increasing the number of the layers from three to four layers, where its value reached 2.1%. At higher burial depths, the pressure reduction rate was clearly lower than that measured at the shallowest burial depth, and the variation in the reduction rate was insignificant due to increasing the number of the geogrid layers. In general, the inclusion of one or two reinforcing layers in the system generates a lightly reinforced system (Sharma et al., 2009). A flexible slab is formed out of the reinforcing layers and the soil layer trapped in-between, which has the ability to obviously mitigate the transferred pressure along its surface. Increasing the number of the reinforcing layers in the system formed a heavily reinforced system. Consequently, the stiffness of the system increases and a rigid slab is generated instead of the flexible one (Tafreshi and Khalaj, 2008). Once a rigid slab is formed, a convergence in the transferred pressure values to the pipe occurs, and adding additional geogrid layers insignificantly contribute in reducing the pressure value, which is clear while using three and four reinforcing layers. Moreover, the contribution of the reinforcing layers in decreasing the transferred pressure to the pipe decreases while increasing the burial depths of the pipe due to the improvement in the arching mechanism.

Consequently, the role of the reinforcing layers in reducing the transferred pressure to the crown of the pipe is obvious at relatively lower burial depths, where arching mechanism has minor contribution, and while using one or two reinforcing layers, where flexible slab is formed.

Pipe deformation

Figure 7.32 depicted the measured data for the normalised deformation of the crown of the pipe due to the variation in the burial depth of the pipe at the end of the loading profile in the four reinforced series.

The increase in the burial depth of the pipe had a major contribution in decreasing its deformation. For series B, where one reinforcing layer was used in the reinforced pipe-soil systems, the values of the normalised crown deformation was 2.21%, 0.37%, 0.285% and 0.235% for *H/D*=1.5, 2, 2.5 and 3, respectively. It was observed that the achieved reduction ratio in the deformation of the crown of the pipe had a remarkable value while increasing the burial depth from *H/D*=1.5 to 2, where it was 83.3%. An insignificant reduction in the pipe deformation occurred due to increasing the burial depth of the pipe more than *H/D*=2, where the average value of the achieved reduction ratio was 3%. For the other reinforced series, similar behaviour of the crown of the pipe was observed with a feasible decrease in the achieved reduction ratio in the deformation of the crown while increasing the burial depth from *H/D*=1.5 to 2. The reduction ratio reached 66.3%, 53.9% and 39.4% for series C, D and E, respectively. Additional increase in the burial depth, more than *H/D*=2, achieved insignificant reduction in the pipe deformation despite the increase in number of the geogrid-reinforcing layers.

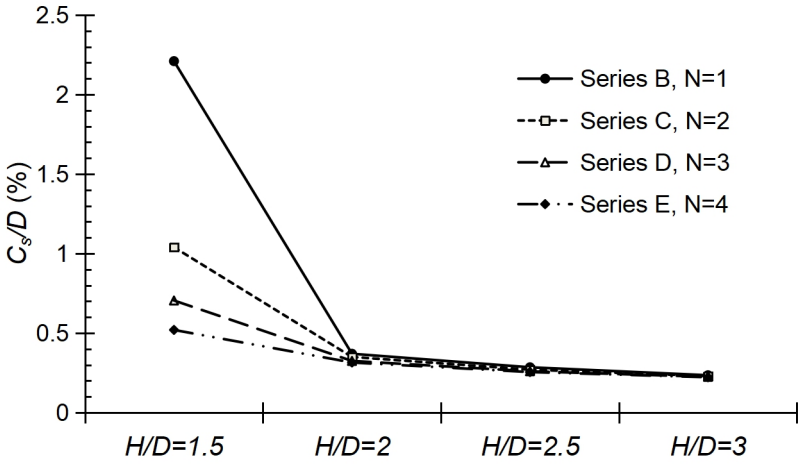

Figure 7.32 Values of normalised crown deformation at variable burial depths

Generally, the occurred deformation in the crown of the pipe is directly related to the transferred value of pressure to the crown of the pipe and the provided lateral support to its spring-lines. Figure 7.33 demonstrated the pressure distribution in the soil for series B. The value of the transferred pressure to the pipe was reduced with the increase in the burial depth, where the increase in the thickness of the soil layer between the pipe and the footing enhanced the contribution of the arching mechanism in mitigating the transferred pressure to the crown. Moreover, the inclusion of the reinforcing layer generated a stiff composite layer, where the transferred pressure was distributed along its plane generating a wider loaded area with a lower pressure value underneath it. This led to an enhanced degree of the provided lateral support to the pipe and a decrease in the crown deformation while increasing the burial depth.

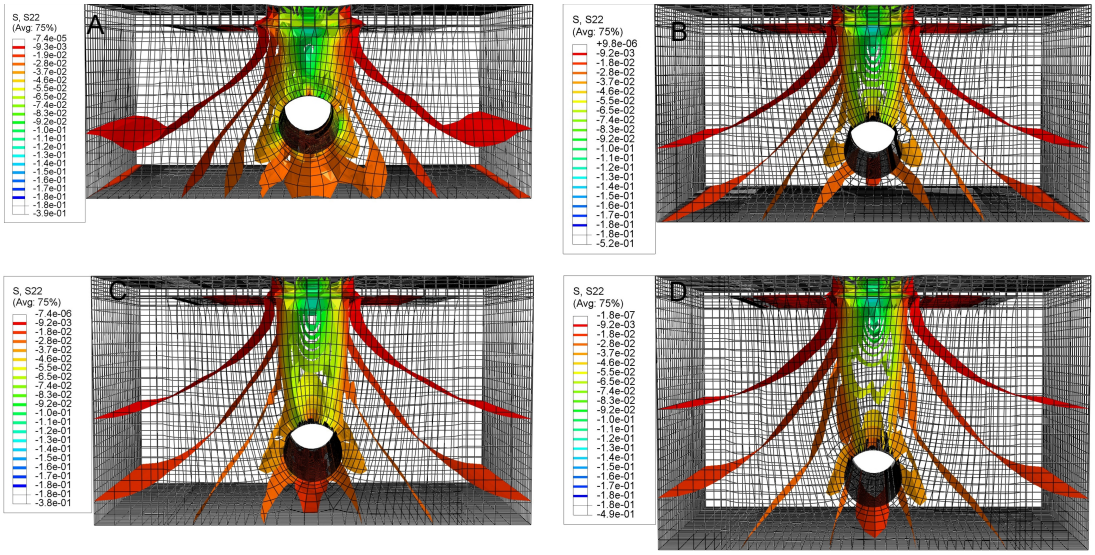

Figure 7.33 Pressure distribution in series B (MPa)
A: *H/D*=1.5, B: *H/D*=2, C: *H/D*=2.5 and D: *H/D*=3

On the other hand, the increase in the number of the reinforcing layers had observable influence in decreasing the crown deformation only at the shallowest burial depth, i.e. *H/D*=1.5. The contribution of the arching mechanism in mitigating the pressure dominated the system at deeper burial depths, where full arching mechanism was formed. Additionally, the reinforcing layers contribution controlled the pressure reduction at shallow burial depth. In series C, two layers of reinforcements were used and the formed stiff layer behaved as a flexible slab distributing the pressure underneath it. The increase in the number of the reinforcing layers, series D and E, increased the stiffness of the reinforced zone and converted it into a rigid slab, where a convergence in the pressure values occurred and the crown of the pipe experienced an almost similar deformation at deeper burial depths, as observed in Figure 7.34.

This explained the insignificant reduction in the deformation of the pipe due to increasing the number of the geogrid layers at deeper burial depths.

Consequently, using two geogrid-reinforcing layers would achieve the optimum reduction in the deformation of the crown of the pipe, and increasing the burial depth of the pipe more than *H/D*=2 would provide insignificant enhancement in decreasing the pipe deformation.

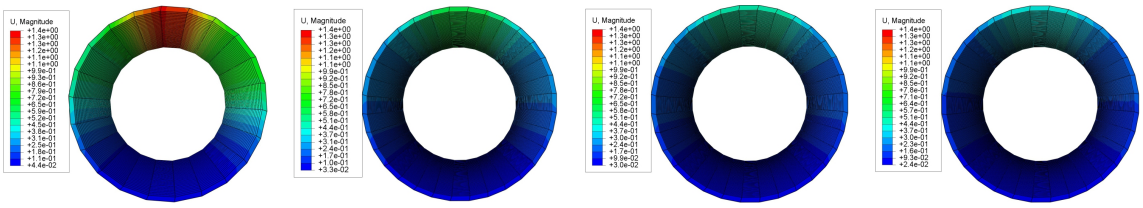

H/D=1.5 (1.4 mm) *H/D*=2 (0.6 mm) *H/D*=2.5 (0.5 mm) *H/D*=3 (0.42 mm)

Series D

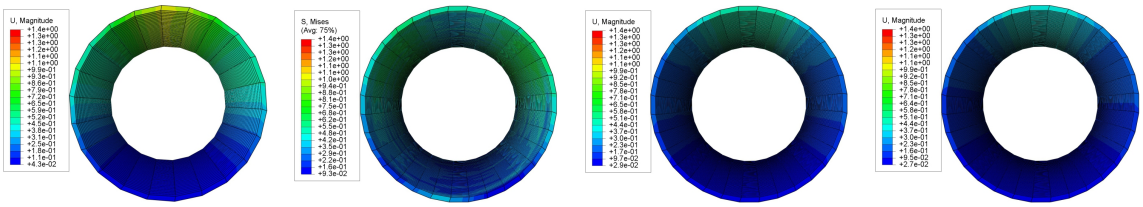

H/D=1.5 (1 mm) *H/D*=2 (0.6 mm) *H/D*=2.5 (0.5 mm) *H/D*=3 (0.41 mm)

Series E

Figure 7.34 Crown settlement for series D and E at different burial depths

Strain of the geogrid reinforcing layers

Due to the application of the loading profile to the tested systems, tensile and compressive strains were generated in the soil. The soil has the ability to sustain the generated compressive strains, however; tensile strains could lead to soil failure. The inclusion of reinforcing layers played a significant role in preventing such failure, where the formed composite material, i.e. reinforced soil, had enhanced properties compared with unreinforced soil, particularly its shearing strength. Figure 7.35-A showed the overall profile of the strain generated in the reinforcing layers according to the burial depth increase for series B, where one reinforcing layer was used.

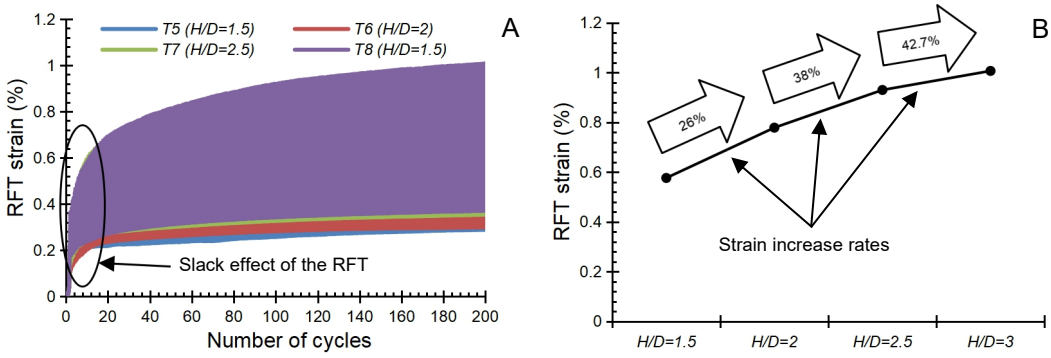

Figure 7.35 Strain generated in the reinforcing layer, series B
A: Overall strain profile. B: Maximum strain value.

It was noted that increasing the burial depth of the pipe had a negative influence on the strain generated in the reinforcing layers, where the reinforcing layers experienced higher tensile strain values with burial depth increase, as presented in Figure 7.35-B. The values of the generated tensile strain were 0.57%, 0.78%, 0.93% and 1% for *H/D*=1.5, 2, 2.5 and 3, respectively, with an increase in the strain generation rate of 26%, 38% and 42.7% for *H/D*=2, 2.5 and 3, respectively, compared with the shallowest burial depth. It was observed that the rate of the increase of the strain generation was significantly decreased after a burial depth of *H/D*=2.5, where the strain rate increased with only 4.7%.

The distance between the pipe and the soil surface could be divided into two zones, upper and lower zones. The pipe itself reinforced the lower zone, since it has higher stiffness compared with the soil, and contributed to the upper zone's stability. When the spacing between the soil surface and the pipe exceeded a certain limit; that is, *H/D*=2.5, the stability of the upper zone was primarily

dominated by the soil properties. Here comes the role of the reinforcing layer, which has a major contribution in the upper zone stability when it is far from the pipe, through sustaining the generated strain in the soil. After *H/D*=2.5, the contribution of the reinforcing layer was no longer dependent on the burial depth of the pipe and the increase in the strain sustained by the reinforcing layer was significantly decreased.

Figure 7.35-A demonstrated that during the first 20 loading cycles the strain rate generated was very fast, and it decreased with the progression of the loading cycles. The slack effect of the reinforcing layers is responsible for this behaviour, where the generated friction between the soil particles and the reinforcing layer forced the layer to stretch and deform before its contribution in the system stability, since it has an extensible nature (Chenggang, 2004; Sieira et al., 2009; Tran et al., 2013). When the layer is fully stretched, as illustrated approximately at the 20th cycle, the slack effect of the reinforcing layer ends (Abu-Farsakh et al., 2013). At this stage, the contribution of the passive earth resistance mechanism between the ribs of the layer and the trapped soil in its apertures dominates the system performance and a decrease in the strain generation rate occurs.

Figure 7.36 illustrated the maximum values of the strain generated in the reinforcing layers at different burial depths for series C, where two reinforcing layers were used. According to the measured values of strain for the upper (*L1*) and lower (*L2*) reinforcing layers, a similar behaviour to that observed in series B occurred, where the increase in the burial depth of the pipe resulted in an increase in the strain values experienced by the reinforcing layers.

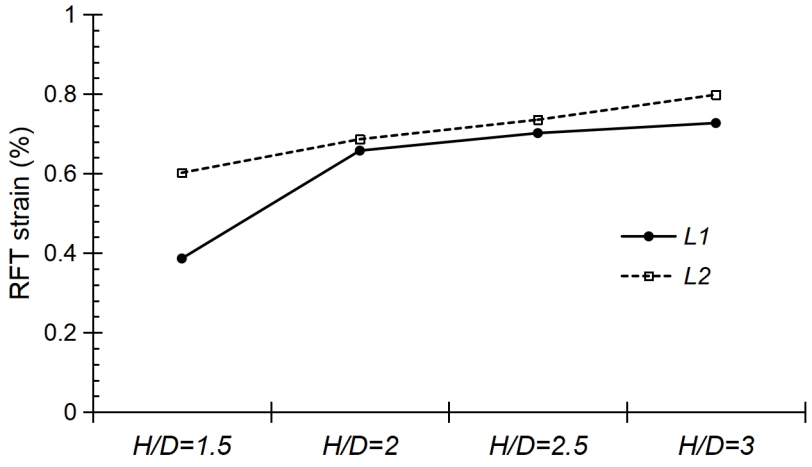

Figure 7.36 Strain generated in the reinforcing layer, series C

On the other hand, measured data illustrated that at any burial depth of the pipe the lower reinforcing layer suffered strain values larger than those sustained by the upper one, matching the findings of Jones and Cooper (2005), however the upper layer underwent the highest deformation as shown in Figure 7.37. The larger deformation of the upper reinforcing layer could be attributed to there being less soil cover above it leading to higher transferred pressure value, lower confinement and higher deformation. Due to the pressure redistributed along the upper layer's surface, the lower layer experienced reduced pressure value leading to lower deformation compared to the upper one.

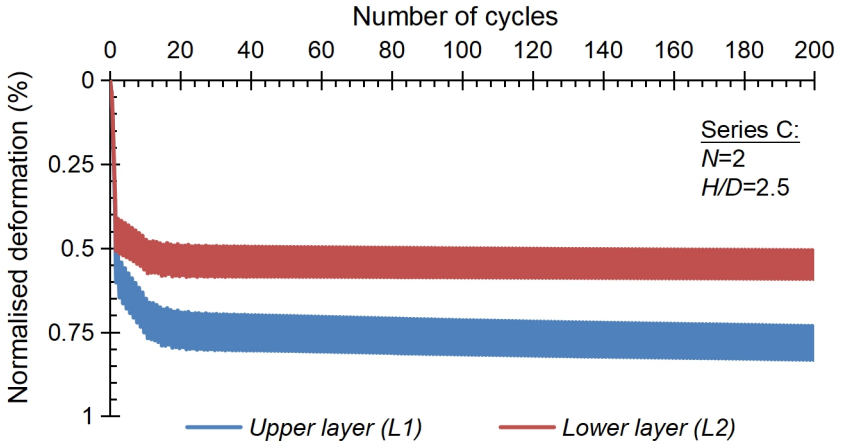

Figure 7.37 Deformation of the reinforcing layers

The increase in the experienced strain by the lower reinforcing layer could be related to the formed flexible slab. In this case, the reinforced zone was subjected to bending stresses that highly affected the lower reinforcing layer generating high value of tensile strain in it. In addition, once the load was applied to this platform its lower surface suffered tensile strain, unlike its upper surface, which might have suffered compressive strain. Consequently, the lower layer suffered higher value of the tensile strain and lower value of deformation compared with the upper layer.

The maximum values for the strain generated in the reinforcing layers due to burial depth increase is demonstrated in Figure 7.38 for series D and E, where three and four reinforcing layers were used.

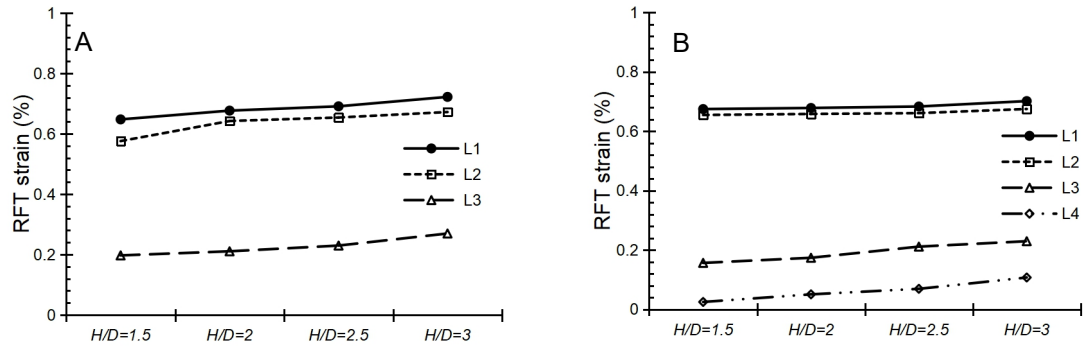

Figure 7.38 Strain generated in the reinforcing layer
A: series D. B: series E.

Where; *L1*, *L2*, *L3* and *L4* represent layer one, two, three and four, respectively. Results illustrated that a similar behaviour to that observed in series B and C happened, where the reinforcing layers experienced higher values of the tensile strain due to the increase in the burial depth of the pipe, regardless of the number of reinforcing layers and their position in the system. This could be attributed to the decrease in the contribution of the pipe in supporting the upper soil zone with burial depth increase, which led to enhanced contribution of the reinforcing layer in sustaining the generated tensile strain in the upper soil zone, i.e. the reinforced soil cover.

Moreover, strain measurements showed that the upper geogrid reinforcing layer (*L1*) suffered the maximum values of the tensile strain, unlike the lower layer (*L3* in series D and *L4* in series E), which suffered the least value of tensile strain. This behaviour contradicted that observed in series C. As observed in the transferred pressure to the pipe section, increasing the number of the inserted reinforcing layers in the system resulted in forming a heavily reinforced system with higher stiffness, which contributed in converting the generated flexible slab, while using two reinforcing layers, into a rigid one, while using three and four reinforcing layers, (Tafreshi and Khalaj, 2008). The formed rigid slab did not deform under bending stresses, unlike the flexible slab, where its upper surface sustained the highest portion of the applied loads and lower value of loads were transferred through the rigid slab until reaching its lower surface. Consequently, the upper reinforcing layer suffered the maximum tensile strain and the subsequent layers sustained lower strain values until reaching the lower layer, which suffered the least value of tensile strain.

Figure 7.38 also showed that the measured strain values in the third layer in series D, the third and the fourth layers in series E were significantly lower than those measured in the first and the second geogrid reinforcing layers. This could illustrate that the inclusion process of two layers of reinforcements would achieve the optimum performance of the reinforced system, and adding additional layers is uneconomical, where it had a minor contribution in sustaining the generated tensile strain.

7.4.2 Second step of the parametric study

In this step, the unit weight of the sand and the number of the reinforcing layers were varying, while keeping the value of the burial depth of the pipe, friction angle of the sand and elastic modulus of the sand constant. According to the first step of the parametric study a *H/D*=2.5 was considered as an optimum burial depth. Consequently, the dimensions of the investigated models in this step were as presented in Table 7.12.

The amplitude of the applied cyclic loading profile in the second step of the parametric study is higher than that applied in the first step, where a monotonic load of 18 kN and load amplitude of 12 kN were selected, as illustrated in Figure 7.39. The frequency of the cyclic loading was similar to that selected in the first step, where its value was 0.5 Hz.

Table 7.12 Dimensions of the investigated parameters in the second step

Soil					Pipe		RFT		
Series	Unit weight (kN/m^3)	Height (mm)	Length (mm)	Width (mm)	*H/D*	*H* (mm)	*u=h* (mm)	*L* (mm)	*N*
F	15.1 (loose)	850	1500	1000	2.5	500	70	1000	0-1-2-3-4
G	16.01 (medium)								
H	16.82 (dense)								

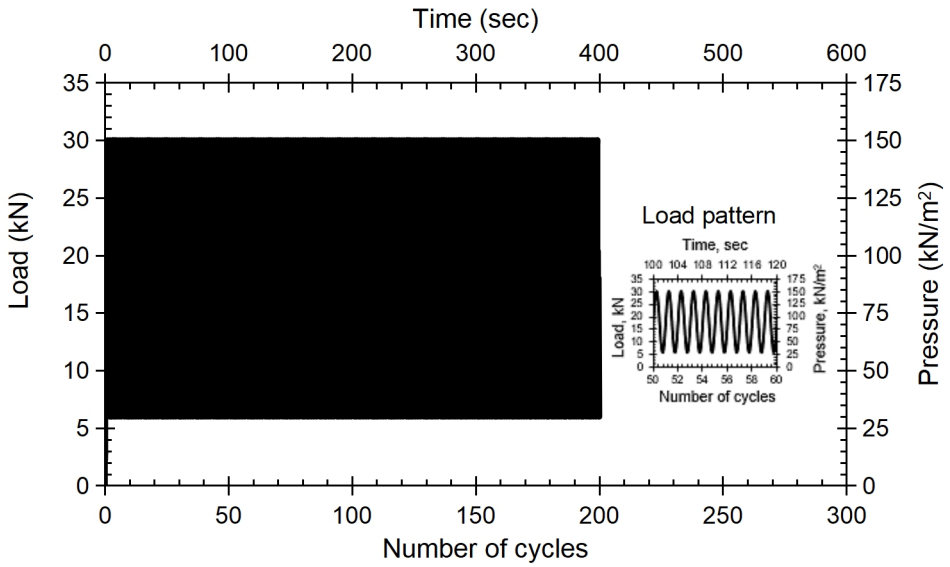

Figure 7.39 Loading profile in the second step of the parametric study

7.4.2.1 Settlement of the footing

The normalised footing settlement due to the variation in the number of the geogrid reinforcing layers is shown in Figure 7.40, for series F, where a soil of loose unit weight was used.

Results illustrated that the maximum footing settlement occurred in the unreinforced case, where its normalised value reached 16.1%. The inclusion of the reinforcing layers contributed in decreasing this value, as presented in Table 7.13, due to the formed load transfer mechanisms between the soil and the reinforcing layers. Moreover, the achieved reduction in F_s/D significantly decreased after N=2, where 3.9% and 2.15% additional reduction occurred due to using three and four layers of reinforcements, respectively. Consequently, the optimum value of the footing settlement was achieved while using two layers of the geogrid reinforcements.

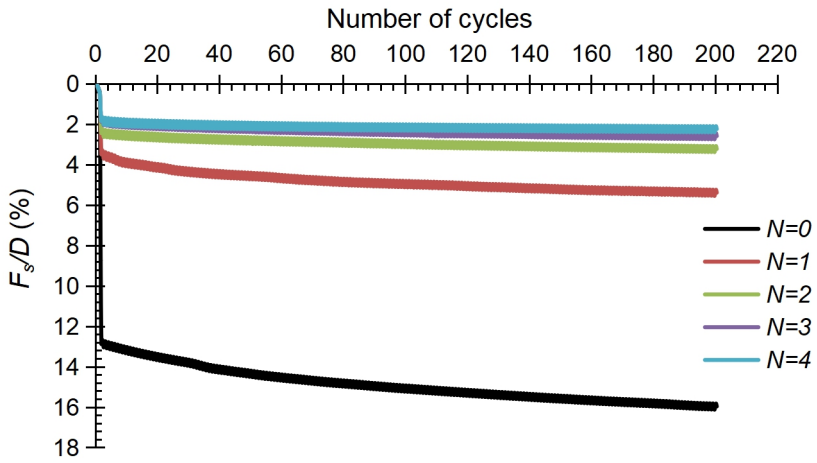

Figure 7.40 F_s/D at variable number of the reinforcing layer, series F

Table 7.13 Reduction ratio of F_s/D in series F

RFT no.	*N*=0	*N*=1	*N*=2	*N*=3	*N*=4
F_s/D (%)	16.1	5.54	3.37	2.74	2.39
Reduction ratio relative to *N*=0 (%)	-	65.6	79.1	83	85.2

A comparison between the obtained results for F_s/D at the end of the applied loading profile due to increasing the number of the reinforcing layers at different unit weights of the soil is presented in Figure 7.41.

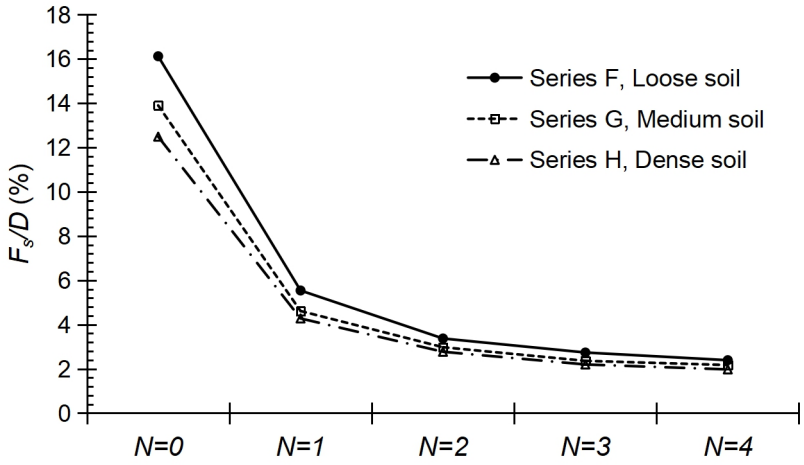

Figure 7.41 Normalised footing settlement at variable unit weights of the soil

It is clear that increasing the unit weight of the soil contributed in decreasing the value of the normalised footing settlement, as presented in Table 7.14. However, after *N*=2, this contribution became insignificant, where a conversion in the achieved footing settlements occurred. Increasing the unit weight of the soil resulted in increasing its stiffness, which is similar to applying higher

compaction efforts to the soil, which would enhance its performance against applied loads. Consequently, increasing the unit weight of the soil decreased the footing settlement.

Table 7.14 Reduction ratio of F_s/D in series G and H

Series G, medium unit weight					
RFT no.	*N*=0	*N*=1	*N*=2	*N*=3	*N*=4
F_s/D (%)	13.9	4.6	2.9	2.4	2.2
Reduction ratio relative to *N*=0 (%)	-	66.8	11.7	4.4	1.4
Reduction ratio relative to series F (%)	13.8	16.7	11.7	13.7	9.2
Series H, dense unit weight					
RFT no.	*N*=0	*N*=1	*N*=2	*N*=3	*N*=4
F_s/D (%)	12.5	4.3	2.7	2.2	1.9
Reduction ratio relative to *N*=0 (%)	-	65.7	77.8	82.4	84.2
Reduction ratio relative to series F (%)	22.5	22.8	17.8	19.7	17.4

Figure 7.42 illustrated the achieved reduction ratio in the footing settlement while using different number of the reinforcing layers relative to the unreinforced case, in series F, G and H.

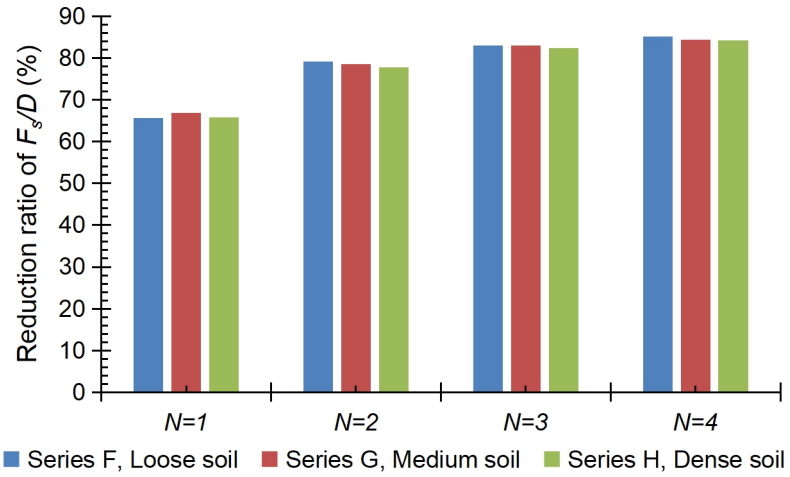

Figure 7.42 Reduction ratio in F_s/D at different number of layers for series F, G and H

While inserting two, three and four geogrid layers of reinforcements; it was noted that the highest reduction ratio in F_s/D was achieved while using loose soil, i.e. in series F. This indicated that the reinforcement contribution while using soil of lower unit weight is more effective than that occurred in soil of higher unit weight. In addition, the maximum benefit of the occurred interaction between the soil and the reinforcing layers was achieved while using loose soil,

which in a good agreement with the findings of Tafreshi and Khalaj (2008). Soil of higher unit weight had higher properties and higher ability to sustain loads, while requiring relatively slight lower contribution from the reinforcing layers.

7.4.2.2 Transferred pressure to the pipe

Figure 7.43 showed measured data for the transferred soil pressure to the crown of the pipe due to the variation in the number of the reinforcing layers at the end of the loading profile for series F, G and H.

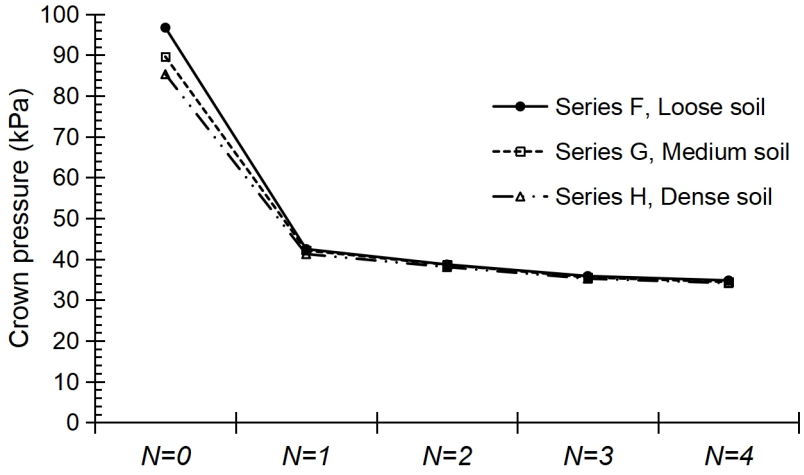

Figure 7.43 Values of crown pressure for series F, G and H

Based on the measured pressure data, it is obvious that the inclusion of the reinforcing layers in the investigated pipe-soil systems resulted in a reduction in the values of the transferred pressure to the crown of the pipe. However, the increase in the layers number had insignificant influence in decreasing the pressure values, regardless the unit weight of the soil, which had obvious contribution in reducing the crown pressure only in the unreinforced case.

Table 7.15 demonstrated the values of the transferred pressure to the crown of the pipe and the achieved reduction rations, relative to both the unreinforced case and series F, due to increasing the number of the geogrid-reinforcing layers in series F, G and H.

Table 7.15 Reduction ratio in the crown pressure in series F, G and H

Series F, loose unit weight					
RFT no.	*N*=0	*N*=1	*N*=2	*N*=3	*N*=4

Pressure (kPa)	96.7	42.46	38.69	35.86	34.78
Reduction ratio relative to *N*=0 (%)	-	56.1	59.9	62.9	64.02
Series G, medium unit weight					
RFT no.	*N*=0	*N*=1	*N*=2	*N*=3	*N*=4
Pressure (kPa)	89.6	42.14	38.62	35.55	34.41
Reduction ratio relative to *N*=0 (%)	-	52.97	56.89	60.32	61.59
Reduction ratio relative to series F (%)	7.34	0.77	0.17	0.87	1.07
Series H, dense unit weight					
RFT no.	*N*=0	*N*=1	*N*=2	*N*=3	*N*=4
Pressure (kPa)	85.3	41.25	38.06	35.23	34.13
Reduction ratio relative to *N*=0 (%)	-	51.64	55.37	58.7	59.98
Reduction ratio relative to series F (%)	11.79	2.87	2.62	1.78	1.88

Figure 7.44 was plotted to inspect the contribution of the increase in the number of the geogrid-reinforcing layers in decreasing the transferred pressure to the crown of the pipe.

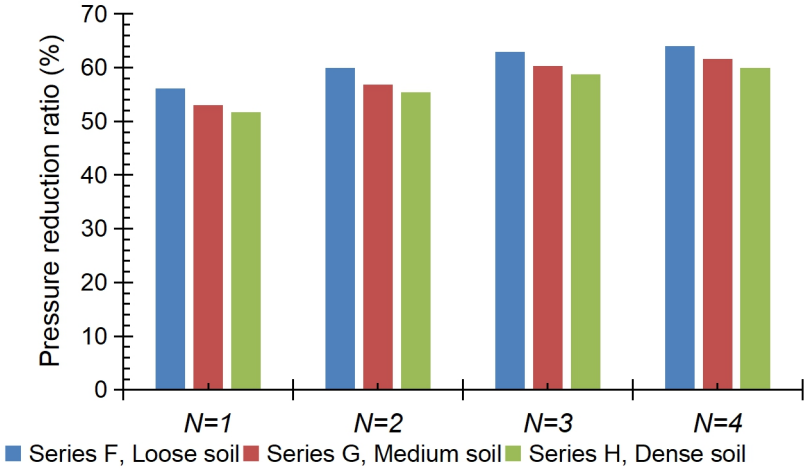

Figure 7.44 Pressure reduction ratio relative to (*N*=0) for series F, G and H

It is clear that small reduction in the pressure values was observed due to increasing the number of the reinforcements, where the inclusion of one reinforcing layer resulted in a pressure reduction ratio of 56.1%, 52.9% and 51.6% for series F, G and H, respectively. These values were increased due to the inclusion of four reinforcing layers to reach values of 64%, 61.6% and 59.98%, respectively, achieving an average additional pressure reduction of 13.4%, which is approximately one-fourth the achieved reduction while using one geogrid-layer. In addition, regardless the number of the layers, the maximum reduction ratios were obtained while inserting the reinforcing layers in loose soil, where maximum benefit of the layers were achieved through the

generated load transfer mechanisms, as medium and dense soils had higher ability to sustain loads compared with loose soils.

7.4.2.3 Deformation of the crown

The normalised crown settlement (C_s/D) due to the increase in the number of the geogrid reinforcing layers for series F, G and H is presented in Figure 7.45.

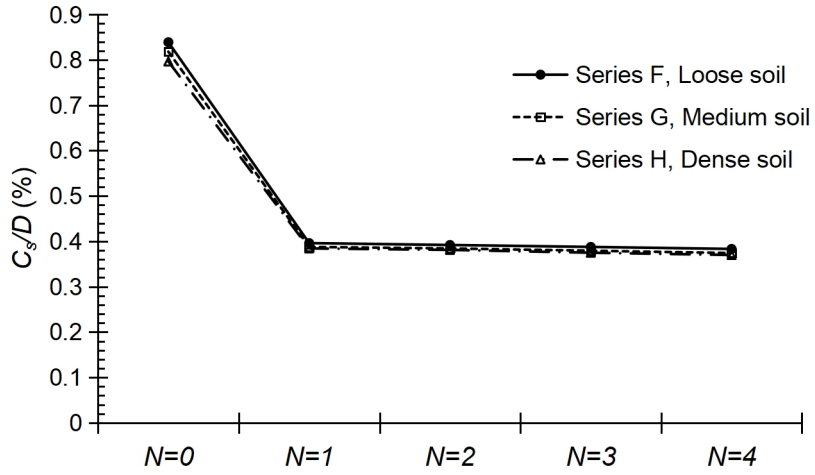

Figure 7.45 C_s/D at different number of geogrid layers for series F, G and H

It is obvious that regardless the unit weight of the soil, the maximum deformation of the crown occurred in the unreinforced case, and with the inclusion of the reinforcing layers, this value decreased, as presented in Table 7.16. The crown deformation was a reflection to the transferred pressure to the pipe as presented in Figure 7.43. The measured reduction in the crown deformation after using one reinforcing layer became insignificant, where the inclusion of one reinforcing layer contributed in decreasing the transferred pressure to the pipe and provided additional lateral support to it.

Figure 7.46 was plotted to further inspect the contribution of varying the unit weight of the soil while inserting variable number of the geogrid reinforcing layers in the investigated pipe-soil system.

Table 7.16 Reduction ratio of C_s/D in series F, G and H

Series F, loose unit weight					
RFT no.	*N*=0	*N*=1	*N*=2	*N*=3	*N*=4

C_s/D (%)	0.84	0.396	0.391	0.387	0.381
Reduction ratio relative to N=0 (%)	-	52.7	53.3	53.7	54.3
Series G, medium unit weight					
RFT no.	N=0	N=1	N=2	N=3	N=4
C_s/D (%)	0.818	0.387	0.384	0.379	0.374
Reduction ratio relative to N=0 (%)	-	52.6	53	53.6	54.2
Reduction ratio relative to series F (%)	2.48	2.13	1.94	2.14	2.36
Series H, dense unit weight					
RFT no.	N=0	N=1	N=2	N=3	N=4
C_s/D (%)	0.796	0.384	0.381	0.374	0.37
Reduction ratio relative to N=0 (%)	-	51.7	52.1	52.9	53.5
Reduction ratio relative to series F (%)	5.06	2.96	2.77	3.3	3.48

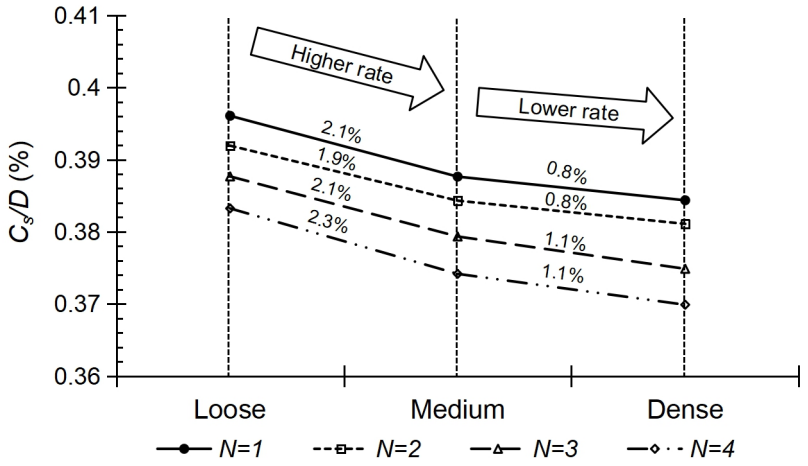

Figure 7.46 Contribution of varying the soil's unit weight in decreasing C_s/D

It was noted that increasing the unit weight of the soil decreased the values of the normalised crown settlement. For example, while inserting one geogrid layer of reinforcement, the measured value of C_s/D was 0.396%, 0.387% and 0.384% for loose, medium and dense unit weights of the soil, respectively. The reduction rate of the crown deformation reached 2.1% and 2.96% for the medium and the dense soil relative to the loose case. It was observed that with the increase in the unit weight of the soil, the crown deformation reduction rate started to decrease, particularly after a soil with medium unit weight. Such behaviour was observed while inserting two, three and four layers of geogrid reinforcements in the investigated systems.

Generally, as observed in the settlement of the footing section, *7.4.2.1*, using soil with higher unit weight would enhance its stiffness. Consequently, the soil resistance to the applied loads would be increased leading to reduction in the

occurred deformation in the pipe. Moreover, using soil of loose unit weight could represent a low-stiffness backfill, which would lead to poor soil support to the pipe and increased pipe deformation. On the contrary, increasing the unit weight of the soil would provide enhanced support to the pipe and reduce its deformation under cyclic loads.

Figure 7.47 illustrated the achieved reduction ratio in the crown settlement while using different number of the reinforcing layers relative to the unreinforced case, in series F, G and H.

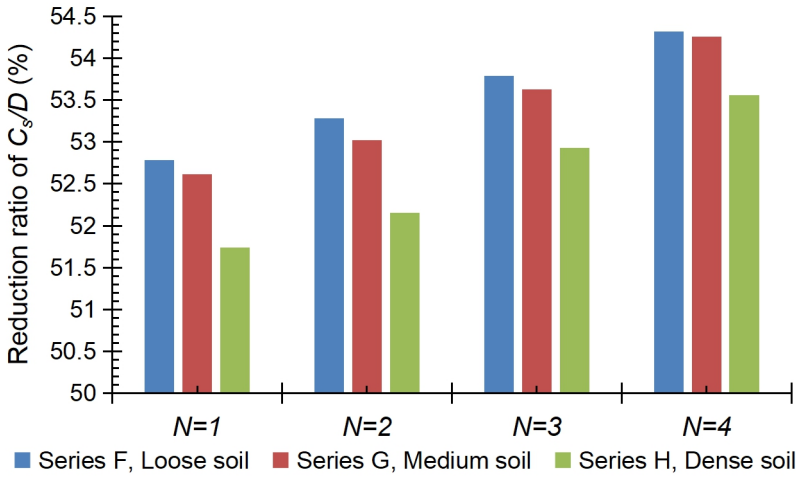

Figure 7.47 Reduction ratio in C_s/D at different number of layers for series F, G and H

Regardless of the number of reinforcing layers, the maximum reduction ratio in the crown deformation occurred while using soil of loose unit weight, and the increase in the soil's unit weight resulted in a decrease in this ratio. This could be attributed to the stiffness of the soil and the provided support to the pipe. Soil of higher unit weigh would have higher stiffness and provide enhanced support to the pipe. This would require lower contribution of the reinforcing layers. On the contrary, the decrease in the unit weight of the soil decreases its stiffness and provides poor support to the pipe, which would require higher contribution of the geogrid layers to enhance the support of the soil to the pipe, to decrease its deformation. This supported the claim, which proposed that the maximum benefit of the reinforcing layers would be achieved while using soil beds of loose unit weight, where the contribution of the reinforcing layers in enhancing the performance of the system become remarkable.

7.4.2.4 Strain of the geogrid reinforcing layers

Figure 7.48-A showed the overall profile of the strain generated in the reinforcing layer due to the variation in the unit weight of the soil, while using one layer of reinforcement.

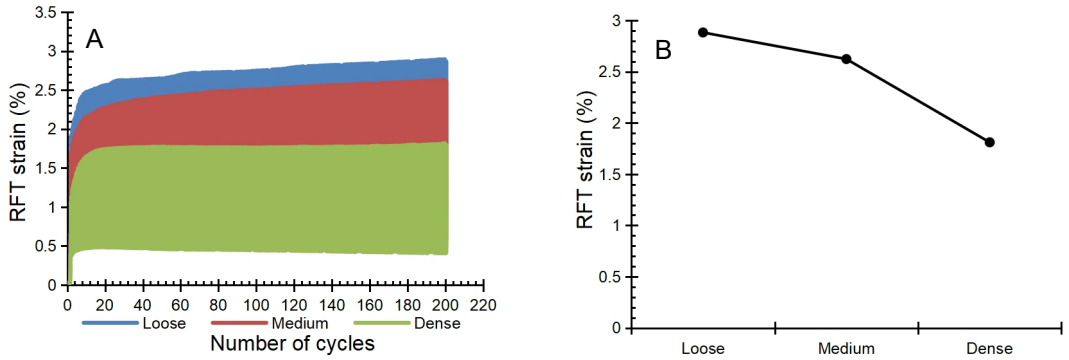

Figure 7.48 Strain generated in the reinforcing layer (*N*=1), series F, G and H
A: Overall strain profile. B: Maximum strain value.

It was noted that increasing the unit weight of the soil had a positive effect on the strain generated in the reinforcing layer, where the reinforcing layers experienced lower tensile strain values while increasing the unit weight of the soil, as presented in Figure 7.48-B. This could be attributed to the enhanced stiffness of soil of higher unit weight, which allowed it to sustain additional tensile strain compared with soil of lower unit weight and seeking lower support from the reinforcing layer.

The generated strain in the reinforcing layers, while using two layers of reinforcements for series F, G and H, is presented in Figure 7.49. As observed while using one layer of reinforcement, the increase in the unit weight of the soil resulted in a decrease in the values of the tensile strain experienced by the two reinforcing layers. Moreover, the formed flexible slab out of the two reinforcing layers and the trapped soil layer between them contributed in increasing the values of the tensile strain sustained by the lower layer (*L2*) compared with those sustained by the upper layer (*L1*), however; the higher deformation of the upper layer.

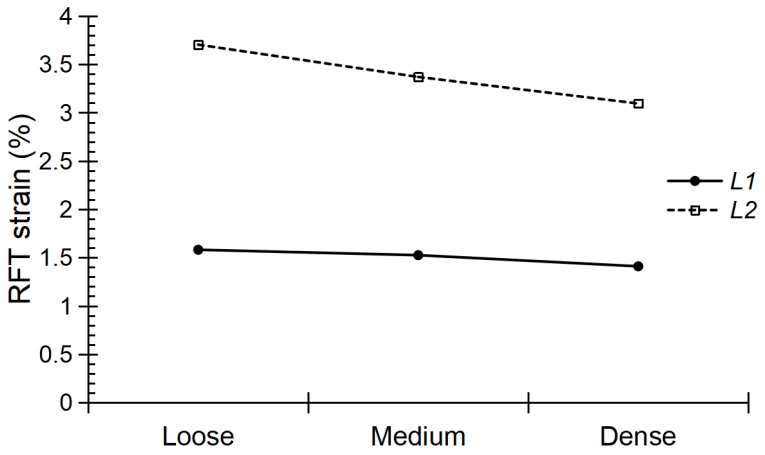

Figure 7.49 Reinforcing layers strain (*N*=2) for series F, G and H

Figure 7.50 showed the generated strain in the reinforcing layers, while using three and four layers of reinforcements for series F, G and H. The increase in the number of the reinforcing layers more than two layers resulted in an increase in the stiffness of the reinforced zone and converted it into a rigid slab instead of a flexible one.

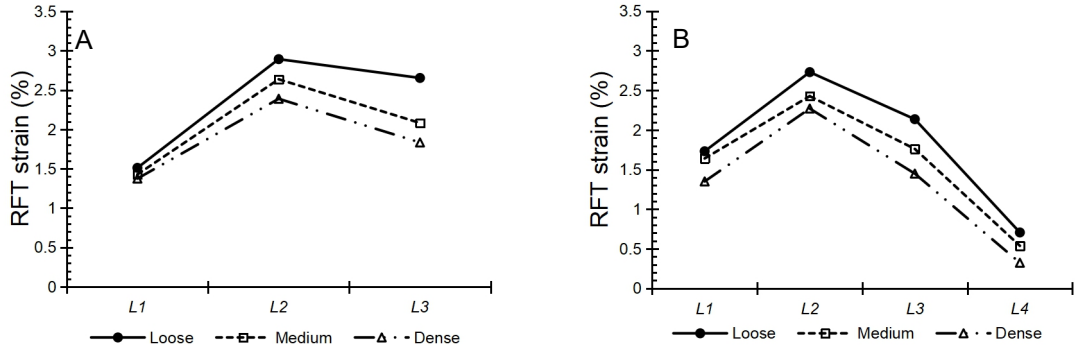

Figure 7.50 Strain generated in the reinforcing layer (*N*=3 and 4), series F, G and H
A: *N*=3. B: *N*=4.

The presented strain values in Figure 7.50 demonstrated that the maximum value of the tensile strain was sustained by the second layer of reinforcements (*L2*), regardless the unit weight of the soil. This could be attributed to the existence of the second layer at the position where the maximum tensile strain was generated inside the soil. Figure 7.51 demonstrated the generated tensile strain in the unreinforced soil in the first and the second steps of the parametric study, where *H/D*=2.5.

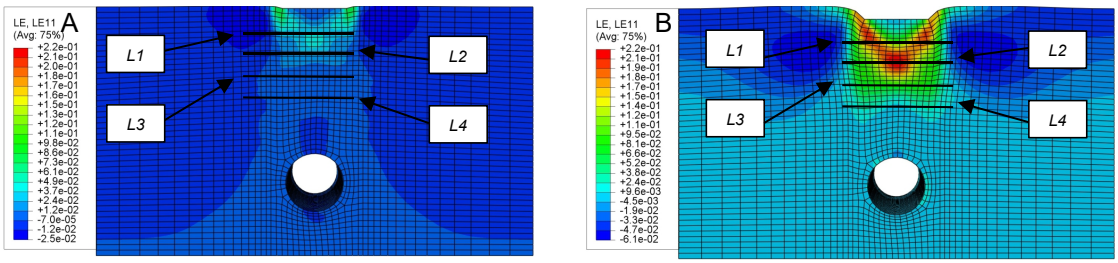

Figure 7.51 Tensile strain in the unreinforced soil at *H/D*=2.5
A: 1st step of the parametric study. B: 2nd step of the parametric study.

It is clear that the strain in the 1st step was lower than that measured in the 2nd step, where loading profile of higher amplitude was subjected to the investigated systems in the 2nd step. In addition, the position of the maximum tensile strain was moved downward to intersect with the second layer (*L2*) instead of the first one (*L1*).

Figure 7.51-A demonstrated that the first reinforcing layer existed in the area where the maximum value of the tensile strain was generated (represented by the green colour). Consequently, the first layer experienced the maximum value of the tensile strain, and the subsequent layers sustained lower strain values, as presented in Figure 7.38.

On the other hand, Figure 7.51-B showed that the second layer of reinforcement existed in the area, where the maximum tensile strain was generated (represented by the red colour). As a result, the second layer sustained the maximum value of the tensile strain, where the other layers sustained lower strain values, as shown in Figure 7.50.

7.5 Summary

In this chapter, the finite element analysis method was used to investigate the behaviour of buried pipe under unreinforced and multi-layers geogrid-reinforced soil while applying cyclic loading profile. According to the outcomes of the numerical study, the following conclusions can be drawn;

1- The modelling process of the geogrid reinforcing layers as a three-dimensional part allowed the prediction of the nearest response to the real case, where the generated load transfer mechanisms between the soil and the ribs of the geogrid-layers were numerically simulated, unlike the membrane modelling process.

2- Increasing the burial depth of the pipe resulted in decreasing both, its deformation and the transferred pressure to its crown. Moreover, the settlement of the footing was decreased. According to the outcomes, the optimum burial depth of the pipe was *H/D*=2.5.
3- The inclusion of the geogrid-reinforcing layers in the investigated systems formed new composite material, i.e. reinforced soil, with higher properties compared with soil, particularly its shearing strength, through the generation of the variable load transfer mechanisms between the soil and the geogrid-layers.
4- Increasing the burial depth of the pipe had negative influence on the generated tensile strain in the geogrid-reinforcing layers, where at deeper burial depths, the contribution of the pipe in reinforcing the system decreased and the reinforcing layers dominated the system stability, which was reflected by the increase in the sustained tensile strain by these layers.
5- The inclusion of the reinforcing layers contributed in forming stiffer layers, at which the transferred pressure was redistributed along wider area, and lower pressure values were transferred to the crown of the pipe. Moreover, enhanced degree of the lateral support was provided to the pipe.
6- At deeper burial depths, increasing the number of the geogrid reinforcing layers had minor contribution in decreasing both, the pipe deformation and the transferred pressure to its crown, as the arching mechanism dominated the system behaviour, where full arching was generated due to the increase in the depth of the soil layer between the footing and the pipe.
7- Increasing the unit weight of the soil had a positive effect in decreasing the transferred pressure to the pipe, its deformation, sustained tensile strain by the reinforcing layers and the settlement of the footing.
8- The inclusion of two reinforcing layers allowed the formation of a flexible slab. Consequently, the sustained tensile strain by the lower layer was higher than that sustained by the upper one, despite the higher deformation of the upper layer.

9- Inserting three and four layers of reinforcements increased the stiffness of the reinforced zone and converted the formed flexible slab into a rigid one.

10- The distribution of the tensile strain through the reinforced zone depended on the value of the applied load and the position where the maximum tensile strain was generated. Consequently, the position of the layer, which sustained the maximum tensile strain varied according to the configuration of the tested system.

11- The maximum benefit of the geogrid-reinforcing layers was achieved when it interacted with soil of loose unit weight, as soil of higher unit weight had higher ability to sustain loads compared with the loose soil. Consequently, the geogrid-reinforcements were required to provide higher contribution, while inserted in systems formed out of soil of loose unit weight.

12- During the second step of the parametric study, the friction angle and the elastic modulus of the soil were kept constant while changing the unit weight of the soil. This would lead to a conservative response of the tested systems.

CHAPTER 8

CONCLUSIONS AND RECOMMENDATIONS FOR FUTURE WORK

8.1 Introduction

In this study, the behaviour of buried pipes under unreinforced and geogrid-reinforced soils while applying incrementally increasing cyclic loading was investigated experimentally using fully instrumented laboratory rig. Moreover, the commercial finite element package, ABAQUS v.14 was used to prepare finite element models to perform a parametric study to provide broader assessment of the controlling parameters in the tested systems. Generally, this study had three main parts, and the main conclusion of each part will be summarised in the following sections.

8.1.1 Part one, experimental investigation of buried flexible pipes

In this part, laboratory large-scale physical models were performed to investigate the behaviour of buried flexible pipes under geogrid-reinforced and unreinforced soil beds while applying incrementally increasing cyclic loading profile. The contribution of two main parameters was investigated in this part, the burial depth of the pipe (H/D=1.5, 2, 2.5 and 3) and the number of the geogrid-reinforcing layers (N=0, 1 and 2). Based on the outcomes of this part, the following conclusions can be drawn;

1- The maximum rate and value of the generated settlement and strain in each tested system occurred during the first 300 cycles of the first loading phase, and with further loading cycles, these rates and values decreased significantly until reaching an almost stable state, at the end of the loading phase. Application of further loading phases resulted in similar behaviour with significantly reduced values.

2- The transition from one loading phase to another led to an increase in the recorded settlements and strains, but with a significantly reduced scale compared with the initial loading phase. This was not the case in the loading phase, where system failure occurred.

3- In the unreinforced case, increasing the burial depth of the pipe had a significant contribution in decreasing the pipe deformation and strain, and it has situational contribution to the footing settlement.
4- In the unreinforced case, after burial depth of *H/D*=2.5, the footing settlement start to increase compared with lower burial depths due to the enhanced degree of soil densification which allows more volume to the footing to settle in. Moreover, the pipe contribution in enhancing the system stability is significantly reduced, where it was too far from the upper soil zone. The results suggest that the behaviour of the whole system relied on pipe location, where it could provide stability according to its stiffness.
5- In the reinforced case, increasing the burial depth of the pipe had a significant contribution in decreasing the pipe deformation and strain in addition to the footing settlement. The existence of the reinforcing layers forces the soil to remain in its position under the generated tensile strains as a result of the passive earth resistance mechanism generation between the reinforcing layers and the trapped soil in between its apertures. This action play a great role in decreasing the footing settlement even at deep burial depths.
6- The increase in the loading cycle number led to a soil densification process, which had significant contribution in reducing the deformation rate of the pipe. The densification process allowed the formation of stiffer soil around the pipe, which provided more lateral support to the pipe leading to reduction in the pipe deformation. The reduced pipe deformation significantly contributed in decreasing the generated strain in the pipe crown and spring-line.
7- The inclusion of the reinforcing layers created a new composite material, which had enhanced properties in comparison with the soil alone. This material had the ability to sustain more loading phases, and provide more protection to the buried pipe.
8- The inclusion of the reinforcing layers had significant contribution in decreasing the generated deformation and strain in the pipe.

9- At the initial loading phases, where the applied load was relatively small, the pipe tended to settle as a whole body with an almost constant settlement rate along its crown and invert. Once the value of the loading phases increased, the crown deformation rate significantly increased compared with the invert increase rate, leading to distortion in the pipe original circular cross-sectional shape.

10- Although sand beds prepared in this experimental investigation were dense, the new formed shape of the pipe cross section after applying loading phases was elliptical.

11- In the case of using multiple-reinforcing layers, the generated strain in the lower layer was always the highest. However, the settlement of the upper layer was remarkably higher than that of the lower layer. The formed flexible slab governed this behaviour. This slab was subjected to bending stresses; consequently, it suffered tensile and compressive strains along its lower and upper surfaces, respectively.

8.1.2 Part two, experimental investigation of buried rigid pipes

In this part, the performance of buried rigid pipes under geogrid-reinforced and unreinforced soil beds while applying incrementally increased cyclic loadings was experimentally investigated using a fully instrumented laboratory rig, varying both the burial depth of the pipe (H/D=1.5, 2 and 2.5), and the number of the geogrid-reinforcing layers (N=0, 1 and 2). Based on the outcomes of this part, the following conclusions can be drawn;

1- Maximum rate and value of deformations and strains occurred during the first 300 cycles of the 1st loading phase. With further loading cycles' application, measured rates and values significantly decreased until reaching almost stable values at the end of the loading phase. With the progression of loading phases, same behaviour is repeated with significant reduced values.

2- Progression of the loading cycles led to a soil densification process, which contributed in reducing the deformation rate of the pipe, and the settlement of the footing.

3- In the unreinforced case, at shallow burial depth, generated cracks along the pipe were observed during the 1st loading phase, where a collapse in the passive arching mechanism was occurred, decreasing the transferred pressure to the pipe, and providing additional lateral support to it. At deeper burial depths, generated cracks along the pipe were observed at further loading phases, as a result of the positive contribution of the load mitigation mechanism.
4- In the unreinforced case, at *H/D*=1.5, during the 1st loading phase, generated deformations and strains of the pipe experienced a non-uniform behaviour, which was matched with the transferred pressure to the pipe.
5- The generated strain patterns along the pipe were similar; however, the generated strains along the invert and the crown of the pipe were much higher than those measured along its spring-line.
6- The densification process of the soil vitally contributed in increasing the stiffness of the soil, in particular the bedding layer, which allowed for more reaction forces to be generated between the bedding layer and the invert of the pipe. These reaction forces applied upward pressure, initiating an invert rebound.
7- At shallow burial depths, the invert rebound occurred faster than those measured at deep burial depths due to the faster densification of the bedding layer. At deep burial depths, the densification of the bedding layer required more loading phases to occur hindering the rebound of the invert.
8- Increasing the burial depth of the pipe had a significant contribution in decreasing its deformations and strains, decreasing transferred pressure to it, decreasing the rates and the values of the footing settlement, and increasing the generated strains in the reinforcing layers. The results suggested that the behaviour of the whole system relied on the pipe location, where it could provide stability to the system according to its stiffness.
9- Due to the crown and invert deformations, cracks were formed along the wall of the pipe distorting its cross-section, where the new formed cross-

section consisted of four segments between the formed cracks, seeking to form an elliptical shape, which was more obvious at shallow burial depths. The inclusion of the reinforcing layers and the increase in the burial depth of the pipe hindered and controlled the generation and propagation of the cracks.

10- In the unreinforced case, pressure transfer inside the soil was governed by two mechanisms; i. passive arching and ii. Load mitigation mechanisms. The inclusion of the reinforcing layers provided one more mechanism, i.e. distributed load over reinforcing layer plane, which depended upon the soil-reinforcement interaction mechanisms, particularly the passive earth resistance.

11- The reinforcing layers inclusion decreased the generated strains and deformations of the pipe and the footing settlement because of the pressure redistribution process. Moreover, it allowed the systems to sustain additional loading.

12- At initial loading phases, the inclusion of the reinforcing layers had obvious influence in decreasing the generated strain in the pipe. However, the increase in the layers number had significant contribution in decreasing the generated strains, while applying advanced loading phases.

13- In Series C, the generated strain in the lower layer was usually higher than that measured in the upper layer, despite the increased deformation of the upper layer. This could be attributed to the formed flexible slab, which suffered tensile and compressive strains along its lower and upper surfaces, respectively.

14- The inclusion of the reinforcing layers achieved the *ITM* concept, where reduced deformations and strains influenced the buried rigid pipe and more loading phases were sustained safely.

8.1.3 Part three, numerical investigation of buried flexible pipes

In this part, the performance of buried pipes in geogrid-reinforced and unreinforced sand beds while applying cyclic loading was numerically investigated. Three-dimensional, 3D, finite element models were first validated

using results of the experimentally investigated cases in Chapter 4, and then a parametric study was performed to investigate the contribution of variable parameters on the performance of the system. The investigated parameters were as follows:

1- Burial depth of the pipe (*H/D*=1.5, 2, 2.5 and 3).
2- Number of the geogrid-reinforcing layers (*N*=0 to 4).
3- Unit weight of the soil (loose – medium – dense).
4- Amplitude of the applied cyclic load.

Based on the outcomes of this part, the following conclusions can be drawn;

1- The modelling process of the geogrid reinforcing layers as a three-dimensional part allowed the prediction of the nearest response to the real case, where the generated load transfer mechanisms between the soil and the ribs of the geogrid-layers were numerically simulated, unlike the membrane modelling process.
2- Increasing the burial depth of the pipe resulted in decreasing both, its deformation and the transferred pressure to its crown. Moreover, the settlement of the footing was decreased. According to the outcomes, the optimum burial depth of the pipe was *H/D*=2.5.
3- The inclusion of the geogrid-reinforcing layers in the investigated systems formed new composite material, i.e. reinforced soil, with higher properties compared with soil, particularly its shearing strength, through the generation of the variable load transfer mechanisms between the soil and the geogrid-layers.
4- Increasing the burial depth of the pipe had negative influence on the generated tensile strain in the geogrid-reinforcing layers, where at deeper burial depths, the contribution of the pipe in reinforcing the system decreased and the reinforcing layers dominated the system stability, which was reflected by the increase in the sustained tensile strain by these layers.
5- The inclusion of the reinforcing layers contributed in forming stiffer layers, at which the transferred pressure was redistributed along wider area, and lower pressure values were transferred to the crown of the pipe.

Moreover, enhanced degree of the lateral support was provided to the pipe.

6- At deeper burial depths, increasing the number of the geogrid reinforcing layers had minor contribution in decreasing both, the pipe deformation and the transferred pressure to its crown, as the arching mechanism dominated the system behaviour, where full arching was generated due to the increase in the depth of the soil layer between the footing and the pipe.
7- Increasing the unit weight of the soil had a positive effect in decreasing the transferred pressure to the pipe, its deformation, sustained tensile strain by the reinforcing layers and the settlement of the footing.
8- The inclusion of two reinforcing layers allowed the formation of a flexible slab. Consequently, the sustained tensile strain by the lower layer was higher than that sustained by the upper one, despite the higher deformation of the upper layer.
9- Inserting three and four layers of reinforcements increased the stiffness of the reinforced zone and converted the formed flexible slab into a rigid one.
10- The distribution of the tensile strain through the reinforced zone depended on the value of the applied load and the position where the maximum tensile strain was generated. Consequently, the position of the layer, which sustained the maximum tensile strain varied according to the configuration of the tested system.
11- The maximum benefit of the geogrid-reinforcing layers was achieved when it interacted with soil of loose unit weight, as soil of higher unit weight had higher ability to sustain loads compared with the loose soil. Consequently, the geogrid-reinforcements were required to provide higher contribution, while inserted in systems formed out of soil of loose unit weight.

8.2 Recommendations for future work

It is recommended to investigate the following points:

1- Using geosynthetic reinforcements in the protection process of buried structures under the application of seismic and uplift loading profiles.

2- Using variable combinations of geosynthetics and EPS geofoams to protect buried structures under different loading profiles.

3- Investigating the effect of the presence of multi-buried structures on the overall behaviour of a geosynthetic-reinforced system while applying centric and eccentric loading profiles.

4- Investigating the circumferential pressure and strain distribution in buried structures under unreinforced and geosynthetic-reinforced soil beds.

5- Investigating the performance of the joints of buried rigid and flexible pipes under geosynthetic-reinforced and unreinforced sand beds while applying dynamic loading profiles.

6- Investigating the influence of loading profiles orientation on the overall performance of buried structures under geosynthetic-reinforced and unreinforced sand beds.

7- Investigating the inclusion effect of geosynthetic-reinforcing layers in soft beds to provide protection to buried conduits.

8- Investigating the detrimental effects of existed voids around buried rigid and flexible pipes, and the influence of adding geosynthetic-reinforcing layers to decrease these effects while applying dynamic loading profiles.

9- Investigating the effect of stiffness variation of geosynthetic-reinforcing layers on the formed load transfer mechanisms and the overall response of buried conduits, while applying dynamic loading profiles.

REFERENCES

Abaqus, V. 2014. 6.14 Documentation. *Dassault Systemes Simulia Corporation*.

Abolmaali, A. & Kararam, A. 2009. Nonlinear finite-element-based investigation of the effect of bedding thickness on buried concrete pipe. *Journal of Transportation Engineering,* 136**,** 793-799.

Abolmaali, A. & Kararam, A. 2011. Nonlinear finite-element modeling analysis of soil-pipe interaction. *International Journal of Geomechanics,* 13**,** 197-204.

Abu-Farsakh, M., Chen, Q. & Sharma, R. 2013. An experimental evaluation of the behavior of footings on geosynthetic-reinforced sand. *Soils and Foundations,* 53**,** 335-348.

Ahmed, M. 2016. *Experimental investigations into the role of geosynthetic inclusions on the earth pressure acting on buried structures.* Doctor of Philisophy, McGill University Libraries.

Ahmed, M., Tran, V. & Meguid, M. 2015. On the role of geogrid reinforcement in reducing earth pressure on buried pipes: experimental and numerical investigations. *Soils and Foundations,* 55**,** 588-599.

Alabdullah, S. F. & Taresh, N. S. 2016. Evaluation of Soil Reinforced with Geogrid in Subgrade Layer Using Finite Element Techniques. *Imperial Journal of Interdisciplinary Research,* 3**,** 174-179.

Alagiyawanna, A., Sugimoto, M., Sato, S. & Toyota, H. 2001. Influence of longitudinal and transverse members on geogrid pullout behavior during deformation. *Geotextiles and Geomembranes,* 19**,** 483-507.

Alamatian, E., Ghadamkheir, M. & Karimpour, B. 2013. Stress estimation on pipeline and effect of burying depth. *International Research Journal of Applied and Basic Sciences,* 6**,** 228-235.

Alzabeebee, S., Chapman, D., Jefferson, I. & Faramarzi, A. The response of buried pipes to UK standard traffic loading. Proc. Inst. Civ. Eng. Geotech. Eng, 2017. 38-50.

Alzabeebee, S., Chapman, D. N., Jefferson, I. & Faramarzi, A. Investigating the maximum soil pressure on a concrete pipe with poor haunch support subjected to traffic live load using numerical modelling. in Proceedings of the 11th Pipeline Technology Conference, 2016 Berlin, Germany.

Anderson, A. O. 1913. *The theory of loads on pipes in ditches: and tests of cement and clay drain tile and sewer pipe,* Ames, Iowa, Iowa State College of Agriculture and Mechanic Arts.

Aqoub, K., Mohamed, M. & Sheehan, T. 2018. Analysis of sequential active and passive arching in granular soils. *International Journal of Geotechnical Engineering***,** 1-10.

Arockiasamy, M., Chaallal, O. & Limpeteeprakarn, T. 2006. Full-scale field tests on flexible pipes under live load application. *Journal of performance of constructed facilities,* 20**,** 21-27.

Asakereh, A., Tafreshi, S. N. M. & Ghazavi, M. 2012. Strip footing behavior on reinforced sand with void subjected to repeated loading. *International Journal of Civil Engineering,* 10**,** 139-152.

Babu, G. S. 2006. *An Introduction to soil reinforcement and geosynthetics*, Universities Press.

Bartlett, S. F. & Lingwall, B. N. Protection of Pipelines and Buried Structures Using EPS Geofoam. *In:* ASCE, ed. Ground Improvement and Geosynthetics, 2014 Shanghai, China. 547-556.

Benzley, S. E., Perry, E., Merkley, K., Clark, B. & Sjaardama, G. A comparison of all hexagonal and all tetrahedral finite element meshes for elastic and elasto-plastic analysis. 1995 1995. Sandia National Laboratories Albuquerque, NM, 179-191.

Berg, R. R., Christopher, B. R. & Samtani, N. C. 2009. Design of Mechanically Stabilized Earth Walls and Reinforced Soil Slopes–Volume II.

Brachman, R. W., Moore, I. & Rowe, R. 2000. The design of a laboratory facility for evaluating the structural response of small-diameter buried pipes. *Canadian Geotechnical Journal,* 37**,** 281-295.

Briancon, L. & Villard, P. 2008. Design of geosynthetic-reinforced platforms spanning localized sinkholes. *Geotextiles and Geomembranes,* 26**,** 416-428.

Bs 1997. BS EN 1295-1:1997 - Structural design of buried pipelines under various conditions of loading - Part 1: General requirements. London: British Standards Institution.

Bs 2003. NA to BS EN 1991-2, UK National Annex to Eurocode 1: Actions on structures - Part 2: Traffic loads on bridges. London, UK: British Standards Institution.

Bs 2009a. BS EN 1401-1:2009 - Plastic piping systems for non-pressure underground drainageand sewerage - Unplasticized poly(vinyl chloride) (PVC-U) - Part 1: Specifications for pipes, fittings and the system. London: British Standards Institution.

Bs 2009b. BS EN 12390-3:2009 - Testing hardened concrete - Part 3: Compressive strength of test specimens. London, UK: British Standards Institution.

Bs 2010a. BS 8006 - Code of Practice for Strengthened/Reinforced Soils and Others Fills. London: British Standards Institution.

Bs 2010b. BS 9295 - Guide to the structural design of buried pipelines. London: British Standards Institution.

Bs 2012. BS EN ISO 527-1, Plastics - Determination of tensile properties - Part 1: General principles. London: British Standards Institution.

Bs 2015. BS EN ISO 10319, Geosynthetics — Wide-width tensile test. London: British Standards Institution.

Bs 2016a. BS1377-1, Methods of test for soils for civil engineering purposes – Part 1: General requirements and sample preparation. London, UK: British Standards Institution.

Bs 2016b. BS EN ISO 9969:2016 - Thermoplastics pipes - Determination of ring stiffness. London: British Standards Institution.

Bueno, B., Viana, P. & Zornberg, J. 2005. A novel construction method for buried pipes using geosynthetics. *Geosynthetics Research and Development in Progress.*

Cao, Z., Han, J., Xu, C., Khatri, D. K., Corey, R. & Cai, Y. 2016. Road surface permanent deformations with a shallowly buried steel-reinforced high-density polyethylene pipe under cyclic loading. *Geotextiles and Geomembranes,* 44**,** 28-38.

Chen, C., Mcdowell, G. & Thom, N. 2012. Discrete element modelling of cyclic loads of geogrid-reinforced ballast under confined and unconfined conditions. *Geotextiles and Geomembranes,* 35**,** 76-86.

Chen, R., Luan, M. & Hao, D. 2011. Improved simulation method for soil-geogrid interaction of reinforced earth structure in FEM. *Transactions of Tianjin University,* 17**,** 220-228.

Chen, W.-F. & Baladi, G. Y. 1985. *Soil plasticity: theory and implementation*, Elsevier, New York.

Chen, W.-F. & Mizuno, E. 1990. *Nonlinear analysis in soil mechanics*, Elsevier, Amsterdam.

Chenggang, B. 2004. Study on the interaction behavior of geosynthetics and soil in China. *Ningbo Institute of Technology, Zhejiang University, China*.

Corey, R., Han, J., Khatri, D. K. & Parsons, R. L. 2014. Laboratory study on geosynthetic protection of buried steel-reinforced HDPE pipes from static loading. *Journal of Geotechnical and Geoenvironmental Engineering,* 140**,** 04014019.

Das, B. M. 2019. *Advanced soil mechanics*, Crc Press.

Dash, S. K. 2011. Effect of geocell type on load-carrying mechanisms of geocell-reinforced sand foundations. *International Journal of Geomechanics,* 12**,** 537-548.

Dong, Y.-L., Han, J. & Bai, X.-H. 2011. Numerical analysis of tensile behavior of geogrids with rectangular and triangular apertures. *Geotextiles and Geomembranes,* 29**,** 83-91.

Drucker, D. C., Gibson, R. E. & Henkel, D. J. 1957. Soil mechanics and work hardening theories of plasticity. *Transactions of the American Society of Civil Engineers,* 122.

Du, X.-L., Lu, D.-C., Gong, Q.-M. & Zhao, M. 2009. Nonlinear unified strength criterion for concrete under three-dimensional stress states. *Journal of engineering mechanics,* 136**,** 51-59.

Elias, V., Barry, P. & Christopher, R. 1997. *Mechanically Stabilized Earth Walls and Reinforced Soil Slopes Design and Construction Guidelines: FHWA Demonstration Project 82, Reinforced Soil Structures WSEW and RSS*, US Department of Transportation, Federal Highway Administration.

Elshesheny, A., Mohamed, M. & Sheehan, T. 2019. Buried flexible pipes behaviour in unreinforced and reinforced soils under cyclic loading. *Geosynthetics International,* 26**,** 184-205.

Elshesheny, A., Nagy, N., Belal, A. & Badawy, A. Finite Element Analysis of Square Footing Resting on Geosynthetic Reinforced Soil. 10th International Conference on Civil and Architecture Engineering ICCAE Cairo, Egypt, May 2014, 2014. 10-21.

Fang, H.-Y. & Daniels, J. L. 2006. *Introductory geotechnical engineering: an environmental perspective*, CRC Press.

Faragher, E., Fleming, P. R. & Rogers, C. D. F. 2000. Analysis of repeated-load field testing of buried plastic pipes. *Journal of transportation engineering,* 126**,** 271-277.

Gilley, C. W. & Gabriel, L. H. 1993. Field performance of cast-in-place nonreinforced concrete pipe. *Transportation Research Record***,** 47-50.

Gourc, J. & Villard, P. Reinforcement by membrane effect: Application to embankments on soil liable to subsidence. Proceedings of the 2nd Asian Geosynthetics Conference, 2000, 2000. 55-72.

Hegde, A., Kadabinakatti, S. & Sitharam, T. 2014. Protection of buried pipelines using a combination of geocell and geogrid reinforcement: experimental studies. *Ground Improvement and Geosynthetics, Geotechnical Special Publication-238, ASCE***,** 289-298.

Hegde, A., Kadabinakatti, S. & Sitharam, T. G. 2016. Use of Geocells to Protect Buried Pipelines and Underground Utilities in Soft Clayey Soils. *Geo-Chicago 2016.*

Hegde, A. M. & Sitharam, T. G. 2015. Experimental and numerical studies on protection of buried pipelines and underground utilities using geocells. *Geotextiles and Geomembranes,* 43**,** 372-381.

Helwany, S. 2007. *Applied soil mechanics with ABAQUS applications*, John Wiley & Sons.

Hsuan Et Al. 2013. Numerical modeling for undrained shear strength of clays subjected to different plasticity indexes. *Journal of GeoEngineering,* 8**,** 91-100.

Hussein, M. & Meguid, M. 2016. A three-dimensional finite element approach for modeling biaxial geogrid with application to geogrid-reinforced soils. *Geotextiles and Geomembranes,* 44**,** 295-307.

Hussein, M. G. & Meguid, M. A. Three-dimensional finite element analysis of soil-geogrid interaction under pull-out loading condition. GeoMontreal, 66th Canadian Geotechnical Conference. Canadian Geotechnical Society, Montreal, Quebec, Canada, 2013. 452-458.

Hussein, M. G., Meguid, M. A. & Mowafy, Y. 2009. On the 3D Modelling of Soil-Geogrid Interaction.

Hussein, M. G., Meguid, M. A., Whalen, J. & Eng, P. 2015. On the numerical modeling of buried structures with compressible inclusion. *GeoQuebec, September, Quebec City,* 8.

Ibrahim, S., Sofia, G. & Teama, Z. 2014. An Approach in Evaluating of Flexible Pavement In Permanent Deformation OF Paved AND Unpaved Roads Over Sand Dunes Subgrade Under Repeated Loads. *J. Environ. Earth Sci,* 4**,** 78-90.

Jewell, R. 1996. *Soil reinforcement with geotextiles*, Construction Industry Research and Information Association.

Jones, C. J. & Cooper, A. H. 2005. Road construction over voids caused by active gypsum dissolution, with an example from Ripon, North Yorkshire, England. *Environmental Geology,* 48**,** 384-394.

Kang, J. S., Han, T. H., Kang, Y. J. & Yoo, C. H. 2009. Short-term and long-term behaviors of buried corrugated high-density polyethylene (HDPE) pipes. *Composites Part B: Engineering,* 40**,** 404-412.

Keatley, D. J. 2009. *Three-Dimensional Nonlinear Analysis of Deeply-Buried Corrugated Annular HDPE Pipe with Changes in Its Profile-Wall.* Ohio University.

Kim, H., Choi, B. & Kim, J. 2010. Reduction of earth pressure on buried pipes by EPS geofoam inclusions. *Geotechnical Testing Journal,* 33**,** 304-313.

Kim, J., Lynch, J. P., Michalowski, R. L., Green, R. A., Pour-Ghaz, M., Weiss, W. J. & Bradshaw, A. Experimental study on the behavior of segmented buried concrete pipelines subject to ground movements. in Proceedings of SPIE Nondestructive Characterization for Composite Materials, Aerospace Engineering, Civil Infrastructure, and Homeland Security, 2009. International Society for Optics and Photonics, 19.

Koerner, R. M. An overview of geogrids. Jubilee Symposium on Polymer Geogrid Reinforcement, London, United Kingdom, 2009.

Kraus, E., Oh, J. & Fernando, E. G. 2013. Impact of repeat overweight truck traffic on buried utility facilities. *Journal of Performance of Constructed Facilities,* 28**,** 04014004.

Larsen, N. G. & Hendrickson, J. G. 1962. A practical method for constructing rigid conduits under high fills. *Highway Research Board Proceedings,* 41.

Latha, G. M. & Somwanshi, A. 2009. Bearing capacity of square footings on geosynthetic reinforced sand. *Geotextiles and Geomembranes,* 27**,** 281-294.

Lay, G. & Brachman, R. 2014. Full-scale physical testing of a buried reinforced concrete pipe under axle load. *Canadian geotechnical journal,* 51**,** 394-408.

Le Hello, B. & Villard, P. 2009. Embankments reinforced by piles and geosynthetics—Numerical and experimental studies dealing with the transfer of load on the soil embankment. *Engineering Geology,* 106**,** 78-91.

Lee, H. 2010. Finite element analysis of a buried pipeline.

Lei, X., Zhicai, Y., Qingwen, R. & Lei, Z. 2013. Fem analysis of dynamic response of buried fiber reinforced plastic matrix pipe under seismic load. *Mathematical Problems in Engineering,* 2013.

Leng, J. 2003. Characteristics and behavior of geogrid-reinforced aggregate under cyclic load.

Liu, C.-N., Ho, Y.-H. & Huang, J.-W. 2009. Large scale direct shear tests of soil/PET-yarn geogrid interfaces. *Geotextiles and Geomembranes,* 27**,** 19-30.

Logan, D. L. 2011. *A first course in the finite element method*, Cengage Learning.

Marston, A. 1922. Second progress report to the joint concrete culvert pipe committee. *Iowa Engineering Experimental Station, Ames, IA*.

Marston, A. The theory of external loads on closed conduits in the light of the latest experiments. Highway Research Board Proceedings, 1930.

Mcaffee, R. P. & Valsangkar, A. J. 2004. Geotechnical properties of compressible materials used for induced trench construction. *Journal of Testing and Evaluation,* 32**,** 143-152.

Mcaffee, R. P. & Valsangkar, A. J. 2008. Field performance, centrifuge testing, and numerical modelling of an induced trench installation. *Canadian Geotechnical Journal,* 45**,** 85-101.

Mcgrath, T. 2005. Performance of Thermoplastic Pipe Under Highway Vehicle Loading.

Mcgrath, T. J., Selig, E. T. & Webb, M. C. 2000. Field tests of concrete pipe performance during backfilling. *In:* I. KASPAR, I. E. (ed.) *Concrete pipe for the new millennium.* Special Technical Publications, ASTM SPT-1368.

Meguid, M. A., Hussein, M. G., Ahmed, M. R., Omeman, Z. & Whalen, J. 2017. Investigation of soil-geosynthetic-structure interaction associated with induced trench installation. *Geotextiles and Geomembranes,* 45**,** 320-330.

Meguid, M. A. & Kamel, S. 2014. A three-dimensional analysis of the effects of erosion voids on rigid pipes. *Tunnelling and Underground Space Technology,* 43**,** 276-289.

Meguid, M. A. & Youssef, T. A. 2018. Experimental investigation of the earth pressure distribution on buried pipes backfilled with tire-derived aggregate. *Transportation Geotechnics,* 14**,** 117-125.

Mehdipour, I., Ghazavi, M. & Moayed, R. Z. 2013. Numerical study on stability analysis of geocell reinforced slopes by considering the bending effect. *Geotextiles and Geomembranes,* 37**,** 23-34.

Mehrjardi, G. T., Ghanbari, A. & Mehdizadeh, H. 2016. Experimental study on the behaviour of geogrid-reinforced slopes with respect to aggregate size. *Geotextiles and Geomembranes,* 44**,** 862-871.

Mehrjardi, G. T. & Tafreshi, S. M. Buried pipes analysis in reinforced sand under repeated loading. Proceedings of the Second BGA International Conference on Foundations, ICOF2008, Dundee, UK, 2008. 1103-1110.

Mehrjardi, G. T., Tafreshi, S. M. & Dawson, A. 2012. Combined use of geocell reinforcement and rubber–soil mixtures to improve performance of buried pipes. *Geotextiles and Geomembranes,* 34**,** 116-130.

Mehrjardi, G. T., Tafreshi, S. M. & Dawson, A. 2013. Pipe response in a geocell-reinforced trench and compaction considerations. *Geosynthetics International,* 20**,** 105-118.

Mir Mohammad, S. & Moghaddas , T., Sn 2001. Soil-structure interaction of buried pipes under cyclic loading conditions. *International Journal of Engineering-Transactions B: Applications,* 15**,** 117.

Mirzababaei, M. 2012. *Reinforcement of clay soils using waste carpet fibres.* PhD thesis. University of Bolton.

Mitchell, J. K. & Villet, W. C. 1987. Reinforcement of earth slopes and embankments. *NCHRP Report*.

Moayed, R. Z., Tamassoki, S. & Izadi, E. 2012. Numerical modeling of direct shear tests on sandy clay. *World Academy of Science, Engineering and Technology,* 61**,** 1093-1097.

Mohamed, M. H. 2010. Two dimensional experimental study for the behaviour of surface footings on unreinforced and reinforced sand beds overlying soft pockets. *Geotextiles and Geomembranes,* 28**,** 589-596.

Moser, A. P. & Folkman, S. L. 2001. *Buried pipe design,* USA, McGraw-Hill New York.

Nagy, N. 2007. *Dynamic soil structure interaction of buried concrete structures under the effect of blast loads.* PhD thesis. The University of Bradford.

Nagy, N., Mohamed, M. & Boot, J. C. 2010. Nonlinear numerical modelling for the effects of surface explosions on buried reinforced concrete structures. *Geomechanics and Engineering,* 2**,** 1-18.

Ni, P., Qin, X. & Yi, Y. 2018. Numerical study of earth pressures on rigid pipes with tire-derived aggregate inclusions. *Geosynthetics International***,** 1-45.

Nobahar, A., Kenny, S. & Phillips, R. 2007. Buried pipelines subject to subgouge deformations. *International Journal of Geomechanics,* 7**,** 206-216.

Palmeira, E. & Andrade, H. 2010. Protection of buried pipes against accidental damage using geosynthetics. *Geosynthetics International,* 17**,** 228-241.

Palmeira, E. M. 2009. Soil–geosynthetic interaction: Modelling and analysis. *Geotextiles and Geomembranes,* 27**,** 368-390.

Perkins, S. & Edens, M. 2003. Finite element modeling of a geosynthetic pullout test. *Geotechnical & Geological Engineering,* 21**,** 357-375.

Peter, J. M., Chapman, D., Moore, I. D. & Hoult, N. 2018. Impact of soil erosion voids on reinforced concrete pipe responses to surface loads. *Tunnelling and Underground Space Technology,* 82**,** 111-124.

Pistrol, J., Falkner, F., Adam, D. & Adam, C. 2012. Comparison of constitutive soil models for the simulation of dynamic roller compaction. *Proc. 6th European Cong. on 'Computational methods in applied sciences and engineering', Vienna, Austria***,** 5925-5939.

Qian, Y., Han, J., Pokharel, S. & Parsons, R. 2011. Stress Analysis on Triangular-Aperture Geogrid-Reinforced Bases over Weak Subgrade Under Cyclic Loading: An Experimental Study. *Transportation Research Record: Journal of the Transportation Research Board***,** 83-91.

Qian, Y., Han, J., Pokharel, S. K. & Parsons, R. L. 2010. Experimental study on triaxial geogrid-reinforced bases over weak subgrade under cyclic loading. *GeoFlorida 2010: Advances in Analysis, Modeling and Design (Geotechnical Special Publication 199)***,** 1208-1216.

Qian, Y., Han, J., Pokharel, S. K. & Parsons, R. L. 2012. Performance of triangular aperture geogrid-reinforced base courses over weak subgrade under cyclic loading. *Journal of Materials in Civil Engineering,* 25**,** 1013-1021.

Rad, N. S. & Tumay, M. T. 1987. Factors affecting sand specimen preparation by raining. *Geotechnical Testing Journal,* 10**,** 31-37.

Rajkumar, R. & Ilamparuthi, K. 2008. Experimental Study on the behaviour of Buried flexible Plastic pipe. *EJGE,* 13**,** 1-10.

Rakitin, B. & Xu, M. 2013. Centrifuge modeling of large-diameter underground pipes subjected to heavy traffic loads. *Canadian Geotechnical Journal,* 51**,** 353-368.

Rogers, C., Fleming, P. & Talby, R. 1996. Use of visual methods to investigate influence of installation procedure on pipe-soil interaction. *Transportation Research Record: Journal of the Transportation Research Board***,** 76-85.

Selvadurai, A. 1989. Enhancement of the uplift capacity of buried pipelines by the use of geogrids.

Sharma, R., Chen, Q., Abu-Farsakh, M. & Yoon, S. 2009. Analytical modeling of geogrid reinforced soil foundation. *Geotextiles and Geomembranes,* 27**,** 63-72.

Sheldon, T., Sezen, H. & Moore, I. D. 2013. Joint response of existing pipe culverts under surface live loads. *Journal of Performance of Constructed Facilities,* 29**,** 04014037 1-9.

Sieira, A. C. C., Gerscovich, D. M. & Sayao, A. S. 2009. Displacement and load transfer mechanisms of geogrids under pullout condition. *Geotextiles and Geomembranes,* 27**,** 241-253.

Spangler, M. G. 1933. *The supporting strength of rigid pipe culverts,* Iowa, (IA): Iowa State College.

Spangler, M. G. 1950. A theory on loads on negative projecting conduits. *Proceedings of the Highway Research Board, 30, Transportation Research Board, Washington, DC,* 30**,** 153–161.

Spangler, M. G. 1958. A practical application of the imperfect ditch method of construction. *Highway Research Board Proceedings,* 37.

Srivastava, A., Goyal, C. R. & Raghuvanshi, A. 2012. Load settlement response of footing placed over buried flexible pipe through a model plate load test. *International Journal of Geomechanics,* 13**,** 477-481.

Tafreshi, S. M. & Khalaj, O. 2008. Laboratory tests of small-diameter HDPE pipes buried in reinforced sand under repeated-load. *Geotextiles and Geomembranes,* 26**,** 145-163.

Tafreshi, S. M. & Khalaj, O. 2011. Analysis of repeated-load laboratory tests on buried plastic pipes in sand. *Soil Dynamics and Earthquake Engineering,* 31**,** 1-15.

Tafreshi, S. M., Mehrjardi, G. T. & Dawson, A. 2012. Buried pipes in rubber-soil backfilled trenches under cyclic loading. *Journal of Geotechnical and Geoenvironmental Engineering,* 138**,** 1346-1356.

Tan, Z. & Moore, I. D. 2007. Effect of backfill erosion on moments in buried rigid pipes. Washington DC: In: Transportation Research Board Annual Conference.

Tang, X. 2011. *A study of permanent deformation behavior of geogrid-reinforced flexible pavements using small scale accelerated pavement testing.* The Pennsylvania State University.

Tensar, I. 2012. Tensar SS Geogrids Product Specifications.

Tensar International 2010. TriAx Brochure. *In:* TENSAR INTERNATIONAL LTD., B. (ed.).

Terzaghi, K. & Peck, R. B. 1967. *Soil mechanics in engineering practice,* New York, John Wiley & Sons.

Tran, V., Meguid, M. & Chouinard, L. 2013. A finite–discrete element framework for the 3D modeling of geogrid–soil interaction under pullout loading conditions. *Geotextiles and Geomembranes,* 37**,** 1-9.

Turan, A., El Naggar, M. H. & Dundas, D. 2013. Investigation of induced trench method using a full scale test embankment. *Geotechnical and Geological Engineering,* 31**,** 557-568.

Vaslestad, J., Johansen, T. H. & Holm, W. 1993. Load reduction on rigid culverts beneath high fills: long-term behavior. *Transportation Research Record***,** 58-58.

Vieira, C. S., Lopes, M. L. & Caldeira, L. Soil-geosynthetic interface shear strength by simple and direct shear tests. Proceedings of the 18th international conference on soil mechanics and geotechnical engineering, 2013 2013 Paris, France. 3497-3500.

Villard, P., Huckert, A. & Briançon, L. 2016. Load transfer mechanisms in geotextile-reinforced embankments overlying voids: Numerical approach and design. *Geotextiles and Geomembranes,* 44**,** 381-395.

Wang, E., Nelson, T. & Rauch, R. Back to elements-tetrahedra vs. hexahedra. 2004. ANSYS Pennsylvania.

Wang, Z., Jacobs, F. & Ziegler, M. 2016. Experimental and DEM investigation of geogrid–soil interaction under pullout loads. *Geotextiles and Geomembranes,* 44**,** 230-246.

Wathugala, G., Huang, B. & Pal, S. 1996. Numerical simulation of geosynthetic-reinforced flexible pavements. *Transportation Research Record: Journal of the Transportation Research Board***,** 58-65.

Witthoeft, A. F. & Kim, H. 2016. Numerical investigation of earth pressure reduction on buried pipes using EPS geofoam compressible inclusions. *Geosynth Int,* 23**,** 1-14.

Wong, L. S., Allouche, E. N., Dhar, A. S., Baumert, M. & Moore, I. D. 2006. Long-term monitoring of SIDD Type IV installations. *Canadian geotechnical journal,* 43**,** 392-408.

Young, O. C. & Trott, J. J. 1984. *Buried Rigid Pipes: Structural Design of Pipelines,* London, Elsevier Applied Science Publishers.

Zhuang, Y. 2009. *Numerical modelling of arching in piled embankments including the effects of reinforcement and subsoil.* University of Nottingham.

Zinkaah, O. H., Ashour, A. & Sheehan, T. 2019. Experimental tests of two-span continuous concrete deep beams reinforced with GFRP bars and strut-and-tie method evaluation. *Composite Structures,* 216**,** 112-126.